University of Cyprus

DEPARTMENT OF CIVIL AND ENVIRONMENTAL ENGINEERING

NONLINEAR MODELING CONSIDERATIONS ON THE SEISMIC RESPONSE OF BASE-ISOLATED BUILDINGS: 2D AND 3D INVESTIGATIONS OF POUNDING

DOCTOR OF PHILOSOPHY DISSERTATION

EFTYCHIA A. MAVRONICOLA

2017

University of Cyprus

DEPARTMENT OF CIVIL AND ENVIRONMENTAL ENGINEERING

NONLINEAR MODELING CONSIDERATIONS ON THE SEISMIC RESPONSE OF BASE-ISOLATED BUILDINGS: 2D AND 3D INVESTIGATIONS OF POUNDING

Eftychia A. Mavronicola

B.Sc. in Civil and Environmental Engineering, University of Cyprus
M.Sc. in Civil Engineering, University of Cyprus

A Dissertation Submitted to the University of Cyprus in Partial Fulfillment of the Requirements for the Degree of Doctor of Philosophy

May 2017

University of Cyprus

DEPARTMENT OF CIVIL AND ENVIRONMENTAL ENGINEERING

NONLINEAR MODELING CONSIDERATIONS ON THE SEISMIC RESPONSE OF BASE-ISOLATED BUILDINGS: 2D AND 3D INVESTIGATIONS OF POUNDING

by

Eftychia A. Mavronicola

Examination Committee:

Dimos C. Charmpis, Associate Professor (*Chairman*)
Department of Civil and Environmental Engineering, University of Cyprus

Stavros A. Anagnostopoulos, Professor Emeritus
University of Patras, Greece

Marios Phocas, Associate Professor
Department of Architecture, University of Cyprus

Panayiotis Roussis, Assistant Professor
Department of Civil and Environmental Engineering, University of Cyprus

Petros Komodromos, Associate Professor
Department of Civil and Environmental Engineering, University of Cyprus

Thesis Advisory Committee:

Dimos C. Charmpis, Associate Professor
Department of Civil and Environmental Engineering, University of Cyprus

Marios Phocas, Associate Professor
Department of Architecture, University of Cyprus

Petros Komodromos, Associate Professor
Department of Civil and Environmental Engineering, University of Cyprus

Thesis supervisor:

Petros Komodromos, Associate Professor
Department of Civil and Environmental Engineering, University of Cyprus

VALIDATION PAGE

Doctoral Candidate: Eftychia A. Mavronicola

Doctoral Thesis Title: Nonlinear modeling considerations on the seismic response of base-isolated buildings: 2D and 3D investigations of poundings

The present Doctoral Dissertation was submitted in partial fulfillment of the requirements for the Degree of Doctor of Philosophy at the **Department of Civil and Environmental Engineering** and was approved on the May 2017 by the members of the **Examination Committee**.

Examination Committee:

Research Supervisor:_____
Petros Komodromos, Associate Professor
Department of Civil and Environmental Engineering, University of Cyprus

Committee Member (Chairman):_____
Dimos C. Charmpis, Associate Professor
Department of Civil and Environmental Engineering, University of Cyprus

Committee Member: _____
Stavros A. Anagnostopoulos, Professor Emeritus
University of Patras, Greece

Committee Member: _____
Marios Phocas, Associate Professor
Department of Architecture, University of Cyprus

Committee Member: _____
Panayiotis Roussis, Assistant Professor
Department of Civil and Environmental Engineering, University of Cyprus

DECLARATION OF DOCTORAL CANDIDATE

The present doctoral dissertation was submitted in partial fulfillment of the requirements for the degree of Doctor of Philosophy of the University of Cyprus. It is a product of original work of my own, unless otherwise mentioned through references, notes, or any other statements.

Eftychia A. Mavronicola

……..

ABSTRACT

Base isolation has proven as an effective design strategy in minimizing structural and non-structural damage under strong ground motions, by introducing flexibility usually at the base of the structure, in order to avoid resonance and reduce excessive seismic loads, accelerations and deformations of the superstructure. However, large relative displacements expected at the isolation level during strong earthquake excitations may lead to structural collisions with the surrounding moat wall and/or adjacent buildings. This research work investigates the consequences of potential pounding incidences on the peak seismic response of base-isolated buildings, initially in two-dimensions and, subsequently, in three-dimensions.

In the conducted analyses, the superstructures are simulated as linear elastic multi-degree of freedom systems with shear-type behavior, while nonlinear modeling is used for the behavior of the seismic isolation system, which consists of lead-rubber bearings. Specifically, the effect of using different nonlinear models for the lead-rubber bearings on the overall peak structural response under unobstructed conditions is initially examined, as that might influence the pounding analysis. Through relevant parametric studies, the influence of the characteristics of the structure and the isolators, and the characteristics of the imposed earthquake excitations on the responses of interest, using either the bilinear inelastic model or the more accurate Bouc-Wen model, are comparatively assessed.

Regarding the modeling of structural impacts in two-dimensions, penalty methods are employed to assess the impact forces that should be applied on the colliding structures. Various impact models have been proposed and used in the scientific literature and, thus, the effect of using each of those impact models on the overall peak response during collisions is examined. In particular, considering collisions of base-isolated buildings against the surrounding moat wall, the effects of impact modeling characteristics under different values of gap sizes and isolator's characteristics, as well as different impact parameters, subjected to multiple near-fault excitations are assessed.

Subsequently, a computational methodology that enables the spatial investigation of collisions, while considering the arbitrary location of contact points and the geometry at the vicinity of impact, is utilized in order to study structural impact in three-dimensions. Nonlinear time-history analyses of base-isolated buildings pounding either with the moat wall or with adjacent fixed-supported buildings are carried out, to investigate the circumstances under which spatial pounding may occur and assess the effect of some important parameters on the corresponding peak structural response. Such parameters include the arbitrary direction of the ground motion with respect to the principal construction axes of the simulated structures.

Therefore, a large number of parametric studies is performed on the structural models using selected pairs of recorded horizontal ground-motion orthogonal components. Records are rotated to various horizontal angles of incidence with respect to the building's structural axes in the range of 0 to 360 degrees. The influence of other parameters, such as the separation distance between the building and the adjacent structures, the geometrical arrangements of the structures, and accidental mass eccentricity at the superstructure, are also studied. The conducted parametric analyses indicate that the peak seismic response is significantly influenced by the directionality of the ground motion. Therefore, the seismic performance of structures should ideally be assessed examining the peak structural response, while bidirectional ground motions are imposed at various incident angles. Finally, the parametric analyses indicate that the effects of impact are more severe for structures with mass eccentricities, in which case the estimation of the critical incidence angle becomes more laborious.

ΠΕΡΙΛΗΨΗ

Η σεισμική μόνωση αποτελεί μια καινοτόμο μέθοδο αντισεισμικής προστασίας, μέσω της οποίας επιτυγχάνεται η μείωση των ζημιών τόσο στη φέρουσα κατασκευή όσο και στα μη-φέροντα στοιχεία, με την εισαγωγή οριζόντιας ευκαμψίας, συνήθως στη βάση της κατασκευής. Με τον τρόπο αυτό, αποφεύγονται φαινόμενα συντονισμού και περιορίζονται τα σεισμικά φορτία, οι επιταχύνσεις και οι σχετικές παραμορφώσεις της ανωδομής. Ωστόσο, οι μεγάλες σχετικές μετακινήσεις που αναμένονται στο επίπεδο της σεισμικής μόνωσης, κατά τη διάρκεια ισχυρών σεισμικών διεγέρσεων, μπορεί να οδηγήσουν σε συγκρούσεις με τον περιμετρικό τοίχο ή/και με γειτονικές κατασκευές. Η παρούσα εργασία εξετάζει διεξοδικά την επίδραση φαινομένων συγκρούσεων στην μέγιστη σεισμική απόκριση σεισμικά μονωμένων κτιρίων, αρχικά στο επίπεδο (2- διαστάσεις), και στη συνέχεια στο χώρο (3-διαστάσεις).

Στις πραγματοποιθείσες αναλύσεις, η ανωδομή της κατασκευής προσομοιώνεται ως γραμμικό ελαστικό πολυβάθμιο σύστημα με συμπεριφορά διατμητικού προβόλου, ενώ για την προσομοίωση της συμπεριφοράς του συστήματος σεισμικής μόνωσης, η οποία αποτελείται από ελαστομερικά συστήματα με πυρήνα μολύβδου, χρησιμοποιούνται μη γραμμικά ανελαστικά μοντέλα. Συγκεκριμένα, η επιρροή της εφαρμογής διαφορετικών ανελαστικών μοντέλων για την προσομοίωση της συμπεριφοράς των μονωτήρων μελετάται αρχικά, ώστε να εξεταστεί πως οι εν λόγω παραδοχές επηρεάζουν τον υπολογισμό της μέγιστης απόκρισης του κτιρίου. Με τη διενέργεια παραμετρικών αναλύσεων, ποσοτικοποιείται μεταξύ άλλων η επίδραση των χαρακτηριστικών του συστήματος μόνωσης και της κατασκευής όταν χρησιμοποιείται το διγραμμικό μοντέλο, αντί το ακριβέστερο μη γραμμικό μοντέλο Bouc-Wen.

Σε σχέση με τη μοντελοποίηση δομικών συγκρούσεων σε 2-διαστάσεις, εφαρμόζονται μέθοδοι ποινής, μέσω των οποίων υπολογίζονται οι δυνάμεις κρούσεις που ασκούνται στις κατασκευές. Η επιρροή της επιλογής από τις διάφορες παραλλαγές τέτοιων μοντέλων κρούσης που προτείνονται και χρησιμοποιούνται στην επιστημονική βιβλιογραφία, στη μέγιστη απόκριση συνεπεία δομικών συγκρούσεων εξετάζεται παραμετρικά. Ειδικότερα, λαμβάνοντας υπόψη συγκρούσεις σεισμικά μονωμένων κτιρίων στη βάση υπό ισχυρές σεισμικές διεγέρσεις κοντινού πεδίου, διερευνάται σε κάθε περίπτωση η επιρροή της χρήσης διαφορετικών μοντέλων κρούσης, μεταβάλλοντας παραμέτρους μεταξύ των οποίων περιλαμβάνεται το πλάτος του διαθέσιμου διάκενου, τα χαρακτηριστικά των σεισμικών μονωτήρων και οι παράμετροι κρούσης.

Στη συνέχεια, εφαρμόζεται μια νέα μεθοδολογία που επιτρέπει τη χωρική μελέτη του φαινομένου κρούσης, σε 3-διαστάσεις, λαμβάνοντας υπόψη το γεγονός ότι δεν είναι εκ των προτέρων γνωστή η θέση των σημείων επαφής και η γεωμετρία στην περιοχή της κρούσης. Διενεργούνται μη-γραμμικές αναλύσεις χρονοϊστορίας σεισμικά μονωμένων κτιρίων που συγκρούονται είτε με τον περιμετρικό τοίχο στη βάση τους είτε και με γειτονικά πολυώροφα κτίρια, ώστε να επισημανθούν οι συνθήκες κατά τις οποίες δυνατό να παρατηρηθούν φαινόμενα συγκρούσεων και να μελετηθούν οι παράμετροι που επηρεάζουν τα μέγιστα μεγέθη απόκρισης. Μεταξύ των παραμέτρων που εξετάζονται, περιλαμβάνεται και η γωνία καταγραφής των δύο οριζοντίων συνιστωσών της διέγερσης.

Ως εκ τούτου, διενεργείται ένας μεγάλος αριθμός παραμετρικών αναλύσεων δομικών μοντέλων χρησιμοποιώντας ζεύγη οριζόντων συνιστωσών ισχυρών σεισμικών διεγέρσεων. Οι άξονες καταγραφής της διέγερσης στρέφονται ως προς τους άξονες αναφοράς του κτιρίου από 0° έως 360°. Επίσης, μελετάται εκτενώς η επιρροή παραμέτρων, όπως το διαθέσιμο διάκενου μεταξύ του σεισμικά μονωμένου κτιρίου και των γειτονικών κατασκευών, της γεωμετρικής χωροθέτησης των κατασκευών καθώς και τυχηματικής εκκεντρότητας μάζας. Οι διενεργηθείσες αναλύσεις καταδεικνύουν ότι η μέγιστη σεισμική απόκριση των κατασκευών επηρεάζεται σημαντικά από τη διεύθυνση της διέγερσης. Συνεπώς, η μελέτη της σεισμικής συμπεριφοράς τους θα έπρεπε να

μελετάται υπό διαξονική διέγερση που επιβάλλεται σε διάφορες διευθύνσεις. Γενικά, η παραμετρική διερεύνηση καταδεικνύει ότι οι επιπτώσεις των συγκρούσεων είναι πιο κρίσιμες για κατασκευές με τυχηματικές εκκεντρότητες μάζας, ενώ σε τέτοιες περιπτώσεις ο προσδιορισμός της κρίσιμης διεύθυνσης της σεισμικής διέγερσης, καθίσταται πιο σύνθετος.

ACKNOWLEDGMENTS

This thesis relates to more than one decade of work at University of Cyprus and specifically within the Archimedes Laboratory. My experience at UCY has been nothing short of amazing. I have been given unique opportunities that helped me develop academically and personally. This includes working at "Archimedes" for over ten years, starting as an undergraduate research assistant in the summer of 2005. This thesis is the result of many experiences I have encountered at UCY from dozens of remarkable individuals who I also wish to acknowledge.

First and foremost, I wish to thank my advisor, Professor Petros Komodromos. He has been supportive since the days I began working in the lab as an undergraduate. I owe him very special thanks because it was through his encouragement and motivation that I continued my studies at the graduate level. It was under his support that I developed a focus and became interested in computer-aided engineering and seismic isolation technology. Petros has supported me academically and emotionally through the rough road to finish this thesis, becoming more of a mentor and a friend, than a professor.

For this dissertation, I would like to thank my thesis advisory committee members: Professor Marios C. Phocas and Professor Dimos Charmpis for their time, interest, and helpful comments. I would also like to thank the other two members of my examination committee, Professor Emeritus Stavros A. Anagnostopoulos and Professor Panayiotis Roussis, for their time and comments towards the improvement of my thesis.

I gratefully acknowledge the funding sources that made my Ph.D. studies possible. My work was supported by Civil and Environmental Engineering Department and the Graduate School of the University of Cyprus.

The members of the lab have contributed immensely to my personal and professional time at UCY. The group has been a source of friendships as well as good advice and collaboration. I am especially grateful for the group of original Archimedes group members: Panayiotis Polycarpou, Loizos Papaloizou, Ernestos Sarris and George Pamboris. Panayiotis deserves a special mention, as some parts of this thesis were developed through a collaborative effort. I thoroughly enjoyed working with him and acknowledge his guidance and contribution in software development, as well as his constructive comments. Other past and present group members that I have had the pleasure to work with or alongside of are graduate students Varnavas Varnava and Panayiotis Andreou.

Furthermore, I would like to thank everybody with whom I have shared experiences during my student and professional life. From the people who played a significant role in my life, to those who with the gift of their company made my days more enjoyable and fulfilling. The warm support of my special friends Charalambos Kartakoulis and Flora Kavoura enabled me to complete this thesis; even been abroad. Also, I want to express my love to Iacovos – Nicoletta – Demos, Marina – Athena – Kimonas, Theodoros – Daphne – Christos-Myron, Stasinos – Michelle, Christos – Anna, Maria and Antonia. They have been a constant source of happiness for me and I really feel very fortunate to have met them. Without their support, my ambitions could hardly have been realized.

I would also like to acknowledge the teachers, professors, and other professionals who either directly inspired me in some way. Some of those that deserve special recognition include my primary school teachers: Christos and Sotiroulla Vouria and my colleague Dr Dinos Poullis.

I cannot finish without saying how grateful I am to my parents, Nitsa and Andreas, for supporting me and encouraging me to take my own decisions and to do my best in all aspects of life, as well as to Chara – Savvas and Hercules for their support and for helping me in fulfilling my goals. Athena's and Averkios's unconditional love was a tremendous source of joy, though these years.

I could not have reached this point in my life without the care, unending support and guidance of my beloved George, whose drive and energy have kept me going all these years. I can never thank him enough for always being there as my best friend and mentor.

Eftychia A. Mavronicola
University of Cyprus
May 2017

στους δασκάλους μου εκείνους·
που αποτέλεσαν πηγή γνώσης, έμπνευσης, και οράματος

TABLE OF CONTENTS

LIST OF FIGURES

LIST OF TABLES

CHAPTER 1 INTRODUCTION

1.1 Seismic Isolation Overview

Advances in structural engineering and earthquake resistant design have significantly reduced human casualties during strong earthquakes. However, severe earthquakes are still among the most destructive phenomena of nature and pose a serious threat to humanity, especially in the developing countries, in which most buildings have been built without satisfying sufficient earthquake resistant requirements. The conventional earthquake-resistant design philosophy primarily aims to protect human lives, by providing sufficient ductility to avoid brittle structural collapses in order to avoid, or at least minimize, human casualties. In the case of very strong earthquakes, conventional earthquake-resistant seismic codes and provisions give emphasis on the avoidance of structural collapse, although damage after a severe earthquake can be extensive, requiring sometimes unavoidable demolishing of heavily damaged structures.

The limitation of conventional earthquake-resistance design to prevent damage has motivated the use of innovate passive and active control approaches. Seismic isolation can be used alternatively to prevent the disastrous consequences of severe earthquake excitations, usually by shifting the fundamental eigenperiods of relatively stiff buildings outside the dangerous for resonance range, in order to reduce the induced seismic loads (Figure 1.1). The elongation of the fundamental eigenperiod of a building is achieved by incorporating flexibility, in the form of seismic isolators, which are usually, installed at the base of the building.

The superstructure of a seismically isolated building is oscillating as an almost rigid body, while the interstory deflections and the absolute floor accelerations are substantially decreased so that potential damage of structural and non-structural components, as well as contents of the building, can be avoided (Higashino and Okamoto, 2006; Komodromos, 2000; Naeim and Kelly, 1999; Skinner *et al.*, 1993). Lateral deformations are confined at the seismic isolation level, where seismic isolators are specifically designed to be capable of accommodating cycles of large strains during earthquake excitations (Figure 1.2).

Therefore, an energy dissipation mechanism must be provided at the isolation level and a sufficiently wide clearance must be ensured around a base-isolated building in order to avoid potential structural pounding with the surrounding moat wall or adjacent structures during severe earthquakes (Mahmoud and Jankowski, 2010; Masroor and Mosqueda, 2013b; Polycarpou and Komodromos, 2010b, 2011).

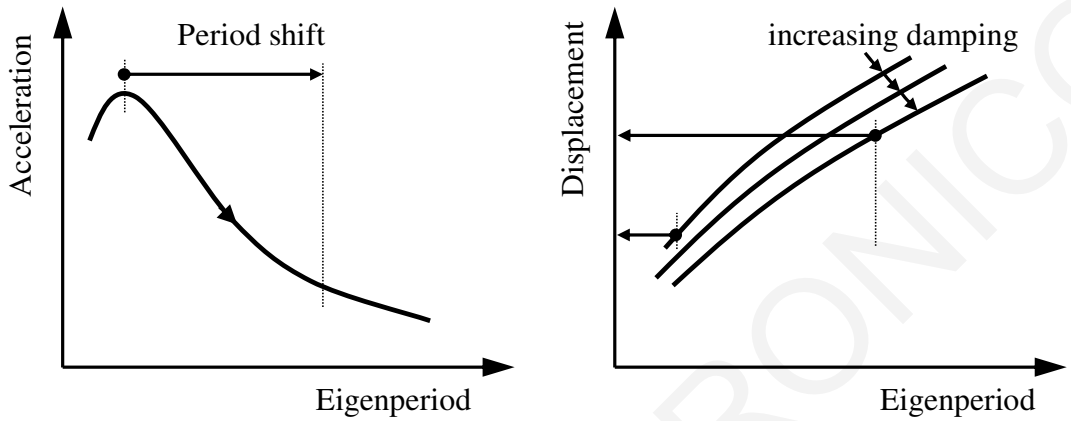

Figure 1.1 Idealized acceleration and displacement response spectrum.

Seismic isolation offers certain advantages when used in important and critical structures for which the disruption of their operations should be prevented, particularly after a severe earthquake, such as command-centers, hospitals, telecommunication centers, etc. Seismic isolation is utilized in both new and existing structures of all types: residential buildings, bridges and viaducts, civil and industrial buildings, cultural heritage (monumental buildings, museums, ceilings of archaeological excavations, museum display cases and unique masterpieces) and industrial components and installations (Basu *et al.*, 2014; Martelli *et al.*, 2012). During the last few decades, seismic isolation has been established as an appealing method for retrofitting and seismic upgrading of existing structures since it requires only minor structural modifications to a building, which are limited at the foundation level, so that the retrofitted structures maintain their original characteristics. Also, seismic isolation is considered a viable strategy for protecting safety-related nuclear structures from the effects of moderate to severe earthquake shaking (Whittaker *et al.*, 2014).

The development and usage of passive control technologies, such as seismic isolation, has been facilitated by the progress in earthquake engineering and technical seismology, advances in computing and innovations in the development and manufacturing of dependable seismic isolators. Various reliable seismic isolation systems have been developed. The most commonly used categories of seismic isolation systems are the *elastomeric bearings* and the *sliding systems*. In general, a seismic isolation system should

provide a mechanism to reduce the induced seismic loads to levels that cannot cause damage, adequate initial horizontal stiffness under minor horizontal loads, such as wind loads, sufficient stiffness in the vertical direction to avoid excessive vertical oscillations and an energy dissipation mechanism to reduce the expected, due to the inserted flexibility, large relative displacements at the isolation level.

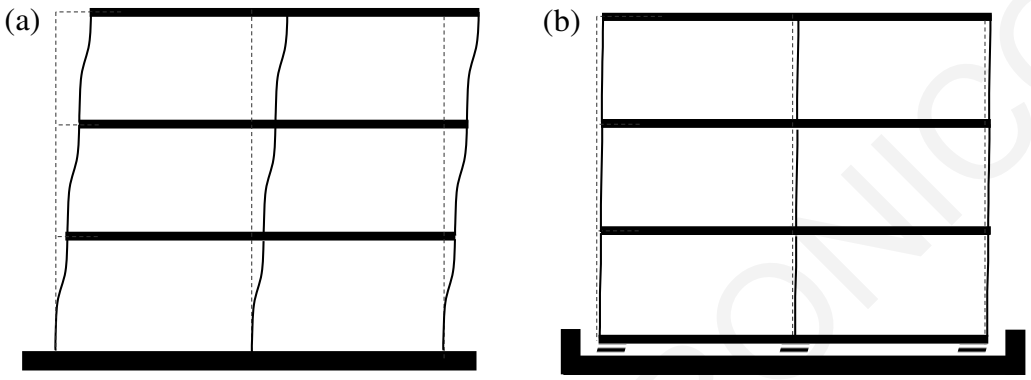

Figure 1.2 Response during an earthquake of: (a) fixed-supported and (b) base-isolated buildings.

Elastomeric bearings (Figure 1.3) provide horizontal flexibility to shift the fundamental eigenperiod of a building outside the dangerous for resonance range, whereas sliding isolation systems prevent, by sliding, the transferring of shear forces above certain magnitudes to the superstructure. In addition, an energy dissipation mechanism must be provided at the level of the seismic isolation system, in order to suppress the expected large relative displacements at that level. This is very important, since it reduces the necessary width of the seismic gap that is required around a seismically isolated building, as well as the probability to experience structural collisions during very strong earthquakes (Komodromos *et al.*, 2007).

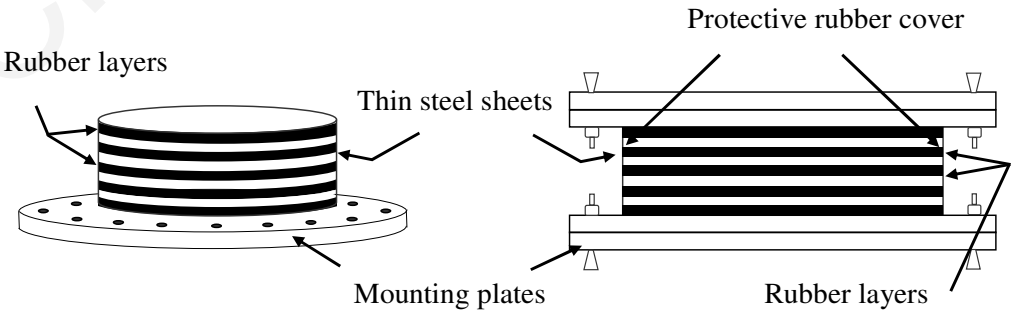

Figure 1.3 Low-damping natural/synthetic rubber bearings.

The additional energy dissipation mechanism can be provided either from auxiliary energy dissipation devices or inherently from the bearings, for example with the

incorporation of lead cores (Figure 1.4) or with the usage of high damping rubber compounds. In addition, a seismic isolation system should provide a mechanism to restore the seismically isolated structure to its original position after the end of a strong earthquake excitation, thus avoiding permanent relative displacements at the isolation level.

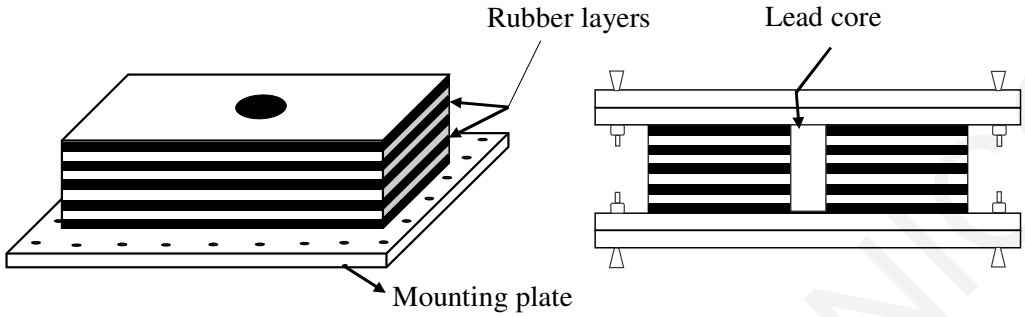

Figure 1.4 Lead Rubber Bearings (LRBs).

The idea of utilizing sliding to seismically isolate a structure has emerged as an effective vibration control approach that may incorporate limitation of the transmitted shear forces to the superstructure, energy dissipation and a restoring mechanism in one unit, as shown in Figure 1.5. Some sliding systems perform very well under a variety of severe earthquake loadings and are quite effective in reducing the large levels of the superstructure's acceleration without inducing large base displacements. However, most currently available systems, such as the Pure Friction System and the Friction Pendulum System, may have some practical limitations when the input excitation level is significantly different from its design level (Pranesh and Sinha, 2000).

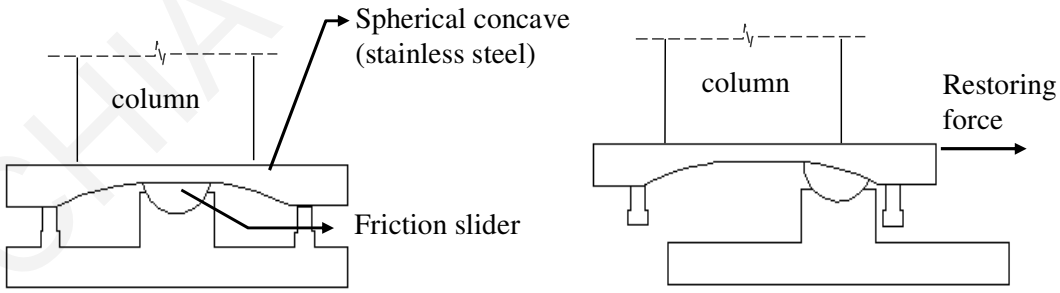

Figure 1.5 Sliding Friction Pendulum System (FPS).

The response of a sliding system does not vary with the frequency content of the earthquake ground motion. In addition, a sliding system is less sensitive to the effects of torsion coupling in asymmetric base-isolated buildings. The variable friction force of some sliding systems makes them effective in controlling the structural response under earthquakes with a broad range of intensities. However, the shear force that can be transmitted to the superstructure depends on the coefficient of friction, which may depend

on the relative velocities of the superstructure and its weight. In addition, the coefficient of friction may change after the experience of strong earthquakes or due to environmental effects, leading to different levels of shear forces that can be transmitted to the superstructure.

1.2 Motivation and Objectives

Earthquake loading is considered the most significant and possibly the most destructive external load, particularly for low- to medium-rise buildings, in high seismicity regions. Although, seismic isolation is currently accepted as an effective design approach for earthquake resistance structures, seismically isolated buildings are expected to experience large relative displacements at the isolation level during strong excitations, especially during near–fault pulse–like ground motions. The modeling of the isolators may influence the proper examination of potential pounding of a seismically isolated building with the surrounding moat wall and/or surrounding buildings. A sharp bilinear model is often used for capturing the hysteretic behavior of the Lead Rubber Bearings (LRBs), which are among the most commonly used seismic isolation systems, although the actual behavior of the LRBs can be more accurately represented utilizing smoothed plasticity, as captured by the Bouc-Wen model. Motivated by the necessity to assess the accuracy of the two inelastic models that can be used, the thesis first examines the suitability of those models to represent sufficiently well the behavior of seismic isolation systems for multistory seismically isolated buildings. Specifically, the potential inaccuracies of the computed peak seismic response when the sharp bilinear model is employed for modeling the LRBs, instead of the more accurate and smoother Bouc-Wen model, are quantified.

Furthermore, considering the limited research work that has been carried out for structural collisions of seismically isolated buildings, the effects of potential collisions on the dynamic response of seismically isolated structures are investigated, as well as the parameters that may affect the response and in what way. Specifically, a two-dimensional (2D) investigation is carried out in order to understand the consequences of collisions on the effectiveness of seismic isolation, taking into account different impact models and assuming that LRBs are utilized for the seismic isolation.

Some basic effects of structural pounding on the dynamic response of buildings can be identified using simplified 2D simulations. However other factors, which are directly related to the spatial movement of the structures, are inadvertently excluded from 2D simulations. Specifically, both orthogonal seismic components of the excitation in the case

of three-dimensional (3D) simulations may significantly affect the overall response of the building, compared to the corresponding unidirectional excitation in the 2D models. In addition, in 2D simulations involving structural pounding, the impacts are assumed to be normal, ignoring any tangential forces developed due to friction. In real cases of structural collisions, friction phenomena exist during an impact and may significantly affect the torsional vibration of the buildings. Therefore, a recently proposed, simple but very efficient, methodology that enables the 3D dynamic analyses of seismically isolated buildings, is utilized to perform spatial simulations of base-isolated buildings, considering potential pounding with both the surrounding moat wall and adjacent buildings. Such an investigation allows us to better understand how potential pounding may affect the performance of seismically isolated buildings.

1.3 Methodology

Although there are several commercially available software that are capable of modeling seismic isolators and, some of them, structural impact with varying degrees of sophistication, the specific needs of this thesis cannot be served with any of the available general-purpose commercial software. Therefore, one of the initial aims of this work is the development and proper extension of suitable software that will enable the effective and efficient performance of numerical simulations and parametric analyses of seismically isolated structures with impact capabilities. Modern object-oriented design and programming approaches is utilized and the Java programming language and relevant technologies are employed in the development of the software application, considering the significant advantages that these technologies offer. The specially developed software needs to provide the desired flexibility, maintainability and extensibility to fulfill the research needs of this thesis, while also facilitating extensions to accomplish future research directions in this research area.

In particular, the numerical simulations that should be performed to address this research problem require the ability to simultaneously simulate multiple structures, using different isolators' models, as well as impact and structural models, while certain characteristics should be varied, in order to parametrically study the problem. Moreover, the aim of this research effort is to initially study the problem in two-dimensions and then extend the investigation, using a specially developed software, in three-dimensions in order to study torsional and other spatial effects.

More specifically, as the computational demands of 3D dynamic analyses involving impact phenomena are often very high, especially in the case of conducting parametric studies, it is crucial to adopt an efficient methodology and software with simple structural and impact modeling. The required time for a dynamic analysis is significantly reduced, compared to general-purpose structural analysis software, allowing the performance of large numbers of parametric studies that examine the effect of certain variables on the peak response of the simulated buildings in various structural arrangements during earthquake-induced pounding.

1.4 Outline

Some basic components and advantages of seismic isolation together with the most commonly used seismic isolation devices have been introduced in this first chapter. In Chapter 2, the various models that can be used to describe the behavior of LRBs are discussed. A comparative study of the two most commonly used nonlinear models is presented in order to identify the effect of the modeling on the computed peak responses of seismically isolated buildings. In addition, the influence of the characteristics of both the simulated base-isolated buildings and the earthquake excitations on the peak responses, using the sharp bilinear inelastic model, instead of the more accurate and smoother nonlinear model, is presented. The nonlinear behavior of the isolation system and a study on its accuracy are finally discussed.

Chapter 3 refers to the modeling of impacts for the numerical simulation of structural pounding, while the major force-based impact models, from the relevant scientific literature, are discussed. Furthermore, the various values of impact parameters incorporated in previous studies is also discussed.

The case of a seismically isolated building pounding against the moat wall in two-dimensions is investigated in Chapter 4, based on the different formulas provided in the scientific literature. A comparison of the models, by determining the impact parameters and the corresponding peak response quantities, is obtained, aiming to identify how certain structural parameters and earthquake characteristics may affect those peak values. Using the developed software, a large number of simulations of seismically isolated buildings is conducted under various near-fault ground motions. The parametric analyses are performed to assess the various impact models that have been proposed considering the seismic response quantities obtained from the corresponding Kelvin-Voigt model analysis, and determine the effect of the excitation's and the isolator's characteristics.

Chapter 5 describes a recently established methodology that has been implemented in a previously-developed software that has been appropriately extended, and how that is extended in order to accomplish the targets of this thesis. Using the developed custom-made software, the effect of pounding on the inelastic response of base-isolated structures, which are simulated as non-linear 3D multi-degree-of-freedom (MDOF) systems with shear-type behavior for their stories in the horizontal direction, subjected to bidirectional earthquake excitations, is examined.

Specifically in Chapter 6, a series of simulations and parametric studies is conducted, considering potential structural pounding of a base-isolated building with the surrounding moat wall at its base due to an inadequate clearance. Initially, a numerical investigation is performed to identify the discrepancies between the bidirectional coupled model and the simplified independent unidirectional modeling of the isolators. Furthermore, the circumstances under which spatial pounding may occur and the effect of some important parameters on the peak structural response considering pounding incidences are thoroughly investigated. Nonlinear time-history analyses are carried out considering the arbitrary direction of the ground motion with respect to the structural axes of the simulated structures. The influence of the isolator's characteristics, the superstructure stiffness and the separation distance between the building and the retaining walls at its base are also investigated, while considering different geometrical arrangements for the moat walls.

The case of a seismically isolated building pounding against adjacent conventionally fixed-base buildings that are in close proximity, as well as the surrounding moat wall, is investigated in Chapter 7. Initially, a large number of parametric analyses are performed in order to examine, among other parameters, the influence of the incidence angle and frequency content of the imposed ground motion. The various configurations of the seismically isolated buildings, regarding the type, characteristics and location of the adjacent structures are also examined in this chapter.

Finally, Chapter 8 summarizes the main conclusions and contributions of this research work, discusses current limitations and proposes suggestions regarding, potential future research investigations pertinent to structural collisions of seismically isolated buildings.

CHAPTER 2 NONLINEAR MODELING CONSIDERATIONS

2.1 Introduction

Nowadays, seismic isolation is often used in high seismicity areas, aiming to mitigate the detrimental effects of strong earthquakes on structures. This innovative earthquake-resistant design technology aims in preventing structural collapse, ensuring life safety, protecting the structure and its content, and safeguarding the uninterrupted operation of the accommodated equipment, even after a very strong ground excitation.

Among the most commonly used seismic isolators are the Lead Rubber Bearings (LRBs), which are constructed of alternating layers of rubber pads and steel plates bonded together, where one or more lead plugs are vertically inserted (Figure 2.1 (a)), in order to provide a high initial stiffness and a hysteretic energy dissipation mechanism. The elastomeric rubber ensures the necessary restoring force to prevent permanent relative displacements at the isolation level, while the lead plug dissipates energy hysteretically during severe earthquakes, as it is forced by the steel plates to deform inelastically in shear after its yield stress is exceeded (Komodromos, 2000).

Numerous hysteretic models of various complexities have been proposed for the behavior of LRBs (Abe *et al.*, 2004; Fenves *et al.*, 1998; Kikuchi and Aiken, 1997; Nagarajaiah *et al.*, 1991). These models, which include bilinear hysteretic responses, have been widely used in general-purpose structural dynamics programs, as well as other formulations that have been found suitable to represent the observed experimental responses. Recent publications attempt to incorporate the deteriorating hysteretic behavior exhibited by LRB's due to the heating of the lead core (Kalpakidis *et al.*, 2010) into an improved model, which has been employed in research studies (Ozdemir, 2014). Temperature effects on the LRB constitutive responses are not considered in this thesis as its main focus is to quantify any discrepancies that might arise between the usage of the sharp bilinear model and the Bouc-Wen model, which is a smooth inelastic model as described in the following paragraph.

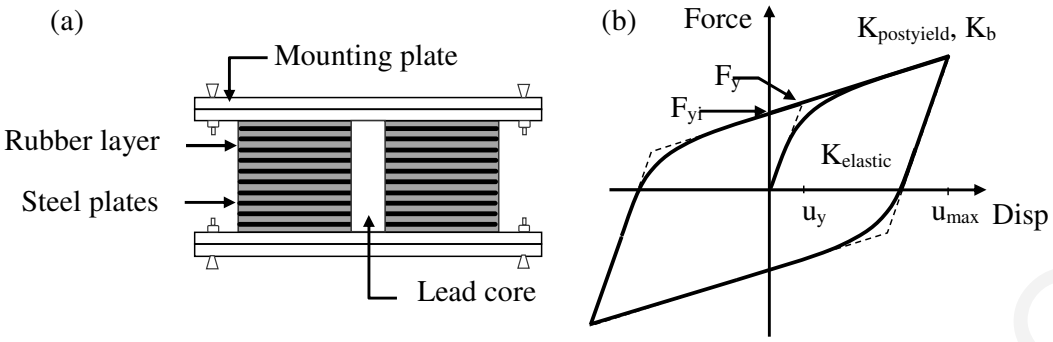

Figure 2.1 (a) Cross-section, and (b) force-displacement behavior of an LRB.

Previous experimental results indicate that the shear force-displacement relationship of the LRBs is highly nonlinear and hysteretic, which can be well represented by the Bouc-Wen model, as shown with a solid line in Figure 2.1(b). In particular, the nonlinear model of Bouc (Bouc, 1967), as extended by Wen (Wen, 1976) and Park *et al.* (Park *et al.*, 1986), is able to capture the hysteretic behavior and the restoring force of the LRBs. This model is commonly employed in the scientific literature (Makris and Black, 2004; Mavronicola and Komodromos, 2012; Nagarajaiah *et al.*, 1991; Varnava and Komodromos, 2013),while Nagarajaiah and Xiaohong (Nagarajaiah and Xiaohong, 2000) have demonstrated that this model provides accurate results in close comparison to experimental data.

Previous studies have examined the influence of the bilinear modeling of the LRBs' behavior and the characteristics of the ground motion on the response of seismically isolated bridges (Hameed *et al.*, 2008; Huang *et al.*, 2000). While preliminary results of the LRBs' characteristics' effect on the response of MDOF structures have been presented (Jangid, 2007; Matsagar and Jangid, 2003; Providakis, 2008), a systematic in-depth investigation on the accuracy of such an approximation is still missing and would be valuable for both research and practical purposes. The comparison presented by Bessasson (Bessason, 1992), considering a single degree-of-freedom (DOF) model, suggested that the bilinear and the Bouc-Wen hysteresis models provide identical results if the controlling parameters for the two models are properly adjusted. However, according to the work of Ramallo *et al.* (Ramallo *et al.*, 2002), the bilinear model causes overestimation of the acceleration levels in base-isolated structures.

Considering that the sharp bilinear model is still in use in the relevant scientific literature, this research investigation aims in identifying any pitfalls that may arise from its usage. The investigation is performed using a software application that has been specifically developed to efficiently and effectively perform large numbers of dynamic simulations and parametric analyses of base-isolated buildings using both the sharp

bilinear and the smooth Bouc-Wen models. Specifically, this chapter provides the comparison of the response of base-isolated buildings using the aforesaid nonlinear hysteresis models under pulse-like excitations, as well as, the assessment of the effect of certain structural parameters and earthquake characteristics on the discrepancies between the usage of those inelastic models. Furthermore, this chapter focuses on quantifying the effect of LRB modeling on the overall peak structural response under seismic excitations, as that might influence the pounding analysis that will follow in later chapters of this thesis. In fact, the accurate estimation of the peak base displacements and other structural deformations will define the possibility of structural impact with the surrounding moat wall or adjacent conventionally fixed-supported buildings.

2.2 Modeling

2.2.1 Modeling of Isolators

It is recognized that an LRB exhibits a nonlinear inelastic response under a seismic action. The Bouc-Wen model provides an analytical relation for the smooth hysteretic behavior and the restoring force of the seismic isolation system, F_b, which can be expressed as a combination of the elastic and plastic force components:

$$F_b = \alpha \frac{F_y}{u_y} u_b + (1-\alpha)\ F_y\ z \tag{2.1}$$

where u_y is the relative displacement corresponding to the yield force F_y; u_b represents the relative displacement at the isolation level; α is the ratio of the post-yield to the pre-yield elastic stiffness and z is a dimensionless hysteretic parameter, with the possible range of z being $|z| \le 1$, which follows a first-order differential equation with zero initial conditions. The internal variable z, which controls the hysteretic behavior, should satisfy the following differential equation:

$$\dot{z} = \frac{1}{u_y}\left\{ A\dot{u}_b - \gamma|\dot{u}_b|\,z\,|z|^{n-1} - \beta\dot{u}_b\,|z|^n \right\} \tag{2.2}$$

where A, β, γ, and n are dimensionless quantities controlling the scale and shape of the hysteresis loop, as shown in Figure 2.2. More precisely, parameters β and γ define the shape of the hysteretic loop (regarding softening or hardening), parameter A controls the restoring force amplitude and the tangent stiffness, while n defines the smoothness of the

transition from an elastic to an inelastic range in the force-deformation relationship. As $n \to \infty$ the hysteresis model is reduced to the bilinear case.

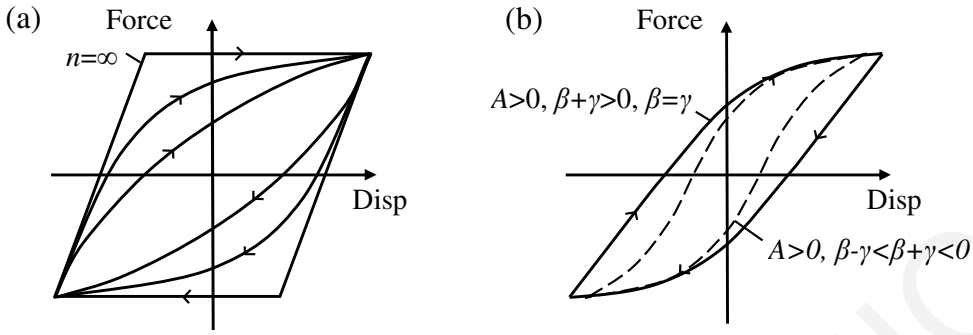

Figure 2.2 (a) The effect of increasing n on the force-displacement hysteretic characteristic for $A>0$, $\beta+\gamma>0$ and $\beta<\gamma$, and (b) example loop shapes for $n=1$ and different combination of A, β, γ.

By adjusting the above parameters, one can construct a variety of restoring forces, such as hardening or softening, narrow or wide-band systems (Sain *et al.*, 1997). It should be mentioned that when $\beta = \gamma = 0$ the relationship between the restoring force and the displacement is linear, while the interaction curve between the forces in the two directions is circular when the conditions $A = 1$ and $\beta + \gamma = 1$ are satisfied (Constantinou *et al.*, 1990; Fenves *et al.*, 1998). When typical parameters for the LRBs, $A = 1$ and $\beta = \gamma = 0.5$ are used, Equation (2.2) simplifies to:

$$\dot{z}(t) = \frac{K_{el}}{F_y}\begin{cases} \dot{u}(t)\left[1 - |z(t)|^n\right] & \text{if } \dot{u}(t)\cdot z > 0 \\ \dot{u}(t) & \text{otherwise} \end{cases} \tag{2.3}$$

The simplified force-displacement behavior of the LRBs can be characterized by three parameters, namely: (i) the characteristic strength, F_{yi}, (ii) the post-yield stiffness, $K_{postyield}$ and (iii) the yield displacement, u_y. In particular, the characteristic strength is defined as the force that is required to yield the lead core, and its normalized version to the weight acting on the isolator, F_{yi}/W_{tot}, is one of the parameters considered in this study. The flexibility of the isolator is quantified through the post-yield stiffness of the system and is generally designed in such a way so as to provide a specific value for the isolation period (Matsagar and Jangid, 2004), T_b, which approximates the post-yield fundamental eigenperiod of the base-isolated building and is expressed as:

$$T_b = 2\pi \sqrt{\frac{m_{tot}}{K_{postyield}}} \tag{2.4}$$

where m_{tot} is the total mass of the base-isolated building. The third parameter evaluated in this study is the yield displacement of the isolation bearings, which typically ranges between 10 to 25 mm, or more. In order to assess the effect of isolator characteristics on the potential inaccuracies of the peak response incorporated through the use of the sharp bilinear model for the LRBs, a significant number of LRBs with varying characteristics are considered. The selection of the specific ranges of the aforementioned parameters included in this study is based on previous research studies that investigated the optimum design parameters for LRBs (Jangid, 2007; Matsagar and Jangid, 2004; Park and Otsuka, 1999).

Several research studies for seismic isolation devices, such as the LRBs, suggested that a bilinear approximation of the shear force-deformation relationship might be adequate (Kampas and Makris, 2012; Kikuchi and Aiken, 1997; Makris and Vassiliou, 2011; Mavronicola and Komodromos, 2011; Robinson, 2011; Skinner *et al.*, 1993; Vassiliou *et al.*, 2013). Following the AASHTO Guide Specifications for Seismic Isolation Design, an LRB can be modelled by a sharp bilinear inelastic model, which is characterized by the yielding of the lead core after a critical shear force is exceeded, as shown with a dashed line in Figure 2.1(b). Prior to the yielding of the lead core, the LRB has an initial stiffness $K_{elastic}$, which is much higher than the post-yield stiffness $K_{postyield}$ that corresponds solely to the stiffness of the rubber.

2.2.2 Structural Modeling

The responses of a 3- and a 5-story base-isolated building are investigated herein. For simplicity, the analyses of the simulated structures are performed in two-dimensions (Figure 2.3), while the superstructure of the seismically isolated building is modelled as a shear-type structure mounted on LRBs with one lateral DOF at each floor and the masses lumped at the floor levels. It is assumed that the superstructure remains linear elastic during the induced earthquake excitations, which is justified by the rationale of using seismic isolation as an earthquake resistant design approach. The seismically isolated MDOF system is subjected to horizontal components of pulse-like excitations. Two typical base-isolated buildings with 340 tons lumped mass at each floor level and a roof mass of 250 tons have been selected and used in the analysis. An additional mass of 340 tons is assumed to be lumped at the seismic isolation level. Each story has a horizontal stiffness of

600 MN/m whereas a viscous damping ratio equal to 2.0% is assumed for the superstructure.

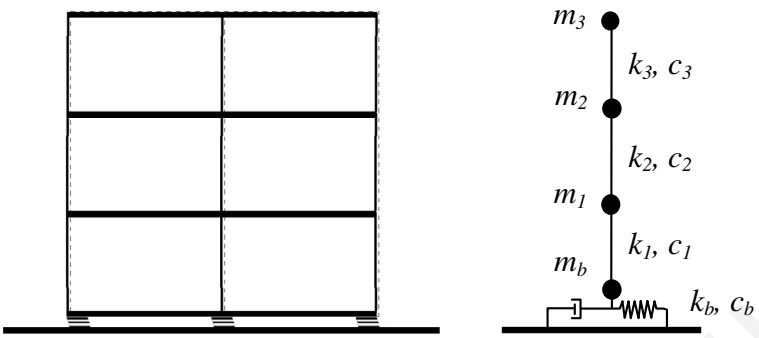

Figure 2.3 Configuration of a 3-story seismically isolated building.

In the case of using a nonlinear model for the isolation system, the energy during the ground excitation is mainly dissipated hysteretically, although some additional viscous damping must be considered, in order to take into account the energy absorbed through other dissipating mechanisms of the isolators, such as friction, heat, sound, etc. This, relatively small amount of dissipated energy, compared to the corresponding hysteretic damping, is taken into account assuming non-classical damping (Polycarpou and Komodromos, 2010b) and a relatively low viscous damping ratio for the seismic isolation system. Therefore, a value of supplemental damping ratio equal to 5.0% has been considered in this study, which is a reasonable assumption considering the purposes of this research investigation.

2.3 Selected Earthquake Records

Previous research studies have shown that seismic ground motions characterized by intense velocities place extreme demands on structures (Makris and Black, 2003; Mavroeidis *et al.*, 2004). A collection of 50 accelerograms of a distinct pulse-type, which correspond to historic records from 18 different seismic events, have been selected from the Pacific Earthquake Engineering Research Center database, Beta Version (PEER Pacific Earthquake Engineering Research Center, 2011). The identification and characterization of records with pulse-like velocities is based on the work of Baker (Baker, 2007), who utilized wavelet transforms. In the present study, further criteria have been imposed for the selection of the 50 ground motions: (a) magnitude of the earthquake $M_w \geq 6.0$; and (b) closest distance to the fault rupture $R_{rup} < 15\,\text{km}$. The selected ground motions have been recorded during the action of the following earthquakes:

1. San Fernando 09/02/1971 (1 Station: Pacoima Dam−upper left abut).
2. Imperial Valley 15/10/1979 (10 Stations: Aeropuerto Mexicali, Agrarias, Brawley Airport, El Centro Array #10, El Centro Array #11, El Centro Array #4, El Centro Array #5, El Centro Array #8, El Centro Differential Array, Holtville Post Office).
3. Irpinia, Italy 23/11/1980 (1 Station: Sturno).
4. Morgan Hill 24/04/1984 (2 Stations: Coyote Lake Dam−southwest abut, Gilroy Array #6).
5. Nahanni, Canada 23/12/1985 (1 Station: Site 2).
6. Palm Springs 08/07/1986 (1 Station: North Palm Springs).
7. Loma Prieta 18/10/1989 (7 Stations: Gilroy – Gavilan Coll., Gilroy Array 1, Gilroy Array 2, Gilroy Array 3, LGPC, Saratoga−Aloha Ave, Saratoga–W Valley Coll).
8. Erzican, Turkey 13/03/1992 (1 Station: Erzincan).
9. Cape Mendocino 25/04/1992 (2 Stations: Cape Mendocino, Petrolia).
10. Landers 28/06/1992 (1 Station: Lucerne).
11. Northridge 17/01/1994 (6 Stations: Jensen Filter Plant Generator, LA Dam, Newhall–West Pico Canyon Rd., Pacoima Dam–downstr, Sylmar Converter Station, Sylmar–Converter Station East).
12. Kobe, Japan 16/01/1995 (2 Stations: KJMA, Takarazuka).
13. Kocaeli, Turkey 17/08/1999 (1 Station: Yarimca).
14. Chi–Chi, Taiwan 20/09/1999 (9 Stations: CHY035, CHY101, TCU049, TCU054, TCU076, TCU082, TCU101, TCU104, TCU136).
15. Duzce, Turkey 12/11/1999 (2 Stations: Bolu, Duzce).
16. Denali, Alaska 03/11/2002 (1 Station: TAPS Pump Station 10).
17. Chi-Chi, Taiwan-03 20/09/1999 (1 Station: TCU076).
18. Chi-Chi, Taiwan-06 25/09/1999 (1 Station: TCU080).

The acceleration and displacement response spectra of the selected ground motions records, considering a viscous damping ratio of 5.0%, are shown in Figure 2.4. The solid black lines in these figures provide the mean values for all selected excitations; whereas the dashed black lines represent the mean plus/minus one standard deviation of the 5.0% damped response spectra.

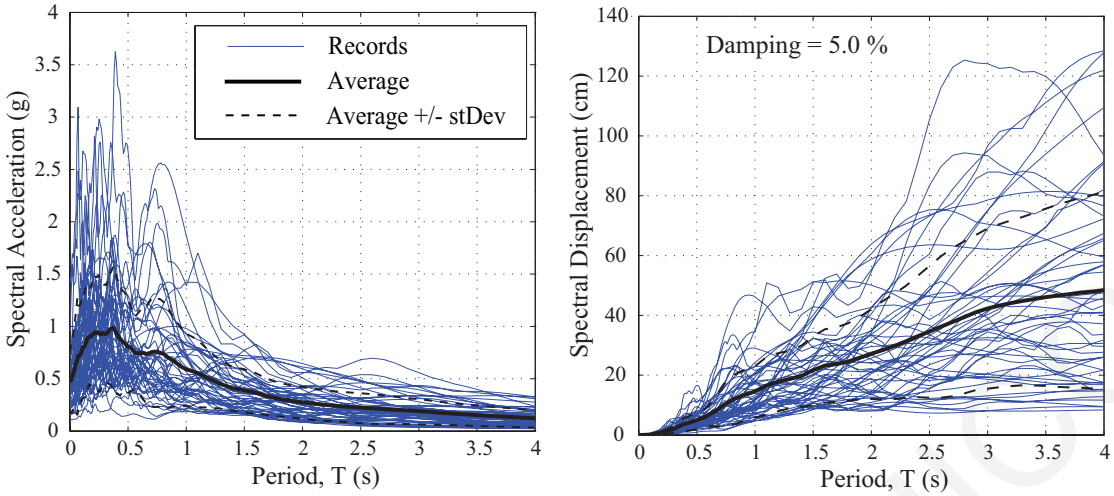

Figure 2.4 Response spectra and average response spectra for the selected pulse-like earthquake excitations.

2.4 Parametric Analyses and Results

In order to effectively perform the necessary numerical simulations for the fulfilment of the aims of this investigation, an extendable software application has been developed, using an object-oriented programming approach and the Java programming language. The specially developed software application enables the efficient performance of dynamic simulations and provides visualization capabilities that can be utilized to effectively monitor the performed numerical simulations and parametric analyses. The software application uses an algorithm that combines the solution of the equations of motion, using the unconditionally stable Newmark's method, and the solution of the differential equation governing the behavior of the Bouc-Wen for the LRBs, based on the implicit Runge-Kutta method with a fixed time-step. Validation of the developed software has been carried out using SAP2000 with very good agreement of the computed results. However, conducting a simulation with SAP2000, or any other general-purpose structural analysis program, requires about 2–3 orders of magnitude more time than what is required to conduct the corresponding analysis with the software specifically developed for this purpose. This significant efficiency of the developed software allows the performance of large numbers of numerical simulations, within a realistic time span.

Dynamic time-history analyses results are presented, in the following subsections for the previously described 3- and 5-story base-isolated buildings under the selected set of pulse-like excitations. The seismic isolation system has been designed so that the fundamental eigenperiods of the seismically isolated 3- and 5-story buildings take values that are sufficiently longer than the fundamental eigenperiods of the corresponding fixed-

supported buildings (0.31 and 0.50 s, respectively). For all performed dynamic analyses, values 1.0, 0.5, 0.5 and 2 are adopted for the Bouc-Wen models' parameters A, β, γ, and n, respectively. These values were proposed in relevant studies (Jin *et al.*, 2008; Nagarajaiah and Xiaohong, 2000; Shrimali and Jangid, 2002), and they are in good accordance with experimental data (Fenves *et al.*, 1998). The time interval for solving the equations of motion has been set to $2 \cdot 10^{-5}$ s.

The peak relative displacements at the isolation level, the peak interstory deflections of all floors and the peak absolute top-floor accelerations are selected as the most important response measures, since they can be directly correlated to the potential damage of a building and its content. In order to quantify the discrepancies of the peak seismic response, while using the two models, the response ratio, which is the ratio of the peak response of the structure utilizing the sharp bilinear (BL) model to the corresponding peak response considering the smooth Bouc-Wen (BW) model, is computed. The response ratio is essentially an index of the accuracy of the sharp bilinear model for the LRBs. Thus, values less than 1.0 indicate underestimation of the peak response, whereas values greater than 1.0 denote overestimation of the peak response values, compared to the peak response obtained while employing the, more accurate, Bouc-Wen model. A statistical analysis of the response ratio for the selected 50 pulse-like ground motions is performed.

In order to distinguish the differences in the response of the 3-story base-isolated building, while using the sharp bilinear and the smooth Bouc-Wen models, indicative curves of the force-displacement nonlinear behavior for the LRBs and the corresponding time-histories of the relative displacements at the isolation level (i.e. base drifts), under the Loma Prieta earthquake, as recorded at the UCSC 16 LGPC Station: Comp FN, are plotted in Figure 2.5. The responses are shown for both nonlinear models, for an isolation period $T_b = 2.0\,\text{s}$, a yield displacement of $u_y = 1.0\,\text{cm}$, and for 3 different values of the normalized characteristic strength F_{yi}/W_{tot}. The peak relative displacements at the isolation level tend to decrease with the increase of the normalized characteristic strength of the isolation system. In general, the computed responses using either of the two models are very similar with only minor discrepancies. The computed responses for the specific earthquake excitation indicate that the base drifts are affected by the characteristics of the seismic isolation system, and can be slightly either underestimated or overestimated, through the usage of the sharp bilinear model for the LRBs. The magnitude and the

occurring time of the base drifts are influenced by the response that precedes the peak, which may justify the variation of the response ratio.

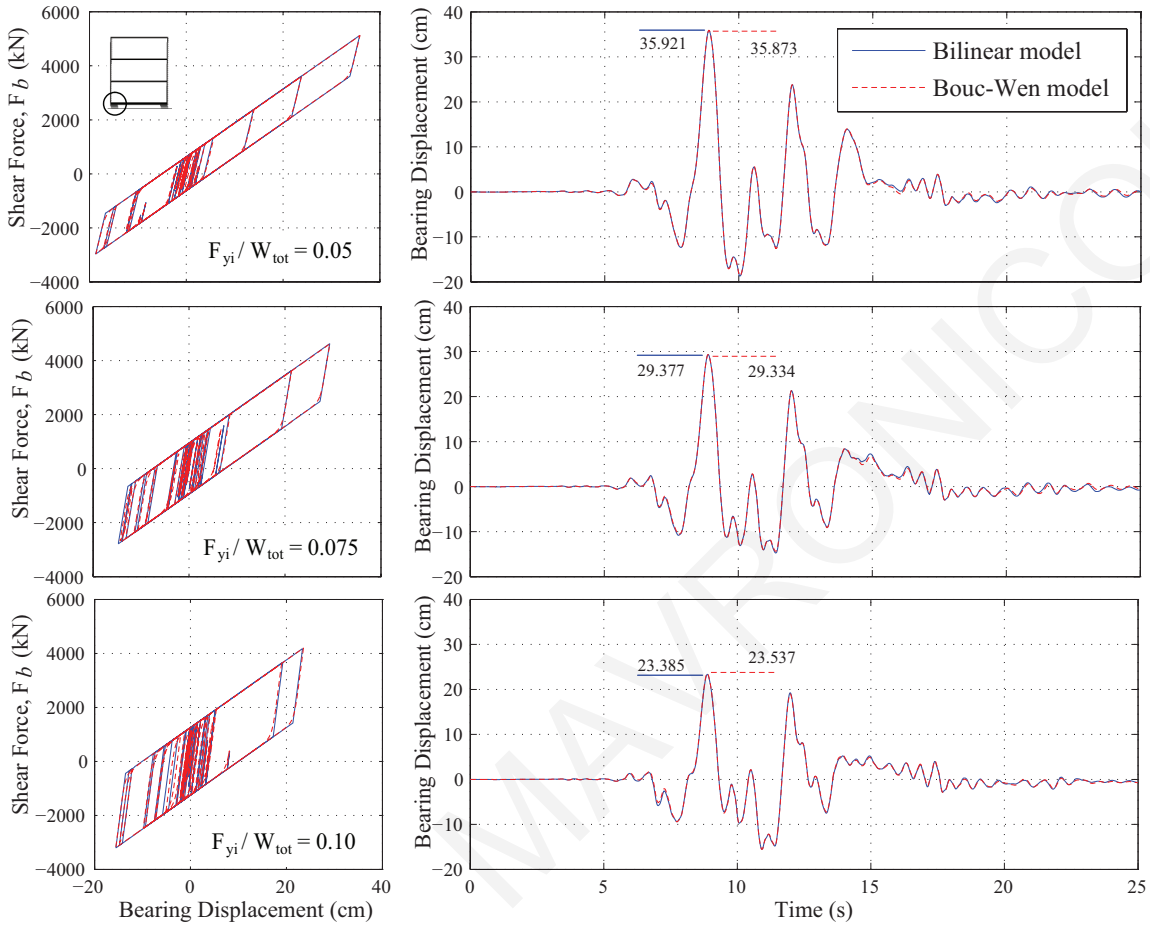

Figure 2.5 Comparison of the force-deformation behavior for both bilinear models and time-variation of base drifts for the 3-story structure under the Loma Prieta earthquake for 3 different values of the normalized characteristic strength ratio.

In Figure 2.6, time-histories of the absolute top-floor acceleration are plotted for both sharp and smooth nonlinear models. In general, the peak top-floor accelerations increase consistently and significantly with the increase of the normalized characteristic strength of the isolation system, and the peak responses computed with the sharp bilinear model are higher than those computed with the more accurate smooth model. Based on the corresponding Fast Fourier Transform (FFT) amplitude spectra shown in the right column of Figure 2.6, it is observed that for both bilinear hysteretic models there is a contribution from a wide range of frequencies to the top-floor accelerations. However, contributions from higher frequencies seem to be more pronounced for the sharp bilinear model. Higher modes of the superstructure are excited for a sharp-cornered hysteretic model, such as the bilinear model, compared to the smoother Bouc-Wen model with the more gradual change of the stiffness upon yielding of the seismic isolation system.

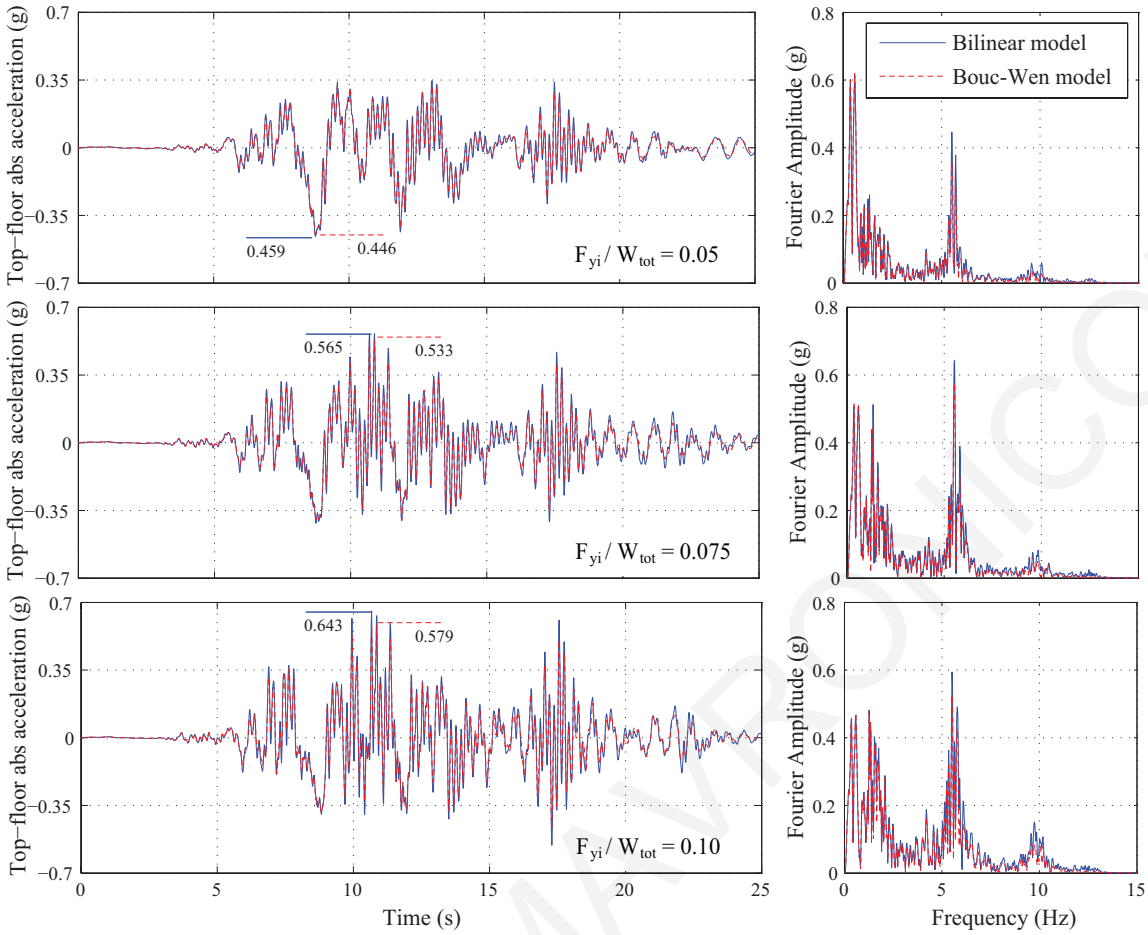

Figure 2.6 Comparison of the time histories and the corresponding FFT spectra of the top-floor acceleration of the 3-story building under the Loma Prieta earthquake ($T_b = 2.0\,\text{s}, u_y = 1.0\,\text{cm}$).

2.4.1 *Effect of Isolators' Yield-Displacement*

A series of parametric studies has been performed with respect to the nonlinear properties of the LRBs, which cover the range of typical seismic isolation systems that are used in practice. For all considered cases, a nonlinear time-history analysis has been performed for the simulated MDOF base-isolated buildings, considering both the sharp and the smooth nonlinear models, under all 50 selected pulse-like ground excitations. In order to understand the influence of the nonlinear hysteretic loop shape on the peak responses of the base-isolated buildings, the variation of the peak response ratio for the 3-story structure is plotted against the yield displacement of the isolators (Figure 2.7). The peak response ratios are provided for three values of the normalized characteristic strength, F_{yi}/W_{tot} (i.e. 0.05, 0.075 and 0.10). The value of the isolation period, T_b, has been kept constant at 2.0 s.

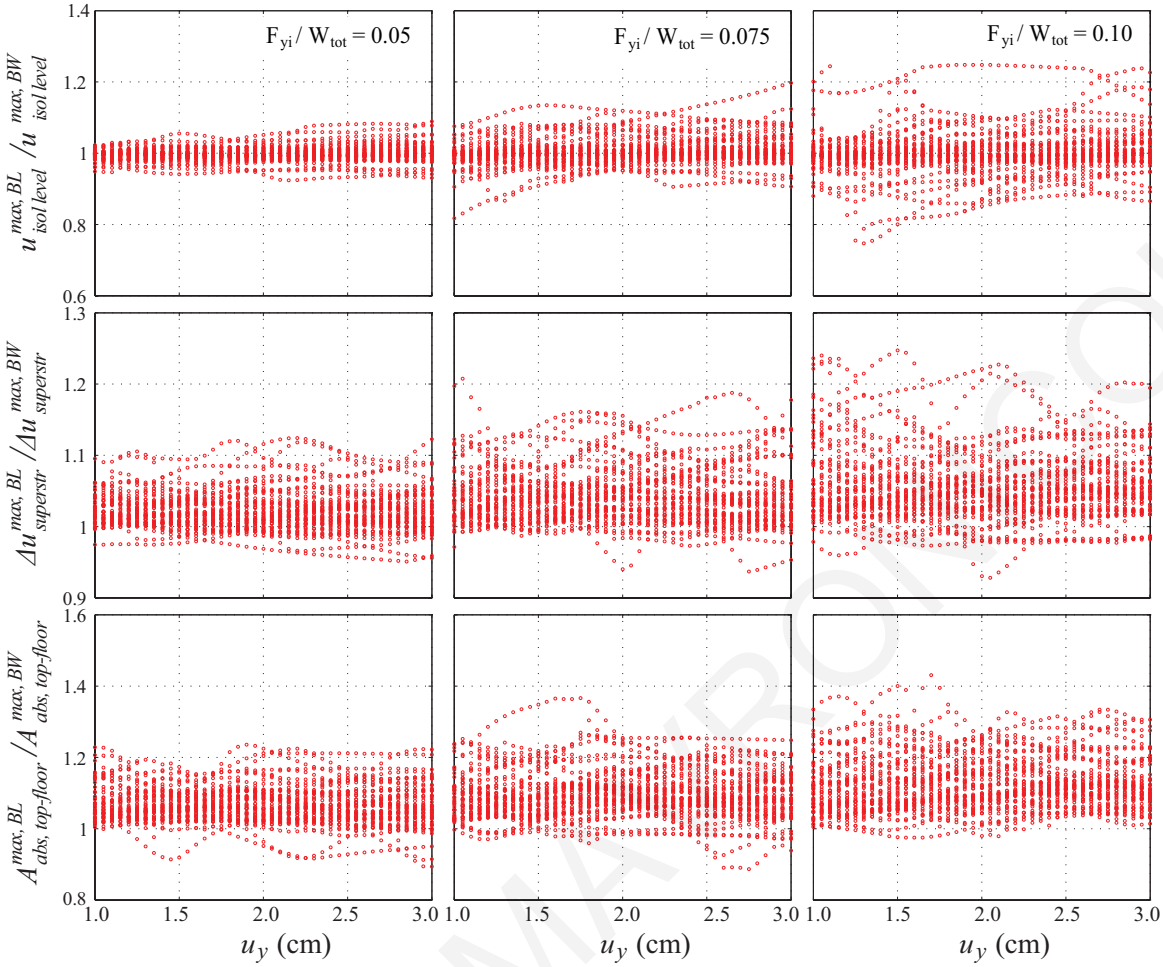

Figure 2.7 Effect of the yield displacement of the isolators on the peak response ratios of the 3-story base-isolated building for different values of $F_{yi}/W_{tot} = 0.05$, 0.075 and 0.10 and $T_b = 2.0\,\mathrm{s}$.

Regarding the discrepancies of the computed peak relative displacements at the isolation level $u_{isol\,level}^{\max,BL}/u_{isol\,level}^{\max,BW}$, no specific pattern can be observed, as the response can be either underestimated or overestimated when the bilinear, instead of the Bouc-Wen, inelastic model is used for the base isolation system. The discrepancies seem to increase with the F_{yi}/W_{tot} ratio. Given that an accurate estimation of the required clearance must be provided around a seismically isolated building in order to avoid any structural pounding during strong earthquakes, it is very important to note that, from a safety point of view, a potential underestimation of the peak relative displacements when the sharp bilinear model is used, should be taken into account using an appropriate safety factor.

On the other hand, the peak response ratios of the superstructure for the peak interstory drifts among all floors $\Delta u_{superstr}^{\max,BL}/\Delta u_{superstr}^{\max,BW}$ and the peak absolute top-floor accelerations $\mathrm{A}_{abs,top-floor}^{\max,BL}/\mathrm{A}_{abs,top-floor}^{\max,BW}$ are, in general, kept at values higher than 1.0, indicating

overestimation of the computed peak response when the bilinear model is used for the LRBs. Furthermore, it is observed that as the normalized characteristic strength of the seismic isolation system increases, the deviation of the peak response ratio is more pronounced. This finding indicates that the response ratio is influenced by the characteristics of both the earthquake excitation and the seismic isolation system, and, therefore, it would be useful to be investigated in a statistical manner, as discussed in subsequent paragraphs.

The various examined cases in this parametric study are presented in Table 2.1. More than 490 different seismic isolation systems have been examined for each building and a total of 98,400 nonlinear time-history analyses have been performed.

Table 2.1 Examined cases in the parametric study.

Parameter	Values	Number of examined cases
Normalized characteristic strength, F_{yi}/W_{tot}	0.05, 0.075, 0.10	3
Yield displacement, u_y	1.0 : 0.05 : 3.0 cm	41
Isolation period, T_b	2.0, 2.5, 3.0 s	3
Exponent n	1.0, 2.0	2
Viscous damping ratio for isolators, ξ_{iso}	2.0, 5.0 %	2
Earthquake ground motion	see Section 2.3	50
Nonlinear hysteretic model for LRB	sharp *vs.* smooth; bilinear model	2
Base-isolated building	3- and 5-story building	2

A graphical representation of the averaged peak response ratios for the 3-story seismically isolated building is presented in Figure 2.8 for three different isolation periods $T_b = 2.0, 2.5$ and 3.0 s. Also, the mean plus/minus one standard deviation of the response ratios are used to describe their main tendency and variability. Despite the highly irregular variations observed in the peak response ratio under each individual ground motion, the average ratios are relatively smooth.

For the examined isolation periods and normalized characteristic strengths, the mean response ratio of the peak relative displacements at the isolation level fluctuate around 1.0, showing a marginal increasing trend with a slight increase with the isolator yield displacement. However, the standard deviations of the response ratio are positively correlated with the normalized characteristic strength, as the response ratios for higher

F_{yi}/W_{tot} ratios show higher standard deviations. The peak response quantities seem to be affected by the characteristics of both the seismic isolators and the selected earthquake excitations. Furthermore, the parametric results indicate that the yield displacement does not considerably influence the average peak responses ratio of the superstructure, which are primarily affected by the post-yield fundamental eigenperiod, the normalized strength of the seismic isolation system and the characteristics of the imposed earthquake excitations.

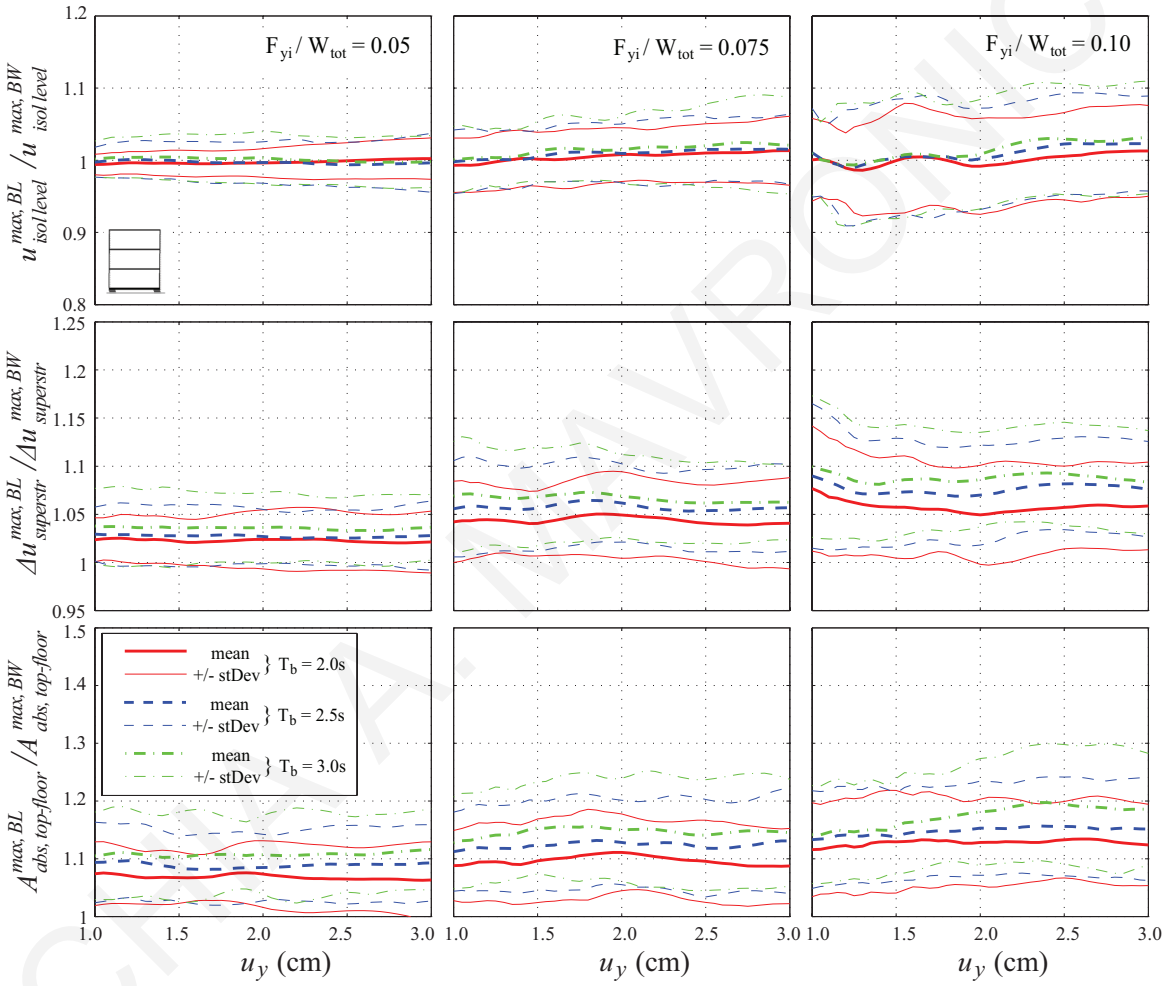

Figure 2.8 Variation of peak response ratios of the 3-story base-isolated building simulated using the sharp *vs.* the smooth bilinear model, for different isolation characteristics.

Furthermore, values of the mean response ratios of the interstory deflections are larger than 1.0, meaning that when the sharp bilinear model is used for LRBs the peak interstory responses are overestimated, and that the overestimation rises with the increase of the normalized characteristic strength. It should also be noted that the mean peak response ratio of the superstructure with an isolation period $T_b = 3.0\,\mathrm{s}$ is consistently higher. In this particular case, the mean $\Delta u_{superstr}^{max,BL}/\Delta u_{superstr}^{max,BW}$ ratio ranges in the vicinity of 1.04 for

$F_{yi}/W_{tot} = 0.05$, while for $F_{yi}/W_{tot} = 0.075$ and $F_{yi}/W_{tot} = 0.10$, the mean peak response ratio increases to approximately 1.07 and 1.09, respectively.

According to the results presented in Figure 2.8 (bottom row), the peak top-floor accelerations are in general overpredicted when the bilinear inelastic model is used, instead of the smoother Bouc-Wen model. As stated before, for sharp bilinear systems, there is an increased contribution of higher eigenfrequencies in the accelerations of the superstructure due to the sudden changes of the stiffness that occur when shifting from the elastic to the post-yield stiffness of the bilinear model. Overall, the average $\mathrm{A}_{abs,top-floor}^{\max,BL}/\mathrm{A}_{abs,top-floor}^{\max,BW}$ ratios and the standard deviation of the response ratio increase with the increase of the F_{yi}/W_{tot} ratio. This tendency is observed for the three investigated isolation periods. In general, the mean peak top-floor absolute acceleration ratio is higher than 1.075 ($F_{yi}/W_{tot} = 0.05$, $T_b = 2.0\,\mathrm{s}$) and reaches values up to about 1.20 ($F_{yi}/W_{tot} = 0.10$, $T_b = 3.0\,\mathrm{s}$), while the mean plus one standard deviation may be as large as about 1.30 for the 3-story base-isolated building.

Similarly-organized results as those presented previously for the 3-story base-isolated building (Figure 2.8), are provided in Figure 2.9 for the 5-story building. A remarkably similar trend is observed for the averaged response ratios as well as for the standard deviations of the ratios in the ranges of the considered seismic isolation system characteristics. Similarly, the deviation of the ` increases with the increase of the F_{yi}/W_{tot} ratio, while in the case of $F_{yi}/W_{tot} = 0.05$, the underestimation of the relative displacements at the isolation level is limited up to 5.0%. These observations, indicate that the usage of the sharp bilinear model may lead to significant overestimation of the peak top-floor acceleration response.

Further to the cases described previously two additional parameters have also been examined. Figure 2.10 shows the averaged peak response ratios of the 3-story base-isolated building while using bilinear models and setting the positive exponential *n*–exponent, which defines the smoothness of the transition from an elastic to an inelastic stiffness in the Bouc-Wen model, equal to 1.0 (first column) for a normalized characteristic strength $F_{yi}/W_{tot} = 10\%$. Comparing the results with those presented previously in the third row of Figure 2.8 for $n = 2.0$, it is observed that the conclusions drawn for the influence of the isolation system characteristics still persist, while the averaged response ratios and the standard deviations of the ratios are kept in higher values. As expected, thanks to the more

gradual change of the stiffness upon yielding of the isolation system $(n=1.0)$ the superstructure response is reduced, and subsequently the response ratios are further increased.

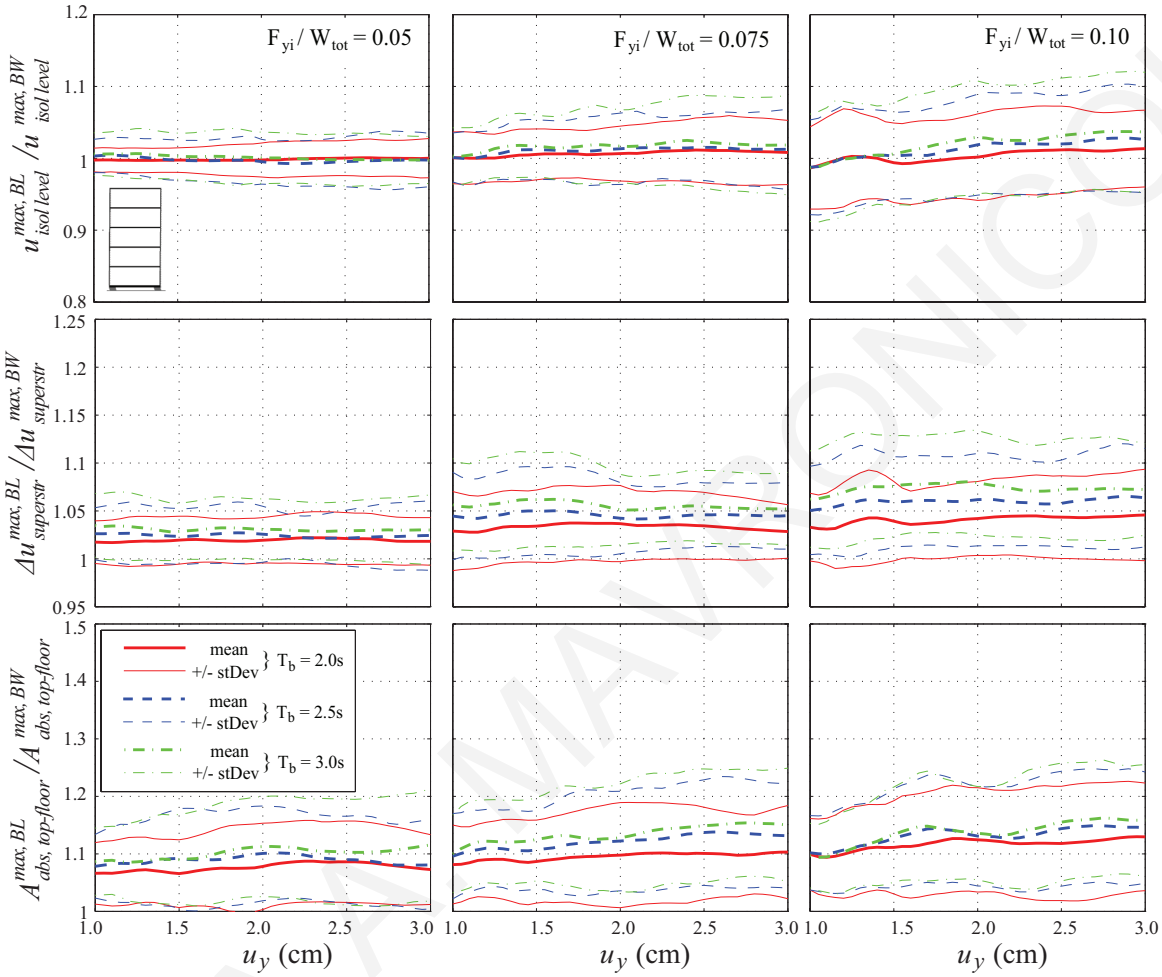

Figure 2.9 Variation of peak response ratios of the 5-story base-isolated building simulated using the nonlinear models, under pulse-like excitations for different isolation characteristics.

Furthermore, in the second column of Figure 2.10 similarly organised results are presented considering that the energy dissipation of the isolation system is restricted to the hysteretic damping that is taken into account explicitly by the nonlinear force-displacement behavior. The results indicate that the isolation damping does not considerably influence the averaged response ratios and the corresponding deviations.

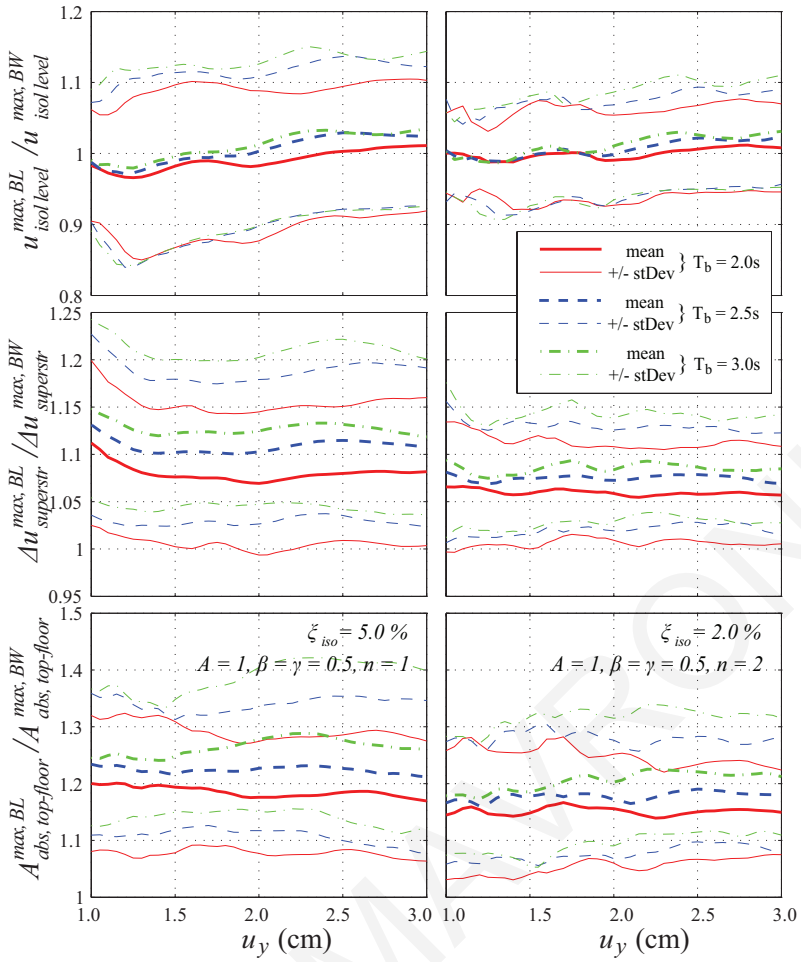

Figure 2.10 Variation of peak response ratios of the 3-story base-isolated building for different supplemental viscous damping ratio, and n exponent for the BW model considering $F_{yi}/W_{tot} = 10\%$.

2.4.2 *Effect of Superstructure's Stiffness*

The scope of this parametric study is to assess the influence of the superstructure's flexibility on the accuracy of modeling the nonlinear LRBs behavior with the sharp bilinear model. Considering that it would be interesting to compare the peak seismic response of the 3- and the 5-story base-isolated buildings, more than 60,000 numerical simulations are conducted by adjusting the interstory stiffness of the superstructure, while using both bilinear models for the seismic isolation system. Figure 2.11 shows the variation of the superstructure response of a 3-story structure against the superstructure's fundamental eigenperiod, T_s. The following values are selected for the seismic isolation characteristics: isolation period, $T_b = 2.0\text{s}$, yield displacement, $u_y = 1.0cm$ and normalized characteristic strength $F_{yi}/W_{tot} = 0.05$.

An examination of the computed responses shows that the peak interstory deflections and the peak absolute top-floor accelerations of the base-isolated structures increase as the fundamental eigenperiod of the superstructure increases. The influence of the superstructure's flexibility on the peak interstory drifts becomes more pronounced as the superstructure's flexibility increases. However, the simulations results indicate that the relative displacements at the isolation level are kept relatively constant as the flexibility of the superstructure is varied. This is in line with the conclusions of previous studies (Kulkarni and Jangid, 2002; Matsagar and Jangid, 2004), who noted that the response of the seismic isolation system regarding the peak base drifts is not really influenced by the flexibility of the superstructure. In contrast, the peak absolute roof accelerations increase when the flexibility of the superstructure increases.

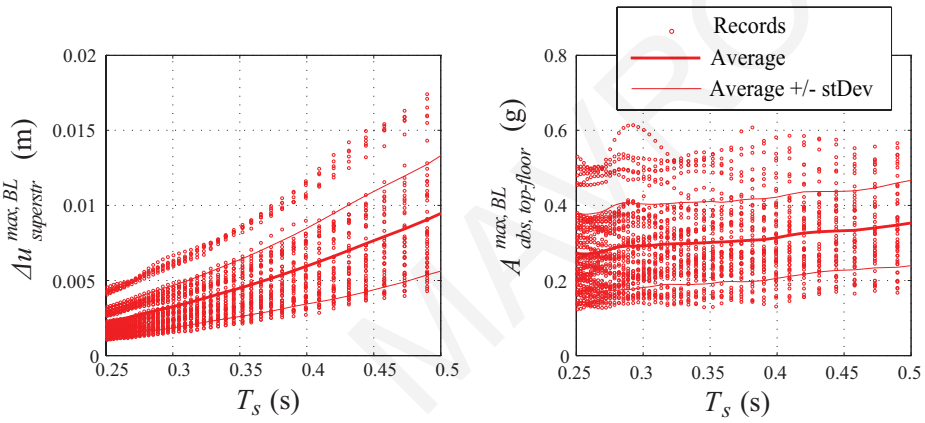

Figure 2.11 Peak response of the interstory deflections, and the absolute top-floor as a function of the superstructure stiffness of the 3-story base-isolated building.

Furthermore, Figure 2.12 provides the variation of the average ratios of the peak relative displacements at the isolation level, interstory deflections and top-floor acceleration for the two buildings against the superstructure's fundamental eigenperiod, T_s for the 50 pulse-like ground motions. The average ratios are shown for three different values of the isolation period based on the post-yield stiffness, yield displacement $u_y = 1.0\,\text{cm}$ and normalized characteristic strength $F_{yi}/W_{tot} = 0.05$. A minor deviation of the mean $u^{\max,BL}_{isol\,level}/u^{\max,BW}_{isol\,level}$ ratios close to 1.0 is observed. Furthermore, the mean peak response ratios of the superstructure are kept to values larger than 1.0.

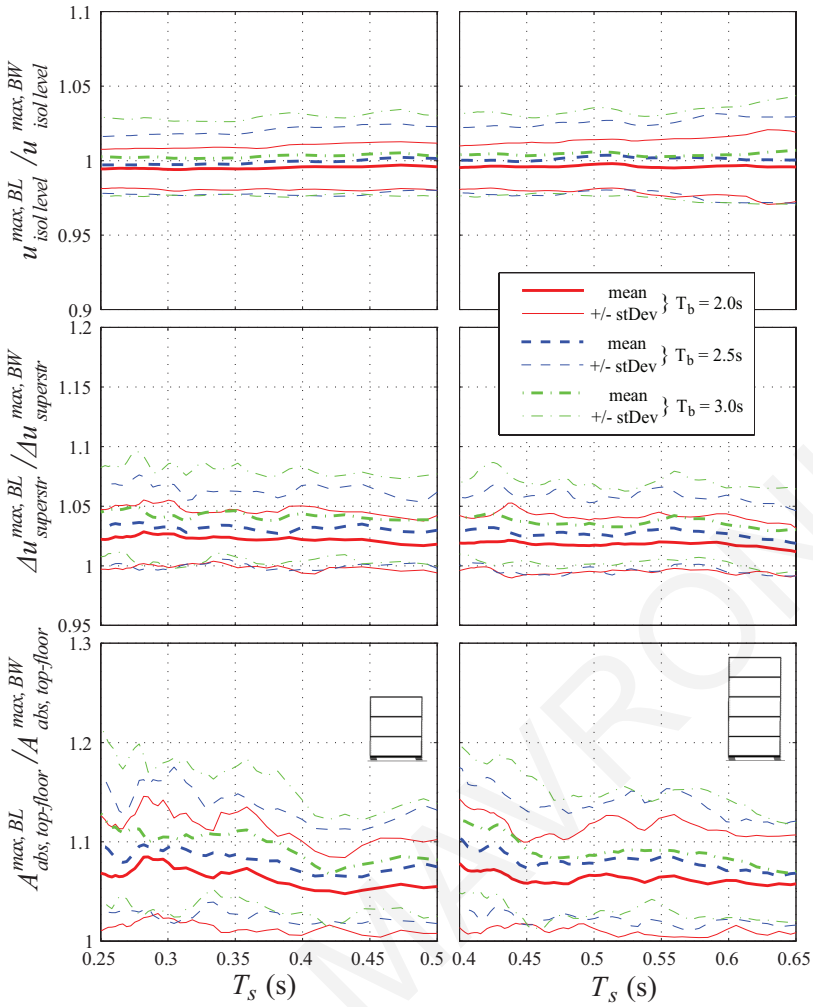

Figure 2.12 Effects of the superstructure's flexibility on the average peak response ratios of the 3- and the 5-story buildings with $F_{yi}/W_{tot} = 5\%$ and $u_y = 1.0\,\text{cm}$.

In general, the mean ratios of the peak interstory drifts among all stories $\Delta u_{superstr}^{\max,BL}/\Delta u_{superstr}^{\max,BW}$ are not significantly influenced by the flexibility of the superstructure and, in general, are kept in the vicinity of 1.04 for $T_b = 3.0\,\text{s}$. On the other hand, as shown by the plots in the bottom row of Figure 2.12, the mean $A_{abs,top-floor}^{\max,BL}/A_{abs,top-floor}^{\max,BW}$ ratio tend to increase with the stiffening of the superstructure. In general, the response ratio deviations are similar for both buildings. The general conclusions drawn in the previous subsection in relation to the effect of the post-yield eigenperiod on the superstructure's response ratios persist. Similar effects of the superstructure's flexibility are exhibited in Figure 2.13, where the corresponding averaged peak response ratios are shown for a normalized characteristic strength $F_{yi}/W_{tot} = 0.10$, for both the 3- and the 5-story buildings.

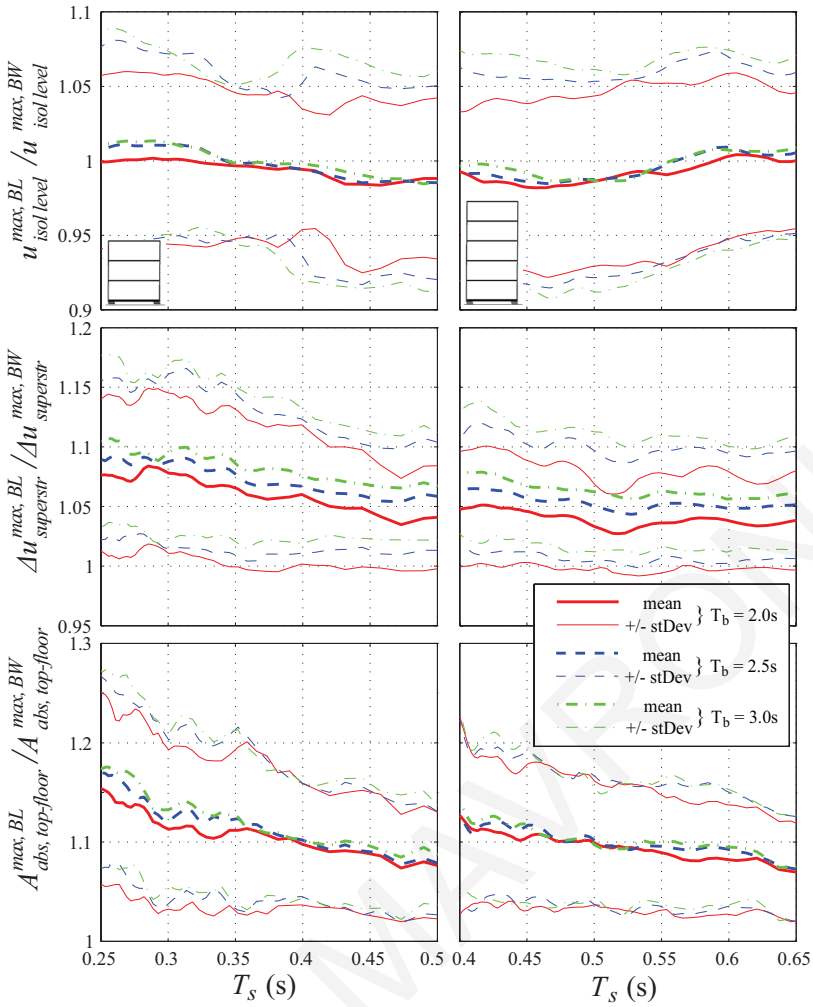

Figure 2.13 Effects of the superstructure's flexibility on the average peak response ratios of the 3- and the 5-story buildings with $F_{yi}/W_{tot} = 0.10$ and $u_y = 1.0\,\text{cm}$.

The average response ratios of the superstructure increase for the higher F_{yi}/W_{tot} ratio. This tendency is observed for all three investigated isolation periods, in line with what has been already presented in previous paragraphs. In general, the mean ratios of the peak interstory drifts are kept higher than 1.06 for $T_b = 3.0\,\text{s}$, while the mean peak top-floor acceleration ratios reach values up to about 1.15, indicating an 15% deviation while using the less accurate bilinear model, in the respective case.

2.5 Conclusions and Remarks

The effect of the modeling of the non-linear behavior of seismic isolation systems with LRBs on the computed peak responses of two typical seismically isolated buildings under pulse-like earthquake excitations has been investigated. The appropriateness of modeling the nonlinear behavior of the LRBs with the sharp bilinear inelastic model has been assessed through simulations and parametric studies performed with specially developed

software. The influence of the characteristics of both simulated base-isolated buildings and the imposed earthquake excitations on the computed peak responses of interest ratios, using the bilinear inelastic model, instead of the more accurate and smoother nonlinear model represented by the Bouc-Wen model with certain parameters, has been quantified through relevant parametric studies.

Considering the dispersion of the ratios of the peak relative displacements at the isolation level, the response can be either underestimated or overestimated when the sharp, instead of the smooth, bilinear model is used for the seismic isolation system. The characteristics of the isolation systems do not considerably influence the mean ratio of the peak relative displacements at the isolation level, which seems to be influenced mostly by the characteristics of the earthquake excitations. However, increasing the ratio of the characteristic strength of the seismic isolation system to the total weight acting on the isolation system increases the standard deviation of the ratios of the peak base drifts. Furthermore, from a design perspective, the slight underestimation of the relative displacements at the isolation level that is introduced due to the usage of the sharp bilinear model is considered to be insignificant when appropriate safety factors are introduced. This finding is vital since there has been a great concern about the possibility of underestimations of the peak relative displacements across the isolators, which may lead to collisions of base-isolated buildings with the surrounding moat walls or adjacent structures during strong near-fault ground motions.

The peak responses of the superstructure, i.e. peak floor accelerations and interstory deflections, are, in general, slightly overestimated when the bilinear model for the LRBs is used, which could be justified by a larger contribution of the higher eigenmodes due to the sudden changes of the stiffness upon yielding of the isolation system, compared to the more accurate and smoother force-displacement curves of the Bouc-Wen model. Moreover, the average ratios of the interstory drifts and the absolute top-floor accelerations appear to increase with an increasing normalized characteristic strength, post-yield fundamental eigenperiods of the LRBs and the stiffening of the superstructure. On the other hand, the mean ratio of the superstructure's peak responses tend to decrease with an increase of the exponent n; in fact as n increases the response approaches that of the bilinear model.

Considering the deviation of the superstructure's peak response, a smooth bilinear model or even more advanced models need to be incorporated to accurately determine the peak responses of base-isolated structures. Therefore, in order to ensure the accurate

capturing of pounding phenomena during seismic excitation simulations, the Bouc-Wen model will be used in the remaining part of this thesis.

CHAPTER 3 STRUCTURAL POUNDING – IMPACT FORCE MODELS

3.1 Overview

Although, seismic isolation can be employed to improve the seismic performance of a structure, the inserted flexibility results in large relative displacements at the isolation level. To accommodate the expected large deformations at the isolation level, a wide seismic gap must be provided as a clearance around a seismically isolated building. This requirement imposes a practical constraint for the utilization of seismic isolation, considering that there are often certain practical restrictions to the size of the available clearance around seismically isolated buildings, especially in cases of retrofitting of existing buildings in densely resided civic centers. Since the width of the available clearance is often limited, a reasonable concern is the risk of structural pounding with the surrounding moat wall or adjacent structures during strong earthquakes (Figure 3.1).

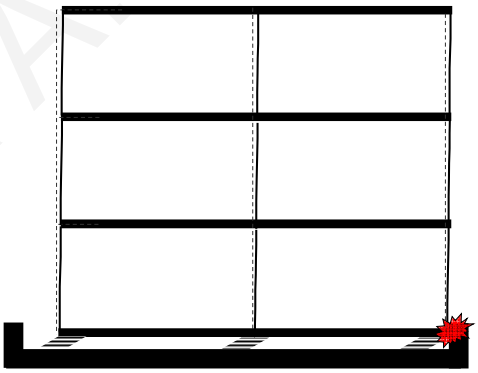

Figure 3.1 Schematic presentation of a base-isolated building pounding laterally with the surrounding moat wall during an earthquake.

Extensive research work on pounding on conventional buildings and civil structures has been carried out (Anagnostopoulos, 1996; Anagnostopoulos and Karamaneas, 2008; Athanassiadou et al., 1994; DesRoches and Muthukumar, 2002; Dimitrakopoulos et al., 2009; Guo et al., 2009; Jankowski et al., 1998; Kim and Shinozuka, 2003; Liolios, 2000; Maison and Kasai, 1990; Papadrakakis et al., 1991; Spiliopoulos and Anagnostopoulos, 1996; Zhu et al., 2002). A fundamental research work of structural pounding of several

single DOF systems in a row using the linear viscoelastic model of collisions had been conducted by Anagnostopoulos (Anagnostopoulos, 1988). In that study, an investigation of the response amplification had been carried out, employing five earthquake motions and multiple problem parameters, such as system configurations, the gap size, the relative sizes of the masses, and the impact element characteristics. The results indicated that in the case of a structure in a row of several adjacent structures, exterior systems tend to suffer more damage due to pounding effects than the interior ones, as for the latter collisions may be even beneficial. Furthermore, it was found that increasing the size of the seismic gap decreases the effects of collisions, while significant differences in the masses of adjacent structures may lead to more pronounced effects of collisions for structures with a smaller mass. Finally, the response amplifications were found to be relatively insensitive to the parameters of the impact elements simulating the collisions.

Structural pounding of seismically isolated buildings during strong earthquakes has begun to be investigated only recently. Maison and Venture (Maison and Venture, 1992) formulated a model to represent the behavior of an existing base-isolated building and employed a linear-elastic contact spring to simulate impacts. Analyses considering impacts of the building with the foundation wall revealed that the peak interstory deflections, shear and accelerations increase significantly due to collisions. Specifically, it was observed that the peak responses could be higher compared to the values of the corresponding fixed-supported structure due to collisions, indicating that such phenomena may negate the benefits of using base isolation.

Tsai (Tsai, 1997) investigated analytically the response of base-isolated buildings considering pounding against the surroundings. In the aforementioned study, the superstructure was modeled as either a viscoelastic or elastoplastic shear beam, while the isolation system was simulated as either linearly elastic or bilinearly elastoplastic. The surroundings were simplified as a spring and a dash-pot separated by a finite seismic gap to the base of the building. The Newmark's implicit integration method was used and the responses of the base-isolated shear beam were computed. The analysis results demonstrated that the sudden change of the stiffness at the base of the shear beam created high acceleration responses, especially if the latter remained elastic. Furthermore, the results indicated that the viscous damping of the moat wall did not seem to affect the beam acceleration during collisions, while the acceleration response was also found to be reduced when the stops exhibit non-linear behavior of which the stiffness is gradually increased with increasing displacement.

Malhotra (Malhotra, 1997), based on wave propagation theory, investigated the effects of impacts on the response of seismically isolated buildings using linear spring elements to simulate pounding with the moat wall. That research study concluded that the base shear force generated by impacts increases with the stiffness of the superstructure of the retaining wall, while it could become higher than the total weight of the seismically isolated building.

Nagarajaiah and Sun (Nagarajaiah and Sun, 2001) evaluated the seismic performance of the base-isolated Fire Command and Control building in Los Angeles during the 1994 Northridge earthquake, and the effect of one-sided pounding with the entry bridge. In particular, the building had experienced impacts with the moat wall as it was observed in the recorded strong motion data. It was reported that the effectiveness of base isolation was reduced due to the unintended occurrence of impact, which increased shear and drift demands. The two-story base-isolated building could not perform as anticipated due to a negligence regarding the securing of the required seismic clearance. The recorded response revealed the presence of sharp acceleration spikes due to the unexpected collisions.

Matsagar and Jangid (Matsagar and Jangid, 2003) examined the seismic response of a multistory seismically isolated building during impact with adjacent structures and the comparative performance of various isolation systems for a shear model of the structure. An impact element in the form of a spring and a dashpot was used to model the adjacent structure. The impact response was studied under the variation of important system parameters, such as gap distance, stiffness of impact element, flexibility of the superstructure and number of stories of the base-isolated building. The results indicated that the peak accelerations of the superstructure increase and the bearing displacements decrease due to impact with an adjacent structure. It was also observed that the acceleration of the superstructure increases with the increase of the isolation gap up to a certain value and then the acceleration decreases with further increase of the gap. The effects of impact were found to be more severe for a building with flexible superstructure, increased number of stories and greater stiffness of the adjacent structure.

Agarwal *et al.* (Agarwal *et al.*, 2007) addressed the upper story pounding of structures in low proximity. More specifically, the case of collisions between two-story buildings that were taken to be either fixed–supported or base–isolated was examined. A variable friction model base isolation was addressed in the model formulation and in this case a Teflon base isolation system was studied. In the numerical simulations, four earthquake records from different sites were used to excite the buildings. The results indicated that the number of

upper story impacts for the fixed-supported and the base-isolated structure configurations and the effect of friction varying base isolation on the number of building impacts is a function of earthquake ground motion characteristics.

Komodromos (Komodromos, 2008) examined the case of collisions of seismically isolated MDOF structures with the surrounding moat wall. Numerical simulations revealed the detrimental effects of structural impacts in the effectiveness of seismic isolation demonstrating that pounding substantially increase floor accelerations, especially as the stiffness of the impact and the flexibility of the isolation system are increased. The peak interstory drifts and the shear forces were also substantially increased during impacts, especially with relatively flexible superstructure. Parametric analyses indicated that the amplification of interstory deflections and floor accelerations with the impact stiffness is more significant up to a certain value of the impact stiffness. Furthermore, potential practical impact mitigation measures were suggested in order to alleviate the sudden changes of the stiffness during impacts and prevent the acceleration peaks due to impacts.

Ye *et al.* (Ye *et al.*, 2009a) investigated the behavior of a base-isolated building during collisions with adjacent structures. In the numerical simulations, the inelasticity of the superstructure was introduced to evaluate the potential damage to the superstructure due to pounding with its adjacent structures. Parametric studies demonstrated that pounding can substantially increase floor accelerations, especially at the ground floor where impacts occur. Higher modes of vibration were excited during collisions, increasing the interstory drifts. Moreover, impact stiffness seems to play a significant role in the acceleration response at the isolation level and the interstory drifts of lower floors of the superstructure. Finally, the numerical results showed that increasing excessively the flexibility of the isolation system, in order to minimize the floor accelerations, may render the base-isolated building more susceptible to pounding under a limited seismic gap.

Komodromos *et al.* (Komodromos *et al.*, 2007), and Polycarpou and Komodromos (Polycarpou and Komodromos, 2010a, 2010b) investigated numerically the effects of collisions with adjacent structures on the response of a typical four-story seismically isolated building during strong earthquakes. The computed peak responses demonstrated that collisions occurring either at the base of the seismically isolated building or at its upper floors are particularly unfavorable for the structure, since they significantly increase the peak absolute floor accelerations and interstory deflections. The parametric analyses showed that even if a sufficient seismic gap is provided, with which pounding with the surrounding moat wall at the base of the building could be avoided, that could not ensure

that the building would not eventually collide with neighboring structures. The results also indicated that the detrimental effects of pounding are more pronounced when the structures adjacent to the seismically isolated building are in resonance with the seismic excitation. Moreover, it was revealed that the values of the impact parameters that were used for the estimation of the impact forces did not significantly affect the peak response of the seismically isolated building during collisions, except on the peak accelerations at the floor of impacts and for the cases of very severe impacts. Finally, the potential utilization of supplemental viscous damping devices was suggested as an effective mitigation measure against the detrimental effects of pounding, with which in some cases the impact could be completely avoided due to the reduction of the maximum horizontal relative displacements of the seismically isolated building.

Polycarpou and Komodromos (Polycarpou and Komodromos, 2011) examined the effectiveness of incorporating rubber shock-absorbers as a potential mitigation measure for pounding of a seismically isolated building with the surrounding moat wall. A series of parametric analyses were performed to assess the effect of the gap size, the earthquake characteristics and the thickness, compressive capacity and damping of the bumpers. The results showed that employing rubber shock-absorbers at impact locations may reduce the maximum impact force, although, the usage of rubber bumpers unavoidably reduces the available clearance around a seismically isolated building and, in some cases, may prove detrimental, depending on various parameters. Both floor accelerations and interstory deflections were reduced when the value of the maximum compressive strain of the rubber bumpers increased, while the flexibility of the moat wall affected significantly the effectiveness of the bumpers.

The Christchurch Women's Hospital was the first base-isolated building in the South Island of New Zealand, opened in 2005. The displacements capacity of the base-isolated building and the superstructure ductility capacity had been designed to meet 2000-year return periods demands. Detailed structural evaluation after the 2010 Darlfield Earthquake and the 2011 Christchurch earthquake revealed that displacement induced damage to non-structural components at the isolation level was also noted at some locations around the perimeter of the building (Gavin and Nigbor, 2012; Gavin and Wilkinson, 2010). In particular, the seismic gap between the Parkside and Women's Hospital, and the moat around the exterior of the building suffered some damage, where coverings impacted the external pit walls (Figure 3.2).

Figure 3.2 Pounding of the base-isolated Christchurch Women's Hospital to the adjacent moat wall (Gavin and Wilkinson, 2010).

Moustafa and Mahmoud (Moustafa and Mahmoud, 2014) assessed the pounding of adjacent fixed-base and base-isolated buildings using input energy, dissipated energy, and damage indices. The relevant results showed that the considered damage indices increased as the separation distance decreased due to the effect of the introduced pounding force. Additionally, adjacent buildings with fixed-bases responded differently from adjacent buildings with isolated-bases. In that study, pounding of fixed-base buildings occurred once or twice compared to base-isolated adjacent buildings in which pounding occurred between one and four times. Furthermore, adjacent fixed-base buildings dissipated more energy hysteretically compared to adjacent base-isolated.

3.2 Numerical Simulation of Impact

In general, the numerical studies that refer to the pounding of either buildings or bridge girders can be categorized in two major groups regarding the methodology of simulating impacts. The first group includes the studies where impact is simulated using the *stereomechanical*, also known as impulse-based, approach (Goldsmith, 1960). These methods assume that the duration of an impact is zero and compute instantaneous changes of the velocities on the basis of the preservation of momentum, taking also into account the coefficient of restitution, which is defined as:

$$e = \frac{v_{1,a} - v_{2,a}}{v_{1,b} - v_{2,b}} \tag{3.1}$$

where v_b and v_a are the velocities before and after collision, respectively, the subscripts 1 and 2 identify the two colliding bodies, and e is the coefficient of restitution (Figure 3.3). As given in Equation (3.1), the coefficient of restitution, which accounts the energy loss during impact, is defined as the ratio of the separation velocities of the two colliding bodies after impact to their approaching velocities. The value of the coefficient of restitution is equal to 0.0 when the collision is fully plastic (i.e. all the energy is dissipated) and

becomes 1.0 when the collision is fully elastic (i.e. no energy is dissipated). The value of e is sensitive to the prior-impact velocity and the material of the colliding elements, as showed by Jankowski (Jankowski, 2010).

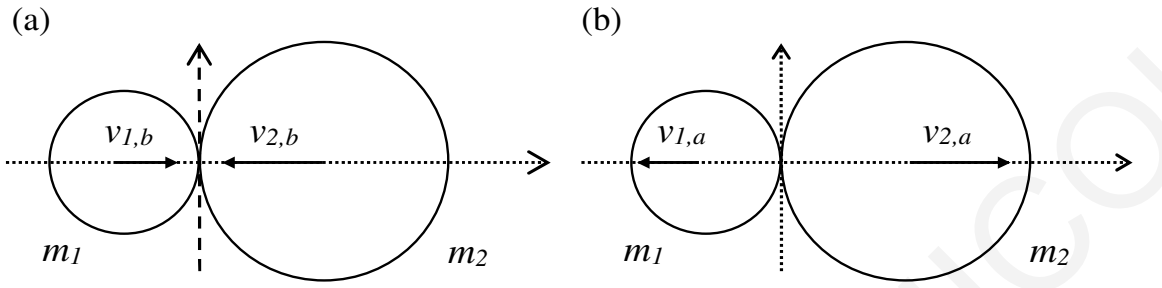

Figure 3.3 Classical theory of impact showing two colliding bodies during (a) the approach and (b) the restitution phase.

The stereomechanical approach of impact is based on the impulse-momentum law for rigid bodies, which specifies the initial and the terminal velocity states, while the duration of impact is neglected. The velocities of the colliding bodies after impact are calculated as:

$$v_{1,a} = v_{1,b} - (1+e)\frac{m_2\left(v_{1,b} - v_{2,b}\right)}{m_1 + m_2}$$
$$v_{2,a} = v_{2,b} - (1+e)\frac{m_1\left(v_{1,b} - v_{2,b}\right)}{m_1 + m_2} \qquad (3.2)$$

The second group involves research studies that use force-based, also known as *penalty*, methods in order to estimate the impact forces that are applied, during impact, on the colliding structures, pushing them apart (Figure 3.4). These methods allow a minor interpenetration between the colliding bodies, which is used together with an impact spring stiffness to assess the impact force at each time-step. In contrast to the impulse-based approach, these methods allow the efficient simulation of dynamic systems with the possibility of multiple impacts occurring at the same time, due to the fact that the computed impact forces are superimposed in the formulation of the corresponding equations of motion. This considerable advantage of the force-based impact models renders them more suitable for simulating pounding of buildings.

The contact element approach is widely used for seismic pounding simulation due to its clear physical meaning and simple algorithmic implementation. This approach uses spring elements, damping elements or their combination to simulate the pounding forces and the energy dissipation during impact. Depending on the force-deformation relationship such

contact elements can be divided into two main categories: linear and nonlinear contact elements.

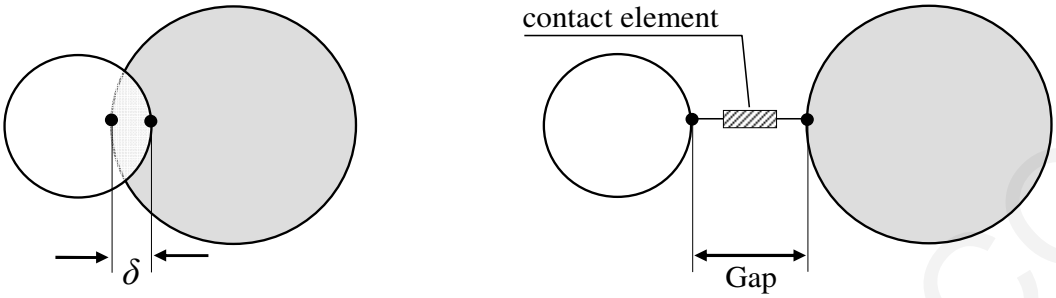

Figure 3.4 Usage of a contact element between impacting bodies.

3.3 Linear Contact Element Models

3.3.1 Linear Elastic Model

A linear impact spring of stiffness k_l can be used to simulate the impact force once the adjacent bodies come into contact. The impact force is expressed as:

$$F_{imp}(t) = k_l \cdot \delta(t) \tag{3.3}$$

where $\delta(t)$ is the penetration depth of the colliding bodies at time t, given in terms of the displacements u_1 and u_2 of the two bodies and the gap between them, as

$$\delta(t) = u_2 - u_1 - gap \tag{3.4}$$

The contact spring is activated as soon as the gap between the adjacent bodies closes and provides the force that is developed during impact as illustrated in Figure 3.5. The linear spring element is the simplest contact element used to model impact and can be easily implemented in commercial software. However, the linear impact spring cannot consider any energy loss during impact. Despite its inability to account for energy dissipation phenomena many researchers have extensively used this model to study pounding between adjacent buildings, primarily due to its simplicity (Filiatrault *et al.*, 1995; Maison and Kasai, 1990; Tsai, 1997).

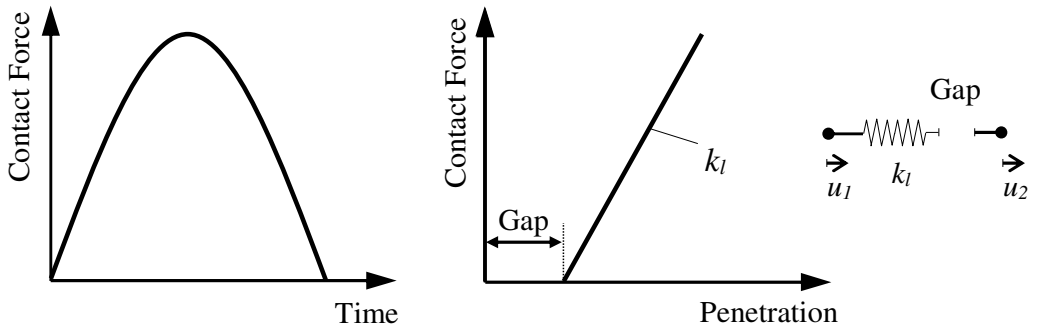

Figure 3.5 Linear spring element.

3.3.2 Kelvin – Voigt Model

The Kelvin-Voigt impact element (i.e. a linear impact spring and an impact damper) is most commonly used to model impact between two colliding structures. Specifically, the Kelvin-Voigt model consists of a linear impact spring and an impact damper acting in parallel to simulate both the deformation and the energy loss during impact. The forces in the contact element may be calculated through the expression:

$$F_{imp}(t) = F_{imp}^{E}(t) + F_{imp}^{D}(t) = k_k \cdot \delta(t) + c_k \cdot \dot{\delta}(t) \tag{3.5}$$

Considering two impacting masses, a relationship may be found between the dashpot constant c_k and the coefficient of restitution e. The resulting mathematical expression for the damping coefficient according to this linear viscoelastic impact model can be assessed as (Anagnostopoulos, 1988, 2004):

$$c_k = 2 \cdot \xi_k \sqrt{k_k \cdot \frac{m_1 \cdot m_2}{m_1 + m_2}} \tag{3.6}$$

where the impact stiffness k_k is determined based on the axial stiffness of the colliding bodies and the impact damping ratio ξ_k is given by the following expression (Anagnostopoulos, 1988, 2004):

$$\xi_k = -\frac{\ln e}{\sqrt{\pi^2 + (\ln e)^2}} \tag{3.7}$$

As it can be seen in Figure 3.6, the viscous impact damper of the Kelvin-Voigt element dissipates energy throughout the approach and restitution phases, but in reality, most of the

energy dissipation takes place during the approach phase and less energy is dissipated during the restitution phase (Goldsmith, 1960).

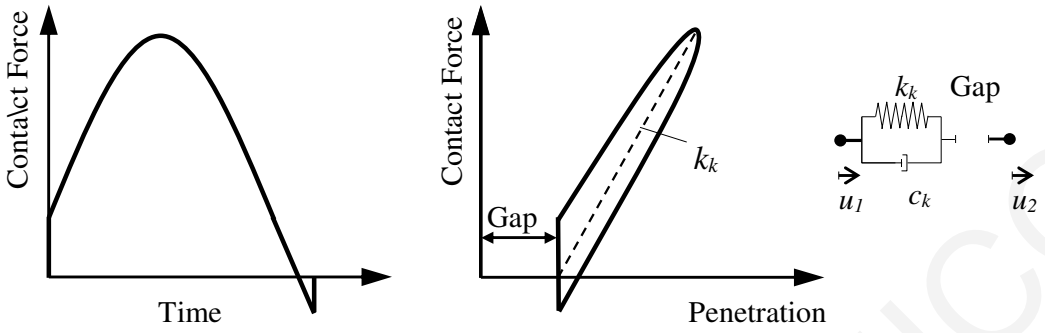

Figure 3.6 Kelvin-Voigt element.

Furthermore, the linear viscoelastic impact model exhibits an initial jump of the impact force values due to the viscous damping term, while the damping force at the end of the restitution phase causes negative (i.e. tensile) forces that pull the colliding bodies together, which is practically unrealistic. However, due to its simplicity, this model has been widely used to simulate structural pounding (Anagnostopoulos and Spiliopoulos, 1992; Jankowski *et al.*, 1998; Zhu *et al.*, 2002).

The tensile forces that arise after the detachment of the colliding bodies can be avoided through a slight adjustment of the linear viscoelastic impact model proposed by Komodromos *et al.* (Komodromos *et al.*, 2007), as shown in Figure 3.7. Furthermore, the modified viscoelastic impact model assumes some permanent plastic deformations, which increase the corresponding available width of the seismic gap. Specifically, the impact force can be computed as:

$$F_{imp}\left(t+\Delta t\right)=\begin{cases} k_k\cdot\delta\left(t\right)+c_k\cdot\dot{\delta}\left(t\right) & \text{for} \quad F_{imp}\left(t\right)\geq 0 \\ 0 & \text{for} \quad F_{imp}\left(t\right)<0 \end{cases} \tag{3.8}$$

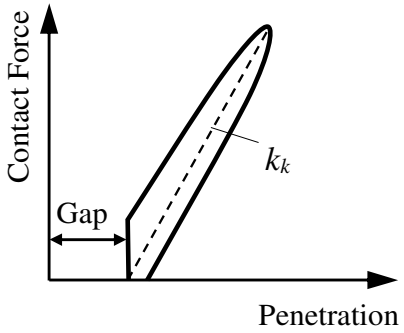

Figure 3.7 Modified Kelvin-Voigt element (Komodromos *et al.*, 2007).

Ye *et al.* (Ye *et al.*, 2009a) proposed a different modification to the Kelvin-Voigt impact model, claiming that the model cannot reasonably reflect the physical nature of structural pounding considering the tensile forces that arise (Figure 3.8). That proposed model preserves the convenience in determining the linear impact spring stiffness, as in the classical Kelvin-Voigt model, while the damping coefficient $\hat{c}_k$ and the damping constant $\hat{\xi}_k$ are given by the following equations:

$$\hat{c}_k(t) = \hat{\xi}_k \cdot \delta(t), \quad \hat{\xi}_k = \frac{3}{2} \cdot \frac{k_k \cdot (1-e)}{e \cdot v_{imp}} \tag{3.9}$$

where v_{imp} is the relative impact velocity of the colliding masses just before impact.

However, other research studies revealed that the utilization of this model does not always avoid the appearance of tensile forces immediately before separation (Mavronicola *et al.*, 2015a; Pant *et al.*, 2010). The existence of tensile forces is possible due to the activation of the dashpot element, which by definition is included in the restitution phase of contact.

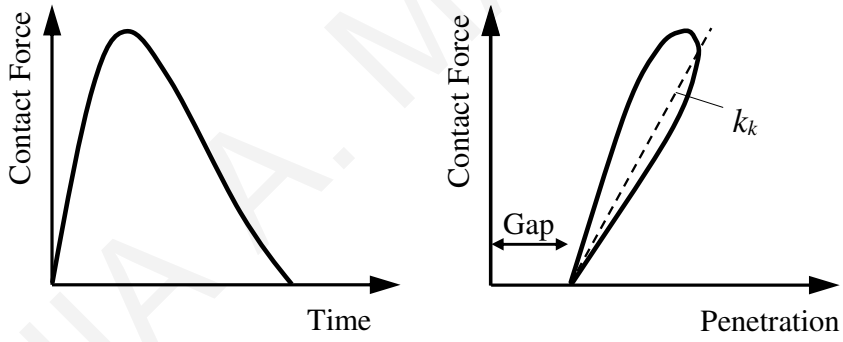

Figure 3.8 Linear viscoelastic impact model (Ye *et al.*, 2009a).

More recently, other variations of the Kelvin-Voigt model have been proposed for modeling the seismic pounding between reinforced concrete moment-resisting frame buildings (Mahmoud and Jankowski, 2011; Pant and Wijeyewickrema, 2012). As shown in Figure 3.9, the main difference from the classical Kelvin-Voigt model lies on the usage of a dashpot, in parallel with the impact spring, that is activated only during the approach phase, in which most of the energy is dissipated.

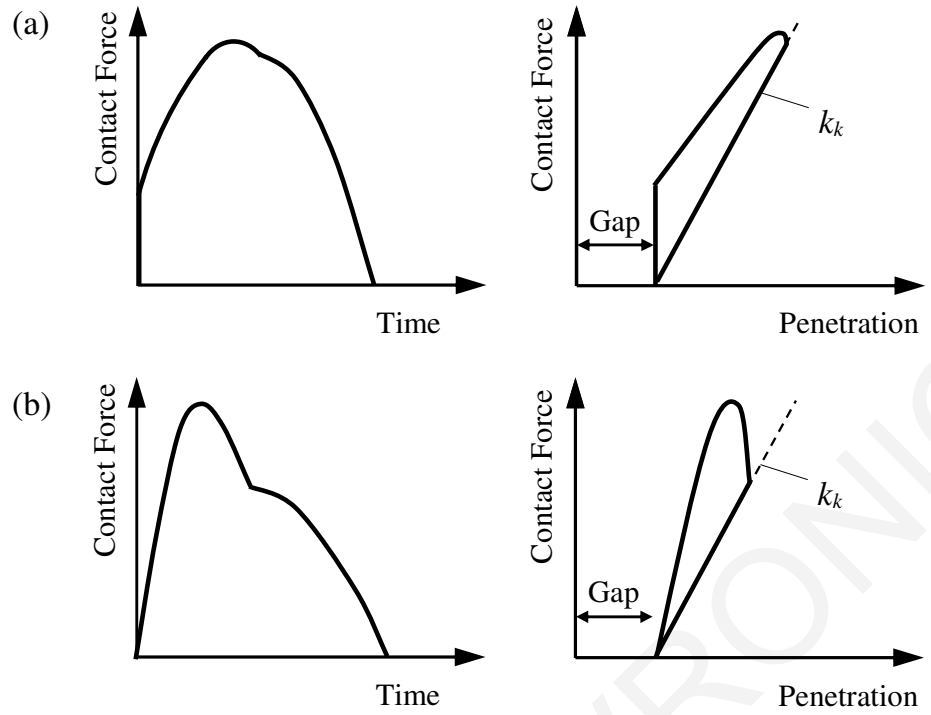

Figure 3.9 Impact models proposed by: (a) Mahmoud and Jankowski, 2011, and (b) Pant and Wijeyewickrema, 2012.

The equation that provides the impact force is written as follows:

$$F_{imp}(t)=\begin{cases} k_k\cdot\delta(t)+\hat{c}_k\cdot\dot{\delta}(t) & \text{for} \quad \delta(t)>0 \text{ and } \dot{\delta}(t)>0 \\ k_k\cdot\delta(t) & \text{for} \quad \delta(t)>0 \text{ and } \dot{\delta}(t)\le 0 \\ 0 & \text{for} \quad \delta(t)\le 0 \end{cases} \tag{3.10}$$

Mahmoud and Jankowski (Jankowski and Mahmoud, 2015; Mahmoud and Jankowski, 2011) proposed the incorporation of a modified viscoelastic impact model, as shown in Figure 3.9(a), in which the damping term is activated only during the approach phase of collision. Two analytical formulas, relating the impact damping ratio ξ_k and the coefficient of restitution e were provided:

$$\xi_k=\frac{1}{\pi}\cdot\frac{1-e^2}{e} \tag{3.11}$$

$$\xi_k=\frac{1-e^2}{e\left(e\left(\pi-2\right)+2\right)} \tag{3.12}$$

Another variation of the Kelvin-Voigt model was proposed by Pant and Wijeyewickrema (Pant and Wijeyewickrema, 2012) to be used for the seismic pounding

between reinforced concrete moment-resisting frame buildings, Figure 3.9(b). The proposed linear viscoelastic model, in which the damping term is activated only during the approach phase of the collision, aims to overcome the negative value of the pounding force that occurs just before separation. The following formulas were proposed for the damping coefficient and the damping ratio, respectively:

$$\hat{c}_k(t) = \hat{\xi}_k \cdot \delta(t), \quad \hat{\xi}_k = \frac{3}{2} \cdot \frac{k_k \cdot (1 - e^2)}{e^2 \cdot v_{imp}} \tag{3.13}$$

Two different approaches have been identified herein for the simulation of the impact damping force. In the Kelvin-Voigt model and the modified versions proposed by Komodromos *et al.* and Mahmoud and Jankowski, the viscous component of the impact force acts at a constant damping coefficient. The effect of a time-dependent damping coefficient has been incorporated in the models of Ye *et al.*, and Pant and Wijeyewickrema, where ξ_k and subsequently c_k become functions of the impact velocity. Figure 3.10 shows the variation of the impact damping ratio as a function of the coefficient of restitution for the five models considered herein.

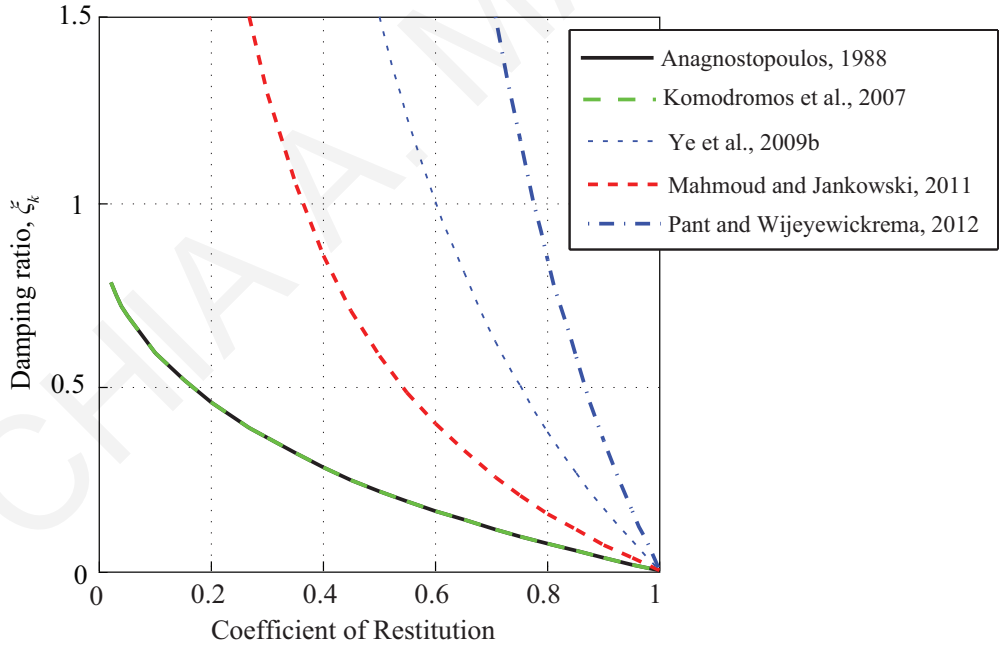

Figure 3.10 Damping ratio *vs.* coefficient of restitution for the five models.

As previously mentioned the models of Ye *et al.*, and Pant and Wijeyewickrema have a velocity dependent damping ratio and, for comparison purposes, only the curves that correspond to a $k_k / v_{imp} = 1$ are considered. It is obvious that each model leads to a significantly different damping ratio that eventually results in variations among the

dissipated energies during impact. Furthermore, it should be noted that in general a $k_k / v_{imp} = 1$ is on the lower end of practical values. Larger values tend to shift the curves of the two models to the right but the general observations persist.

3.4 Non-Linear Contact Element Models

3.4.1 Hertz Model

The Hertz contact law had been originally proposed for static collision of two bodies, in which stresses and deformations near the contact point are described as a function of the geometric and elastic properties of the bodies (Goldsmith, 1960). Although, this approach fails to include energy dissipation during impact, the use of the Hertz model for dynamic impact has been justified on the basis that it appears to predict accurately most of the impact parameters that can be experimentally verified (Goldsmith, 1960). Many researchers have adopted the Hertz contact law to model collisions. The force in the contact element, as shown in Figure 3.11, can be expressed as:

$$F_{imp}(t) = k_h \cdot \delta(t)^n \tag{3.14}$$

The use of the Hertz contact law has an intuitive appeal in modeling pounding, since one would expect the contact area between the colliding structures to increase as the contact force increases, leading to a non-linear stiffness described by the Hertz coefficient, n. The Hertz coefficient is typically taken as $3/2$, which corresponds to the case of a sphere penetrating a flat surface. The nonlinear spring stiffness depends on the material properties of the colliding structures and the contact surface geometry.

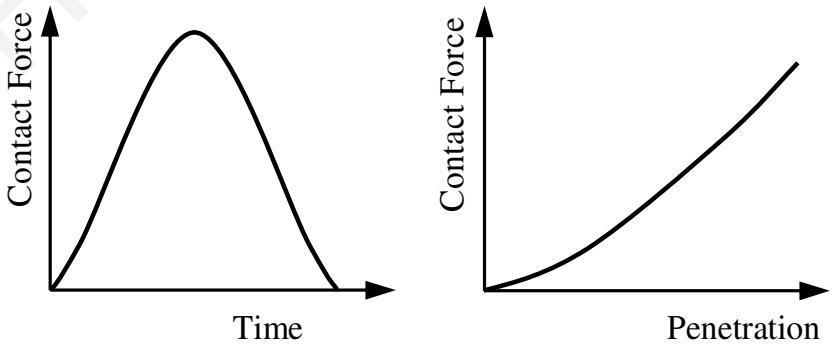

Figure 3.11 Contact force-penetration relationship for the Hertz model.

3.4.2 Nonlinear Viscoelastic Model

Since the Hertzian elastic model cannot represent energy dissipation during contact, Jankowski proposed a nonlinear viscoelastic model in order to include an energy dissipation mechanism (Jankowski, 2005). Therefore, a nonlinear damper parallel to the nonlinear impact spring of stiffness is incorporated in the approaching phase of the contact, while the energy dissipation is omitted during the restitution phase. The impact force *vs.* time curve obtained from this impact model is shown in Figure 3.12.

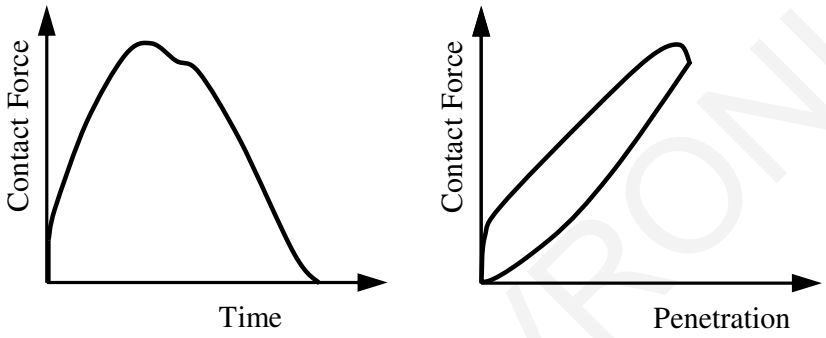

Figure 3.12 The nonlinear viscoelastic impact model.

Thus, the pounding force during impact $F_{imp}(t)$ is expressed as:

$$F_{imp}(t)=\begin{cases} k_h \cdot \delta(t)^{1.5} + \hat{c}_h \cdot \dot{\delta}(t) & \text{for} \quad \dot{\delta}(t) > 0 \\ k_h \cdot \delta(t)^{1.5} & \text{for} \quad \dot{\delta}(t) \le 0 \end{cases} \tag{3.15}$$

where $\delta(t)$ describes the deformation of the colliding structures, $\dot{\delta}(t)$ denotes the relative velocity between them and k_h is the impact stiffness parameter, which depends on material properties and the geometry of the colliding bodies. Furthermore, the impact element's damping coefficient can be obtained at any instant of time from the formula:

$$\hat{c}_h(t) = 2 \cdot \hat{\xi}_h \sqrt{k_h \sqrt{\delta(t)} \frac{m_1 \cdot m_2}{m_1 + m_2}} \tag{3.16}$$

where $\hat{\xi}_h$ denotes an impact damping ratio correlated with the more widely known coefficient of restitution. Incorporating the indentation term to the equation of the damping ratio the discontinuity at the beginning of the approach phase, which is a characteristic of the linear viscoelastic impact model, is theoretically eliminated. The derived analytical formulation relating the impact damping ratio and the coefficient of restitution is given by:

$$\hat{\xi}_h = \frac{9\sqrt{5}}{2} \cdot \frac{1-e^2}{e\left(e\left(9\pi-16\right)+16\right)} \tag{3.17}$$

3.4.3 Hertz Model with Nonlinear Damper

Since the Hertz model does not include the energy dissipation during contact, the Hertz model with nonlinear damping has been developed. More specifically, Muthukumar and DesRoches (Muthukumar and DesRoches, 2006) proposed a nonlinear damper in conjunction with the Hertz model. Figure 3.13 displays the shape of the force-displacement graph of the proposed Hertz Damped model, while the impact force is given by:

$$F_{imp}\left(t\right) = k_h \cdot \delta\left(t\right)^n + c_h\left(t\right) \cdot \dot{\delta}\left(t\right) \tag{3.18}$$

in which the non-linear damping coefficient $c_h\left(t\right)$ is related to the penetration depth, in order to prevent tensile forces after the two bodies separate, and is expressed as:

$$c_h\left(t\right) = \xi_h \cdot \delta\left(t\right)^n \tag{3.19}$$

Therefore, equating the energy loss during stereomechanical impact to the energy dissipated by the damping force, an appropriate expression for the damping constant ξ_h was proposed in terms of the impact stiffness, the coefficient of restitution and the relative approaching velocity of the two colliding bodies, as follows:

$$\xi_h = \frac{3}{4} \cdot \frac{k_h \cdot \left(1-e^2\right)}{v_{imp}} \tag{3.20}$$

Ye *et al.* (Ye *et al.*, 2009b) based on a reexamination of the Hertz contact model with nonlinear damping concluded that the formula used to determine the impact damping ratio, was incorrect for simulating pounding in structural engineering. More specifically, that research work concluded that the coefficient of restitution calculated from the output of the model was different from the predefined value utilized in the computation. The error increased while decreasing the value of the input coefficient. Therefore, a more accurate formula for the damping constant, $\hat{\xi}_h$, was derived, and is shown with a solid line in Figure 3.13.

$$\hat{\xi}_h = \frac{8}{5}\frac{k_h \cdot (1-e)}{e \cdot v_{imp}} \tag{3.21}$$

Similar research work was carried out by Barros *et al.* (Barros *et al.*, 2013), and a new impact model with three springs and dashpot was derived, while a new damping ratio was suggested to calculate the dissipated energy.

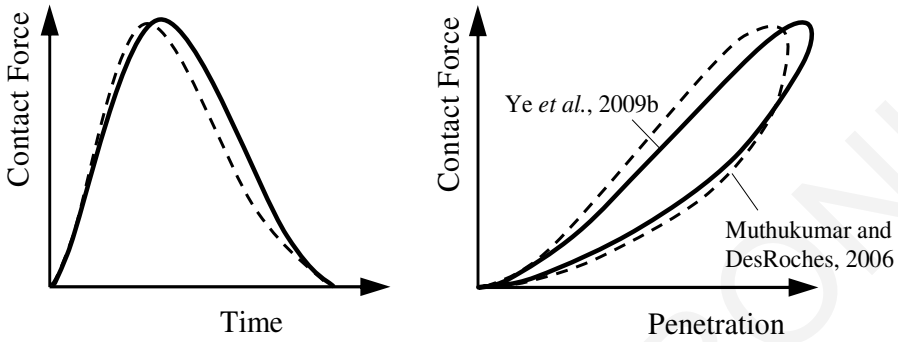

Figure 3.13 Contact force-penetration relationship for Hertzian impact models.

In order to evaluate the values of the previously described models regarding the calculation of the velocities after impact, the computed values of the coefficient of restitution obtained from pounding simulations are compared with the provided values of the coefficient. Two colliding masses and a range of values of the coefficient of restitution are used in order to assess the accuracy of the aforementioned impact models. For each predefined value of the coefficient of restitution, each of the impact models is used to perform an impact simulation, compute the impact velocity after impact and, thus, the corresponding computed value for the coefficient of restitution, e.

Figure 3.14 compares the pre-specified (nominal) and the computed values for the impact models under consideration, which ideally should coincide. The results presented in Figure 3.14 suggest that there is a significant difference between the prespecified coefficient and the one numerically obtained utilizing the corresponding formula proposed by Muthukumar and DesRoches. On the other hand, the results show that the assumption of a direct relationship between the impact velocity and the indentation is reasonable for pre-specified coefficients of restitution larger than 0.5. Considering that for most practical purposes the coefficient of restitution for structural impact varies within the range of 0.5 to 0.75 (Jankowski, 2005), the accuracy of the proposed formulas is satisfactory.

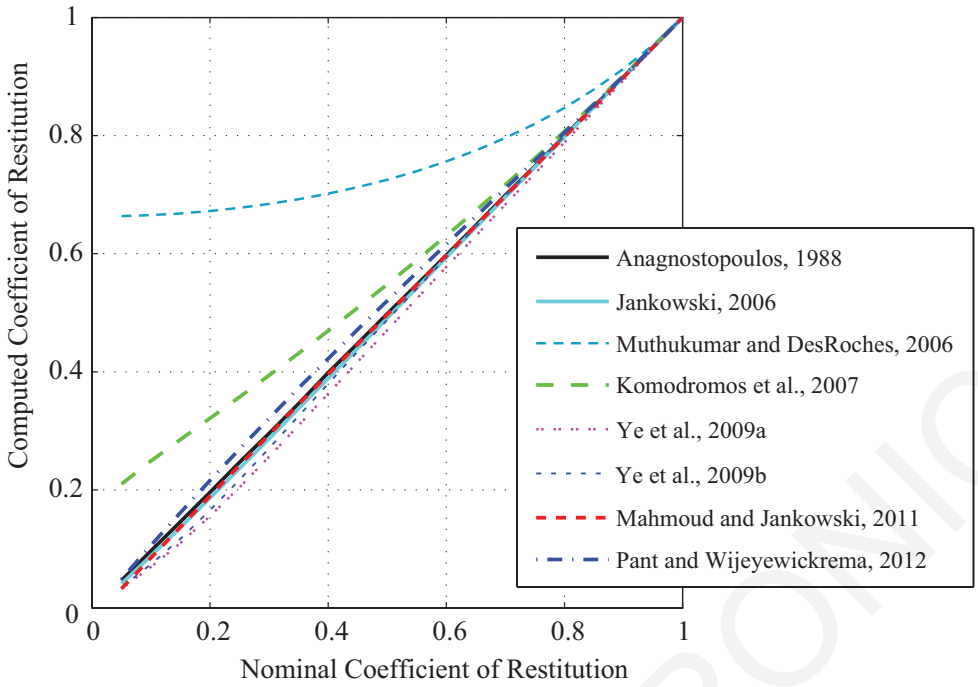

Figure 3.14 Comparison of the pre-specified and numerically computed coefficient of restitution.

3.5 Estimation of the Impact Parameters

3.5.1 Coefficient of Restitution

The energy loss can be expressed in terms of the coefficient of restitution, e. According to the work-energy principle, the coefficient of restitution should be $0 \le e \le 1$. A coefficient of restitution equal to 1 corresponds to a fully elastic impact, while a fully plastic impact is represented by a coefficient equal to 0. The coefficient of restitution depends on many factors, such as the geometry of the bodies in contact, the approach velocity, the material properties and the duration of contact (Goldsmith, 1960).

In case of collision between two different materials, the following formula is used to compute the equivalent coefficient of restitution (Goldsmith 1960):

$$e = \frac{e_1 \cdot E_1 + e_2 \cdot E_2}{E_1 + E_2} \tag{3.22}$$

where e_i, E_i are the coefficient of restitution and modulus of elasticity for material i (where $i = 1, 2$), respectively.

Anagnostopoulos (Anagnostopoulos, 1988) used a value of the coefficient of restitution equal to 0.65 based on experimental data and, after a systematic examination, concluded that the coefficient of restitution has a negligible effect on the displacement response of

building during pounding, except from the case of perfectly elastic impact. In general, a value of $e = 0.5$ to 0.7 is usually employed in numerical simulations (Anagnostopoulos and Spiliopoulos, 1992; Jankowski, 2005, 2008; Jankowski *et al.*, 1998; Mahmoud *et al.*, 2013; Mahmoud and Jankowski, 2011; Papadrakakis *et al.*, 1991).

Although some common values of the coefficient of restitution are usually given for various types of materials, experimental studies have shown that these values are highly depended on the impact velocity and suggested certain formulas to be used. Based on shaking table tests results, an optimization approach was proposed (Guo *et al.*, 2009) for identifying the parameters of the linear and the nonlinear viscoelastic impact models. That study concluded that the coefficient of restitution of the bridge model during impacts ranges from 0.62 to 0.75, and that strong impacts dissipate more energy during collisions.

Jankowski (Jankowski, 2010) investigated the influence of the impact velocity on the coefficient of restitution, performing similar experiments on common building materials. The experiment involved dropping a ball of the tested material from different heights. The ball was dropped onto a fixed flat surface of the same material, and the ball's pre- and post-collision velocities were recorded. These velocities were then used to determine the coefficient of restitution of each impact for different building materials, as shown in Figure 3.15. The general trend for the typical building materials, such as: steel, concrete, timber and ceramic, shows a decrease in the coefficient of restitution as the prior-impact velocity increases, with the highest values exhibited for ceramic-to-ceramic impact and the lowest for timber-to-timber impact.

More specifically, Jankowski measured values of 0.4 to 0.8 and incorporated relationships, such as those provided in Equation (3.23), to predict the coefficient of restitution, based on the type of the material and the impact velocity.

$$\begin{aligned}
e_c &= -0.0040 \cdot v_{imp}^3 + 0.0474 \cdot v_{imp}^2 - 0.2116 \cdot v_{imp} + 0.8141 \quad \text{for ceramic-to-ceramic impact} \\
e_c &= -0.0070 \cdot v_{imp}^3 + 0.0696 \cdot v_{imp}^2 - 0.2529 \cdot v_{imp} + 0.7929 \quad \text{for concrete-to-concrete impact} \\
e_c &= -0.0039 \cdot v_{imp}^3 + 0.0440 \cdot v_{imp}^2 - 0.1867 \cdot v_{imp} + 0.7299 \quad \text{for steel-to-steel impact} \\
e_c &= -0.0043 \cdot v_{imp}^3 + 0.0479 \cdot v_{imp}^2 - 0.1971 \cdot v_{imp} + 0.7067 \quad \text{for timber-to-timber impact}
\end{aligned} \tag{3.23}$$

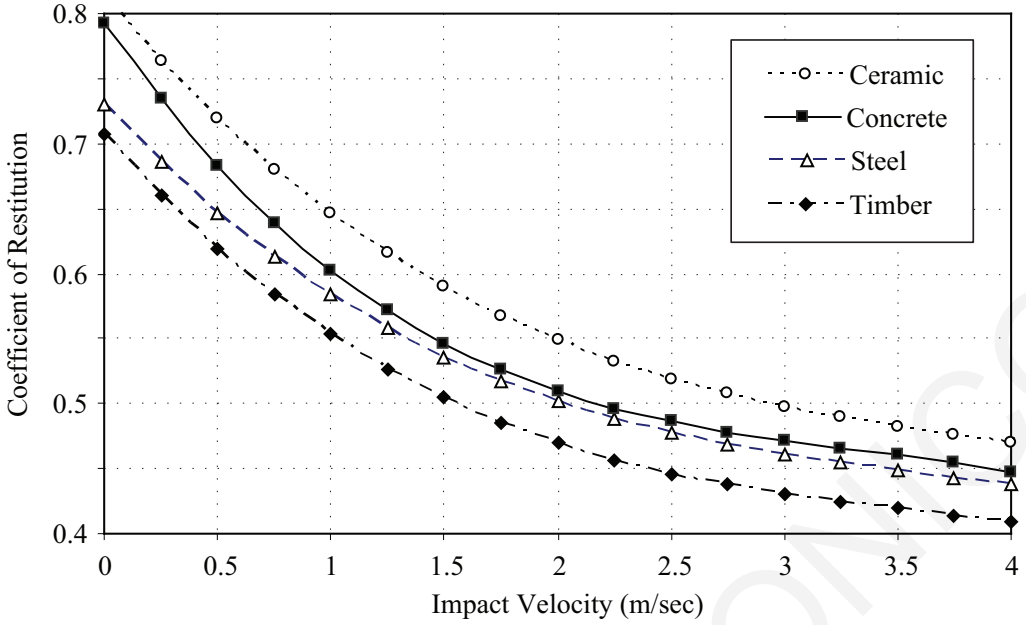

Figure 3.15 Coefficient of restitution in respect to impact velocity (Jankowski, 2010).

Leibovich *et al.* (Leibovich *et al.*, 2012) measured the coefficient of restitution and the impact acceleration for plane ended circular concrete rods suspended as pendulums. Two different cases of bars with equal and unequal lengths were considered. The calculated coefficients of restitution were 0.5 to 0.7 for the pounding between equal bars.

3.5.2 Impact Stiffness

A primary issue for properly utilizing the contact-element models in structural pounding analysis is to select appropriate values for the impact parameters, especially the value of the impact stiffness. A wide range of diverse values has been used in the scientific literature for different kinds of impact problems, since its exact value is practically unknown. The values of the impact stiffness is described as a function of the geometric and elastic properties of the colliding bodies (Goldsmith, 1960). For two spheres of radii R_1 and R_2 in contact the generalized stiffness is calculated as:

$$k_h = \frac{4}{3\pi}\left(\frac{1}{\lambda_1+\lambda_2}\right)\sqrt{\frac{R_1 \cdot R_2}{R_1+R_2}} \tag{3.24}$$

In formula, λ_i is a material parameter defined as:

$$\lambda_i = \frac{1-v_i^2}{\pi E_i}, \quad i=1,2 \tag{3.25}$$

where v_i and E_i are the Poisson's ratio and the modulus of elasticity, respectively, of sphere *i*.

For contact between a spherical body and a plane surface body, the generalized stiffness coefficient depends on the radius of the sphere and the material properties, as expressed by the formula (Goldsmith, 1960):

$$k_h = \frac{4}{3\pi}\left(\frac{1}{\lambda_1 + \lambda_2}\right)\sqrt{R_1} \tag{3.26}$$

Assuming the colliding bodies to be spherical, the radius of an equivalent colliding sphere, can be estimated as:

$$R_i = \sqrt[3]{\frac{3m_i}{4\pi\rho}} \qquad i = 1,2 \tag{3.27}$$

where m_i is the colliding mass and ρ is the density of concrete.

Anagnostopoulos (Anagnostopoulos, 1988) assumed an impact stiffness value for the linear viscoelastic impact model equal to twenty times the stiffness of the stiffer structure considered in the analysis. He also examined the effect of choosing different values for the impact parameters on the response during collisions. It was found that a ten-fold decrease of the impact stiffness does not cause any substantial differences in the displacement response of the pounding buildings. Nevertheless, for a 100 times reduction of the impact stiffness, the amplification of the response due to collisions was significantly reduced. Furthermore, it was noted that despite the insensitivity of the displacement response to the impact stiffness value, the acceleration response is highly affected by this parameter.

Van Mier *et al.* (van Mier *et al.*, 1991) experimentally examined the case of impact between concrete bodies, and found that the impact stiffness, considering a non-linear impact spring, should vary from 40 to 80 $KN/mm^{1.5}$ in order to match experimental results. Maison and Kasai (Maison and Venture, 1992) considered that the impact linear spring stiffness was equal to the in-plane stiffness of the slab. They varied the impact stiffness from 87.6 to 8756 KN/mm, assuming different widths of the building's plan, and argued that no significant effect had been observed on the response during collisions. However, it was observed, that for small values, the effect of impact stiffness on the response was increased.

For the impact stiffness of the linear spring impact model (Watanabe and Kawashima, 2004) conducted a numerical simulation to clarify the appropriate stiffness of impact spring and the time interval of numerical integration based on wave propagation theory. Bridge decks simulated as elastic rods and analysis results indicated that the impact stiffness can be taken as the axial stiffness of the contact bodies as follows:

$$k_l = \frac{E \cdot A}{L} \tag{3.28}$$

where E is the elastic modulus of the material of the colliding bodies, while A and L are the section area and length of the structure in the axial direction, respectively. This approach for determining the spring stiffness has been widely accepted for the pounding analysis of buildings and highway bridges by using the impact model based on the linear spring, including the Kelvin impact model (Jankowski *et al.*, 1998; Maison and Venture, 1992).

Experimental results indicated that the actual contact stiffness are significantly smaller than the theoretical values, although the structural response can be effectively predicted by using the identified or given stiffness values (Guo *et al.*, 2012). For example, the axial stiffness of the bridge model calculated from the theoretical approaches should be larger than 10^7 N/m. However, the actual impact stiffness, which can capture the pounding effects is $1.55 \cdot 10^5$ N/m, as given in (Zhu *et al.*, 2002). In (Guo *et al.*, 2009) the theoretical value and identified value of the impact stiffness are found to be $2.80 \cdot 10^9$ N/m and $3.67 \cdot 10^7$ N/m, respectively. The enormous difference may be due to the inconsistency between the assumptions for deriving the model and the actual conditions of the structures.

3.6 Concluding Remarks

The pounding force generated between two colliding structures depends on a number of factors, such as the contact surface geometry, the impact velocity, material properties and the masses of the colliding structures. In this chapter, the major force-based impact models that have been employed in the scientific literature have been described. The advantages and drawbacks of the impact force models, when used for modeling of structural pounding, have also been discussed.

In the following chapter, structural pounding is investigated in two-dimensions and pounding forces are simulated with the help of the linear models presented in Section 3.3. The use of linear impact models is relevant in 2D (planar) simulations as the absence of any torsional effects ensures that the structure collides perpendicularly to the moat wall.

Non-linear impact force-penetration phenomena that might arise from material effects can be captured through the viscous damping terms that are included in all models. The discrepancies that might arise from the use of the different impact models is parametrically investigated in Chapter 4.

CHAPTER 4 PLANAR INVESTIGATION OF STRUCTURAL POUNDING

4.1 Planar 2D Modeling

This chapter focuses on the investigation of impact modeling effects on the overall structural response of base-isolated buildings. The dynamic analyses of the simulated building, taking into account structural pounding, are performed in two-dimensions, while the superstructure of the seismically isolated building is modeled as a shear-type structure mounted on LRBs with one lateral DOF at each floor and the masses lumped at the floor levels. Collisions are assumed to happen between the moat wall and the base floor, which is the most common case of structural impact for a base-isolated building due to the large relative displacements at the isolation level. The seismically isolated MDOF system is subjected to horizontal components of near-fault ground motions, while for simplicity purposes, it is assumed that the superstructure maintains a linear elastic behavior during the induced earthquake excitations.

In contrast to the response for an independently vibrating structure, the pounding force response between two structures also depends on theirs masses and clearance between them. The equation of motion for a MDOF system subjected to pounding under an earthquake excitation can be expressed as follows:

$$\overline{M}\cdot\ddot{\overline{U}}(t)+\overline{C}\cdot\dot{\overline{U}}(t)+\overline{K}\cdot\overline{U}(t)+\overline{F}_{imp}(t)=-\overline{M}\cdot\bar{i}\cdot\ddot{u}_g(t) \tag{4.1}$$

where $\overline{F}_{imp}(t)$ is the vector representing the pounding forces at the floors level. The use of an appropriate numerical model for the pounding forces during collision between structures is essential for precise determination of the peak responses.

In the case of a ground motion, $\ddot{u}_g(t)$, the inertia forces are expressed as:

$$\overline{F}^{I}(t)=\overline{M}\cdot\ddot{\overline{U}}(t)+\overline{M}\cdot\bar{i}\cdot\ddot{u}_g(t) \qquad \text{where} \qquad \bar{i}=\begin{bmatrix}1 & 1 & \dots & 1\end{bmatrix}^T \tag{4.2}$$

The damping forces are expressed in terms of the relative velocities of the floors velocities and the damping matrix of the MDOF system, taking also into account the impact damping forces during collisions:

$$\overline{F}^{D}(t)=\begin{cases}\overline{C}\cdot\overline{\dot{U}}(t) & \text{no impact}\\ \overline{C}\cdot\overline{\dot{U}}(t)+\bar{e}\cdot\overline{F}^{D}_{imp}(t) & \text{during impact}\end{cases} \tag{4.3}$$

Each of the terms e_i of the vector $\bar{e}$, which has a dimension equal to the number of the DOFs, is equal to zero when no contact is detected in the corresponding DOF *i,* while it takes the value of 1 whenever an impact occurs at the corresponding floor, assuming only the possibility of slab-to-slab collisions. When the linear elastic model is used for simulating the seismic isolation system, the elastic forces are formed based on the floor relative displacements and the stiffness matrix, taking into account the impact forces in case of collisions:

$$\overline{F}^{E}(t)=\begin{cases}\overline{K}\cdot\overline{U}(t) & \text{no impact}\\ \overline{K}\cdot\overline{U}(t)+\bar{e}\cdot\overline{F}^{E}_{imp}(t) & \text{during impact}\end{cases} \tag{4.4}$$

When the nonlinear model is used for the isolation system, the elastic forces of the superstructure are computed based on the stiffness matrix and the corresponding relative displacements at time *t*, while for the isolation system the forces are computed considering the hysteretic behavior proposed by Wen (1976):

$$\overline{F}^{E}(t)=\begin{cases}\overline{f}_{s}\left(u(t),\dot{u}(t)\right) & \text{no impact}\\ \overline{f}_{s}\left(u(t),\dot{u}(t)\right)+\bar{e}\cdot\overline{F}^{E}_{imp}(t) & \text{during impact}\end{cases} \tag{4.5}$$

$\overline{F}^{D}_{imp}(t)$ and $\overline{F}^{E}_{imp}(t)$ are the damping and elastic contact forces during impact, respectively, which are calculated according to the corresponding impact model. The impact forces are non-zero only whenever the relative displacements exceed the available clearance, leading to collisions with the adjacent structure.

The Newmark numerical integration method is used for solving the nonlinear equations of motion. The Newmark's parameters are set to $\beta=0.25$ and $\gamma=0.5$, which ensures the unconditional stability of the solution. Moreover, the Runge-Kutta method with a fixed

time-step is employed to solve the equation that describes the Bouc-Wen behavior of the isolators in each iteration.

4.2 Numerical Simulation

The dynamic analyses of the simulated buildings, taking into account structural pounding, are performed in two-dimensions, while the superstructure of the seismically isolated building is modeled as a shear-type structure mounted on LRBs with one lateral DOF at each floor and the masses lumped at the floor levels, as shown in Figure 4.1(a).

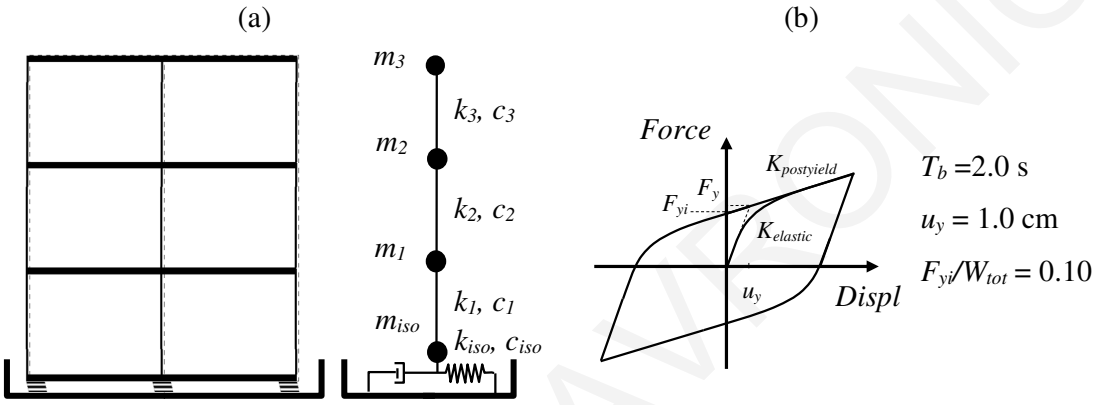

Figure 4.1 (a) Configuration of a 3-story seismically isolated building, and (b) smooth bilinear inelastic model for the behavior of the seismic isolation system.

In the simulations, collisions are assumed to happen between the moat wall and the base mat at the isolation level, which is the most common case of structural impact for a base-isolated building due to the large relative displacements that usually occur at the isolation level. The linear viscoelastic model and its aforementioned modifications are used to compare the resulting peak structural responses during potential collisions of a 3-story base-isolated building with the surrounding moat wall, under the Loma Prieta earthquake (UCSC 16 LGPC Station) and the Northridge earthquake (DWP 74 Sylmar-Converter Station), Fault-Normal component. The characteristics of the base-isolated structure are those provided in Section 2.2.2. The impact stiffness is taken to be equal to $2,500\,\mathrm{KN/mm}$, the coefficient of restitution is taken to be equal to 0.7 for all cases, while the mass of the surrounding moat wall is assumed to be equal to 500 tons.

Table 4.1 presents the peak structural responses of the base-isolated structure with the separation gap equal to 20 cm for both excitations, considering the five aforedescribed impact models. The maximum impact velocities (on both sides) and the impact incidences are also provided. It shall be noted that the number of impacts may deviate between the various models that are considered. In general, the differences in the computed responses

of the classical linear viscoelastic model and the slightly modified by Komodromos *et al.* model are very small. As expected, the two models have almost identical responses due to the fact that their only difference is the tensile force at the end of the detachment phase. Nevertheless, there is a considerable variation of the peak base-floor acceleration computed considering the classic Kelvin-Voigt model and the corresponding results of the Ye *et al.*, the Mahmoud and Jankowski and the Pant and Wijeyewickrema models.

Table 4.1 Peak responses of the 3-story base-isolated building with a seismic gap equal to 20 cm, considering different impact models.

Peak Response		Loma Prieta earthquake					Northridge earthquake				
		1	2	3	4	5	1	2	3	4	5
Base displacement (cm)		20.47	20.47	20.45	20.41	20.39	21.12	21.13	21.06	20.98	20.91
Top-floor displacement (cm)		23.60	23.60	23.60	23.57	23.56	28.14	28.15	28.11	28.09	28.01
Interstory deflection (cm)		1.82	1.82	1.77	1.79	1.77	4.14	4.14	4.02	4.05	3.97
Base-floor acceleration (m/sec^2)		34.2	34.2	38.08	32.90	42.71	71.88	71.99	80.57	68.62	92.07
Top-floor acceleration (m/sec^2)		22.57	22.57	22.30	22.29	22.13	49.51	49.51	48.56	48.43	47.6
Remaining plastic deformation (cm)		-	0.04	-	-	-	-	0.11	-	-	-
Max impact velocity (m/sec)		0.48	0.48	0.48	0.48	0.48	1.06	1.06	1.06	1.07	1.07
Impact incidences (#)	Left	0	0	0	0	0	2	3	2	3	3
	Right	2	2	2	2	2	2	2	2	2	2

***1:** Kelvin-Voigt model (Anagnostopoulos, 1988); Modified Kelvin-Voigt **2:** Komodromos et al., 2007, **3:** Ye et al., 2009, **4:** Mahmoud and Jankowski, 2011 **5:** Pant and Wijeyewickrema, 2012.*

The observed variations can be explained through Figure 4.2 and Figure 4.3. Specifically, these two figures present the impact force – indentation diagrams and the time-histories of the impact force at the base of the seismically isolated building for the 5 different impact models, subjected to the Loma Prieta and Northridge excitations. Solid lines represent impacts on the left side of the building, whereas dashed lines correspond to collisions on its right side.

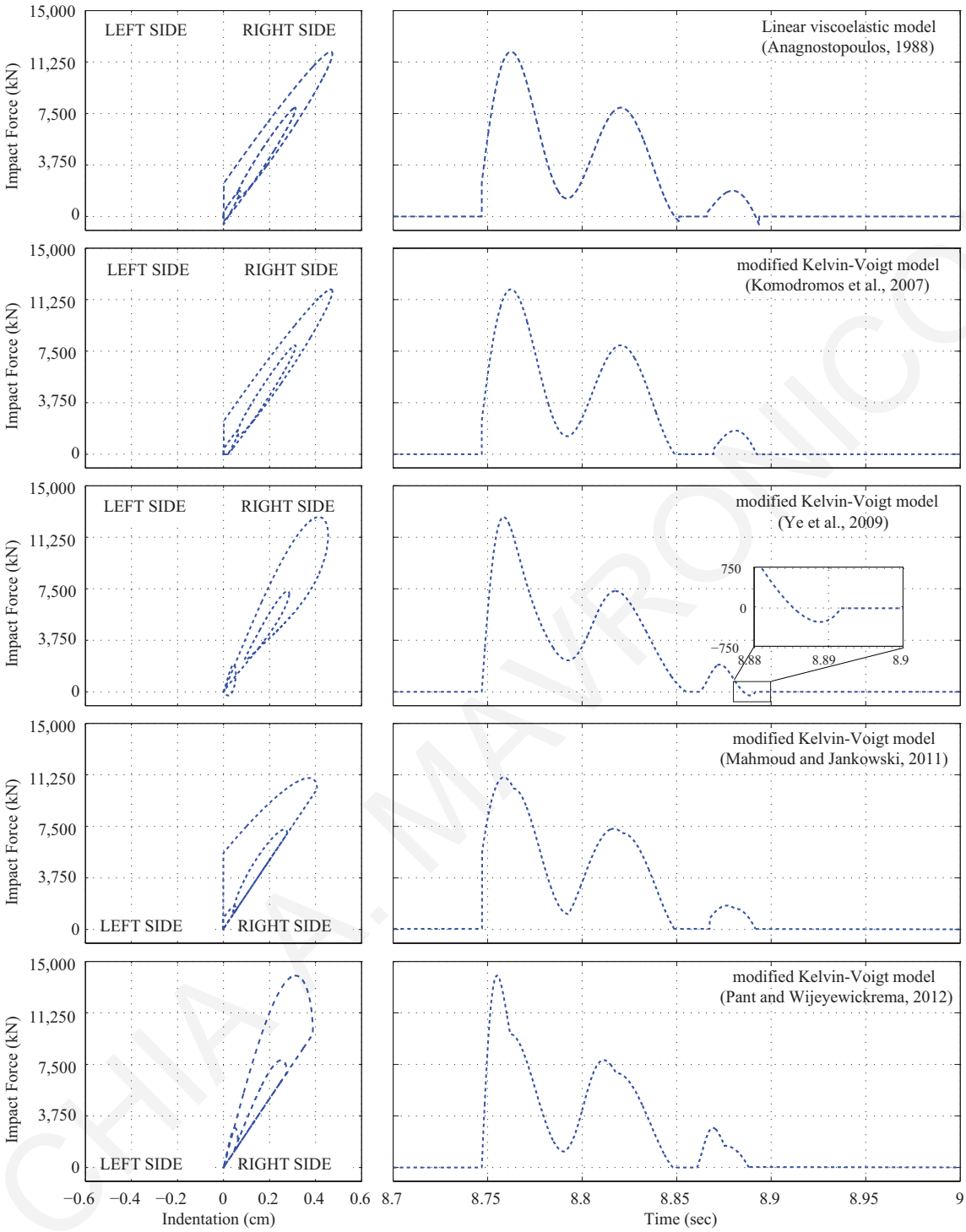

Figure 4.2 Plots of the impact force in terms of indentation and time-histories; of the 3-story base-isolated building, under the Loma Prieta earthquake, with a seismic gap of 20 cm, considering 5 different impact models.

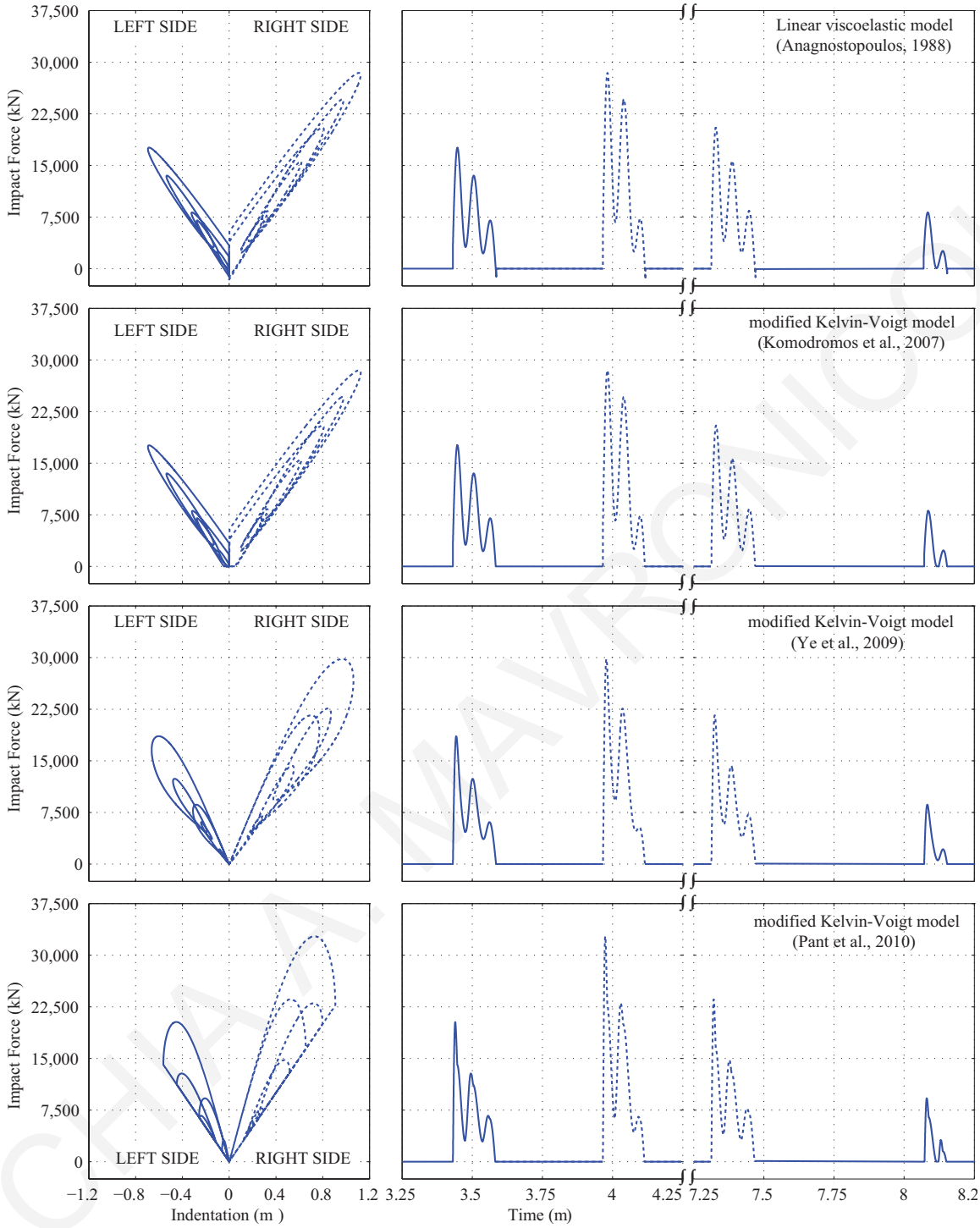

Figure 4.3 Plots of the impact force in terms of indentation and time-histories; of the 3-story base-isolated building, under the Northridge earthquake, with a seismic gap of 20 cm.

It is observed that the values of the maximum impact force calculated through the Kelvin-Voigt model and the modified version proposed by Komodromos *et al.* are essentially equal. This observation is also valid for the Northridge earthquake responses, where the peak response occurs due to the second impact. However, the maximum impact force using the models proposed by Ye *et al.*, Mahmoud and Jankowski and Pant and

Wijeyewickrema is significantly higher. This deviation justifies the higher discrepancies among model responses observed in the base acceleration results (Table 4.1). Despite the large differences in the calculated impact forces, the displacement response of the structure is found to be relatively insensitive to the impact model that is used. These dynamic simulations reveal that the utilization of the Ye *et al.* model does not always avoid the appearance of tensile force immediately before separation. The existence of tensile forces in the case of the Loma Prieta earthquake, as shown in Figure 4.2 (third row), is possible due to the activation of the dashpot element, which by definition is included in the restitution phase of contact. It should be noted, however, that in the case of the Northridge excitation (third row of Figure 4.3) the model does not produce tensile forces.

4.3 Extending a Specially Developed Software

In order to efficiently conduct this research work, an effective software, able to perform large numbers of dynamic analyses of MDOF systems while considering possible impact phenomena is necessary. In addition, the option of using different impact models is essential, as well as the ability of investigating parametrically the effects of certain factors. Taking into account these specific needs, a specialized software application has been accordingly modified and extended. Specifically, object-oriented programming and the Java programming language have been employed in the design and development of the aforementioned software application, taking into account the significant advantages that these modern software development approaches provide. In particular, the Java programming language is used for the computational part, while the Java Swing is employed for the Graphical User Interface (GUI) and the computer graphics, as shown in Figure 4.4.

Therefore, a software has been developed, which is capable of performing efficiently 2D numerical simulations and parametric studies of MDOF systems exhibiting shear beam behavior under dynamic loading with automatic impact detection and handling capabilities. Moreover, the software allows both linear and bilinear models to be used for the simulation of the seismic isolation system. Furthermore, the smooth nonlinear model for the behavior of the isolators and the previously descripted impact models for the simulation of structural collisions have also been incorporated in the software to facilitate the efficient execution of all necessary simulations and parametric. A general flow-chart of the analysis procedure is illustrated in Figure 4.5.

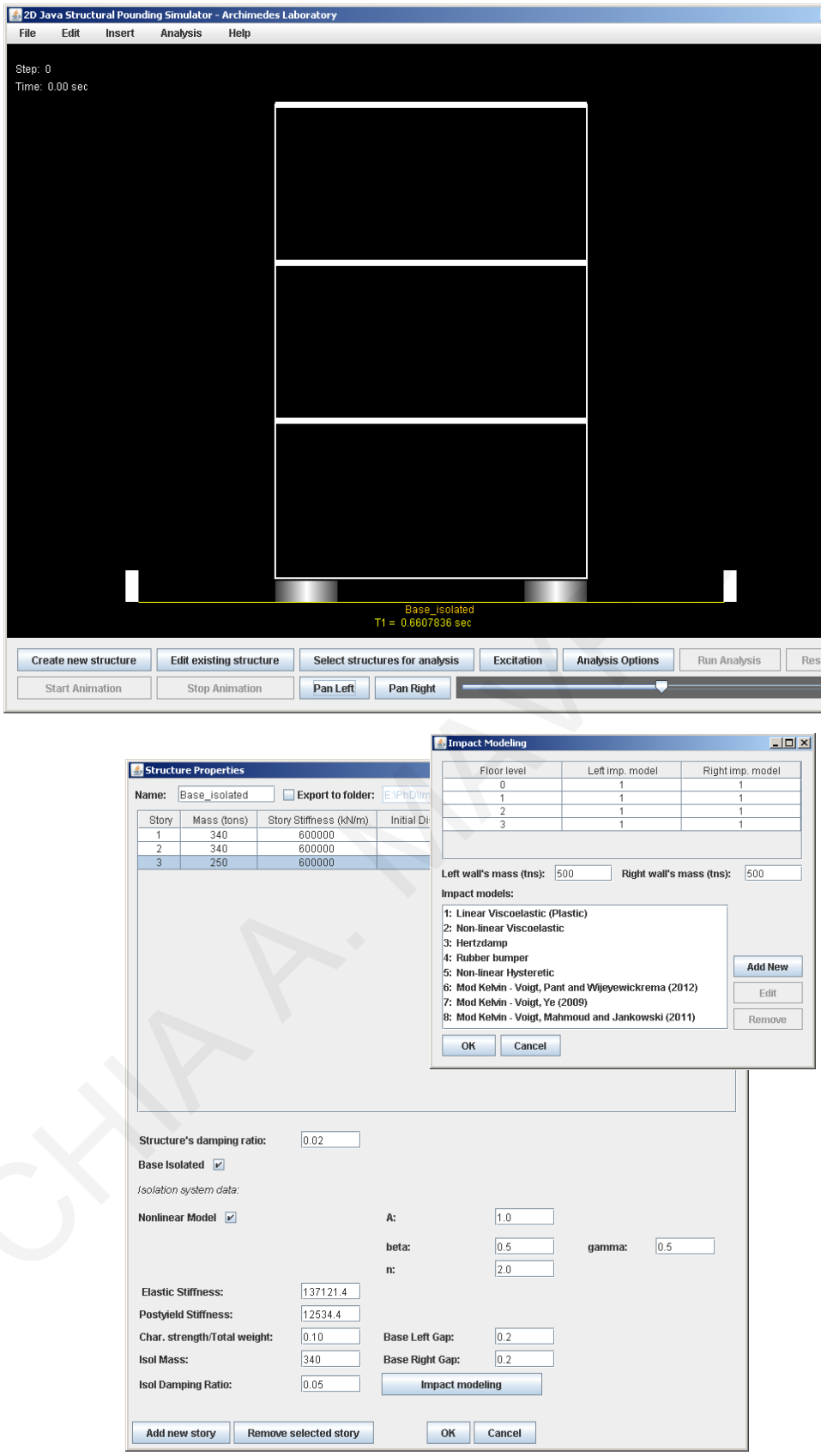

Figure 4.4 Windows and dialogs of the Graphical User Interface (GUI) of the software.

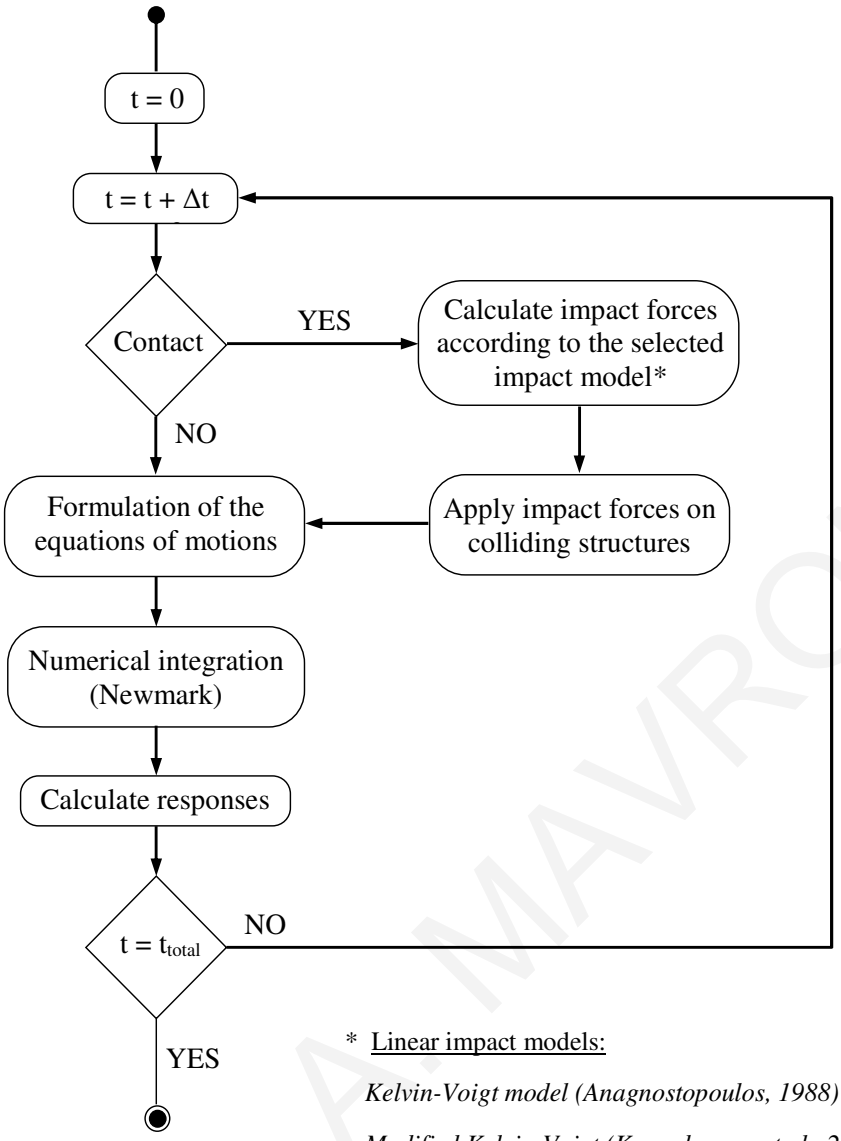

Figure 4.5 A concise flow chart of the developed software.

The developed software provides the ability to perform large numbers of numerical simulations in order to investigate the effects of certain parameters, such as structural characteristics, the size of the separation gap, earthquake characteristics, etc. Some of the pertinent capabilities of the developed software are provided below:

- Input data from a text file and import a recorded accelerogram from a data file.

- Option of selecting a linear or a nonlinear model for the isolation system.
- Impact detection when the available gap between neighboring structures is exceeded and calculation of impact forces based on the selected impact model.
- Ability of exporting the time history results in text files.
- Option of performing parametric analyses by varying a user – selected parameter.

4.4 Parametric Studies

Two typical base-isolated buildings, a 3- and a 5-story building as described in Section 2.2.2, are used in the simulations, while a finite seismic gap on either of their sides is considered, in order to compare the peak responses estimated using the aforedescribed impact models. A smooth bilinear inelastic model is used to simulate the base isolation system, with an isolation period based on the post-yield stiffness of 2.0 s, normalized characteristic strength $F_{yi}/W_{tot} = 0.05$ and yield displacement equal to 1.0 cm, unless otherwise stated. For all performed dynamic analyses, the values of 1.0, 0.5, 0.5 and 2 are adopted for the Bouc-Wen models' parameters A, β, γ and n, respectively.

Five near-fault ground motions (Table 4.2) are used in the simulations of this study in order to examine the effects of the characteristics of the earthquake excitation on the seismic response of the seismically isolated building during collisions.

Table 4.2 Earthquake records that are used in the simulations.

NGA#	Event	Station	M_w	PGA (g)
779	Loma Prieta 1989-10-18	UCSC 16 LGPC	6.93	0.944
821	Erzican, Turkey 1992-03-13	95 Erzincan	6.69	0.486
828	Cape Mendocino 1992-04-25	CDMG 89156 Petrolia	7.01	0.615
1084	Northridge-01 1994-01-17	DWP74 Sylmar-Converter Sta	6.69	0.594
2627	Chi-Chi, Taiwan-03 1999-09-20	CWB 99999 TCU076	6.2	0.524

The selected earthquake records accelerograms, which have been taken from the PEER database (PEER Pacific Earthquake Engineering Research Center, 2011), are characterized by low-frequency content, in order to induce large relative displacements to the seismically isolated building, since this is one of the most decisive factors for the occurrence of collisions in such structures. The acceleration response spectra of the selected earthquake records are plotted together in Figure 4.6. The graph includes response spectra for the fault-normal components used in the analysis.

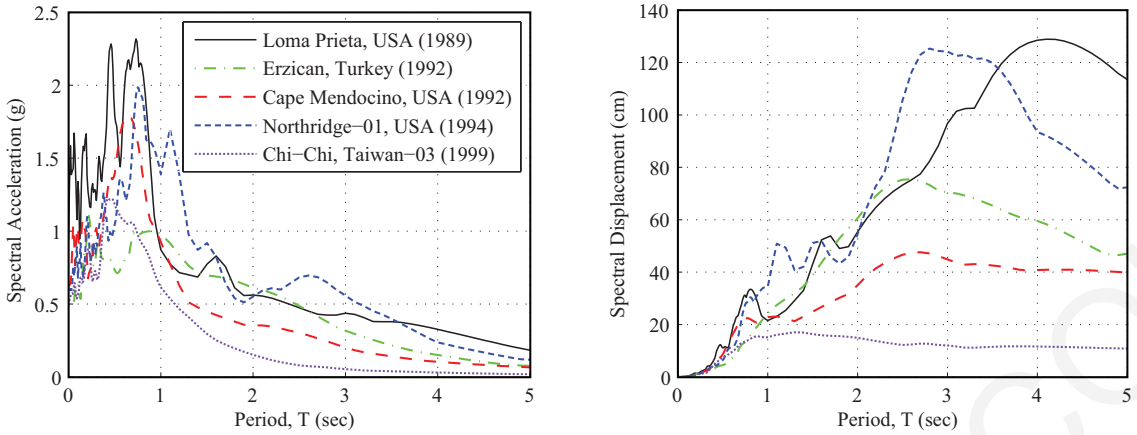

Figure 4.6 Acceleration and displacement response spectra (Comp FN) for the 5 earthquake records, considering a viscous damping ratio of 5.0%.

The various parameters investigated and their range examined herein are presented in Table 4.3. Certain influencing parameters are purposely varied in order to assess how they may affect the effectiveness of the seismic isolation during collisions. Also, the effect of using different impact models for the calculation of the impact forces on the overall seismic response during pounding is examined in this section, performing more than 14,500 nonlinear time-history analyses.

Table 4.3 Examined cases in the conducted parametric study.

Parameter	Values	Examined cases	Total number of analyses
Proximity to the moat wall			
Gap size	10 : 0.2 : 30 cm	up to 95	3,280
Impact parameters			
Coefficient of restitution, e	0.5 : 0.01 : 1.0	51	2,550
Impact stiffness, k_k	500 : 75 : 5000 MN/m	61	3,050
Characteristics of isolation system			
Isolation period, T_b	1.5 : 0.02 : 3.0 s	76	
Normalized characteristic strength, F_{yi}/W_{tot}	0.05, 0.10	3	5,700
Yield displacement, u_y	1.0 cm, 2.5 cm		

4.4.1 Influence of Gap Size and Excitation Characteristics

The seismic gap width is systematically varied in the range of 10 to 30 cm with a step of 0.2 cm, in order to investigate its effect on the overall peak responses. The 3-story base-isolated building is analyzed under the selected near-fault ground motions, while the moat wall is assumed to be present on both sides of the building. Figure 4.7 presents the peak floor accelerations and the maximum interstory drifts of the base-isolated building using the recorded accelerogram from the Loma Prieta earthquake as a function of the seismic

gap width considering the five impact models. Each subplot corresponds to the response of a particular floor, or interstory response for the case of interstory deflections. It is apparent that the most severe peak floor accelerations occur at the base level where collisions occur. Subsequently, the maximum interstory deflections occur at the 1-0 interface, between the first floor and the isolation level.

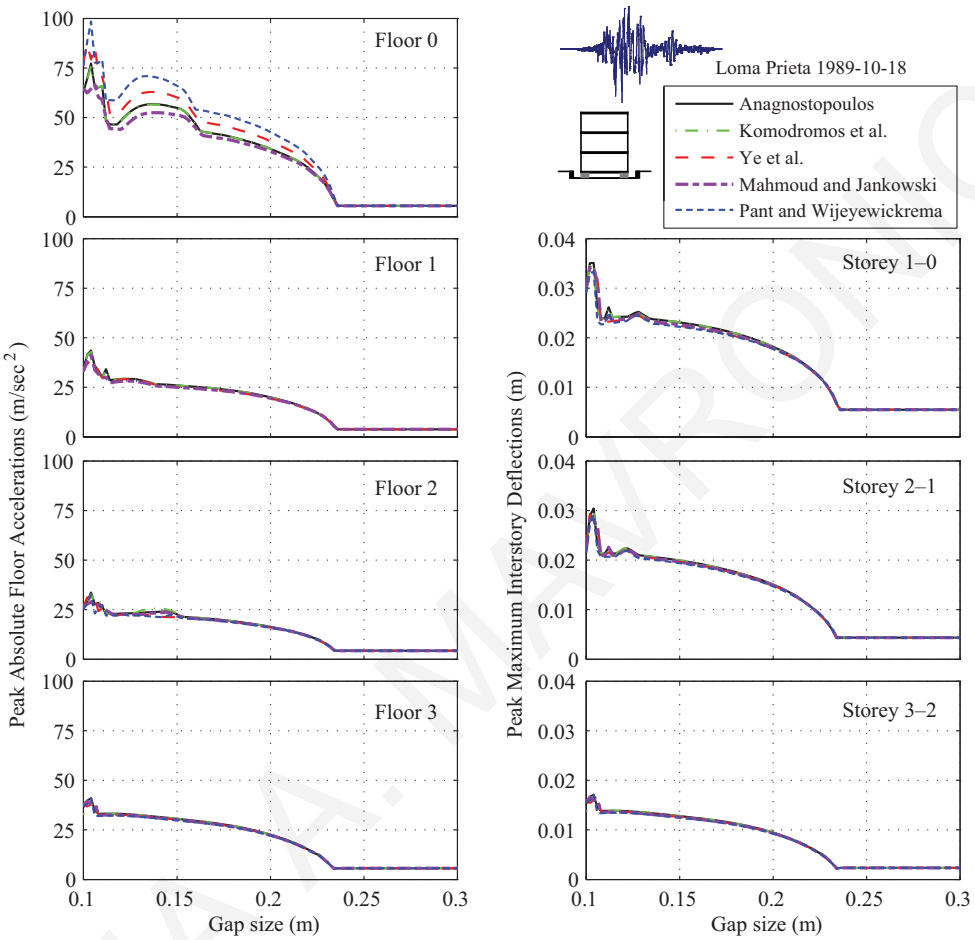

Figure 4.7 Maximum responses of the 3-story base-isolated building, under the Loma Prieta earthquake in terms of the width of the seismic gap.

Figure 4.8 presents the peak floor accelerations and the maximum interstory drifts amplification among all floors of the 3-story base-isolated building as a function of the seismic gap width for all considered excitations, using the classical Kelvin-Voigt model with the formula provided by Anagnostopoulos (Anagnostopoulos, 1988, 2004) for the estimation of the impact damping coefficient. Different models for the isolators are also considered. The differences between the peak response curves for each ground motion are significant. This indicates that the frequency content and the predominant frequencies are the most important characteristics of the seismic excitations, influencing greatly the peak response during collisions. The effect of the isolator behavior on the response deviation is minor; comparing the results provided in Figure 4.8(a) and (b).

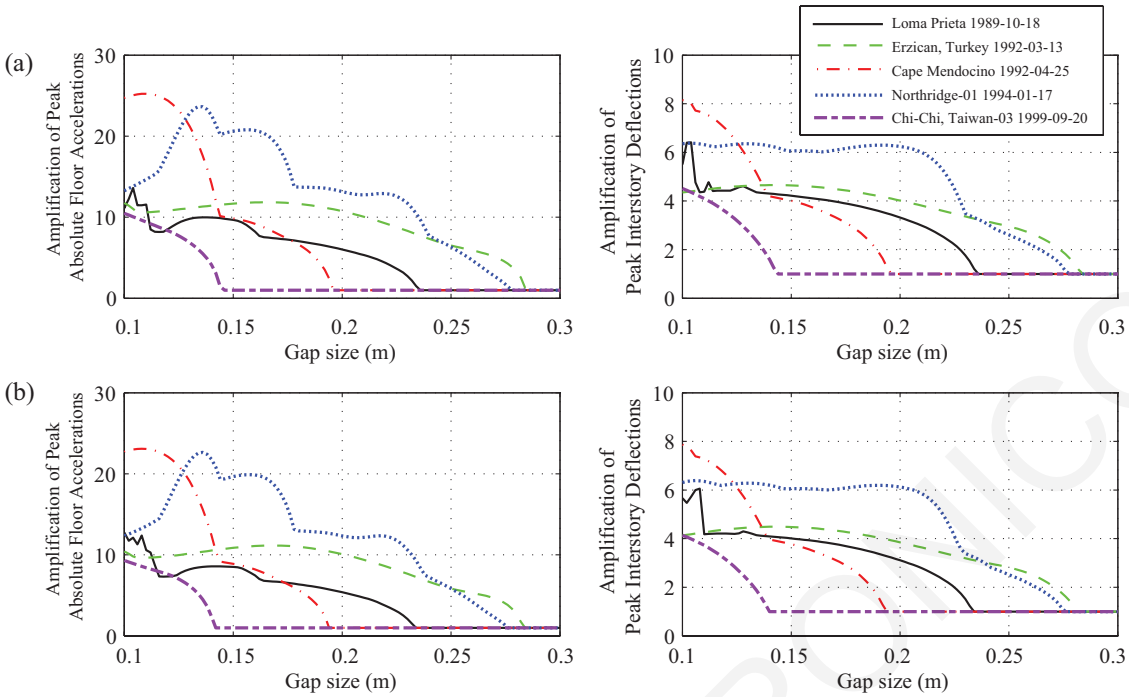

Figure 4.8 Peak floor response amplification of the 3-story building due to collisions with the moat wall considering the classical Kelvin-Voigt impact element: (a) smooth Bouc-Wen model and, (b) sharp bilinear model; for the isolators.

In order to more easily compare the results among the five impact models, all peak responses are normalized with respect to the classical Kelvin-Voigt model. The linear viscoelastic model using the formula provided by Anagnostopoulos for the estimation of the impact damping coefficient has been considered as a base model due to its wide usage in numerical simulations. Figure 4.9 presents the normalized peak absolute floor accelerations (first column), showing that the Kelvin-Voigt impact model and the modified model proposed by Komodromos *et al.,* in which a permanent deformation is allowed, lead to almost identical responses. In general, the peak floor accelerations are underestimated by about 5% when the impact element proposed by Mahmoud and Jankowski, is utilized with respect to the linear viscoelastic impact model. On the other hand, normalized response ratios are, in general, kept at values higher than 1.0, indicating overestimation around 10 and 25% when the contact elements proposed by Ye *et al.* and the Pant and Wijeyewickrema, respectively, are used. It is interesting to note that the response deviation remains almost constant. The differences in the peak floor accelerations predicted by the various impact models appear to relate with their capacity to either overestimate or underestimate, with respect to the Kelvin-Voigt model, the peak impact force.

It is observed that the values of the maximum interstory deflections calculated through the Kelvin-Voigt model and the modified version proposed by Komodromos *et al.* are essentially equal. While, the peak interstory deflections are, in general, underestimated

when the impact models proposed by the Ye *et al.*, Mahmoud and Jankowski and Pant and Wijeyewickrema are used, compared to the corresponding peak responses computed using the classical Kelvin-Voigt model. In general, the underestimation of the peak response while using the aforementioned modified models tends to increase as the width of the seismic gap reduces. The underestimation of the peak response for seismic gap widths 20% smaller than the maximum base drifts, for each earthquake record appears to fall within a range of 1-3% for all modified linear impact models. Such an underestimation of the response can be considered as insignificant. These peak responses are in line with the capacity of the models to dissipate energy in various extends, as indicated in Figure 3.10; the higher the dissipation capacity, the lower the interstory deflections.

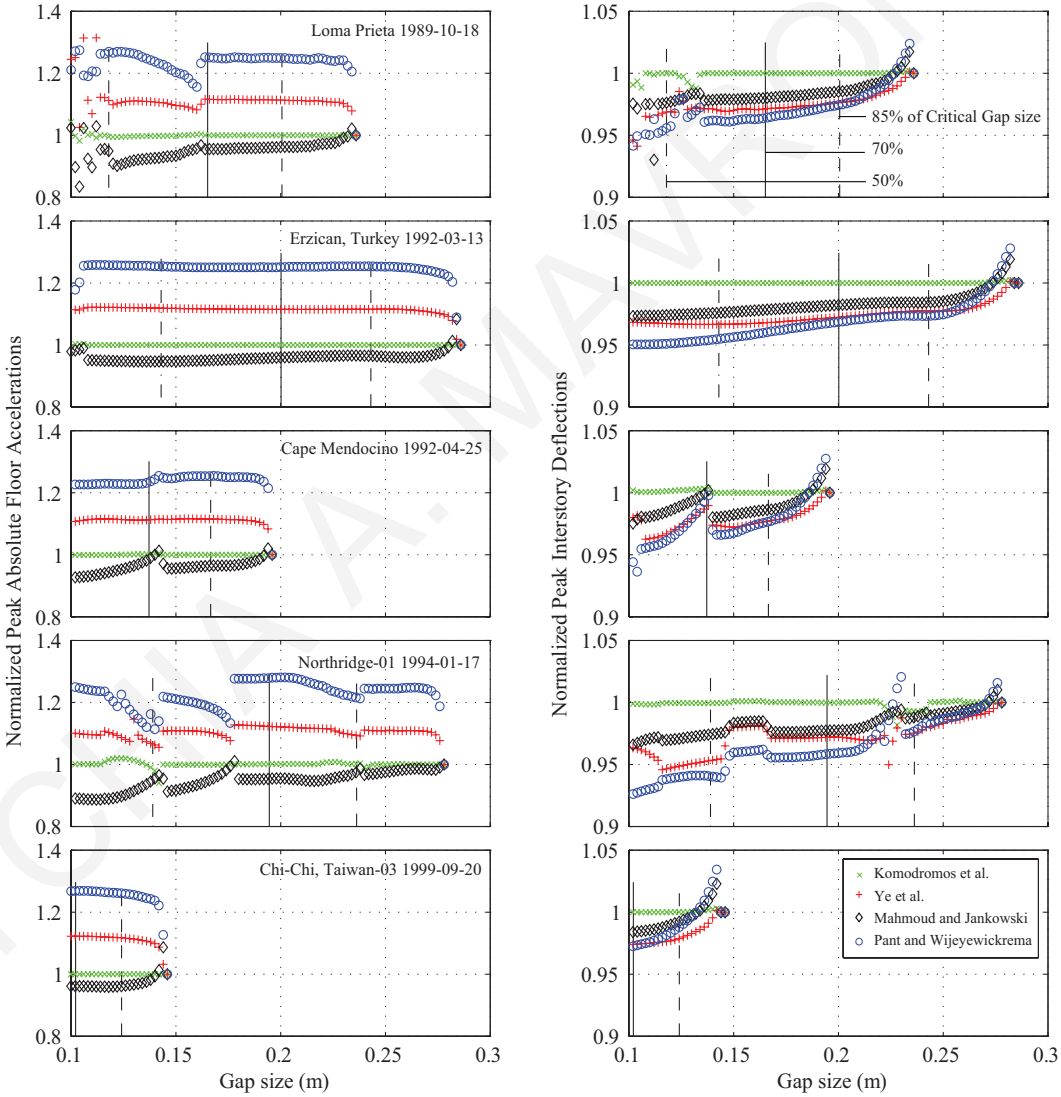

Figure 4.9 Peak responses using the modified linear impact models normalized to the corresponding peak response obtained with the classical Kelvin-Voigt model; in terms of the width of the seismic gap.

The ratio of peak responses when the classical Kelvin-Voigt model element is used and the normalized peak response when the modified models are utilized are provided in Figure 4.10 for the 5-story base-isolated building. Identical or very similar results are observed, mainly regarding the shape of the curves. Nevertheless, the nature of the results of the two buildings during pounding to the surrounding moat wall is consistent.

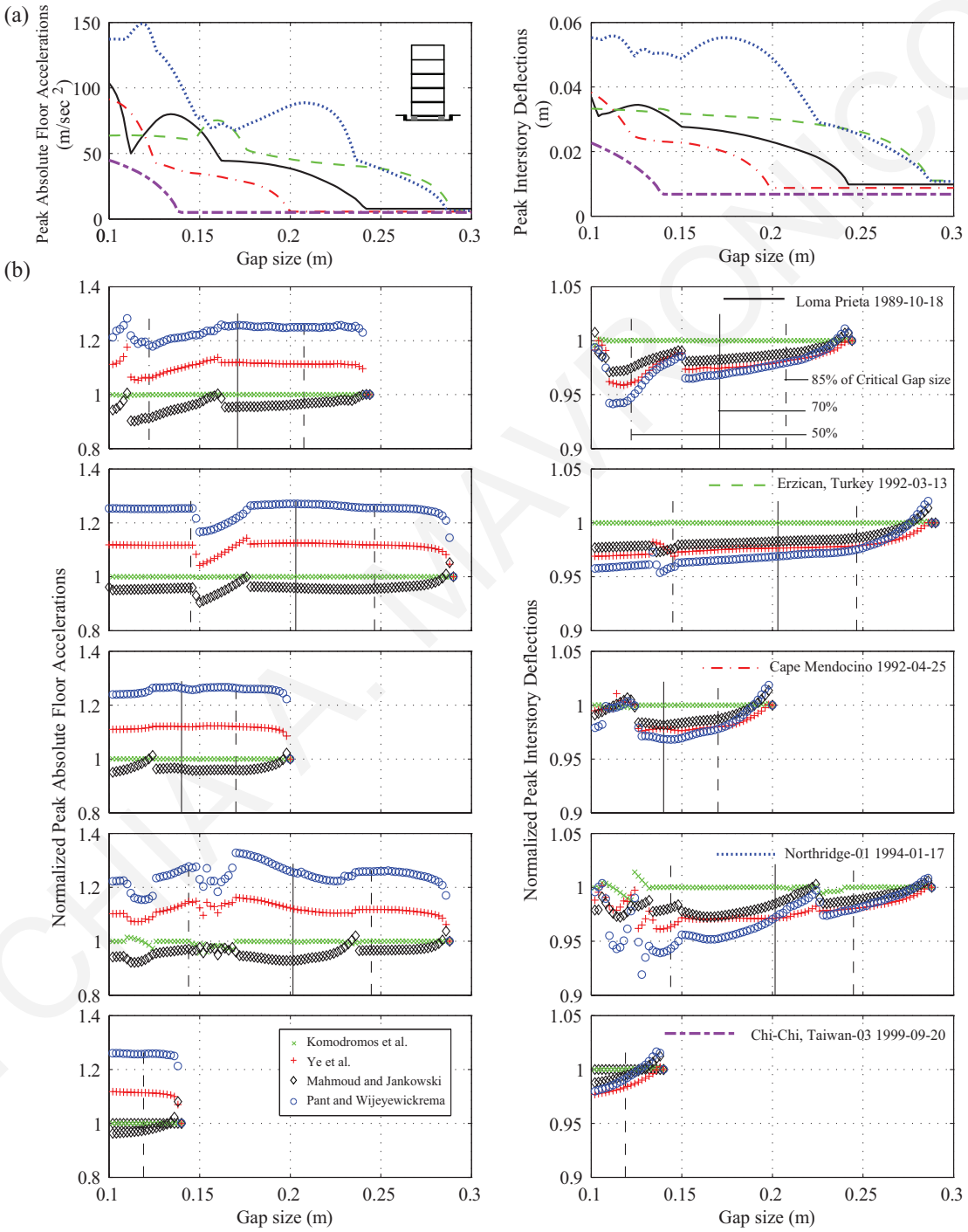

Figure 4.10 (a) Peak response of the 5-story base-isolated building considering the Kelvin-Voigt contact element, and (b) normalized peak response considering modified models in terms of the width of the seismic gap.

4.4.2 Influence of Impact Parameters

In order to examine the effect of the impact stiffness's and the coefficient of restitution's values on the computed peak seismic responses of the 3- and 5-story seismically isolated buildings during collisions, another series of parametric studies is performed. The impact stiffness, k_k, of the linear impact spring is varied in the range of 500 to 5,000 KN/mm, assuming a coefficient of restitution equal to 0.7. In addition, the coefficient of restitution is varied between 0.5 and 1.0, while the impact stiffness for the linear viscoelastic impact models is taken to be equal to 2,500 KN/mm. The pounding force between the moat walls is modeled using each of the five aforedescribed impacts models.

Figure 4.11 presents the impact incidences obtained from the time-history analysis carried out for the Loma Prieta ground motion considering the 5 different impact models for various impact parameters. For this investigation, the 5-story base-isolated building is simulated, assuming a seismic gap 15% smaller than the maximum unobstructed relative displacement at the isolation level under each one of the selected near-fault ground motions, in order to ensure the occurrence of structural pounding. It should be noted that, for this particular excitation, the first impact incidence delivers the peak responses.

As shown in the first row of Figure 4.11, the coefficient of restitution does not influence considerably the peak impact force for the Kelvin Voigt model and the model with the slight modification proposed by Komodromos *et al.* On the other hand, the peak impact force as computed while using the recommended modifications by Ye *et al.,* Mahmoud and Jankowski, and Pant and Wijeyewickrema depends significantly on the coefficient of restitution. The computed results indicate that the contact element proposed by Mahmoud and Jankowski exhibits a high initial jump, especially for lower values of the coefficient of restitution, upon impact. The authors have acknowledged that the modified formula is inferior to the original formulation in all their studied cases and recommended the original formula for use in the study of structural collisions (Mahmoud and Jankowski, 2011).

Furthermore, the results highlight the significant influence of the impact stiffness on the peak impact force due to pounding with the adjacent moat wall, as shown in the second row of Figure 4.11. In general, large peak forces are coupled with higher values of the impact stiffness and small deformations across all impact models. It is apparent that the models proposed by Ye *et al.* and Pant and Wijeyewickrema, produce significantly higher magnitude impact forces than the classical linear viscoelastic impact model, mainly due to the damping of the contact elements.

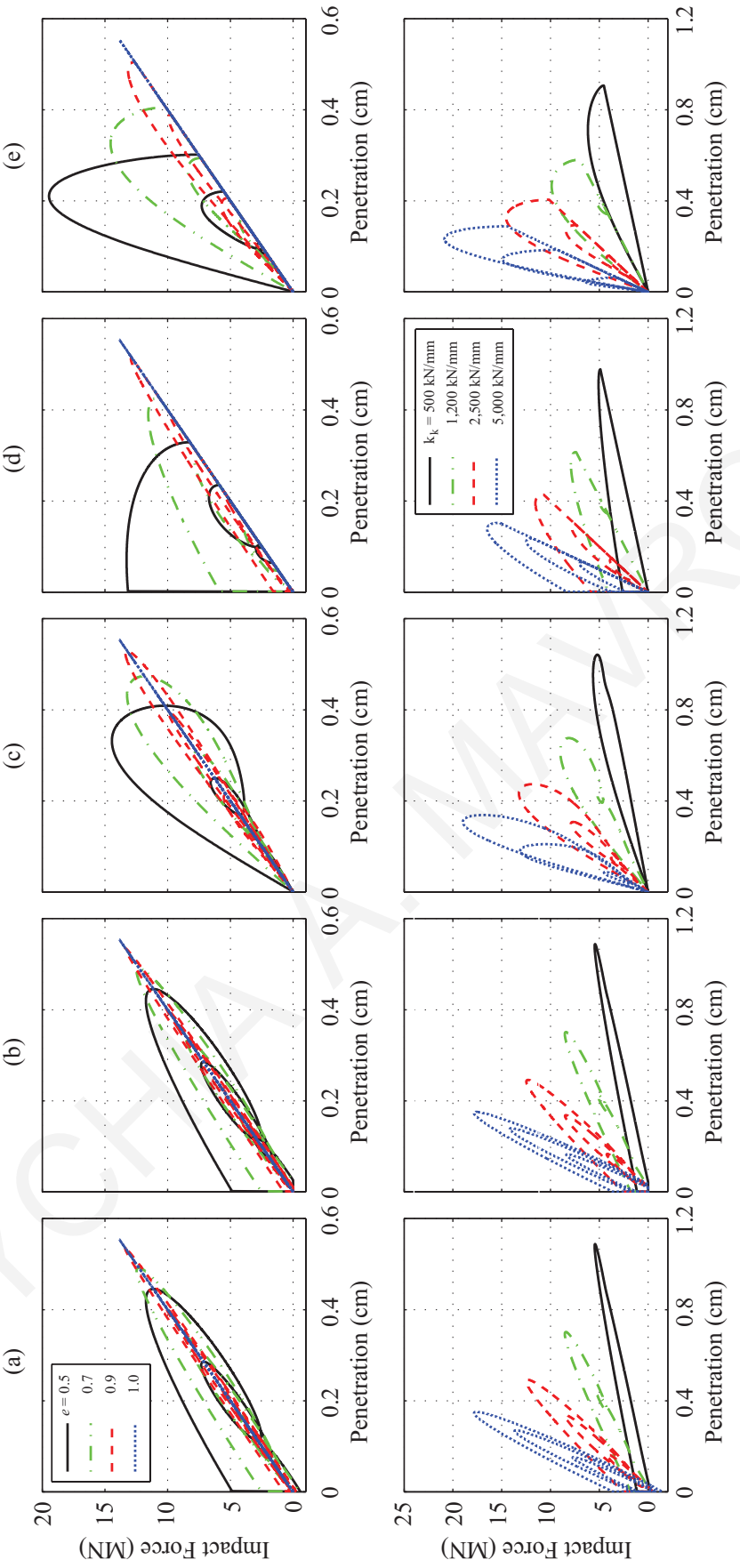

Figure 4.11 Comparison of the impact forces, under the Loma Prieta ground motion, considering the (a) classical Kelvin-Voigt, (b) Komodromos *et al.*, (c) Ye *et al.*, (d) Mahmoud and Jankowski, and (e) Pant and Wijeyewickrema impact models, for various impact parameters.

The enclosed areas between the loading and unloading curves of an impact-force *vs.* indentation curve, correspond to the amount of energy dissipated hysteretically during impact. A comparison of the amount of dissipated energy during impact reveals that the values computed by the modified contact models proposed by Ye *et al.,* Mahmoud and Jankowski, and Pant and Wijeyewickrema are higher than the dissipated energy during impact computed by the classical Kelvin-Voigt model.

The variation of the amplification of peak floor accelerations and peak interstory deflections of the examined base-isolated buildings that are computed considering the classical Kelvin-Voigt model in terms of the two impact parameters are now discussed. The peak response amplification of the 3- and the 5-story base-isolated building in terms of the coefficient of restitution under the five selected ground motions are presented in Figure 4.12(a) and Figure 4.13(a), respectively. The amplification factor is defined as the ratio of the maximum response considering the impact model when collisions occur, divided by the corresponding maximum response values without collisions. It is observed that the amplification of the peak floor accelerations shows a marginally increasing trend with a slight increase of the coefficient of restitution, reaching their maximum values when the impact becomes purely elastic. In general, the characteristics of the excitation influence considerably the magnitude of the amplification due to collisions. This finding is in line with the corresponding conclusion of Athanassiadou *et al.* (Athanassiadou *et al.*, 1994).

Figure 4.12(b) shows the normalized peak response of the 3-story building for the 4 modified impact models with respect to the classical Kelvin-Voigt model, with the same usage of the line-types as those used in the plots of Figure 4.12(a) regarding the imposed earthquake excitation. Similarly-organized results, as those presented previously in Figure 4.12(b) for the three-story base-isolated building, are provided in Figure 4.13(b) the five-story base-isolated building. The results indicate that the modification proposed by Komodromos *et al.* does not significantly change the peak structural response. On the other hand, the peak floor acceleration ratios, as estimated using the Mahmoud and Jankowski contact element, are overestimated, with respect to the corresponding response computed with the classical Kelvin-Voigt model, for e lower than 0.65 with an increasing tendency, reaching values up to about 20% for $e = 0.5$. For a coefficient of restitution between 0.65 and 1.0 the response is slightly underestimated. It should be noted that the range of underestimation depends on the values of the impact stiffness, something that is further investigated in the following paragraphs.

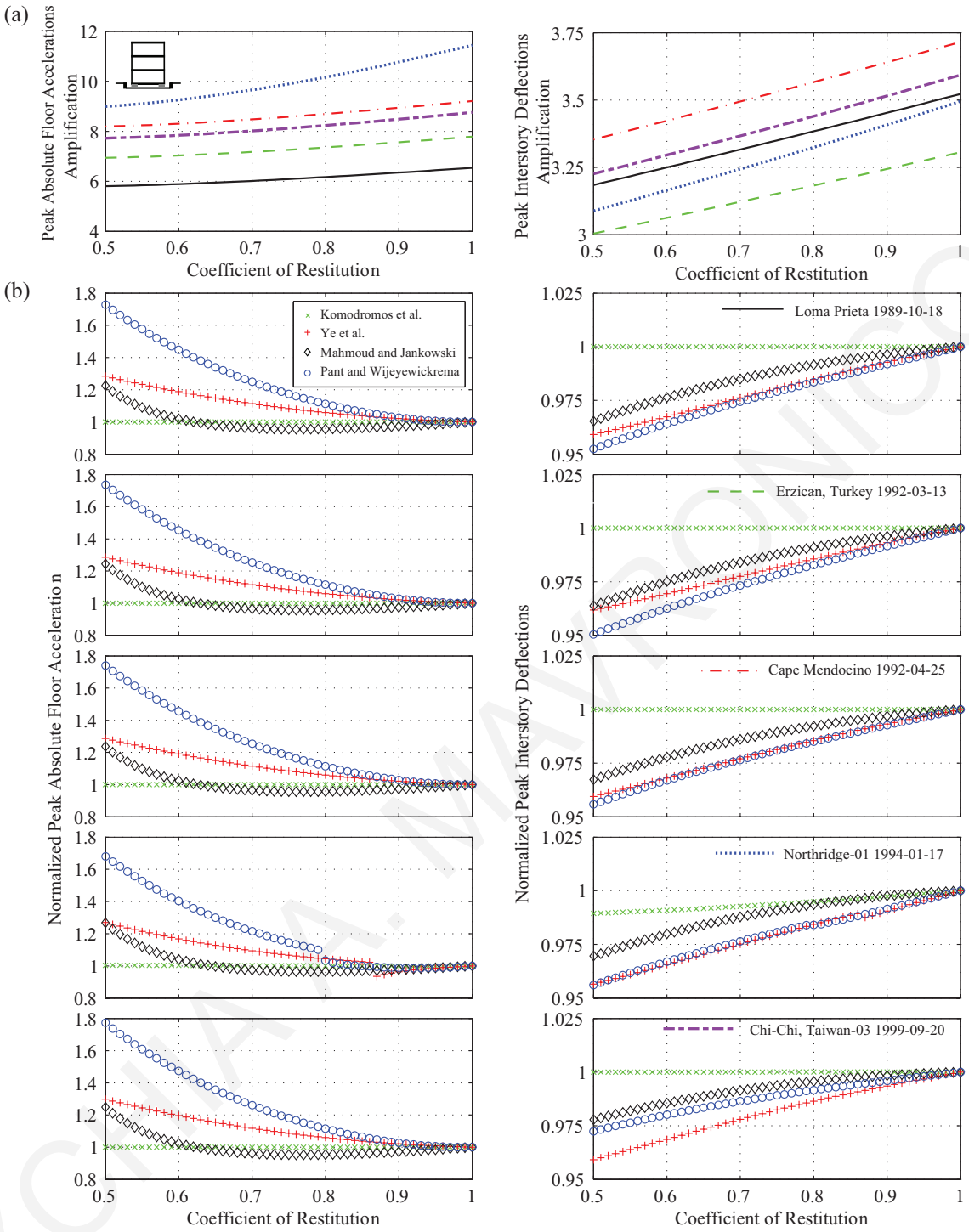

Figure 4.12 Amplifications of peak responses while considering the classical Kelvin-Voigt contact element, and (b) normalized peak responses while considering the 4 other impact models, in terms of the coefficient of restitution, under the 5 ground excitations.

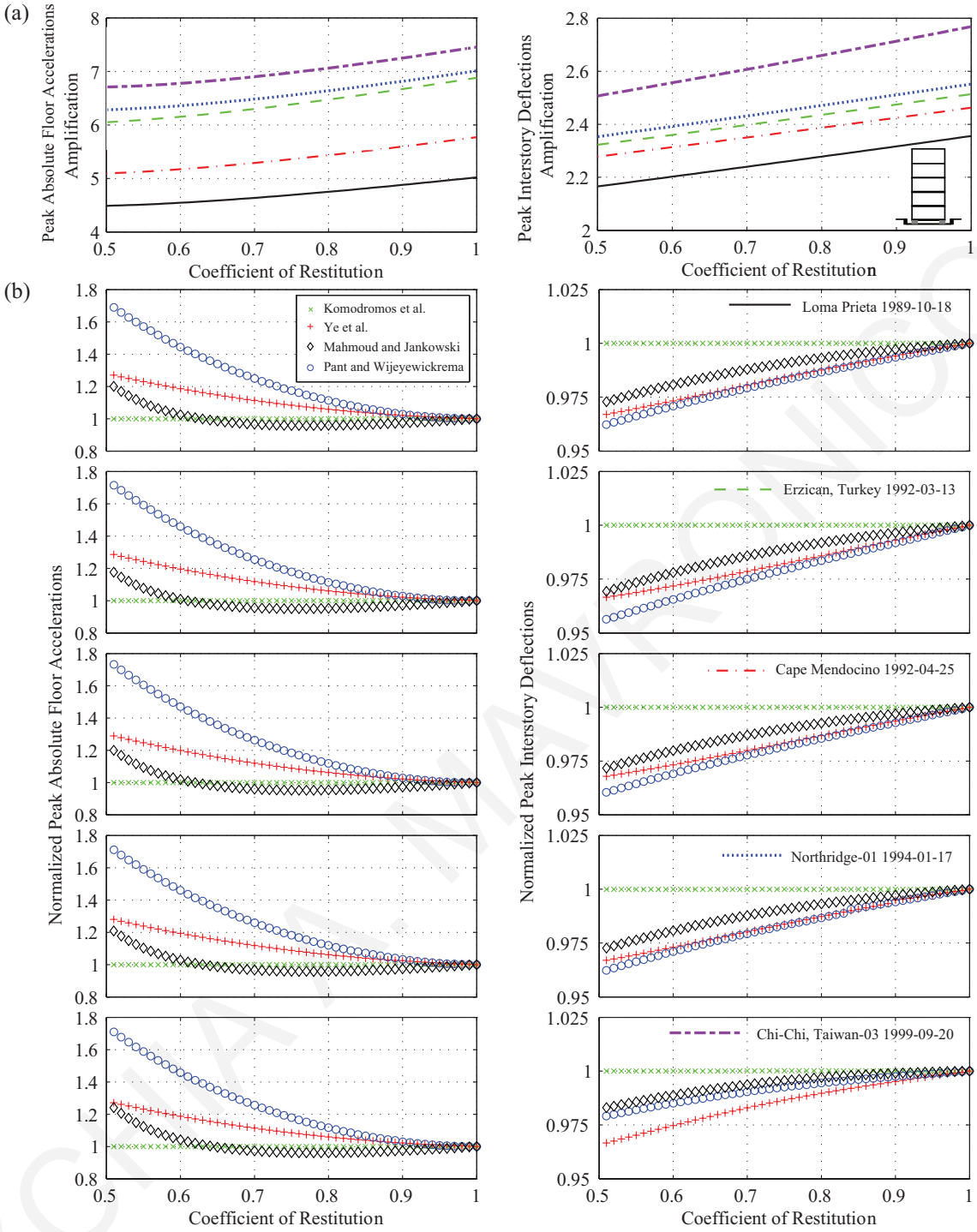

Figure 4.13 Peak response amplification considering the Kelvin-Voigt contact element for each of the five selected earthquake excitations, and (b) normalized peak response considering modified models, in terms of coefficient of restitution.

Furthermore, using Ye *et al.* and Pant and Wijeyewickrema models lead to a significant overestimation of the peak absolute floor acceleration, i.e. of the magnitude of 1.7 and 1.3 for e=0.5, respectively, as the coefficient of restitution influences more significantly the peak impact forces derived from those models than those derived from the classical Kelvin-Voigt model. Furthermore, the development of higher impact forces during

collision leads to higher peak floor accelerations. The capacity of the models to generate different magnitudes of peak forces during impact is evidenced in Figure 4.11. Moreover, the peak interstory deflections computed using the models proposed by Ye *et al.*, Mahmoud and Jankowski and Pant and Wijeyewickrema lead to an underestimation of the response up to 4% with respect to the corresponding peak responses computed using the classical Kelvin-Voigt model. This can be justified by considering that the corresponding amount of dissipated energy in the Kelvin-Voigt model for a given coefficient of restitution is the lowest among all modified models. For all cases, the underestimation of the peak interstory deflections tends to decrease with the increase of the value of the coefficient of restitution.

The peak absolute floor accelerations of the 3-story building due to pounding of the base-isolated building with the moat wall under each one of the 5 selected near-fault ground motions, which are presented in Figure 4.14(a), tend to increase for higher values of the impact stiffness, as it is varied from 500 to 5,000 $\mathrm{KN/mm}$. This finding suggests that the value of the impact stiffness should not be much higher than the stiffness of the superstructure to avoid large peak floor accelerations, which can be destructive for sensitive equipment that may be housed in the building, upon impact. Hence, potential incorporation of a flexible material with low impact stiffness between the building and the adjacent walls, which may act as a collision bumper, could be an effective measure to minimize the detrimental effects of impacts, under certain circumstances. Furthermore, the peak interstory drift amplifications increase rapidly when the impact stiffness increases up to the value of $650-800\,\mathrm{KN/mm}$, while for the rest of the examined range the amplifications of the peak response remain almost insensitive to this parameter. The simulation results also reveal that the excitation characteristics influence considerably the amplification of the peak response.

Figure 4.14(b) depicts the normalized peak responses computed using the 4 modified impact models, while considering as reference the classical linear viscoelastic impact model. The results indicate that using the Ye *et al.* and Pant and Wijeyewickrema models lead to an overestimation of the peak absolute floor accelerations, as the magnitudes of the contact forces during impact are much higher in those cases, while the response is slightly underestimated when the model of Mahmoud and Jankowski is used for the structural pounding. The computed results indicate that the overestimation of the amplification of the response tends to increase up to 15 and 33%, for the Ye *et al.* and Pant and

Wijeyewickrema models, followed by an exponential-type trend that tends to 10 and 20% increases, respectively.

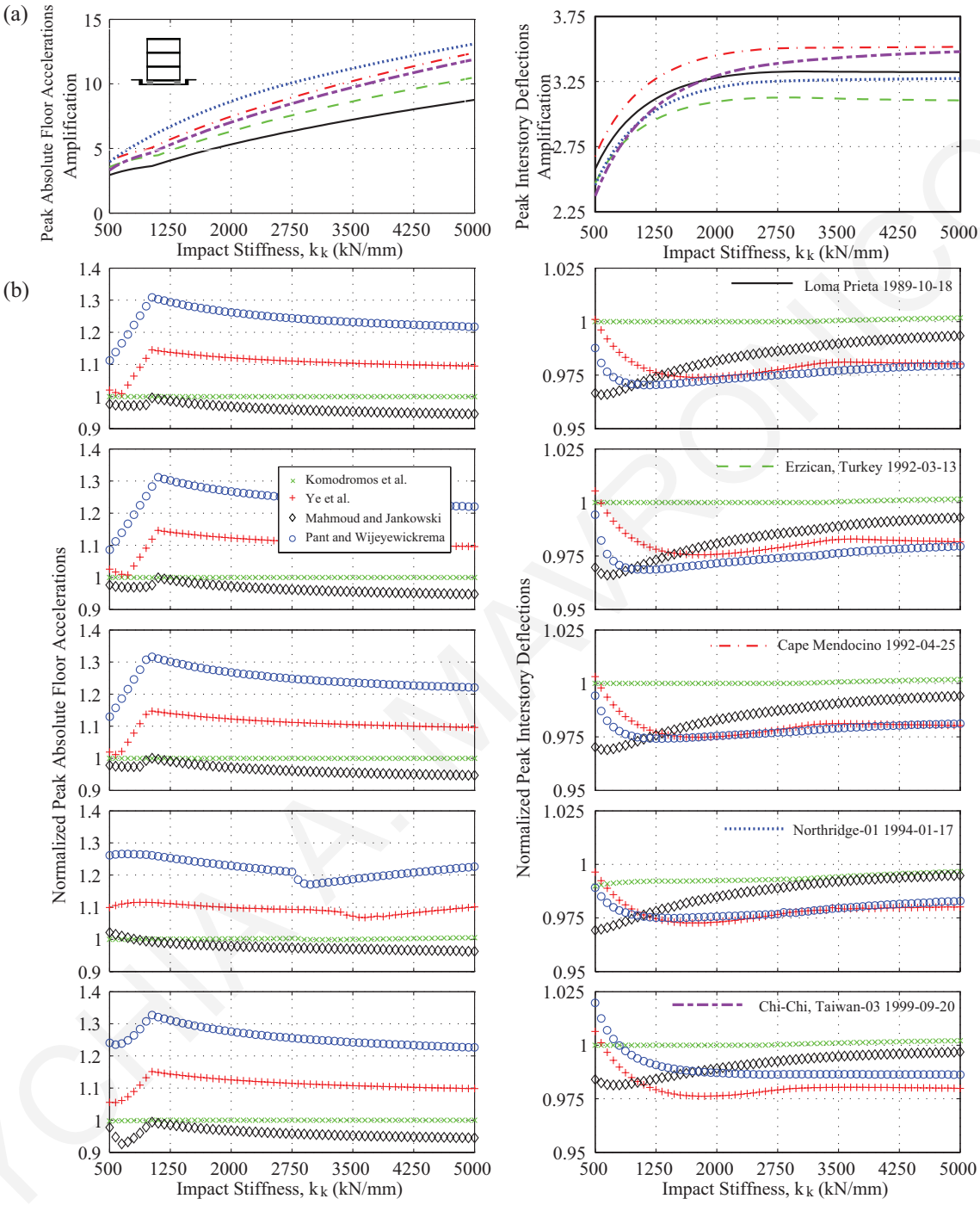

Figure 4.14 Influence of the impact stiffness on the (a) amplification of the peak response considering the Kelvin-Voigt contact element for each of the five selected earthquake excitations, and (b) normalized peak response considering the 4 modified linear impact models, for each excitation.

An examination of the response for each floor (Figure 4.15) shows that the kinks appearing in the variation of the normalized peak floor acceleration relate to an interchange between the floors that dominate the global structural response. More specifically, for low

k_k values the top floor appears to exhibit the peak floor acceleration, whereas as k_k increases the response is dominated by the base floor accelerations, which relates to the level of impact with the moat wall. It should be noted that the variation of the normalized floor accelerations depends on the impact parameters, but does not seem to be sensitive to the characteristics of the seismic excitation. Regarding the peak interstory drifts obtained considering the 4 modifications of the classical linear viscoelastic impact model, the computed peak interstory drifts are relatively underestimated, up to 2.5%, compared to the corresponding peak responses computed while using the classical Kelvin-Voigt impact model.

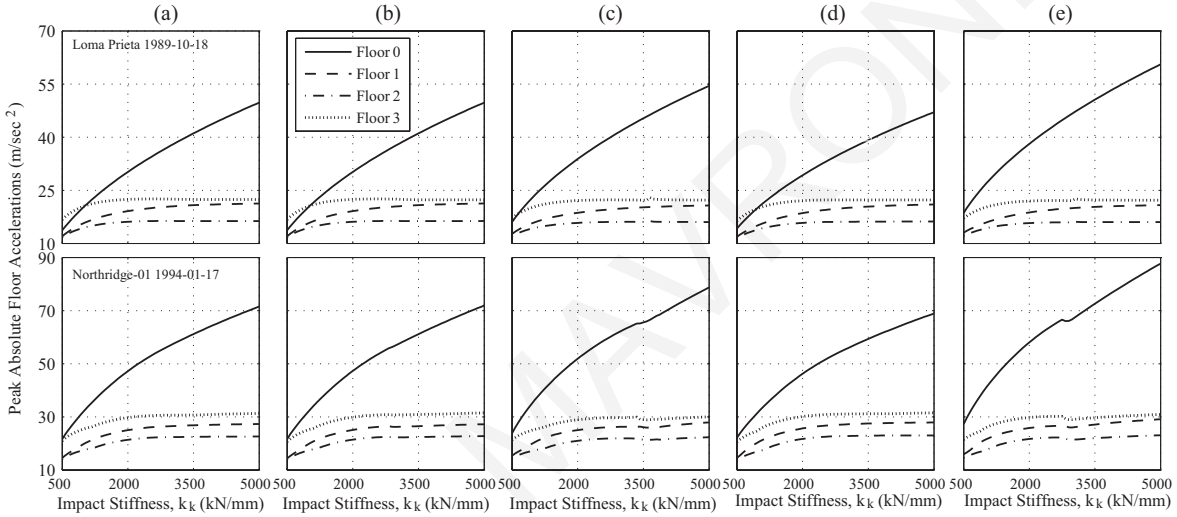

Figure 4.15 Influence of the impact stiffness on the peak floor accelerations considering (a) classical Kelvin-Voigt, (b) Komodromos *et al.,* (c) Ye *et al.*, (d) Mahmoud and Jankowski and (e) Pant and Wijeyewickrema impact models, under near-fault ground motions.

In the case of the 5-story base-isolated building, the corresponding normalized response values are of the same magnitude as in the case of the 3-story building, as shown in Figure 4.16(b). The variation of the peak impact force introduced when modified models are used as illustrated in the first row of Figure 4.11, can justify such a significant deviation of the peak absolute floor accelerations.

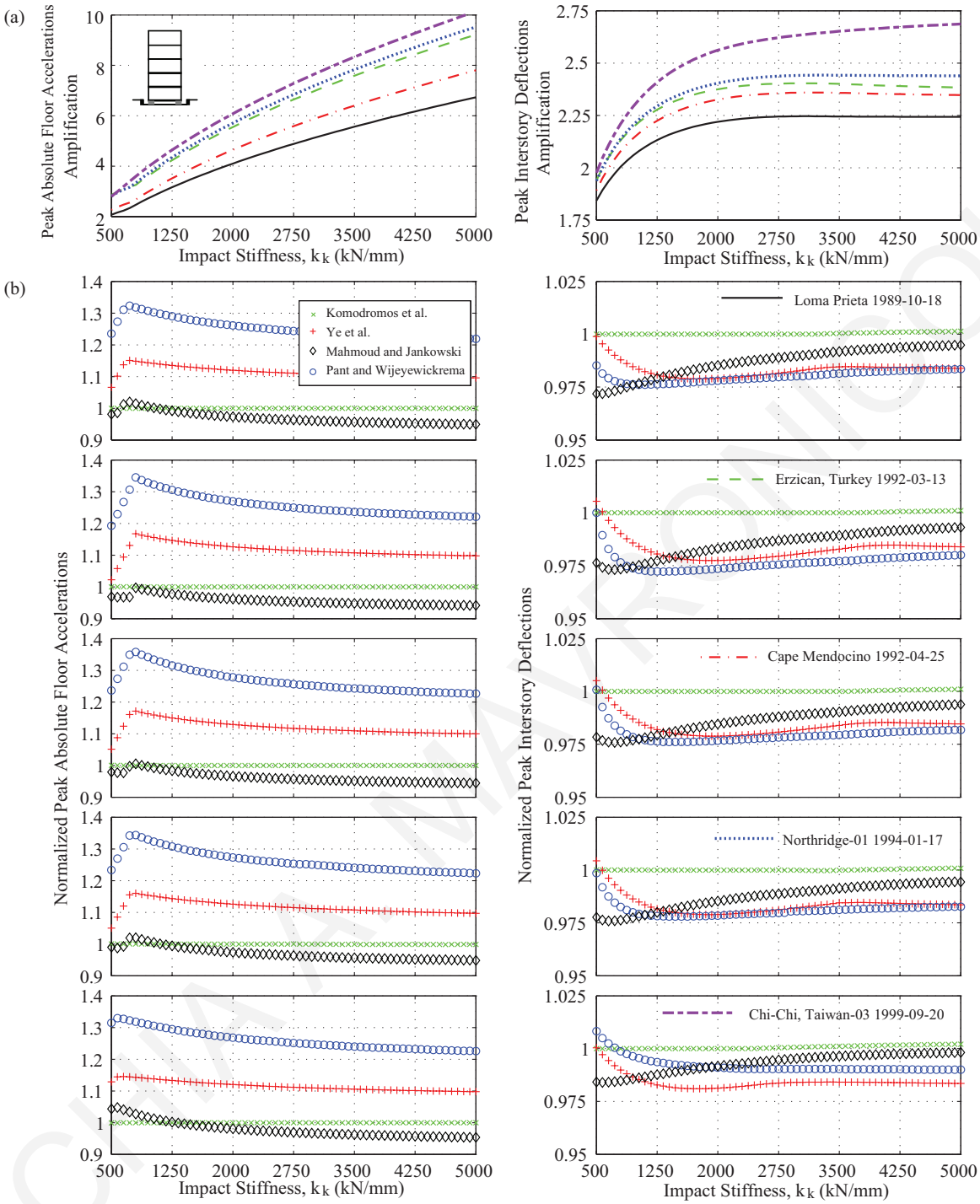

Figure 4.16 (a) Amplifications of the peak responses while considering the Kelvin-Voigt contact element, and (b) the normalized peak responses, while considering the 4 other impact models, in terms of the varying impact stiffness under the 5 ground excitations.

4.4.3 Influence of Isolation System Characteristics

In order to investigate the effect of the isolation characteristics on the amplification of the peak responses, the smooth Bouc-Wen model is used for the seismic isolation system with an isolation eigenperiod, T_b, which approximates the post-yield fundamental eigenperiod

of the 5-story base-isolated building, varying between 1.5 and 3.0 s. For all considered cases, a nonlinear time-history analysis is performed for the simulated MDOF base-isolated building for different combinations of the normalized characteristic strength (0.05 and 0.10) and the isolators' yield-displacements (1.0 and 2.5 cm). The impact parameters considered are those that have been used in the previous subsection.

Figure 4.17 presents the peak response amplifications considering the classical Kelvin-Voigt model, for all excitations considering gap size equal to 20 cm and assuming equal gaps on both sides of the buildings. The simulation results indicate that there is a substantial increase of the response amplification in the case of normalized characteristic strength equal to 5%, and, in general, the response amplification increases rapidly with the increase of the isolation period. It should be noted that a seismic gap of 20 cm would be sufficient to avoid any structural pounding during the Chi-Chi earthquake; thus, the corresponding amplification factors remain constant at 1.0. As already discussed, the more restricted the available seismic gap compared to the maximum unobstructed displacement under each one of the selected near-fault ground motions the higher the peak response amplification. Therefore, the previous finding can be justified considering that with the increase of the normalized characteristic strength the isolation system becomes relatively stiff, and the bearing displacement decreases, while the relative bearing displacements become higher for higher values of the isolation period.

Moreover, the case of having an isolator yield displacement equal to 2.5 cm is also examined and the respective results are illustrated in Figure 4.17(c). In general, it is observed that the response amplification reaches higher values compared to the corresponding response amplification considering yield displacement of 1.0 cm for the isolation system, as shown in Figure 4.16(a). Previous studies showed that the bearing displacements present a marginal increasing trend with the increase of the maximum isolator yield displacements (Matsagar and Jangid, 2004). Therefore, the results suggest that the earthquake characteristics in combination with the characteristics of the seismic isolation system and the difference between the available seismic gap and the maximum relative displacements of the building for each earthquake record seem to play a significant role in the severity of the structural impact and its consequences.

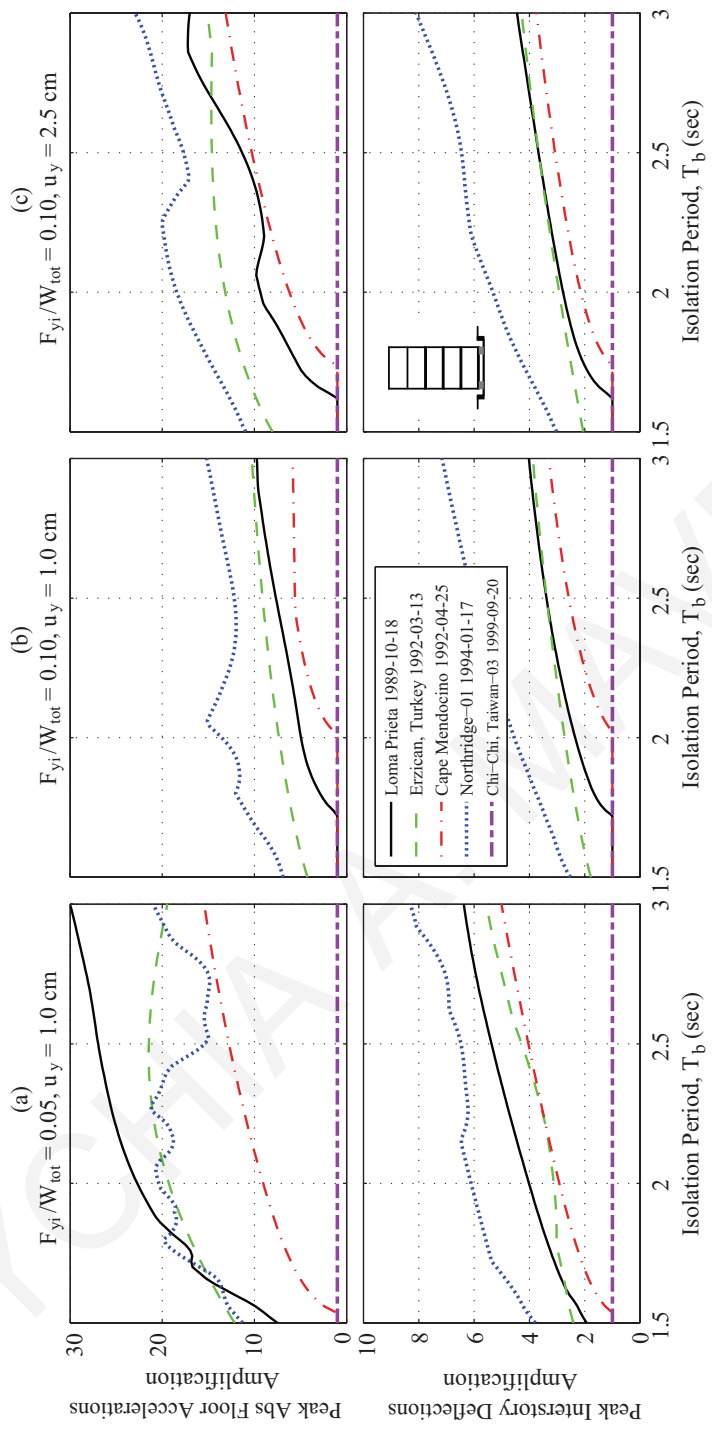

Figure 4.17 Amplifications of the peak floor accelerations and interstory deflections, using various seismic isolation systems, in terms of the period of the isolation system using the Kelvin-Voigt impact model, with a 20*cm* gap size at both sides.

The amplifications of the peak floor accelerations and interstory deflections, using the 4 aforementioned modifications of the classical Kelvin-Voigt, normalized with respect to the corresponding peak responses computed with the latter impact model are provided in Figure 4.18 and Figure 4.19, respectively. The variation in the normalized responses under the selected near-fault excitations is presented for different values of the normalized characteristic strengths and the isolators' yield displacements, in terms of the seismic isolation period.

The plots of Figure 4.18 indicate that the seismic isolation period, the normalized characteristic strength and the yield-displacement of the isolation system do not considerably influence the normalized peak floor acceleration. Furthermore, the normalized peak response ratios do not seem to be affected by the difference between the available gap size and the maximum response displacement of the corresponding MDOF system. Additionally, the Kelvin-Voigt impact model and the modified linear viscoelastic model proposed by Komodromos *et al.*, lead to almost identical responses for the absolute floor accelerations, while when the contact element proposed by Mahmoud and Jankowski is used, the response is slightly underestimated compared to the former two models. On the other hand, the peak response obtained using Ye *et al.* and the Pant and Wijeyewickrema models are much higher than those obtained using the classical Kelvin model, fluctuating around 10 and 25% higher, respectively.

The variations of the normalized interstory deflections for various characteristics of the seismic isolators are shown in Figure 4.19. The peak responses considering the classical Kelvin-Voigt model and the contact elements proposed by Komodromos *et al.* are, in general, identical to each other. Interestingly, the simulation results indicate that the underestimation of the normalized peak interstory drifts considering the rest of the impact models, tend to increase as the isolation period increases. The results indicate that the difference between the seismic gap and the maximum relative displacement of the corresponding MDOF system influence the variation of the normalized interstory deflections.

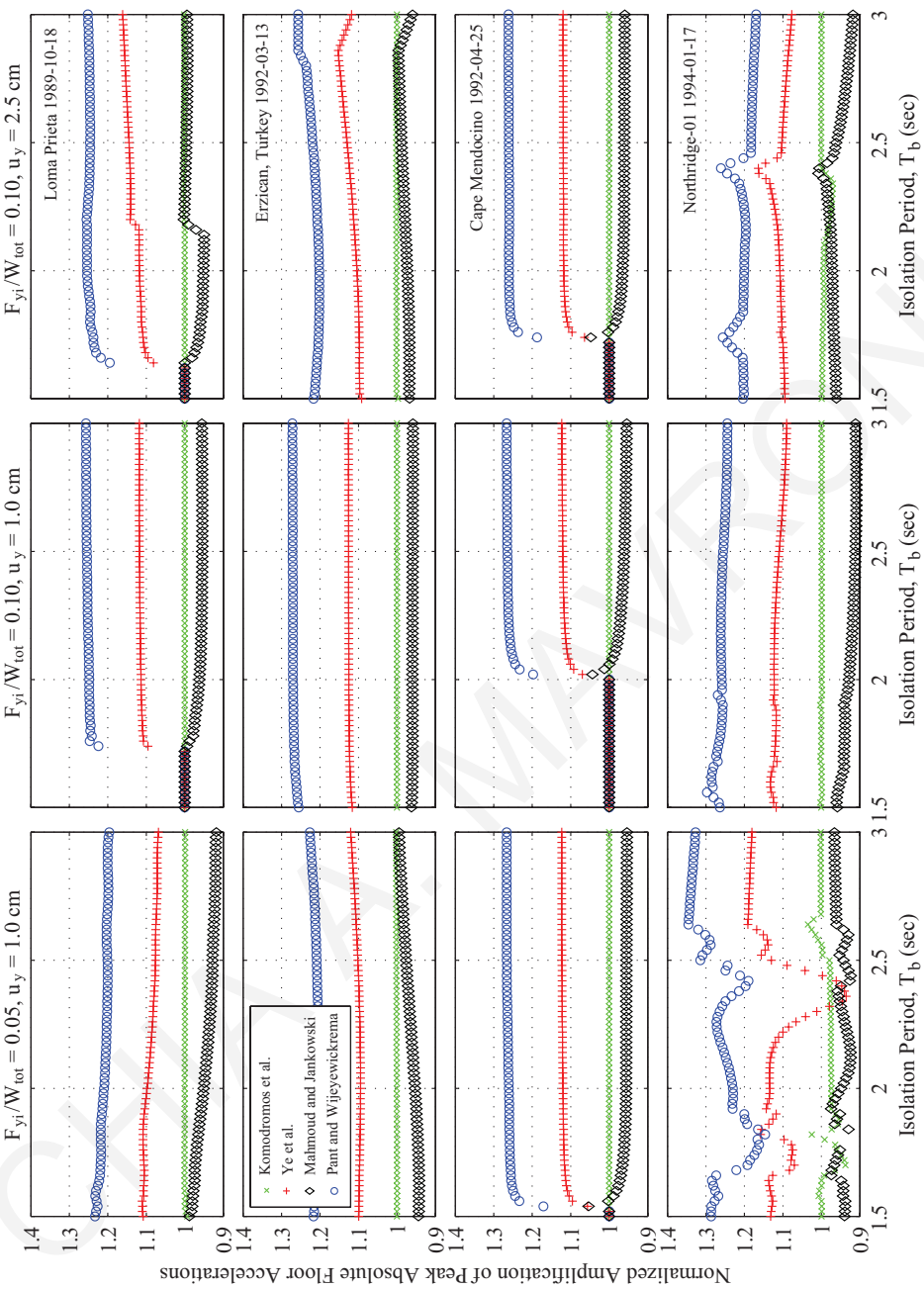

Figure 4.18 Normalized peak absolute floor accelerations using the four impact models with respect to the corresponding peak responses using the classical Kelvin-Voigt impact model, in terms of the isolation period.

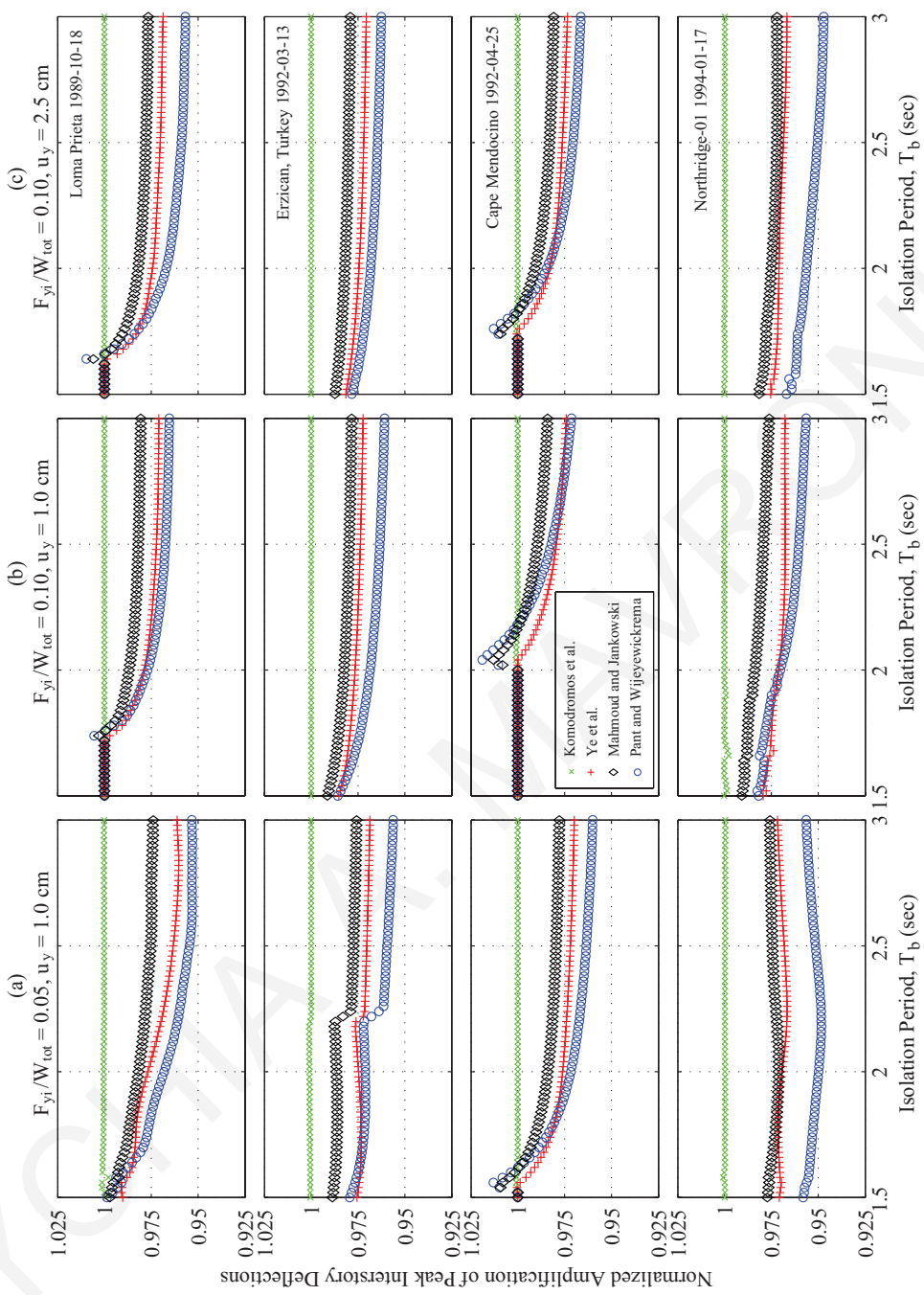

Figure 4.19 Peak interstory deflections, using the modified linear impact models, normalized to the corresponding peak response obtained with the classical Kelvin-Voigt impact model, in terms of the isolation period.

4.5 Major Findings

The seismic performance of base-isolated buildings pounding against the surrounding moat wall has been evaluated using near-fault pulse-like ground motions. Four recently proposed variations of the classical linear viscoelastic impact model have been compared considering as a base model the classical Kelvin-Voigt impact model. The relative performance of the base-isolated structure has been evaluated based on the peak absolute floor accelerations and maximum interstory drifts.

The presented results refer to typical base-isolated buildings with specific structural characteristics under different cases of gap sizes and characteristics of the isolators, as well as different impact parameters, subjected to a range of different near fault excitations. From the trends of the computed results of the current study the following conclusions have been drawn:

- The impact model proposed by Mahmoud and Jankowski aimed at eliminating the tensile force just before separation of the colliding bodies, while reassessing the relationship between ξ_k and e. However, after this improvement, the sudden jump at the beginning of impact may still appear in the model.
- The minor modification proposed by Komodromos *et al.* of the linear viscoelastic impact model does not influence considerably the peak response values.
- The maximum impact forces obtained using the impact models proposed by Ye *et al.* and Pant and Wijeyewickrema are much higher than those obtained using the classical linear viscoelastic impact model with the formulas provided by Anagnostopoulos, leading to a relative overestimation of the peak absolute floor accelerations.
- The absolute floor accelerations for all modified models appear to be a function of the impact stiffness and the coefficient of restitution. When either the impact stiffness or the coefficient of restitution is reduced, the deviations of the peak response tend to increase.
- The maximum interstory deflections of the building are, in general, slightly underestimated when the modified impact models are used. Those response deviations are related to the capacity of the models to dissipate energy in various extends and, in general, tend to increase as the available gap size and the coefficient of restitution decrease.

- The characteristics of the seismic excitation and the properties of the isolators do not seem to influence the variation of the normalized peak responses.

CHAPTER 5 STRUCTURAL POUNDING IN THREE-DIMENSIONS: MODELING CONSIDERATIONS

5.1 Introductory Remarks

The problem of earthquake-induced pounding has been the subject of great scientific interest. While several recent numerical studies have quantified the effects of seismic pounding of buildings, the majority of researchers simulate the problem in two-dimensions (Dimitrakopoulos et al., 2009; Jankowski and Mahmoud, 2015; Komodromos, 2008; Mahmoud and Jankowski, 2010; Matsagar and Jangid, 2003; Mavronicola et al., 2015a, 2015b, 2016; Polycarpou et al., 2015a; Ye et al., 2009a), in an attempt to avoid the complexities associated with the 3D problem and the consequently excessive computational cost. However, the effect of crucial factors, such as the consideration of both orthogonal seismic components, friction phenomena that occur during pounding, eccentric impacts, irregularities, or asymmetries in the plan view of the colliding structures, which may excite the torsional vibration of a building and further increase the possibility of impacts during earthquakes, are essential parameters that can only be considered through 3D simulations.

The previous chapters have concentrated on the modeling and simulation of earthquake-induced collisions in the simplified 2D analysis, omitting the effect of important factors that are directly related to the spatial movement of the structures and should also be taken into account. The remaining chapters of this thesis are devoted to 3D modeling and simulation of earthquake-induced collisions. This chapter begins with a review of the relevant available research studies in the scientific literature followed by the presentation of the modeling methodology that is adopted in this thesis for modeling impact in three-dimensions.

5.2 Literature Review

While the majority of research studies on structural impacts approach the problem in the simplified 2D domain, there is a number of recent research works that extent the simulation in the more realistic 3D space and which are reviewed below.

Matsagar and Jangid (Matsagar and Jangid, 2010) investigated the seismic response of a single-story asymmetric structure supported on various base isolation systems during impact with adjacent structures. The adjacent structures, surrounding the base-isolated structure on all four sides, were modeled using springs and dashpots. The torsional impact responses of isolated structures were studied under the variation of important system parameters such as the gap size, the stiffness of adjacent structures, the flexibility of the superstructure and different eccentricities of the base-isolated structure. Based on the findings of that research work, the superstructure acceleration increases and the base displacement decreases when impact with adjacent structures occurs. Furthermore, it was observed that superstructure accelerations increase with an increase of the isolation gap up to a certain value, decreasing thereafter. The effects of impact were found to be severe for systems with flexible superstructures, stiffer adjacent structures and increased eccentricities.

Jankowski (Jankowski, 2009, 2012) simulated a case of pounding between the Olive View Hospital main building and one of its independently standing stairway towers during the San Fernando earthquake of 1971 using commercial software. In that work, a detailed 3D pounding-involved response analysis of two adjacent structures had been conducted using the finite element method with a non-linear model of material behavior. The results revealed the significant influence of pounding in the spatial response of the structure. Although this approach provides accuracy in the results, it lacks the desired efficiency, especially when performing parametric studies where large numbers of analyses are required.

Uz and Hadi (Uz and Hadi, 2011) carried out a parametric investigation of pounding involved response of two base-isolated buildings of unequal heights. Nonlinear analyses were used, modeling the structures with inelastic MDOF lumped mass systems. In addition, the nonlinear viscoelastic model to assess the proper impact force during collisions was incorporated regarding the 3D pounding between two adjacent four- and three- story buildings. According to that research work, pounding of the structures during a ground motion excitation has a significant influence on the behavior of the lighter building in the

longitudinal direction, leading to a substantial amplification of its response. In contrast, the computed results of the response analysis indicated that the behavior of the heavier building in the longitudinal, transverse, and vertical directions is practically unchanged by potential pounding of structures.

Sato *et al.* (Sato *et al.*, 2011) conducted a series of full-scale shaking table tests using the E-Defense shaking table facility on a base-isolated four-story reinforced concrete hospital structure. A variety of furniture items, medical appliances and service utilities were placed on the hospital specimen in a realistic manner. In that test, natural rubber bearings with a parallel U-shaped steel damper (NRB+U) were adopted, as well as high-damping rubber bearings (HDRB), with which the bearing itself dissipates energy. For the NRB+U case, the clearance between the superstructure and surrounding blocks was set at 500 mm, while for the HDRB it was set at 300 mm, intending to allow slight pounding during the test. In fact, pounding occurred once, but the velocity at the instant of pounding was close to zero ($0.06\,\mathrm{m/s}$). The floor acceleration increase was about twice as large as the value observed when no pounding occurred. The enhanced acceleration, however, lasted only for 0.2 s, and it had no effect on responses except for the following case; a high-oxygen pressure unit placed on the first floor moved horizontally by 20 mm by this pounding.

The effects of seismic pounding on the structural performance of a base-isolated reinforced concrete building were investigated by Pant and Wijeyewickrema (Pant and Wijeyewickrema, 2012), aiming to evaluate the influence of adjacent structures and the separation between structures on the pounding response. In particular, the seismic pounding of a typical four-story base-isolated reinforced concrete building with retaining walls at the base and with a four-story fixed-base building was studied. 3D finite element analyses of the base-isolated building were carried out considering various seismic excitations. It was found that the structural performance of the building was substantially influenced by the pounding. The investigated base-isolated building showed good resistance against shear failure and the predominant mode of failure due to pounding was flexural.

Extensive shake table tests were conducted by Masroor and Mosqueda (Masroor and Mosqueda, 2012) on fixed-base and base-isolated structures with and without a moat wall for comparison purposes, under extreme ground motions. The effect of various moat wall properties was investigated, including stiffness and gap distance. It was demonstrated that the response amplification and resulting damage depends on the gap distance, moat wall

properties, and impact velocity. Acceleration amplified significantly at the base level where pounding occurred. Peak interstory drift ratios increased uniformly at all stories for softer pounding experiments with more flexible walls or lower impact velocities. As the pounding forces increased, increased drifts were observed throughout the structure with substantial larger amplifications in upper floors.

Masroor and Mosqueda (Masroor and Mosqueda, 2013a) proposed an new impact element considering moat wall flexibility, based on impact theory and observations during experimental simulations. Sensitivity analysis conducted showed that the simplified impact model could provide reasonable results considering uncertainty in assigning model parameters. The contact force generated depended on impact velocity, geometry, and material properties at the contact surface, and the global dynamic characteristic of the moat wall. The simulations showed that the generated contact forces can induce yielding in the superstructure and amplify the response acceleration at all stories of the building,

Pant and Wijeyewickrema (Pant and Wijeyewickrema, 2014) considered a 3D finite element model of a code-compliant four-story building in order to investigate its seismic performance under bidirectional far-fault non-pulse-like ground motions and near-fault pulse-like ground motions scaled to represent two levels of shaking. Seismic pounding of the building with the retaining walls at the base was simulated using a newly developed special purpose contact element that accounts for friction. Nonlinear behavior of the superstructure as well as the isolation system was considered, while contact elements were used only at the corner nodes of the base slab. The performance of the building was evaluated separately for far-fault non-pulse-like ground motions and near-fault pulse-like ground motions, which were scaled to represent two levels of shaking: the design earthquake level and the risk-targeted maximum considered earthquake (MCE_R) level. Nonlinear time-history analyses were carried out considering lower bound as well as upper bound properties of the isolators. The influence of the separation distance between the building and the retaining walls at the base was also investigated. In the case of seismic pounding, MCER-level near-fault motions were found to be detrimental, where the effect of pounding was mostly concentrated at the first story. In addition, it was determined that considering unidirectional excitation instead of bidirectional excitation for the MCE_R-level near-fault motions provided highly unconservative estimates of superstructure demands.

Finally, Polycarpou *et al.* (Polycarpou *et al.*, 2014) presented an efficient methodology for numerically simulating in three-dimensions adjacent buildings that may experience pounding during strong earthquakes. The proposed approach to the numerical problem of

spatial impact modeling that does not require the *a priori* determination of the contact points, taking also into account the geometry at the vicinity of an impact.

5.3 Mathematical Representation

The aforementioned methodology proposed by Polycarpou *et al.* (Polycarpou *et al.*, 2014) is employed in this research work, considering the buildings as 3D MDOF systems with shear-type behavior for their stories in the horizontal directions. The slab at each floor level of the superstructure is represented by a rigid diaphragm that is mathematically simulated as a convex polygon, while the masses are considered to be lumped at the floor levels, having three dynamic DOFs, i.e. two translational, parallel to the horizontal global axes, and one rotational along the vertical axis. Therefore, considering ground excitations only in the horizontal directions, which is the most important case, no displacement occurs in the vertical direction, since the translational dynamic DOF of the structure refer only to horizontal planes. Accordingly, it is assumed that the impact forces occur only in horizontal planes.

5.3.1 Stiffness Matrix

The global stiffness matrix is composed, based on the 3×3 stiffness matrices of the floors, which are, in turn, composed by superposing the 3×3 stiffness matrices of the columns of the corresponding floors. Let us consider a typical plan of a floor i ($i = 1,...,N$) and a column j ($j = 1,...,n$), where n is the total number of columns at the floor i while N is the total number of stories of the simulated building (Figure 5.1). The horizontal stiffness values of a column c_{ij} in the two orthogonal directions (*I* and *II*) parallel to the horizontal global axes (*X* and *Y*) are given by the following expressions:

$$\begin{aligned} k_{cj}^{I} &= k_{1,cj} \cdot \cos^2\left(r_{cj}\right) + k_{2,cj} \cdot \sin^2\left(r_{cj}\right) \\ k_{cj}^{II} &= k_{1,cj} \cdot \sin^2\left(r_{cj}\right) + k_{2,cj} \cdot \cos^2\left(r_{cj}\right) \end{aligned} \quad \text{where} \quad \begin{aligned} k_{1,cj} &= 12\,E_j I_{22,j} / h_j^3 \\ k_{2,cj} &= 12\,E_j I_{11,j} / h_j^3 \end{aligned} \qquad (5.1)$$

In the above equations, r_{cj} is the rotation angle of the principal axes (1 and 2) of the section of the column with respect to the global axes, $k_{1,cj}$ and $k_{2,cj}$ are the horizontal stiffness terms in the principal directions of the column j, E_j is the Young's modulus, $I_{11,j}$ and $I_{22,j}$ are the moments of inertia of the cross section of the column j along the axes 1 and 2, while h_j is the height of the column. The torsional stiffness of the column is defined as:

$$k_{cj}^{\theta} = G_j \cdot J_{c,j} / h_i \tag{5.2}$$

where G_j is the shear modulus and $J_{c,j}$ is the torsional constant of the column's j section.

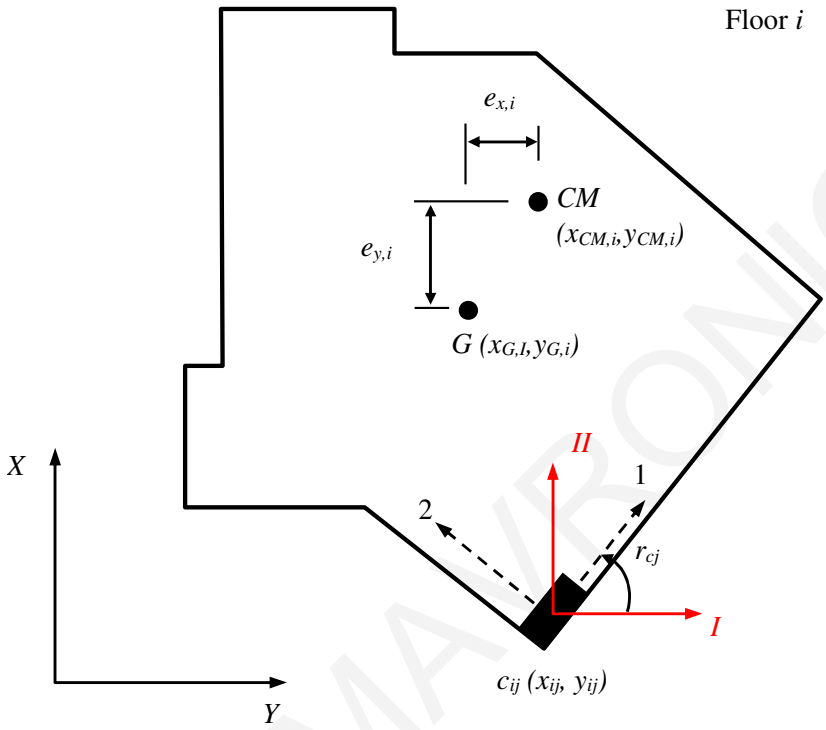

Figure 5.1 Representation of a typical floor diaphragm as a polygon, with the dynamic degrees of freedom at the center of the mass, and the location and orientation of a typical column.

Accordingly, the local stiffness matrix of the column is:

$$\overline{k}_{cj}^{'} = \begin{bmatrix} k_{cj}^{I} & 0 & 0 \\ 0 & k_{cj}^{II} & 0 \\ 0 & 0 & k_{cj}^{\theta} \end{bmatrix} \tag{5.3}$$

At floor i, the horizontal displacements at the head of a column c_{ij} in the local coordinate system (axes I and II) can be expressed in terms of global coordinates (axes X and Y) using the following transformation:

$$\overline{d}_{ij}^{\,local} = \overline{T}_{ij} \cdot \overline{d}_i^{\,global} \quad \Leftrightarrow \quad \begin{bmatrix} u_{ij} \\ v_{ij} \\ \theta_{ij} \end{bmatrix} = \begin{bmatrix} 1 & 0 & -y_{ij} \\ 0 & 1 & x_{ij} \\ 0 & 0 & 1 \end{bmatrix} \cdot \begin{bmatrix} u_i \\ v_i \\ \theta_i \end{bmatrix} \tag{5.4}$$

where $\overline{T}_{ij}$ is the transformation matrix, which can be used to express the local stiffness matrix of the column *j* in global coordinates as follows:

$$\overline{k}_{cj} = \overline{T}_{ij}^{T} \cdot \overline{k}_{cj}^{'} \cdot \overline{T}_{ij} = \begin{bmatrix} k_{cj}^{I} & 0 & -y_{ij} \cdot k_{cj}^{I} \\ 0 & k_{cj}^{II} & x_{ij} \cdot k_{cj}^{II} \\ -y_{ij} \cdot k_{cj}^{I} & x_{ij} \cdot k_{cj}^{II} & k_{cj}^{\theta\theta} \end{bmatrix} \tag{5.5}$$

where $k_{cj}^{\theta\theta} = y_{ij}^{2} \cdot k_{cj}^{I} + x_{ij}^{2} \cdot k_{cj}^{II} + k_{cj}^{\theta}$.

Therefore, the 3×3 stiffness matrix of the whole story is formed by summarizing the stiffness matrices of all columns of the story as calculated using Equation (5.5). The composition of the $3N \times 3N$ global stiffness matrix of the building is performed by superposing the N stiffness matrices of the stories and the general form of the stiffness matrix with respect to the origin of the global coordinate system is provided as follows:

$$\overline{K} = \begin{bmatrix} \overline{k}_1 + \overline{k}_2 & -\overline{k}_2 & 0 & 0 & \cdots & 0 \\ -\overline{k}_2 & \overline{k}_2 + \overline{k}_3 & -\overline{k}_3 & 0 & \cdots & 0 \\ 0 & -\overline{k}_3 & \overline{k}_3 + \overline{k}_4 & -\overline{k}_4 & 0 & \vdots \\ 0 & 0 & \overline{k}_4 & \ddots & \cdots & 0 \\ \vdots & \vdots & \vdots & \vdots & \overline{k}_{N-1} + \overline{k}_N & -\overline{k}_N \\ 0 & 0 & \cdots & 0 & -\overline{k}_N & \overline{k}_N \end{bmatrix} \tag{5.6}$$

In case of considering a Bouc-Wen model to simulate the non-linear behavior of structural components, the stiffness matrix of the system is composed after checking the status of each individual column, based on the deformation of the column and the sign of the relative velocity at the particular time instance. Therefore, when a bilinear model is selected for one or more seismic isolators of the structure the above procedure for the determination of the global stiffness matrix of the system is performed at each time step.

5.3.2 Mass Matrix

The mass of each floor is considered to be concentrated at a specific point, which is called "center of mass", and coincides with the center of gravity of the floor when the mass is evenly distributed in plan. In general, the position of the center of mass is defined by the eccentricities $e_{x,i}$ and $e_{y,i}$ in the *X* and *Y* directions, respectively, in relation to the coordinates $x_{G,i}$ and $y_{G,i}$ of the floor's center of gravity (Figure 5.1). The mass matrix of the floor *i*, with respect to its center of mass, is:

$$\overline{m}_i^{CM} = \begin{bmatrix} m_i & 0 & 0 \\ 0 & m_i & 0 \\ 0 & 0 & J_{CM,i} \end{bmatrix} \tag{5.7}$$

where m_i is the total mass of the story and $J_{CM,i}=m_i \cdot J_{G,i}+m_i\left(e_{x,i}^2+e_{y,i}^2\right)$ is the mass polar moment of inertia of the floor's slab with respect to its center of mass and expressed in relation to the corresponding polar moment of inertia at the center of gravity $J_{G,i}$. Thus, the corresponding mass matrix of the floor, expressed in the global coordinate system, is:

$$\overline{m}_i = \overline{T}_{CM,i}^T \cdot \overline{m}_i^{CM} \cdot \overline{T}_{CM,i} = \begin{bmatrix} m_i & 0 & -\left(y_{G,i}+e_{y,i}\right)m_i \\ 0 & m_i & \left(x_{G,i}+e_{x,i}\right)m_i \\ -\left(y_{G,i}+e_{y,i}\right)m_i & \left(x_{G,i}+e_{x,i}\right)m_i & J_{CMi,00} \end{bmatrix} \tag{5.8}$$

where $J_{CMi,00} = m_i \cdot J_{CM,i} + m_i\left(x_{CM,i}^2 + y_{CM,i}^2\right) = m_i \cdot J_{CM,i} + m_i\left[\left(x_{Gi}+e_{Xi}\right)^2 + \left(y_{Gi}+e_{Yi}\right)^2\right]$

$$\overline{T}_{CM,i} = \begin{bmatrix} 1 & 0 & -\left(y_{G,i}+e_{y,i}\right) \\ 0 & 1 & \left(x_{G,i}+e_{x,i}\right) \\ 0 & 0 & 1 \end{bmatrix} \tag{5.9}$$

Therefore, the *3N×3N* global mass matrix has the following diagonal form:

$$\overline{\overline{M}} = \begin{bmatrix} m_1 & 0 & \dots & 0 \\ 0 & m_2 & \dots & 0 \\ \vdots & \vdots & \ddots & \vdots \\ 0 & 0 & \dots & m_N \end{bmatrix} \tag{5.10}$$

5.3.3 Damping Matrix

The corresponding $3N\times3N$ damping matrix of the system is computed assuming Rayleigh damping, based on specifying the values of two viscous damping ratios ζ_i and ζ_j at the corresponding eigenfrequencies of the system ω_i and ω_j:

$$\overline{C} = \alpha \cdot \overline{\mathrm{M}} + \beta \cdot \overline{\mathrm{K}} \qquad \text{where} \qquad \begin{bmatrix} \alpha \\ \beta \end{bmatrix} = \begin{bmatrix} 1/(2\omega_i) & \omega_i/2 \\ 1/(2\omega_j) & \omega_j/2 \end{bmatrix}^{-1} \cdot \begin{bmatrix} \zeta_i \\ \zeta_j \end{bmatrix} \tag{5.11}$$

5.4 Equations of Motions

The equations of motion of each simulated building can be expressed in matrix form as follows:

$$\overline{M}\cdot\ddot{\overline{U}}(t)+\overline{C}\cdot\dot{\overline{U}}(t)+\overline{K}\cdot\overline{U}(t)+\overline{F}_{imp}=-\overline{M}\left[\overline{I}_L\cdot\ddot{u}_g^L(t)+\overline{I}_T\cdot\ddot{u}_g^T(t)\right] \tag{5.12}$$

where $\overline{M}$, $\overline{C}$ and $\overline{K}$ are the mass, damping and stiffness matrices, respectively; $\overline{U}(t)$ is the vector of the relative displacements in the global coordinate system at time t; $\overline{F}_{imp}$ is the vector of the computed impact forces, acting on each DOF, while $\overline{I}_L$ and $\overline{I}_T$ are the influence vectors coupling the DOFs of the structure to the two ground motion components $\ddot{u}_g^L(t)$ and $\ddot{u}_g^T(t)$ in the longitudinal and transverse directions, respectively.

The influence vectors for the two horizontal components are provided by the following expressions:

$$\overline{I}_L=\left[\overline{I}_{L,1}\quad\overline{I}_{L,2}\quad\ldots\quad\overline{I}_{L,n}\right],\qquad \overline{I}_T=\left[\overline{I}_{T,1}\quad\overline{I}_{T,2}\quad\ldots\quad\overline{I}_{T,n}\right]$$

$$\textit{where}\quad \begin{aligned}\overline{I}_{L,1}&=\overline{I}_X\cdot\cos\theta+\overline{I}_Y\cdot\sin\theta\\ \overline{I}_{T,1}&=-\overline{I}_X\cdot\sin\theta+\overline{I}_Y\cdot\cos\theta\end{aligned}\quad\textit{and}\quad \begin{aligned}\overline{I}_X&=\left[1\quad 0\quad 0\right]^T\\ \overline{I}_Y&=\left[0\quad 1\quad 0\right]^T\end{aligned} \tag{5.13}$$

The excitation angle θ is the angle between the principal directions L and T of the excitation orthogonal components, with respect to the global axes of the system X and Y, respectively (Figure 5.2).

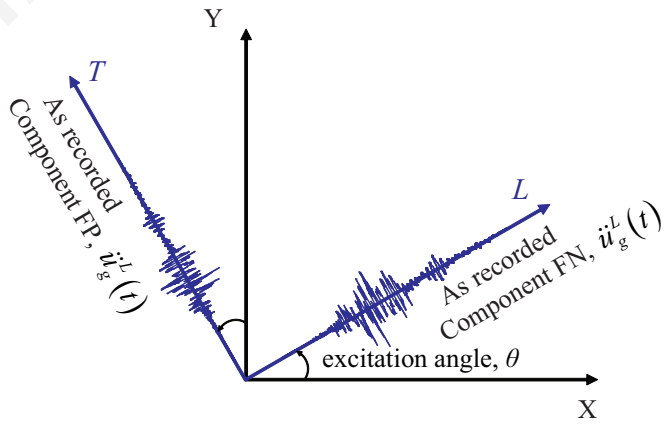

Figure 5.2 Horizontal ground of motion angle of incidence.

In order to study the effects of ground motion rotation, the two horizontal components of ground acceleration are rotated and resolved to the structural degrees of freedom

(Athanatopoulou, 2005; Polycarpou et al., 2015b). A similar approach, which is often used in the scientific literature (Liang and Lee, 2003; Slafak and Bendimerad, 1988) to study ground motion incidence angle is to rotate the structure and transform the original ground motion components to the rotated structural degrees of freedom.

The time-history analysis involves the numerical integration of the above differential equations at each time step and the calculation of the resulting displacements, velocities and absolute accelerations at each DOF of each building. Based on the resulting displacements, an automatic contact detection check is performed for potential pounding incidences between the floors of the adjacent structures, which would lead to the computation of the arising impact forces to be applied at the corresponding DOFs. The differential equations of all simulated structures are directly integrated simultaneously using the Newmark method, which computes the resulting displacements at time $t+\Delta t$. The contact detection and resolution of the contact forces are performed automatically at each time-step of the analysis, based on the deformed position of each floor diaphragm in space. For this reason, the time-step size, Δt, is selected to be small enough (usually in the range of 1 to $2 \cdot 10^{-5}$ s) to maximize the accuracy of the solution. When an interaction between adjacent structures is detected, the resulting impact forces $\overline{F}_{imp}$ are computed according to the impact model and the methodology that is presented in the following subsections.

5.5 Impact Modeling

As already mentioned in Chapter 3, the majority of the force-based impact models that are available in the scientific literature calculate the impact force as a function of the interpenetration depth between the colliding bodies. This method is widely known as the 'penalty method' in contact mechanics, because a virtual overlap is allowed between the two bodies in order to calculate the arising impact forces. However, the use of the interpenetration depth as the key variable entails a significant drawback in the case of 3D impact modeling. Specifically, that approach assumes that the calculated impact force depends only on the indentation, regardless of the overall geometry at the contact region. For example, the method assumes that the impact force between two floor slabs, which collide with a specific impact velocity, increases in magnitude in the same way for both cases of side-to-side and corner-to-side impact practically is not correct.

Therefore, based on the above observation and in order to take into account the geometry at the contact region, the area of the overlapping region, instead of the interpenetration depth, should be used as the key variable in the calculation of the impact

forces. Figure 5.3 describes schematically how the employed impact model works. In particular, when two bodies, which in the proposed methodology are modelled as polygons, come in contact, they form an overlapping region, which in most of the cases is either a triangle or a quadrilateral. The developed algorithm uses the geometry of the overlapping region at each time-step, defined by the coordinates of its nodes, in order to determine: (i) the location of the action point of the impact forces, (ii) the direction of the impact forces, based on the definition of the contact plane, and (iii) the magnitude of the impact forces, as described below:

5.5.1 Location of the Action Point of the Impact Force

The location of the application point of an impact force is a very important issue in the case of simulating collisions of buildings in 3D. While in the case of 1D impact models the location of the resultant force vector clearly is at the point of contact, in the case where contact conditions exist over a finite surface area on both bodies, the exact point where the contact force should be applied is not obvious. For the specific problem of modeling impact between rigid diaphragms, the contact forces in the normal and tangential directions are assumed to act on the centroid C of the overlapping region, and are applied at the corresponding position of the bodies in contact, as shown in Figure 5.3.

5.5.2 Direction of the Impact Forces – Contact Plane

The normal and tangential contact directions are determined in order to be able to apply the corresponding normal and tangential impact forces as well as the Coulomb's law of friction. Taking into account the assumptions of the current problem and, specifically, considering the case of colliding diaphragms (rigid plates) of constant thickness, the contact plane is actually a line. In particular, the contact plane is assumed to be parallel to the line that is determined by the two nodes P_1 and P_2 of the intersections between the boundaries of the two colliding bodies (Figure 5.3). Since the impact forces are applied at the centroid C of the overlapping region, the contact plane is passing through that point. The methodology that is used defines a normal and a tangential direction in such a way that ensures that a directional jump does not occur between two sequential time-steps of the analysis. Specifically, the contact plane smoothly changes direction, while the overlapping contact area changes from triangular to quadrilateral and vice-versa.

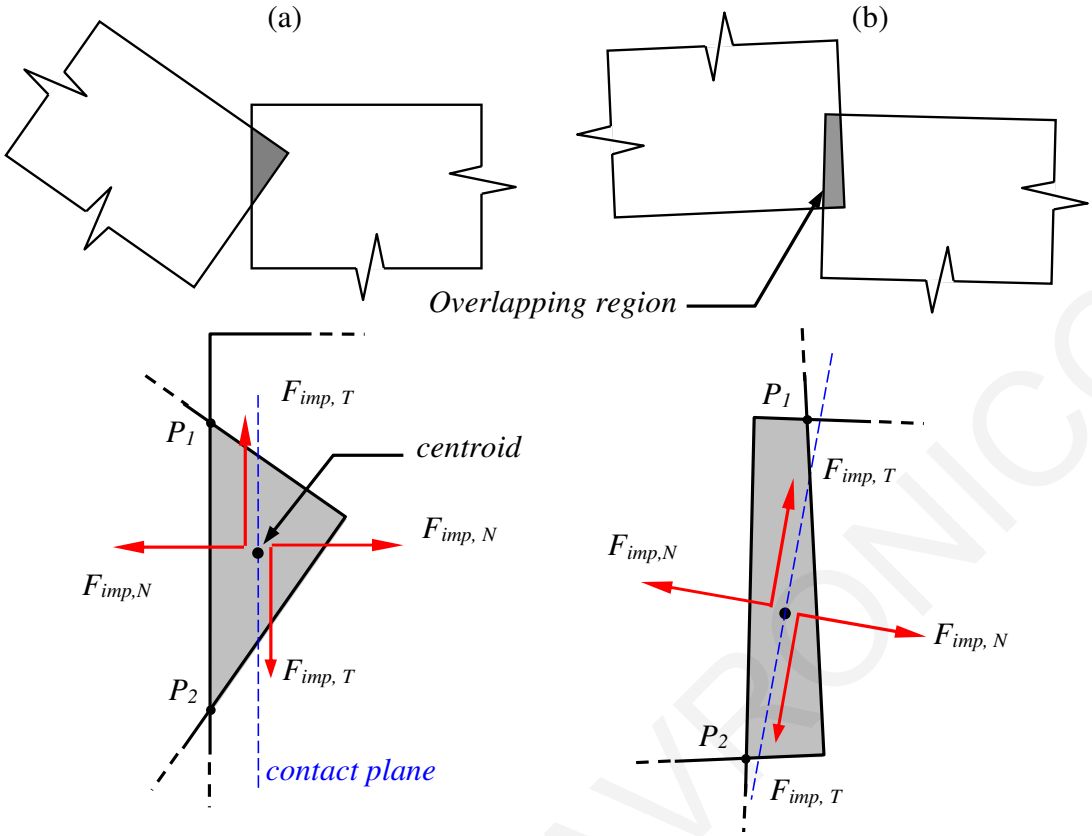

Figure 5.3 Schematic representation of the contact plane based on the geometry of the indentation region, which can be either (a) a triangle or (b) a quadrilateral.

5.5.3 *Calculation of Elastic Impact Forces*

According to basic concepts of the 'penalty' method, contact springs are automatically formed whenever two rigid bodies are detected to be in contact, in order to calculate the resulting impact forces that push them apart. In the modeling approach adopted herein, the stiffness of the impact spring is used together with the area of the overlapping region, A_c, to calculate the elastic impact force in the normal direction. Specifically, the elastic impact forces in the normal and tangential directions are computed by the following equations, at each iteration time-step:

$$\begin{aligned} F_{imp,N}^{elastic} &= A_c \cdot k_{imp,N} \\ F_{imp,T}^{elastic} &= {}^{prev}F_{imp,T}^{elastic} + u_{rel,T} \cdot k_{imp,T} \end{aligned} \tag{5.14}$$

The indices N and T in the above equations indicate the normal and tangential directions, respectively, while $k_{imp,N}$ (in $\mathrm{KN/m^2}$) and $k_{imp,T}$ (in $\mathrm{KN/m}$) are the impact stiffness coefficients in the normal and tangential directions, respectively, and $u_{rel,T}$ is the relative displacement along the tangential direction.

5.5.4 *Impact Damping*

An impact stiffness coefficient is used along with the area, A_c, of the overlapping region to calculate the elastic impact force in the normal direction, while the tangential impact force is computed in terms of the relative displacement, $u_{rel,T}$, of the two bodies in contact in the tangential direction. In addition, as in the case of 1D impact models, a viscous impact dashpot is used, in parallel with the impact spring, to account for the dissipation of energy during impact (e.g. plastic, thermal, acoustic energy) in each impact direction, providing the damping impact force based on the corresponding relative velocity of the bodies. Therefore, the corresponding total impact forces in the normal and tangential directions, respectively, taking into account the impact damping, are given by the following expressions:

$$\begin{aligned} F_{imp,N} &= F_{imp,N}^{elastic} + F_{imp,N}^{damp} \\ F_{imp,T} &= F_{imp,T}^{elastic} + F_{imp,T}^{damp} \end{aligned} \tag{5.15}$$

The viscous damping force is assumed to be velocity-dependent and, therefore, the magnitude of the damping force in each impact direction (normal and tangential) is computed using the corresponding relative velocity of the bodies that are in contact, together with an impact damping coefficient:

$$\begin{aligned} F_{imp,N}^{damp} &= \dot{u}_{rel,N} \cdot c_{imp,N} \\ F_{imp,T}^{damp} &= \dot{u}_{rel,T} \cdot c_{imp,T} \end{aligned} \tag{5.16}$$

where $\dot{u}_{rel,N}$, $\dot{u}_{rel,T}$, $c_{imp,N}$ and $c_{imp,T}$ are the relative velocities and the impact damping coefficients in the normal and tangential directions, respectively.

The values of the impact damping coefficients can be approximated in the same manner as in the case of 1D impact models, based on the coefficient of restitution, which can be provided for various materials and the active masses of the colliding rigid bodies. Specifically, the impact damping coefficient can be expressed in terms of the impact damping ratio ξ_{imp}, the impact stiffness k_{imp} and the masses of the colliding bodies as follows (Anagnostopoulos, 1988, 2004):

$$c_{imp} = 2 \cdot \xi_{imp} \sqrt{k_{imp} \cdot \frac{m_1 \cdot m_2}{m_1 + m_2}} \tag{5.17}$$

The impact damping ratio is expressed in terms of the coefficient of restitution e:

$$\xi_{imp} = -\frac{\ln e}{\sqrt{\pi^2 + (\ln e)^2}} \tag{5.18}$$

As already mentioned, for the proposed impact model, the impact damping coefficient of Equation (5.17) has to be determined separately for the normal and the tangential directions of the impact force, since the impact stiffness coefficients in these two directions of contact are not the same. In the normal direction, the impact stiffness's units are in $\mathrm{KN/m^2}$ and therefore a conversion is needed to $\mathrm{KN/m}$ in order to result in the correct units for the corresponding damping coefficient. Therefore, instead of the term $k_{imp,N}$, the ratio between the normal elastic impact force and the indentation at the corresponding time-step is used:

$$c_{imp,N} = 2 \cdot \xi_{imp} \sqrt{\frac{F_{imp,N}^{elastic}}{\delta_N} \cdot \frac{m_1 \cdot m_2}{m_1 + m_2}} \tag{5.19}$$

The indentation δ_N is computed at each time-step, based on the geometry of the overlapping region, which is separated in two cases, according to Figure 5.3:

$$\delta_N = \begin{cases} 2\dfrac{A_c}{d(P_1, P_2)} & \text{for triangle} \\ \dfrac{A_c}{d(P_1, P_2)} & \text{for quatrilateral} \end{cases} \tag{5.20}$$

where $d(P_1, P_2)$ is the distance between the intersecting nodes P_1 and P_2 of the colliding polygons (Figure 5.3). Finally, for the mass terms of Equation (5.19), the corresponding total masses of the two colliding floors are used.

In the case of the tangential direction, the computation of the impact damping term is simpler, since the tangential impact stiffness term can be used directly in Equation (5.17) as follows:

$$c_{imp,T} = 2 \cdot \xi_{imp} \sqrt{k_{imp,T} \cdot \frac{m_1 \cdot m_2}{m_1 + m_2}} \tag{5.21}$$

Apparently, the impact damping ratio is the same in both normal and tangential directions if the coefficient of restitution is considered to be independent of the impact

velocity and dependent only on the type of the colliding materials. However, in the case where the coefficient of restitution is computed in terms of the impact velocity, which varies in each impact direction, a different impact damping ratio can be computed in each direction of an impact using an experimental formula given in Equation (3.23).

5.5.5 Friction during Impact

The Coulomb friction law is used to limit the tangential impact force below a certain magnitude that depends on the magnitude of the normal impact force and the static and kinetic friction coefficients of the contact surfaces:

$$\begin{aligned} &\text{if } \left|F_{imp,T}\right| \le \left|F_{imp,N} \cdot \mu_s\right| \quad \rightarrow \quad F_{imp,T} = F_{imp,T}^{elastic} + F_{imp,T}^{damp} \\ &\text{if } \left|F_{imp,T}\right| > \left|F_{imp,N} \cdot \mu_s\right| \quad \rightarrow \quad F_{imp,T} = F_{imp,N} \cdot \mu_k \end{aligned} \tag{5.22}$$

where μ_s and μ_k are the static and kinetic friction coefficients, which are applied in the 'stick' (i.e. no sliding occurs) and 'slide' mode of contact, respectively.

5.5.6 Impact Stiffness Coefficients

In the developed software that is used, a simple approximation is followed in order to determine a reasonable value for the impact stiffness and impact damping in both normal and tangential directions of the contact plane, in cases where their values are not defined explicitly by the user. As it is well known, the impact stiffness value depends mainly on the material characteristics of the colliding structures and the geometry at the vicinity of an impact. Assuming that the contact geometry is taken into account with the use of the area of the overlapping region instead of the indentation depth, then the impact stiffness should be directly related to the moduli of elasticity of the colliding bodies. Based on fundamental theories of contact mechanics (Goldsmith, 1960; Layton, 1999; Popov and Heß, 2015), it is assumed that the normal impact stiffness value can be approximated as follows:

$$k_{imp,N} = \left(\frac{1-\nu_1^2}{E_{dyn,1}} + \frac{1-\nu_2^2}{E_{dyn,2}} \right)^{-1} \tag{5.23}$$

where:

$$E_{dyn,i} = 5.82 \left(E_{st,i} \right)^{0.63}, \qquad \text{in GPa} \tag{5.24}$$

is the dynamic elastic modulus for normal strength concrete, as it has been determined through relevant experiments (Mohammed and Al-Amawee, 2006), expressed in terms of

the static elastic modulus $E_{st,i}$, while ν_i is the Poisson's ratio for the body *i*. In a similar manner, the tangential impact stiffness is approximated using the shear moduli of the colliding bodies:

$$k_{imp,T} = \left(\frac{2-\nu_1}{G_{dyn,1}} + \frac{2-\nu_2}{G_{dyn,2}} \right)^{-1} \tag{5.25}$$

where:

$$G_{dyn,i} = \frac{E_{dyn,i}}{2(1+\nu_i)} \tag{5.26}$$

The above-described methodology for predicting the impact stiffness coefficients is based on the assumption that the material of the colliding bodies maintains an elastic behavior during impacts. However, during pounding, the colliding structures, especially in the case of concrete structures, experience local damage, exhibiting highly non-elastic behavior at the vicinity of impact (van Mier *et al.*, 1991). Therefore, the impact stiffness is not actually constant but gradually decreases during an impact due to the local plastic damage of the colliding structures. Probably, it would be more appropriate to use a smaller equivalent impact stiffness value in order to take into account this local inelastic behavior of concrete.

5.6 Hysteretic Isolator Property

A coupled plasticity model is used for the bidirectional lateral response of the isolation system (Figure 5.4). The plasticity model is based on the hysteretic behavior proposed by Wen (1976) and Park *et al.* (1986) and recommended by Nagarajaiah *et al.* (1991). For a LRB the mobilized forces are described by the following equations:

$$\begin{aligned} F_b^x &= \alpha_x \frac{F_y^x}{u_y^x} u_b^x + (1-\alpha_x)\ F_y^x\ z_x \\ F_b^y &= \alpha_x \frac{F_y^y}{u_y^y} u_b^y + (1-\alpha_y)\ F_y^y\ z_y \end{aligned} \tag{5.27}$$

where F_b^x, F_b^y is the restoring force of *X* and *Y* directions, F_y^x, F_y^y is the yield load *X* and *Y* directions, u_b^x, u_b^x are the horizontal shear displacements of the bearing in *X* and *Y* directions, z_x, z_y are the dimensionless evolutionary variables. It should be noted that

when considering bi-directional coupled action and the direction of the restoring force, z_x, z_y should satisfy $\sqrt{z_x^2 + z_y^2} \le 1$ and the summation of initial deformation should be zero (Figure 5.5(a)). Those two variables can be obtained from:

$$\begin{Bmatrix} \dot{z}_x \, u_y^x \\ \dot{z}_y \, u_y^y \end{Bmatrix} = \begin{Bmatrix} A \, \dot{u}_b^x \\ A \, \dot{u}_b^y \end{Bmatrix} - \begin{bmatrix} z_x^2 \left(\gamma \operatorname{sgn}\left(\dot{u}_b^x \, z_x\right) + \beta\right) & z_x \, z_y \left(\gamma \operatorname{sgn}\left(\dot{u}_b^y \, z_y\right) + \beta\right) \\ z_x \, z_y \left(\gamma \operatorname{sgn}\left(\dot{u}_b^x \, z_x\right) + \beta\right) & z_y^2 \left(\gamma \operatorname{sgn}\left(\dot{u}_b^y \, z_y\right) + \beta\right) \end{bmatrix} \begin{Bmatrix} \dot{u}_b^x \\ \dot{u}_b^y \end{Bmatrix} \quad (5.28)$$

in which u_y^x, u_y^y, $\dot{u}_b^x$, $\dot{u}_b^y$ are the horizontal yield displacement and the shear deformation velocity in the *X* and the *Y* directions, respectively.

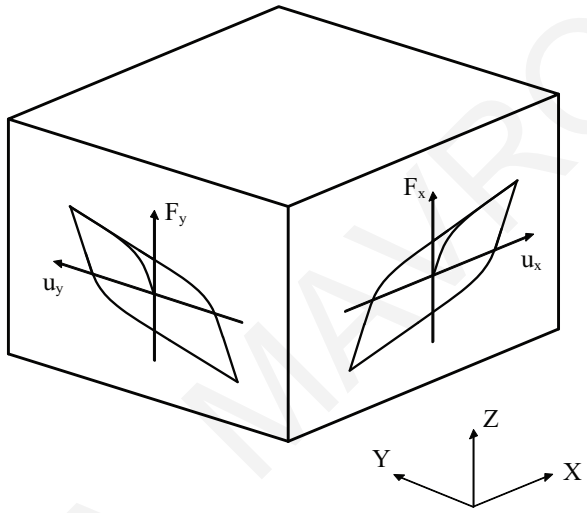

Figure 5.4 Hysteretic isolator property for biaxial shear deformation.

By setting $A = 1$ and $\beta = \gamma = 0.5$, Equation (5.28) is simplified into:

$$\begin{Bmatrix} \dot{z}_x \\ \dot{z}_y \end{Bmatrix} = \begin{bmatrix} 1 - a_x \, z_x^2 & -a_y \, z_x \, z_y \\ -a_x \, z_x \, z_y & 1 - a_y \, z_y^2 \end{bmatrix} \begin{Bmatrix} \dfrac{K_{el}^x}{F_y^x} \dot{u}_b^x \\ \dfrac{K_{el}^y}{F_y^y} \dot{u}_b^y \end{Bmatrix} \quad (5.29)$$

where:

$$a_x = \begin{cases} 1 & \text{if } \dot{u}_b^x \cdot z_x > 0 \\ 0 & \text{otherwise} \end{cases}, \quad a_y = \begin{cases} 1 & \text{if } \dot{u}_y^x \cdot z_y > 0 \\ 0 & \text{otherwise} \end{cases}.$$

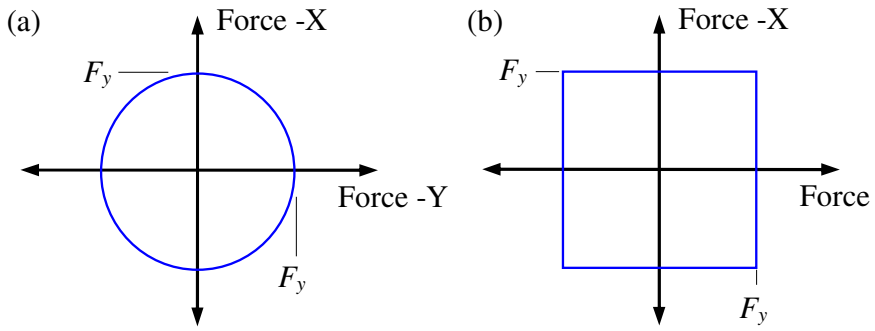

Figure 5.5 Bi-directional coupling in isolators force-deformation response: (a) coupled circular yield surface, and (b) uncoupled yield surface.

It should be noted that independent uniaxial plasticity properties can also be specified for each deformational DOF; all internal deformations are independent and yielding at one DOF may not affect the behavior of the other deformations, as shown in Figure 5.5(b).

5.7 Discussion of the Analysis Results

The results from the dynamic analysis of a base-isolated building obtained using the developed software (3DPOUND) are indicatively presented in this section, and are compared with the results utilizing the commercial software SAP2000 (Figure 5.6). Initially, nonlinear dynamic analyses of a typical three-story building, when sufficient clearance is provided around the structure (no pounding case), is used to study peak responses considering mass eccentricities.

5.7.1 No Pounding Case

A three-story, three-by-three bay base-isolated reinforced concrete moment-frame building has been chosen for this example. The location of the center of mass is set to have eccentricities $e_{s,x} = e_{s,y} = 0.60\,\text{m}$. The retaining walls extend from ground level up to the base level of the building. All column sections of the simulated building have dimensions $45\times45\,\text{cm}^2$. The bay width of the building in both directions is 5.5 m. The story height of the building is 3.2 m. The elastic modulus of concrete is taken to be equal to 30 GPa with a Poisson's ratio equal to 0.2. A uniformly distributed mass is considered, which corresponds to a 250 tons lumped mass for the roof mass and a 340 tons lumped mass for each floor level, including the base of the building. For the determination of the Rayleigh damping matrix, the viscous damping ratio for the first and the fourth eigenfrequencies are set to 0.05 and 0.02, respectively.

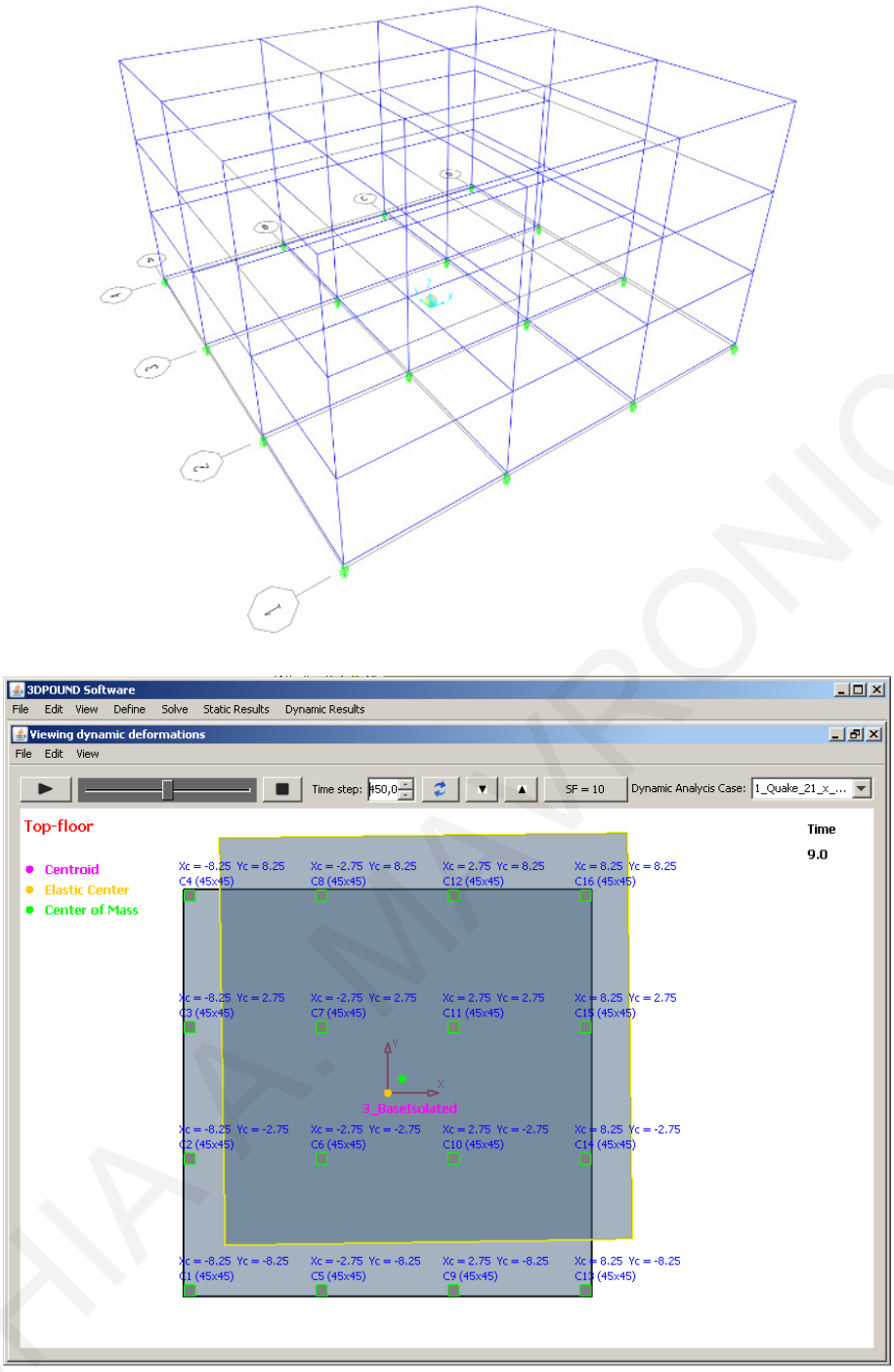

Figure 5.6 SAP2000 and 3DPOUND models.

A coupled plasticity model is used for simulating the bidirectional lateral response of the seismic isolators. Values 1.0, 0.5, 0,5 and 2 are adopted for the Bouc-Wen models' parameters A, β, γ and n, respectively. Identical bearings are provided under each of the 16 column bases, with the same stiffness and damping properties in the two principal directions. For each isolator, $T_b^x = T_b^y = 2.0\,\text{s}$, $u_y^x = u_y^y = 1.0\,\text{cm}$ and $F_{yi}^x / W = F_{yi}^y / W = 10\%$ are considered. A pair of accelerograms consisting of the X and Y components of Loma Prieta, 1989 earthquake excitation (LGPC station), are selected for the time-history

analyses of the seismically isolated structure, which are performed using SAP2000 and 3DPOUND (Figure 5.6). The angle of incidence is set in both cases at 30°.

The results of the nonlinear analysis from the custom-made software and the SAP2000 model are shown in Figure 5.7, Figure 5.8 and Figure 5.9. The results from the dynamic analysis of a torsionally flexible base-isolated building using the developed software are contrasted and benchmarked against the results using the SAP2000 software. It can be seen that, the numerical results are nearly identical. The minor deviation that exists between the custom-made software and the commercially available, general purpose, SAP2000 software verifies the accuracy of the developed algorithm and the validity of the results presented hereafter.

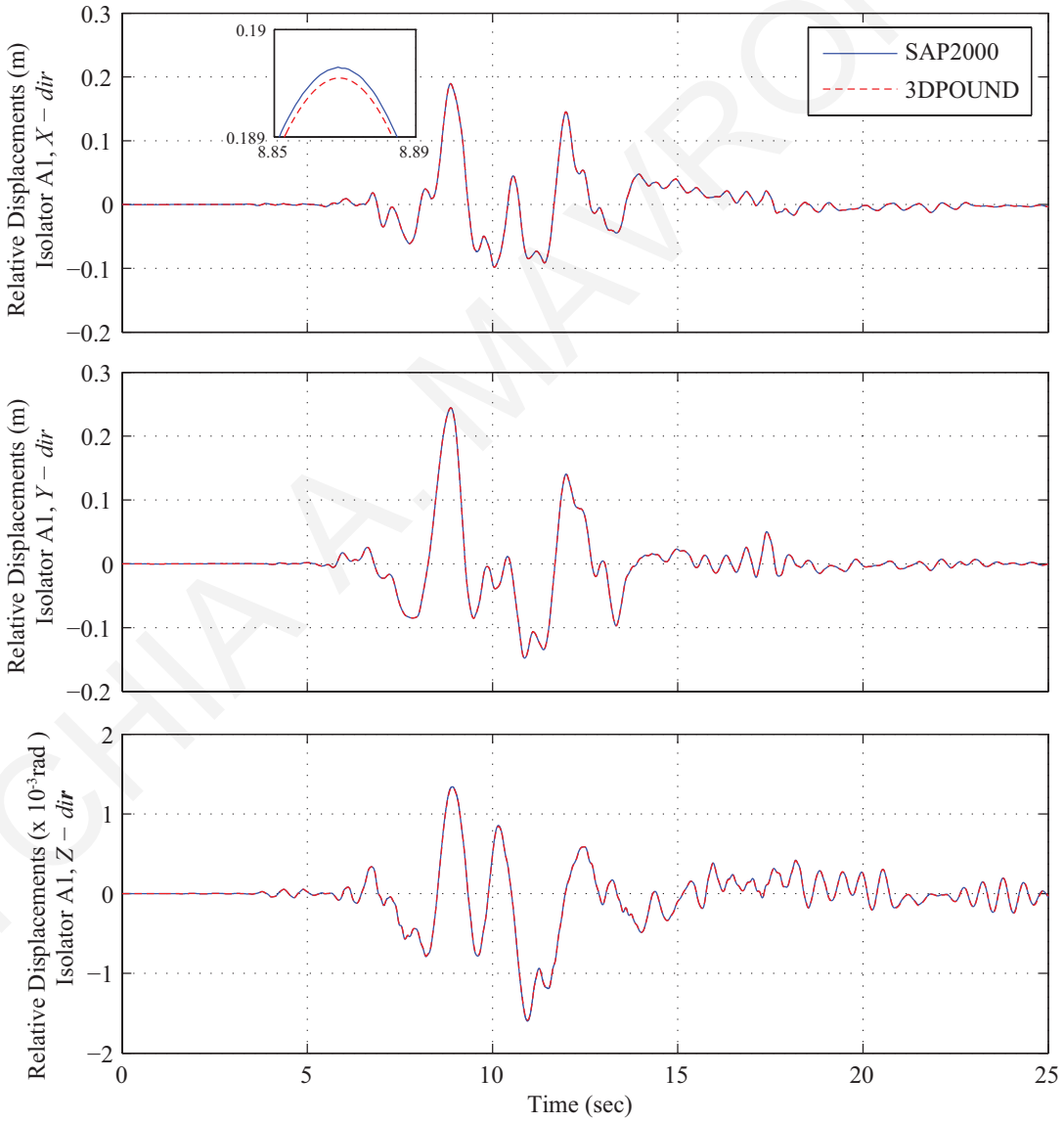

Figure 5.7 Time-variation of base drifts for the 3-story base-isolated structure (column A_1) under the Loma Prieta earthquake, using the commercial software SAP2000 and the custom-made 3DPOUND.

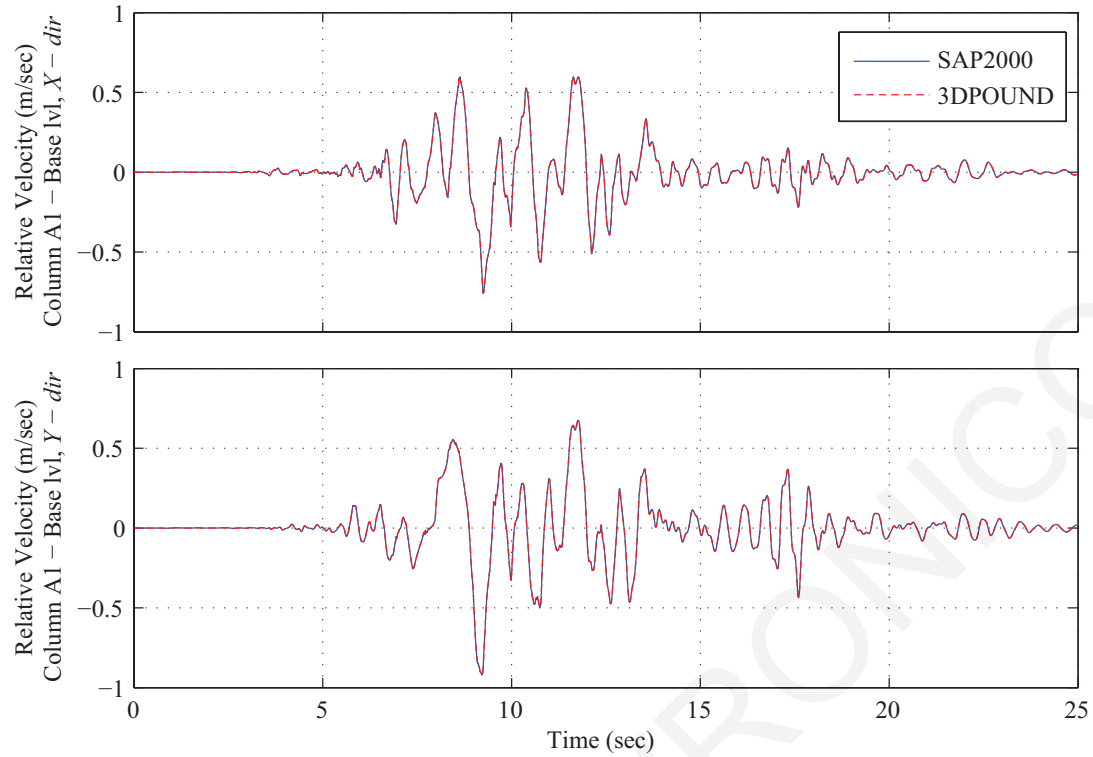

Figure 5.8 Time-variation of relative velocity at the isolation level (corner column A_1) for the 3-story base-isolated structure under the Loma Prieta earthquake utilizing SAP2000 and 3DPOUND software.

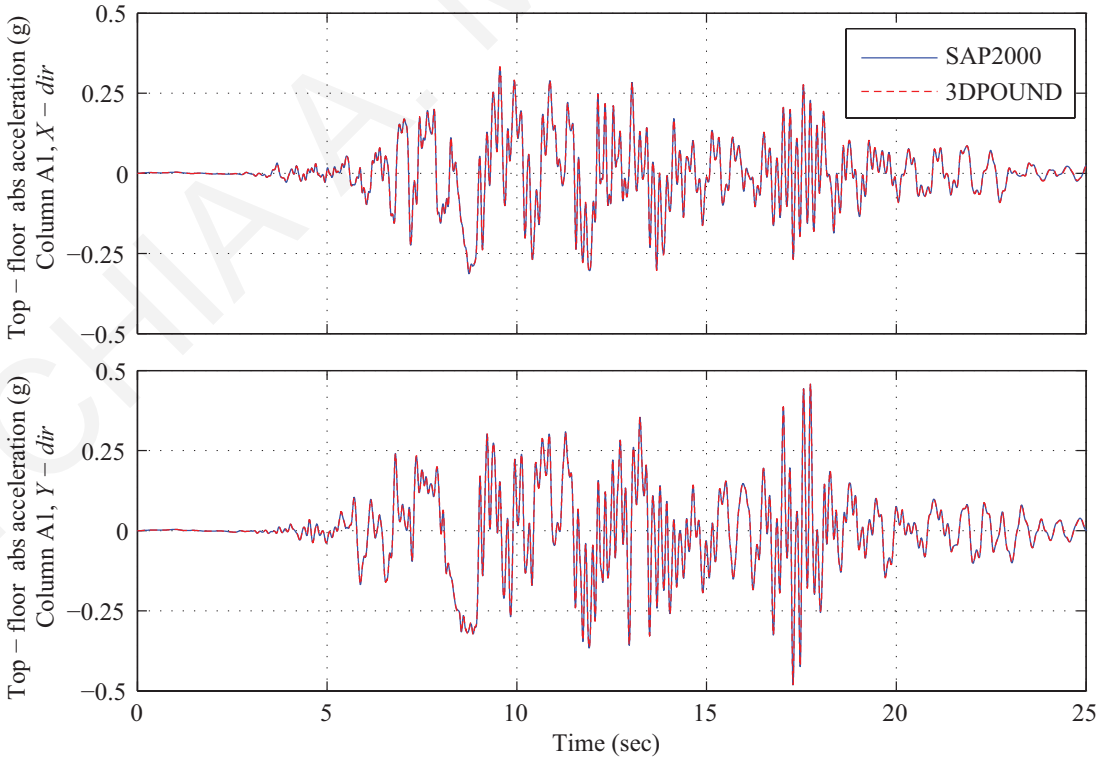

Figure 5.9 Comparison of absolute acceleration at the top – floor (corner column A_1) for the 3-story structure utilizing SAP2000 and 3DPOUND, in X and Y directions.

5.7.2 Pounding to Adjacent Moat Wall

A different three-story base-isolated building is considered in this subsection, with isolator characteristics of $T_b^x = T_b^y = 2.0\,\text{s}$, $u_y^x = u_y^y = 1.0\,\text{cm}$ and $F_{yi}^x / W = F_{yi}^y / W = 10\%$. The new building has the same stiffness characteristics but a different mass distribution eliminating any eccentricities, $e_{s,x} = e_{s,y} = 0$ (Figure 5.10). The selection of the particular building, regular and symmetric, has been made in order to more easily identify the effects of the various parameters on the response during pounding. Due to symmetry, the first two eigenmodes are translational along the two horizontal axes. The fundamental eigenperiod of the corresponding fixed-supported building are $T_{fixed}^x = T_{fixed}^y = 0.31\,\text{s}$.

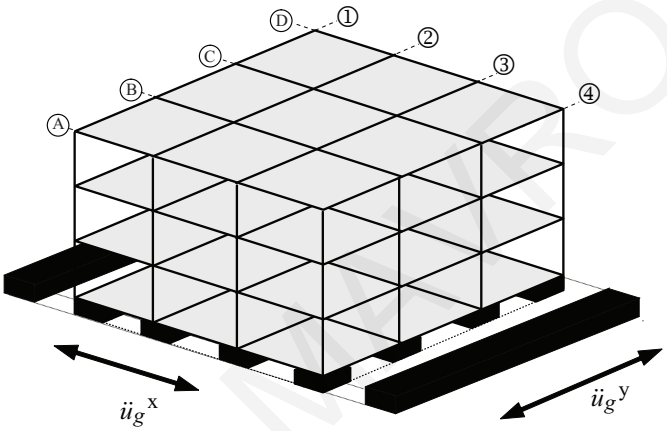

Figure 5.10 The three-story base-isolated building considered in the present study.

In the case under examination, impacts can occur only at the base isolation level whenever the distance from the surrounding moat wall, i.e. the seismic gap, is exceeded. The seismic gap is taken to be equal to 15 cm. The retaining walls extend from ground level up to the base level of the building. The moat wall on each one of the two sides of the building is modelled as a single-mass system, with three dynamic DOF, as in the case of a single-story structure. The moat wall is taken to be 100 cm thick and 100 cm high, resulting to a substantially stiff barrier, while it's mass is taken to be 5 tons/m, in order to take into account the contribution of the backfill soil. The normal impact stiffness $k_{imp,N}$ is $2.58 \cdot 10^7\,\text{KN/m}^2$, while the corresponding tangential impact stiffness $k_{imp,T}$ is $5.74 \cdot 10^6\,\text{KN/m}$. The static and kinetic friction coefficients are taken to be $\mu_s = 0.8$ and $\mu_k = 0.6$, respectively, while no impact damping is considered in this analysis, for simplicity and in order to be able to discuss the results on a specific basis.

The plots in Figure 5.11 present the times-histories of the normal and tangential impact forces at the ground floor. The incidence angle of the excitation under consideration is set to 0°. Figure 5.12 presents, in more detail, the impact forces, generated due to pounding of the base-isolated building to the moat wall located at the west side, for two different time instances: t = 8.5953 s, which corresponds to the first impact, and t = 8.6831 s, which corresponds to the third impact. In particular, the normal impact force is plotted with respect to both time and normal indentation, $\delta_{N,}$ whereas the tangential impact force is also provided with respect to time. It is interesting to observe the differences between the impact forces generated on the two presented time instances.

During the first impact, as no rotation occurs yet with the colliding structures, the overlapping region forms a rectangle, of which the area is linearly increasing with the indentation depth. Therefore, the impact force is linearly increasing with the interpenetration depth, corresponding to the case of a linear impact model. However, when torsional vibration occurs between the colliding structures at the ground floor, the overlapping region becomes a triangle, of which the area is increasing in a nonlinear manner with the indentation depth, resembling the nonlinear evolution of the contact area with depth. This is clearly observed in the force-indentation diagram of Figure 5.12(b), which corresponds to the case of a nonlinear impact model.

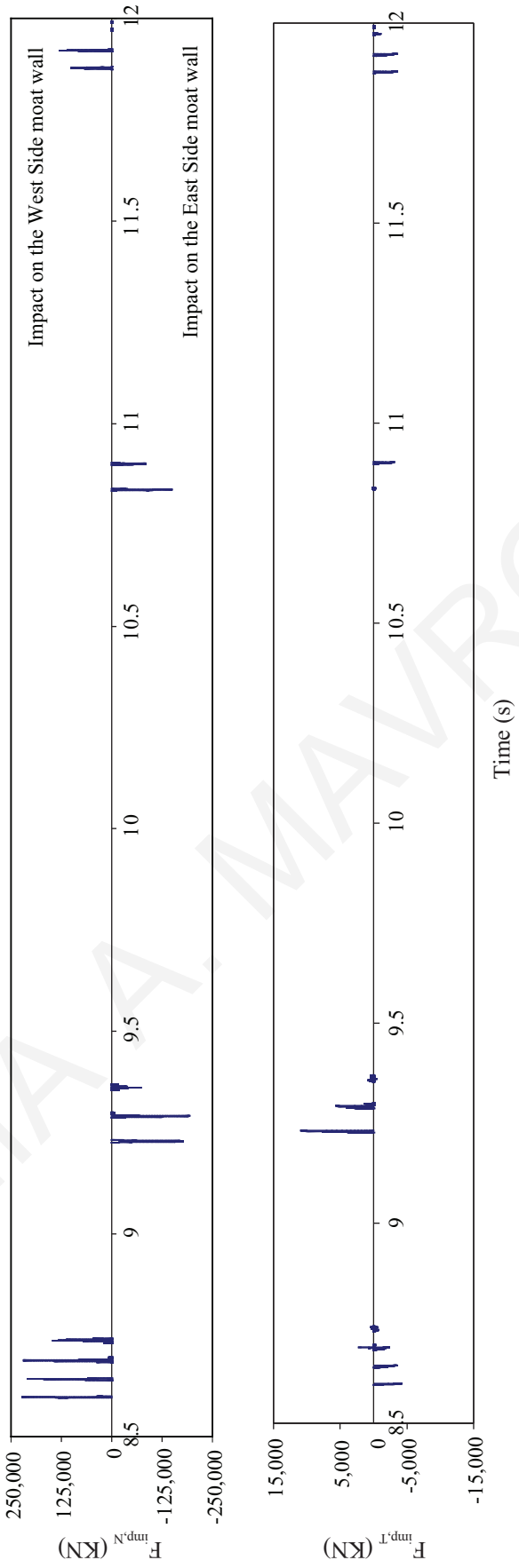

Figure 5.11 Normal (N) and tangential (T) impact force time histories at the base, when separation gap is limited to 15 cm at both sides.

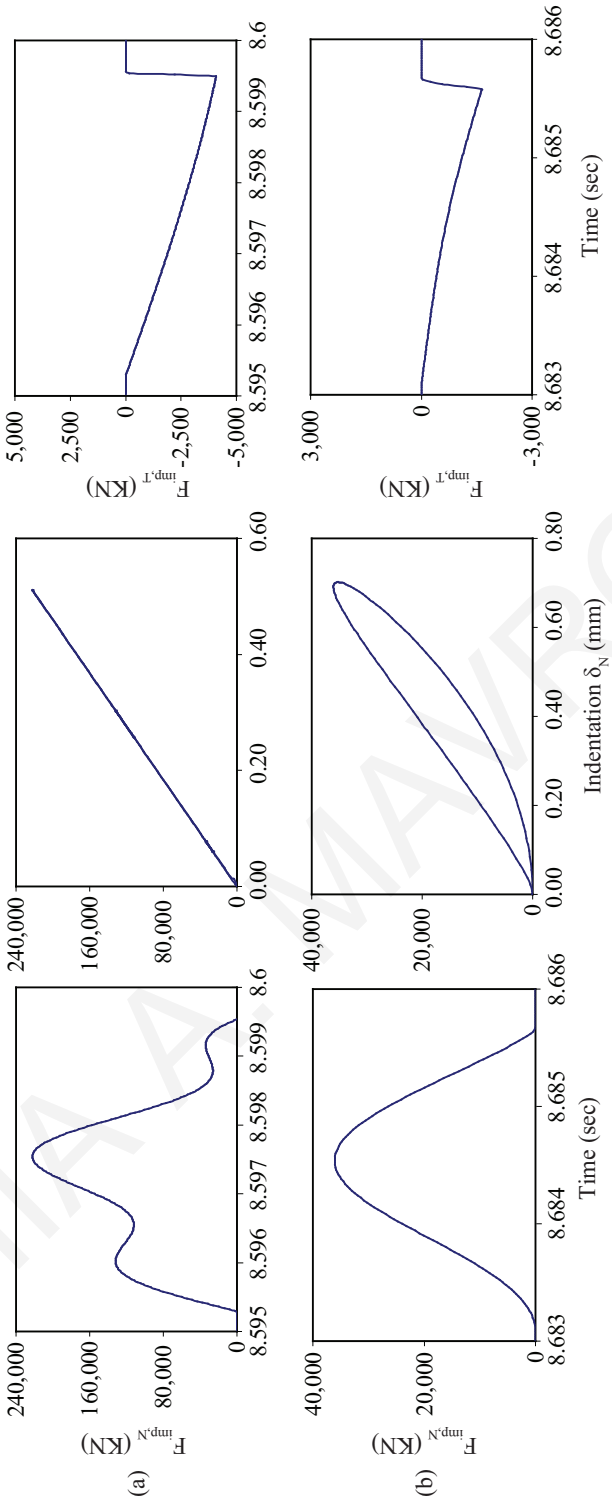

Figure 5.12 Impact forces at (a) during first impact at 8.5953 s, and (b) during impact at 8.6831 s.

5.8 Concluding Remarks

The methodology presented in this chapter for modeling 3D dynamic modeling of base-isolated buildings with the ability to capture impact forces is used in the following chapters for parametrically investigating the effect of several important variables that may affect the overall dynamic response, when structural pounding occurs. The possibility of impacting against moat walls or against surrounding structures, including adjacent buildings, is considered separately in Chapter 6 and Chapter 7, respectively. More specifically, the peak responses of seismically isolated buildings utilizing LRBs are studied while varying important parameters, such as the incidence angle of seismic excitations, the available seismic clearance and mass eccentricities, under the action of bidirectional horizontal excitations. A large number of numerical simulations are performed using a specially developed software that implements an efficient approach to model impacts, taking into account arbitrary locations of contact points.

CHAPTER 6 THREE-DIMENSIONAL BASE-ISOLATED BUILDINGS POUNDING TO MOAT WALLS

6.1 Introductory Remarks

The research work presented in this chapter utilizes the computational methodology described in Chapter 5, aiming to thoroughly investigate the circumstances under which spatial pounding of base-isolated buildings may occur and assess the effect of some important parameters on the peak seismic response due to potential structural pounding. Nonlinear time-history analyses of three-story base-isolated structures are carried out, considering the arbitrary direction of the ground motion with respect to the principal construction axes of the simulated structures.

Although, the methodology provides the ability of considering impacts at all floor levels of the seismically isolated building, the analyses presented in this chapter consider only the possibility of having impacts at the isolation level, whenever the seismic gap is exceeded during very strong seismic excitations. The influence of the isolators' characteristics and the separation distance between the building and the retaining walls at its base are also investigated, while considering different geometrical arrangements for the surrounding moat walls. The influence of eccentricities arising because of actual or accidental mass eccentricities at the superstructure is also studied.

The present analysis results, which quantify the contribution of the angle of excitation and the 3D impact effects on the overall peak structural response of a base-isolated building, might influence the design strategy chosen for the seismic upgrading of existing buildings. Furthermore, it is shown that existing design methodologies for defining the required seismic gap of new structures, in order to avoid potential collisions, might fall short, compared to the actually required clearance when 3D effects, such as those related to the angle of excitation or torsional vibrations, are not taken into consideration.

Although the implemented methodology supports the simulation of more complicated structures with structural or mass irregularities both in plan and height, the selection of double symmetric buildings, as presented in Section 5.7, is made in order to more easily

identify the effects of the various parameters on the peak seismic response during pounding.

Specifically, a three-story, three-bay by three-bay, base-isolated reinforced concrete moment-frame building is chosen as a typical seismically isolated structure (Figure 6.1(a)). The building is symmetric with coinciding centers of mass and stiffness. All columns of the simulated building have square sections of $45\times45\,\mathrm{cm}^2$. The bay width of the building in both directions is 5.5 m, while each story height is 3.2 m. The elastic modulus of concrete is assumed to be 30 GPa and the Poisson's ratio 0.2. A uniformly distributed mass of 250 tons is considered for the roof mass, while a 340 tons mass is assumed at each floor level, including the base level. For the determination of the Rayleigh damping matrix, the viscous damping ratios for the first and the fourth eigenfrequencies are taken as 0.05 and 0.02, respectively. Due to symmetry, the first two eigenmodes are translational along the two horizontal axes.

A coupled plasticity model is used for simulating the bidirectional lateral response of the seismic isolators. Identical bearings are provided under each of the 16 column bases, with the same stiffness and damping properties in the two principal directions. For each bearing element an isolation period based on the post-yield stiffness of 2.0 s, and a yield displacement equal to 1.0 cm, in both directions, are considered. However, two different values of the normalized characteristic strength defined as the ratio of the force required to yield the lead core normalized by the weight acting on the isolator, $F_{yi}^{x}/W = F_{yi}^{y}/W = 0.05$ and 0.10, are considered, in order to examine the influence of the isolators' characteristics on the nonlinear behavior of symmetric buildings due to seismic pounding (Figure 6.1(b)).

The moat wall is modeled as a single-mass system, with three dynamic DOF, as in the case of a single-story structure and extends from the ground level up to the base level of the building. Specifically, the moat wall is 100 cm thick and 100 cm high, resulting in a substantially stiff barrier, while it's mass is assumed to be 5 tons/m, in which the contribution of the backfill soil is taken into consideration. Normal impact stiffness and tangential impact stiffness values of $k_{imp,N} = 2.58\cdot10^{7}\ \mathrm{KN/m}^2$ and $k_{imp,T} = 5.74\cdot10^{6}\ \mathrm{KN/m}$, respectively, which are characteristic values for normal strength concrete (Polycarpou *et al.*, 2014), are used. The static and kinetic friction coefficients are taken as $\mu_s = 0.8$ and $\mu_k = 0.6$, respectively. A value of 0.65 for the coefficient of restitution has been used for concrete structures in many relevant studies, and is also adopted herein (Anagnostopoulos and Karamaneas, 2008; Jankowski, 2005).

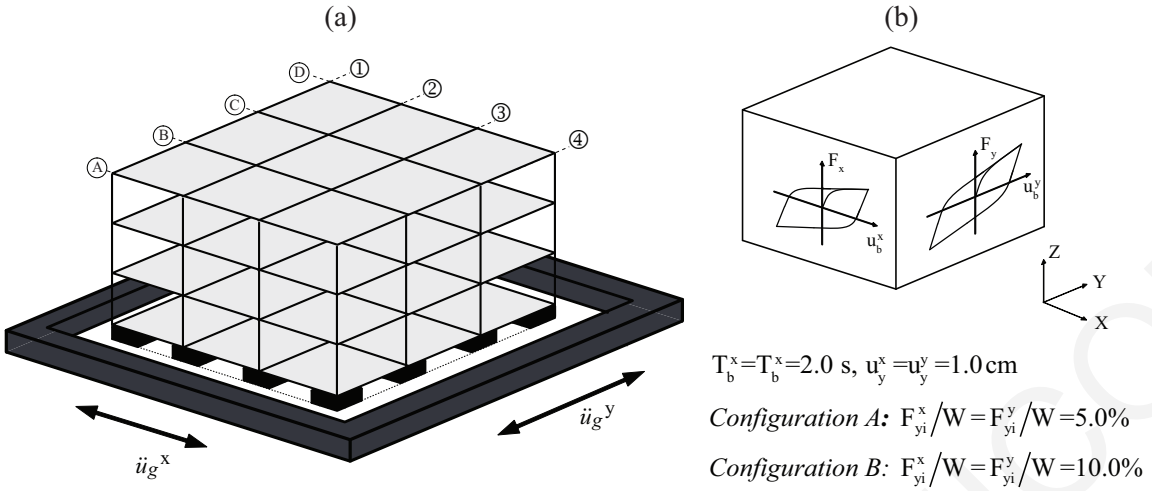

Figure 6.1 (a) Three-story base-isolated building, and (b) hysteretic isolator properties for biaxial shear deformation; considered in the present study.

Structural pounding may occur in cases of base-isolated buildings without other adjacent buildings when the width of the available seismic clearance around them is exceeded by the large horizontal relative displacements that are expected, during strong earthquake excitations, at the isolation level due to the inserted flexibility (Gavin and Wilkinson, 2010; Nagarajaiah and Xiaohong, 2000). Such impact incidences are more likely to happen under strong, near-fault, pulse-like ground motions, which amplify further the relative displacements at the isolation level (Malhotra, 1997; Matsagar and Jangid, 2003, 2010; Tsai, 1997).

In this research work, a set of 20 accelerograms of a distinct pulse-type earthquakes, which correspond to historic records from 11 different seismic events (Table 6.1), have been selected from the PEER Database, Beta Version (PEER Pacific Earthquake Engineering Research Center, 2011). The identification and characterization of records with pulse-like velocities has been based on the work of Baker (Baker, 2007), who utilized wavelet transforms. In the present study, further criteria have been imposed for the selection of the ground motions: (a) an earthquake magnitude of $M_w \geq 6.0$; and (b) a distance to the fault rupture of $R_{rup} < 15\,\text{km}$. These earthquake selection criteria have been imposed on the basis of maximizing the expected base relative displacement demands of base-isolated buildings.

Table 6.1 Summary of the main characteristics of the selected horizontal seismic excitations that are used in this research work.

EQ No.	NGA seq. no.	Event	Year	Station	Mw	FN component			FP component		
						PGA (g)	PGV (cm/s)	PGD (cm)	PGA (g)	PGV (cm/s)	PGD (cm)
1	179	Imperial Valley-06	1979	El Centro Array #4	6.53	0.36	77.9	58.7	0.47	40.1	20.7
2	183	Imperial Valley-06	1979	El Centro Array #8	6.53	0.47	48.6	36.8	0.59	52	30.8
3	184	Imperial Valley-06	1979	El Centro Differential Array	6.53	0.42	59.6	38.7	0.44	51.4	27.8
4	292	Irpinia- Italy-01	1980	Sturno	6.9	0.23	41.4	22.1	0.31	45.5	23.4
5	779	Loma Prieta	1989	LGPC	6.93	0.94	97	62.5	0.54	72.1	30.5
6	802	Loma Prieta	1989	Saratoga - Aloha Ave	6.93	0.36	55.5	29.4	0.38	43.3	15.8
7	821	Erzican- Turkey	1992	Erzincan	6.69	0.49	95.4	32.1	0.42	45.3	16.5
8	825	Cape Mendocino	1992	Cape Mendocino	7.01	1.27	57.6	13.8	1.43	118.3	38.2
9	828	Cape Mendocino	1992	Petrolia	7.01	0.61	81.9	25.5	0.63	60.4	26
10	983	Northridge-01	1994	Jensen Filter Plant Generator	6.69	0.52	67.3	42.6	1.07	65.3	23.3
11	1013	Northridge-01	1994	LA Dam	6.69	0.58	77.1	20.1	0.42	40.7	16
12	1045	Northridge-01	1994	Newhall - W Pico Canyon Rd.	6.69	0.43	87.7	55.1	0.28	74.7	21.8
13	1084	Northridge-01	1994	Sylmar - Converter Sta	6.69	0.59	130.3	54	0.8	93.3	53.3
14	1176	Kocaeli- Turkey	1999	Yarimca	7.51	0.28	48.2	43	0.31	72.9	55.9
15	1489	Chi-Chi- Taiwan	1999	TCU049	7.62	0.28	44.8	66.3	0.25	57.3	49
16	1511	Chi-Chi- Taiwan	1999	TCU076	7.62	0.3	63.4	31.8	0.42	63.4	35.1
17	1515	Chi-Chi- Taiwan	1999	TCU082	7.62	0.25	56.1	71.6	0.2	49.3	58.1
18	1605	Duzce- Turkey	1999	Duzce	7.14	0.36	62.2	46.5	0.52	79.5	48.2
19	2114	Denali- Alaska	2002	TAPS Pump Station #10	7.9	0.33	95.5	92.4	0.27	121.3	116.2
20	2627	Chi-Chi- Taiwan-03	1999	TCU076	6.2	0.52	59.3	9.6	0.16	19.5	3.6

NGA seq. no.: Next generation attenuation project database sequence number
FN: Fault normal; FP: Fault parallel; PGA: Peak ground acceleration; PGV: peak ground velocity; PGD: peak ground displacement

Peak unobstructed base relative displacements and corresponding peak interstory drifts of all floors for all ground motions, considering different isolation system characteristics are plotted in Figure 6.2(a) and (b), respectively. Lines with a slope equal to one, and deviations of ±15 and ±30% are also shown for reference. In Figure 6.2(a), $u_b^{coup,i\text{-}dir}$ and $u_b^{uncoup,i\text{-}dir}$ are the unobstructed peak base displacements in *X* and *Y* directions under coupled and uncoupled interaction of the restoring forces of LRB, respectively. As described in Section 5.6, the LRBs model couples the two orthogonal directions through a circular interaction surface. The force-deformation responses in the two directions can be uncoupled by assuming a square interaction surface. The responses in the two directions are then independent and can be represented by two bilinear springs.

It is observed that, for most of the near-fault ground motions, the peak base displacements are, in general, greater under coupled isolator's behavior, and are kept lower than ±30% for all cases considered in this research study. Coupling which occurs in the bi-directional yield surface of typical seismic isolation systems (Figure 5.5), causes a reduction in resisting forces orthogonal to the direction of initial displacement beyond yield. Such a reduction in the effective stiffness leads to an amplification of the relative displacements at the isolators' level. However, the extent of the amplification highly depends on the magnitude of the forces acting on the isolator and the phasing of the orthogonal ground motion components. Since the phase of the orthogonal horizontal components of the excitations is arbitrary in nature, the degree of displacement's amplification is also arbitrary. Therefore, peak displacement differences between the two approaches, i.e. considering uncoupled or coupled behavior, are significant depending on the ground motion that is used as an earthquake excitation.

Figure 6.2 (b) suggests that, in general, the maximum interstory deflection ratios of all floors are not accurately estimated in the uncoupled isolator's model. In most cases, the superstructure response under uncoupled analysis, $\Delta U_{superstr}^{uncoup,i\text{-}dir}$ is higher than that of the corresponding coupled analysis, $\Delta U_{superstr}^{coup,i\text{-}dir}$. This implies that by ignoring the fact that loading a bearing in one direction affects the load resisted in an orthogonal direction, would lead to an overestimation of the superstructure's peak response. The differences persist even when the separation gap between the building and retaining walls is limited to 20 cm and impact occurs (according to the plotted results in Figure 6.2(c)). Response deviations in the latter case depend on both isolator and excitation characteristics and, in general, are retained within ±30%.

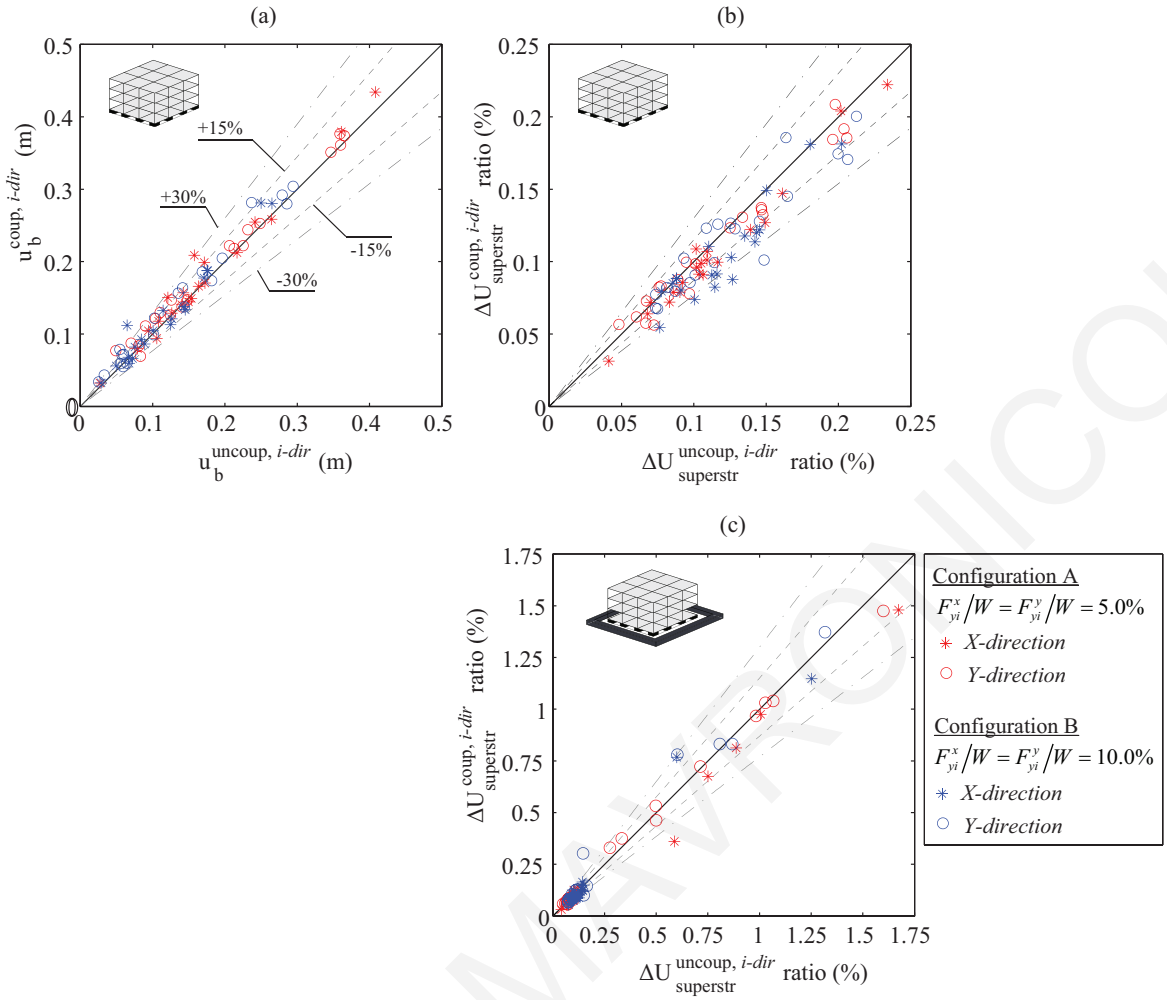

Figure 6.2 Comparison of structural responses between coupled and uncoupled isolators behavior: (a) peak unobstructed relative displacements at the isolation level, (b) envelope of peak interstory deflections, when a sufficient gap is provided around the building, (c) envelope of the maximum interstory deflections when separation gap is limited to 20 cm, leading to structural pounding.

The accurate description of the shear force–deformation response of the base isolation bearings can be crucial for design and analysis purposes. Due to the coupled behavior of the isolation bearing response, the contribution of the plastic force in the *X*-direction varies due to motion demands in the perpendicular *Y*-direction. The coupled model shows considerable interaction effects in hysteresis loops. Therefore, in the following sections, the seismic response of the base-isolated structure is investigated under bidirectional excitations of real ground motions, and the coupled Bouc-Wen model is used in order to more realistically capture the shear force–deformation behavior.

6.2 Critical Angle of Seismic Incidence

Several researchers have addressed the issue of the incident angle of the ground excitation in seismic design. Penzien and Watabe (Penzien and Watabe, 1974) had first described the

methodology for determining the principal axes of a multi-component excitation. Based on the principal component theory, several closed form equations and procedures to determine the critical incident angle for a given ground motion have been proposed (Kostinakis *et al.*, 2015; Lopez *et al.*, 2000; López and Torres, 1997; Wilson and Button, 1982). However, the effect of the orientation of the seismic action, i.e. the angle in which the horizontal seismic components are applied with respect to the structural axes has been mostly studied for fixed-supported structures and highway bridges (Kalkan and Kwong, 2014; Kostinakis et al., 2012; Magliulo et al., 2014; Polycarpou et al., 2015b; Taskari and Sextos, 2015; Torbol and Shinozuka, 2012). However, none of the previous studies investigated in a systematic manner the effect of the seismic excitation direction on the dynamic performance of base-isolated reinforced concrete buildings. This highlights the need to explore the sensitivities of base-isolated building responses to the effects of the incident angle while using nonlinear time history analysis.

6.2.1 Base-isolated Buildings Response without Pounding

During dynamic analysis, the orientation of imposed horizontal ground motion components is commonly applied along the principal structural axes, without further consideration. By rotating each of the 20 selected seismic record pairs, with respect to the system's principle axes of construction, from 0° to 360°, with a 5° interval, 73 alternative excitation cases can be considered. In order to identify potential differences in the peak response of base–isolated buildings due to the incidence angle of the ground motion, the peak relative displacements at the isolation level and peak interstory drift ratios over all stories (in the *X*-direction and the *Y*-direction, as well as the corresponding resultant) are presented in Figure 6.3. It is noted that the peak resultant relates to the peak square root of the sum of the squares of the components in X and Y directions. The peak responses of two seismically-isolated buildings, with different isolators' characteristics in each case are illustrated in Figure 6.3(a) and (b), considering various orientations of each of the 20 near-fault earthquakes.

The simulation results indicate that the influence of the incidence angle on the seismic demand varies significantly depending on both isolator characteristics F_{yi}^{x}/W, F_{yi}^{y}/W and frequency content of each examined ground motion. The variability is considerably larger for some ground-motion pairs (for example, EQs No. 5, 7, 12, and 19), as compared to the minor variability observed for EQ No. 2, 3, 15, and 17, which is consistent for base and story drifts in both directions. Based on the presented outcome, maximum relative

displacements at the isolation level in each direction can vary by a factor of 1.2 (20%) up to 7.2 (720%) over the possible angles of interest, in the particular case. Similarly, interstory deflections in each direction depend highly on the incidence angle with extremities that their discrepancy reaches a ratio of up to 3.6 (360%). These are considered to be significant variations that can play a decisive role in the design process of such structures.

Also, it should be noted that, although the peak examined responses in each direction depend highly on the incidence angle, the maximum resultant of the responses, defined as the maximum value of the vector sum of the response values in the two structural axes (noted by red squares), remains relatively unaffected by the angle of incidence. It should be noted that the variation of the peak response with the angle of incidence is equivalent for both *X*- and *Y*-directions, thus, only a single marker is used in Figure 6.4. The correspondence, however, between the *X*- and *Y*-directions is shifted by 90 degrees (i.e. complementary angles), since the examined buildings are symmetrical in both directions. This is further elaborated with the aid of polar plots as presented below.

Furthermore, Figure 6.4 permits the following observations: (1) Since the maximum responses in the two horizontal directions are not attained at the same time instant, the maximum vectorial sum is not directly obtained by the algebraic summation of the maximum *X* and *Y* response values. (2) The peak resultant values under examination are not directional independent. Note that this finding pertains only to base-isolated structures symmetric in both directions with uniform mass and stiffness distributions. Under a preliminary investigation, it has been found that any deviation for the aforementioned conditions would lead to non-circular peak responses and, subsequently, the effect of the angle of incidence on the structural response would become significant. (3) Maximum interstory deflections in each direction over all non-redundant orientations are generally polarized in the direction along which the peak relative displacements at the isolation level is observed. This implies that the excitation angle plays an insignificant role for design purposes in the absence of structural pounding. Nevertheless, this cannot be generalized to cases with collisions, a situation which is considered next. (4) The angle of incidence is an important aspect in the computed seismic response, but difficult to be taken into account in a systematic way. Therefore, standard regulatory provisions should be established for both design and assessment of such structures.

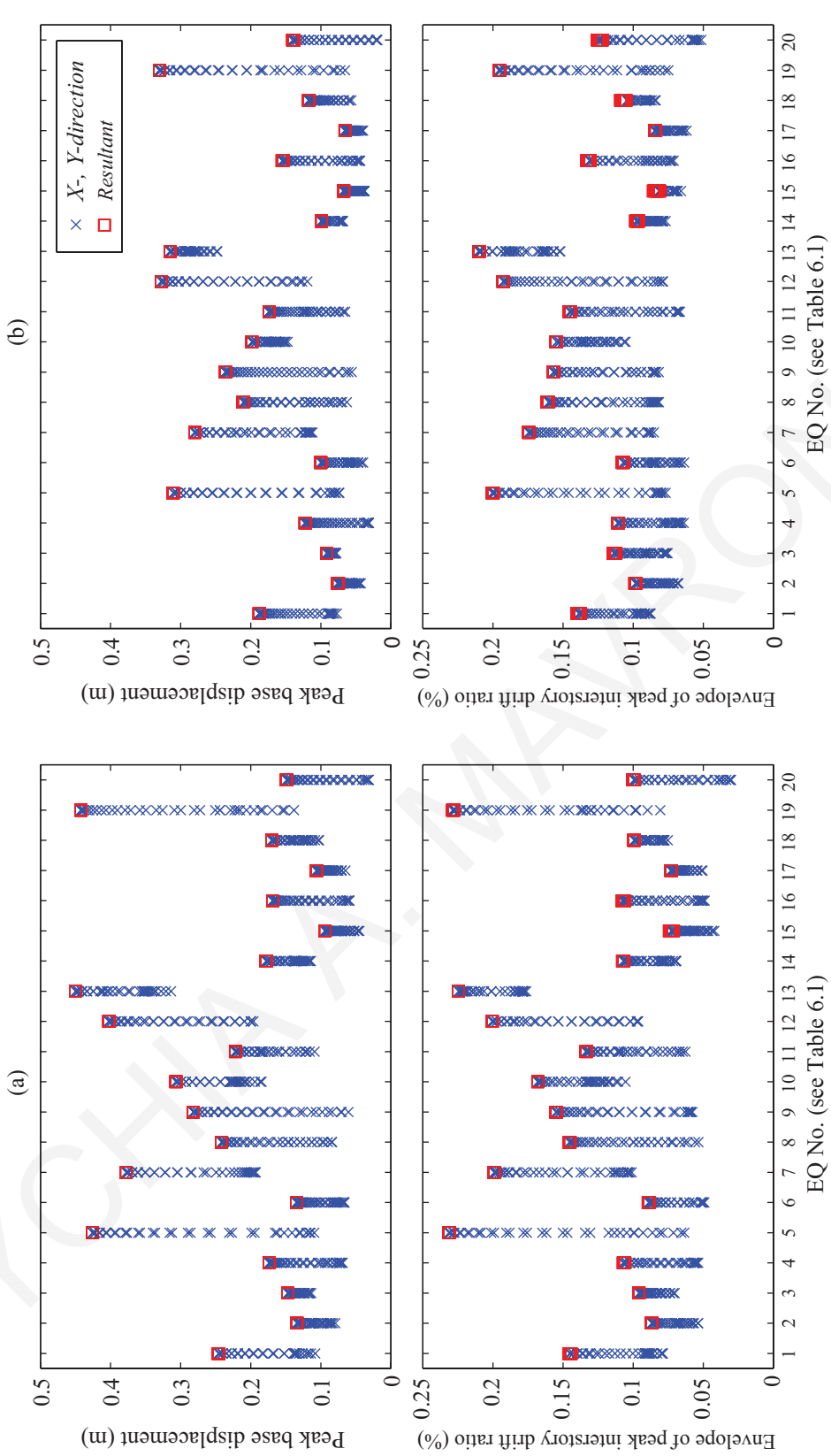

Figure 6.3 Variation of the peak response of the base-isolated buildings subjected to near-fault pulse-like ground motions for different angles of incidence considering two different values of normalized characteristics strength in both directions for the i^{th}-isolator: (a) 0.05, and (b) 0.10, while 73 angles of incidence have been considered for each excitation, each one indicated by a point marked with x.

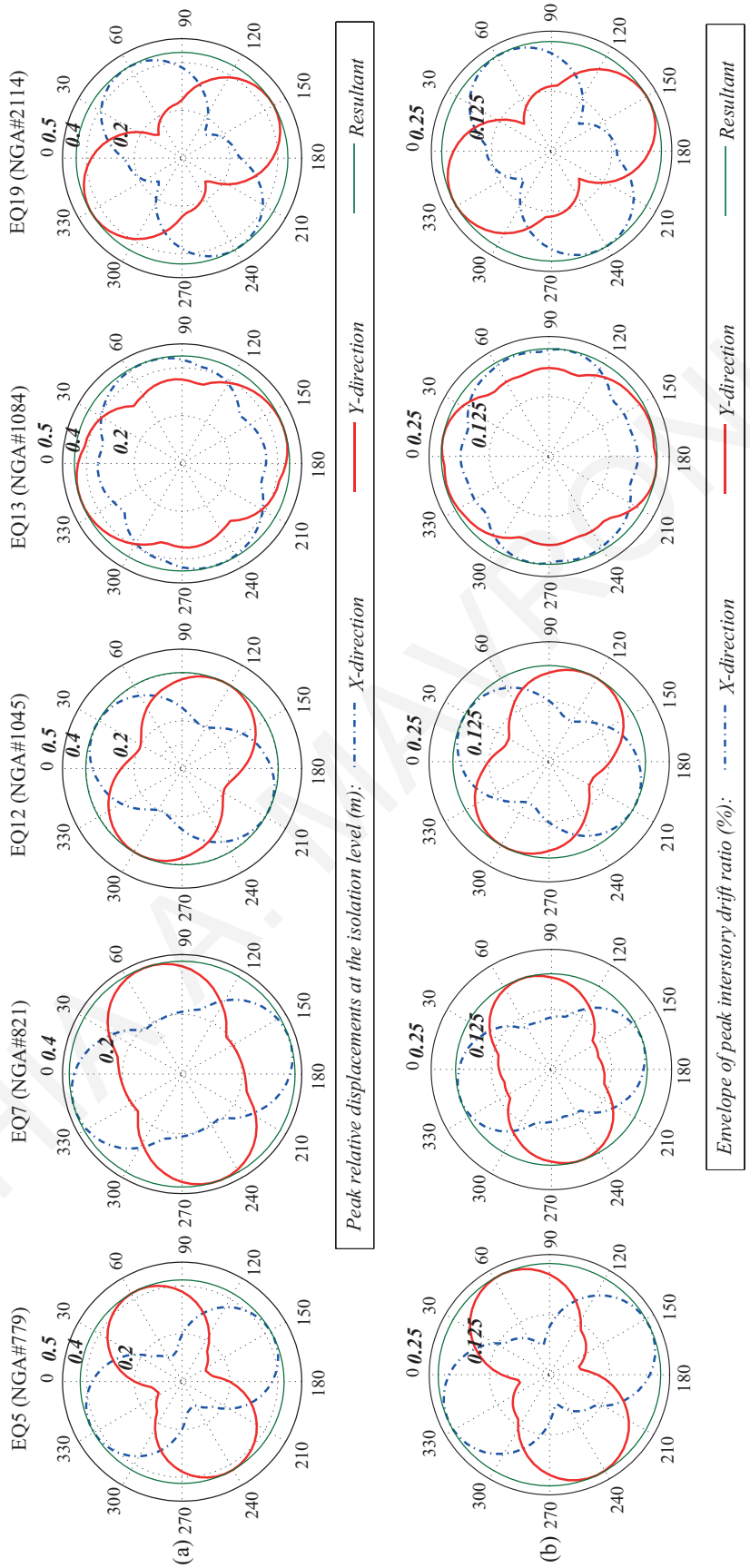

Figure 6.4 (a) Peak unobstructed base drifts, and (b) maximum interstory drifts of the building's corner column A_1 in terms of the excitation angle, considering normalized characteristic strength of 0.05 in both directions for the i^{th}-isolator.

Another consideration relates to the performance of seismic isolation under the selected near-fault earthquakes at arbitrary directions of the seismic action. In order to examine this aspect, the ratio of the fixed-base building to the base–isolated structure response is calculated for the peak resultant interstory drifts among all floors over all angles. While a presentation of the peak response of the fixed supported building is provided only for 5 selected ground motions for brevity, the examined ratio appears to strongly depend on the excitation frequency content, fluctuating between 1.35 and 9.75, having only a minor dependency on the angle of incidence. Figure 6.4(b) and Figure 6.5 demonstrate, for the two buildings considered herein, that the critical angles significantly differ in the *X* and *Y* directions. Therefore, it can be deduced that the effect of the excitation characteristics in the interstory drifts is considerably influenced by the dynamic characteristics of the structure.

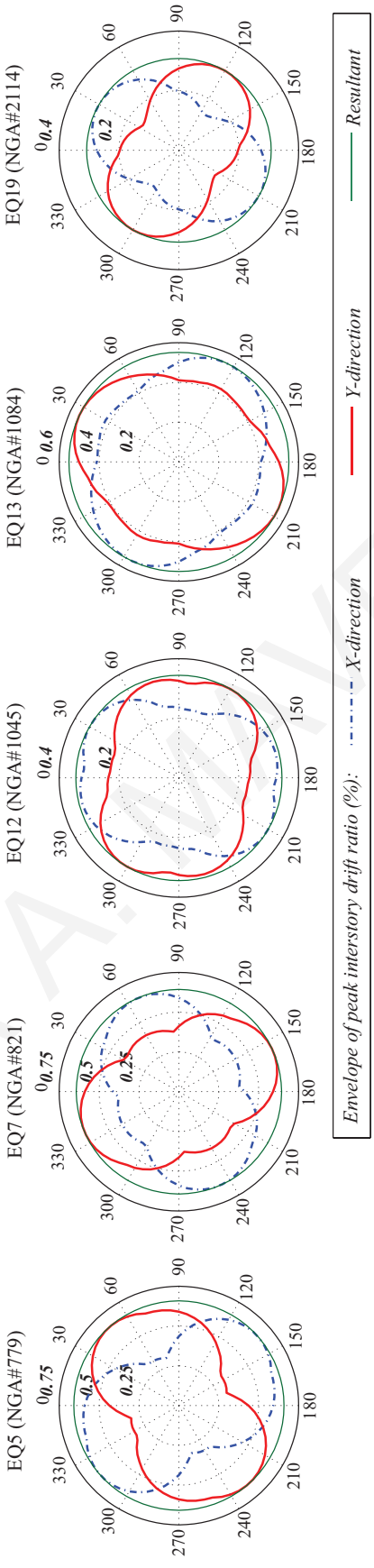

Figure 6.5 Maximum interstory drifts of the fixed-supported building's corner column A_1 in terms of the excitation angle.

6.2.2 Structural Response considering Seismic Pounding

The response of three base-isolated building case studies are discussed next, assuming an available seismic gap between the simulated structure and the retaining walls of 20 cm. For the simulations presented in this section, the 10 earthquakes that cause base displacements in *X*- or *Y*-direction larger than 20 cm in the unobstructed case (first row in Figure 6.4(a)) have been selected. The effect of structural collisions on the peak response is discussed in view of different isolator's characteristics and geometrical arrangements for the moat walls. The abbreviations *X* or *XY* indicate the directions of motion, which are restricted by the presence of moat walls around the building, while the suffix, 5 or 10, is used to represent the normalized characteristic strength ratio of the isolator in percent. Three different case studies are considered herein:

Case Study X-5:

Base-isolated building with retaining walls on two sides (*X*-direction)

LRBs: $T_b^x = T_b^y = 2.0$ s, $u_y^x = u_y^y = 1.0$ cm, $F_{yi}^x / W = F_{yi}^y / W = 5.0\%$

Case Study XY-5:

Base-isolated building with retaining walls on all four sides (*X*- and *Y*- directions)

LRBs: $T_b^x = T_b^y = 2.0$ s, $u_y^x = u_y^y = 1.0$ cm, $F_{yi}^x / W = F_{yi}^y / W = 5.0\%$

Case Study XY-10:

Base-isolated building with retaining walls on all four sides (*X*- and *Y*- directions)

LRBs: $T_b^x = T_b^y = 2.0$ s, $u_y^x = u_y^y = 1.0$ cm, $F_{yi}^x / W = F_{yi}^y / W = 10.0\%$

The envelopes of the peak interstory drift ratios of the corner column A_1, over all stories of the structure, are shown in Figure 6.6, for various angles of the seismic incidence. The results are obtained for the three different case studies presented above during the action of the 10 selected earthquakes that potentially cause impact. Each subplot corresponds to the peak response of a particular excitation, while the gap size around the building is set at 20 cm.

The peak interstory drift ratio when seismic pounding is not considered (second row of Figure 6.3) is very small, with maximum values retained below 0.25%, suggesting no structural damage to the building. On the other hand, the occurrence of collisions lead to major damages in base-isolated structures suggested by the simulated interstory drift ratios in the range of 0.5-1.5% (Figure 6.6), which most of the times correspond to moderate structural damage. A notable exception is the damage range for the Northridge earthquake, falling in the range of 1.5-2.5% interstory drift ratios, which usually correspond to severe structural damage.

In the case of unidirectional base displacement restriction and isolation systems with the lower bound of normalized characteristic strength of $F_{yi}^{x}/\mathrm{W} = F_{yi}^{y}/\mathrm{W} = 0.05$ (Case Study X-5) illustrated in Figure 6.6(a), the polar plots of the peak responses resemble 8-shapes, exhibiting a pronounced dependence of the peak response on the incidence angle. Similarly, the envelopes of peak interstory drift ratios for the Case Study XY-5, Figure 6.6 (b), also depend on the incidence angle, exhibiting two maxima in orthogonal directions. This finding lies on the fact that, although retaining walls are placed on each of the four sides of the building, amplification of responses relates to the impact occurrences with respect to the excitation angles, which subsequently leads to petal-like shape responses.

A closer look at the results presented in Figure 6.6(b) and Figure 6.4 reveals that the maximum interstory drift ratios for each excitation due to pounding seems to be polarized in the direction in which the peak unobstructed base relative displacement is observed. Furthermore, the occurrence of impacts generates a significant response dependency on the angle of excitation. As a consequence, the consideration of the directionality of planar ground motions becomes an essential parameter that should be investigated during the design process. In order to emphasize the importance of the discrepancies that might occur between the maximum and the minimum interstory drift ratios, it is indicatively noted that the range of values that are obtained for Case Study X-5 correspond to a mean maximum to minimum ratio within the range of 3.5 – 7.5 with a mean value of 5.4.

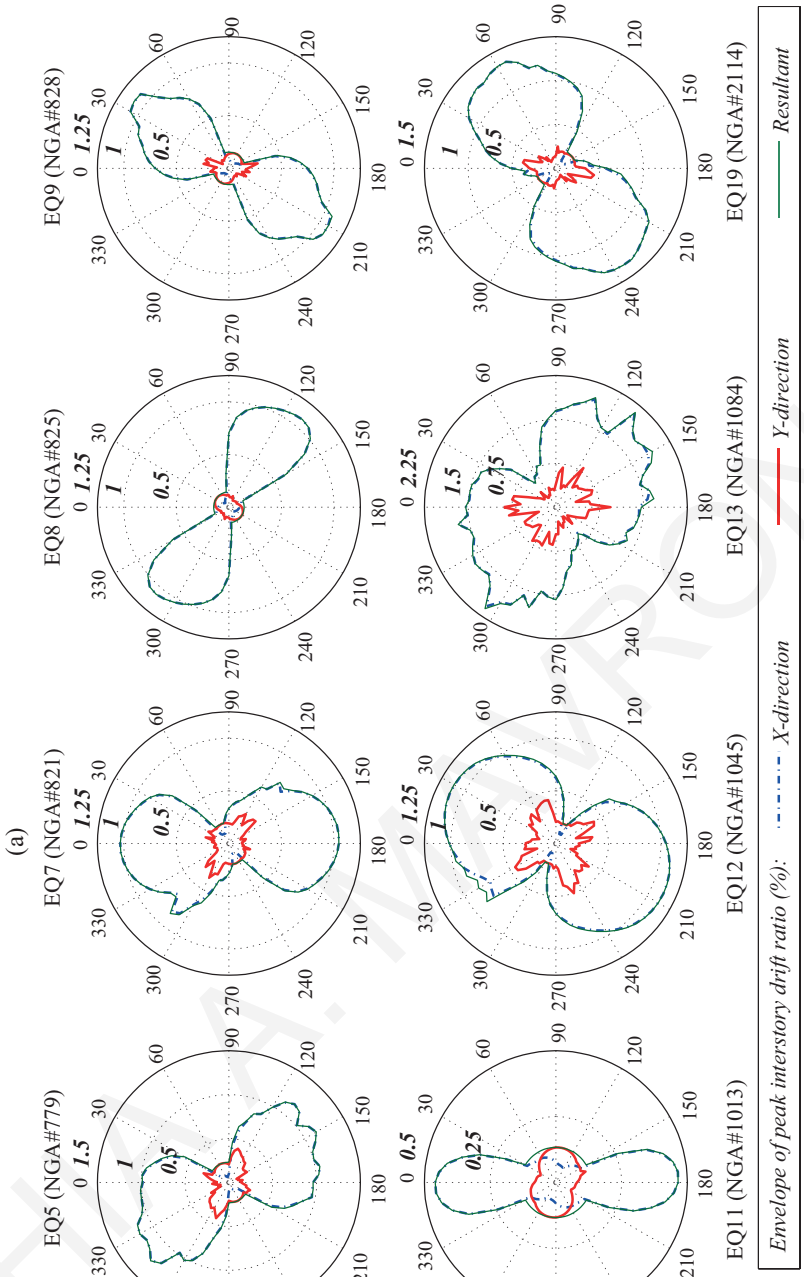

Figure 6.6 Polar plot envelopes of peak interstory drift ratios of column A_1 for various excitation angles and different geometrical arrangements of moat walls (a) Case Study X-5, (b) Case Study XY-5, and (c) Case Study XY-10.

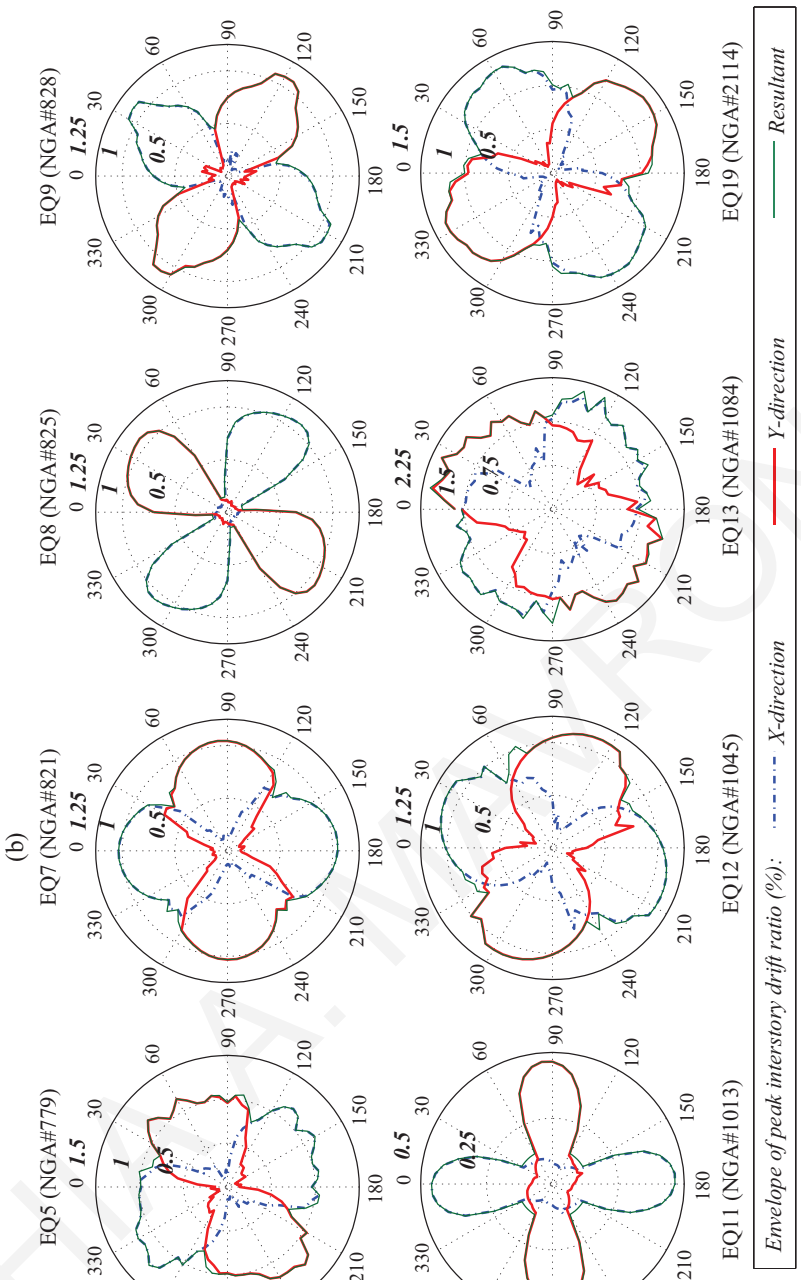

Figure 6.6 Polar plot envelopes of peak interstory drift ratios of column A_1 for various excitation angles and different geometrical arrangements of moat walls (a) Case Study X-5, (b) Case Study XY-5, and (c) Case Study XY-10. (cont'd)

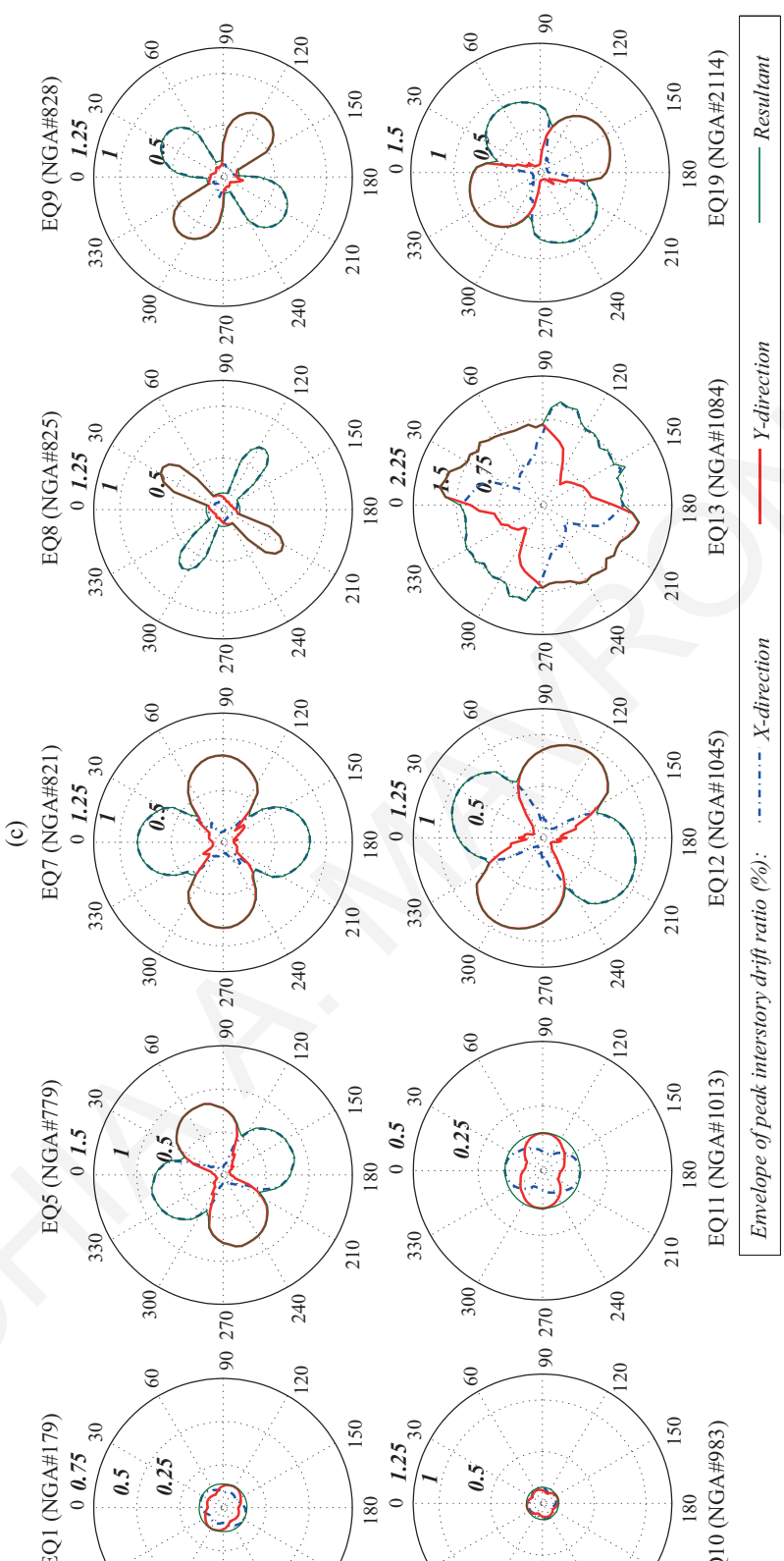

Figure 6.6 Polar plot envelopes of peak interstory drift ratios of column A_1 for various excitation angles and different geometrical arrangements of moat walls (a) Case Study X-5, (b) Case Study XY-5, and (c) Case Study XY-10. (cont'd)

Similarly-organized results, as those presented previously in Figure 6.6(b) for the three-story base-isolated building, are provided in Figure 6.6(c), for seismic isolators with normalized characteristic strength equal to 10%. A remarkably similar trend is observed indicating that the increase in drift demands due to pounding in Case Study XY-10 is less than the corresponding to Case Study XY-5 for all examined ground motions. In the absence of any structural pounding under near-fault ground motions, the peak relative displacements at the isolation level are significantly lower for isolators with higher normalized characteristic strength. Therefore, the influence of collisions in the response of the base-isolated building can be more detrimental when isolators with higher characteristic strength are incorporated since the corresponding maximum unobstructed displacement of the base-isolated building is more likely to exceed the available clearance around the base-isolated building.

Figure 6.7 shows polar plots of the corresponding peak resultant interstory drifts ratios at each floor of the base-isolated building, for Case Study XY-5, under the 10 earthquakes that potentially cause impact. It is apparent that the most severe peak interstory deflections occur at the base level where collisions occur. Subsequently, the maximum responses occur at the 1-0 interface. The influence of the excitation angle persists for the upper floors.

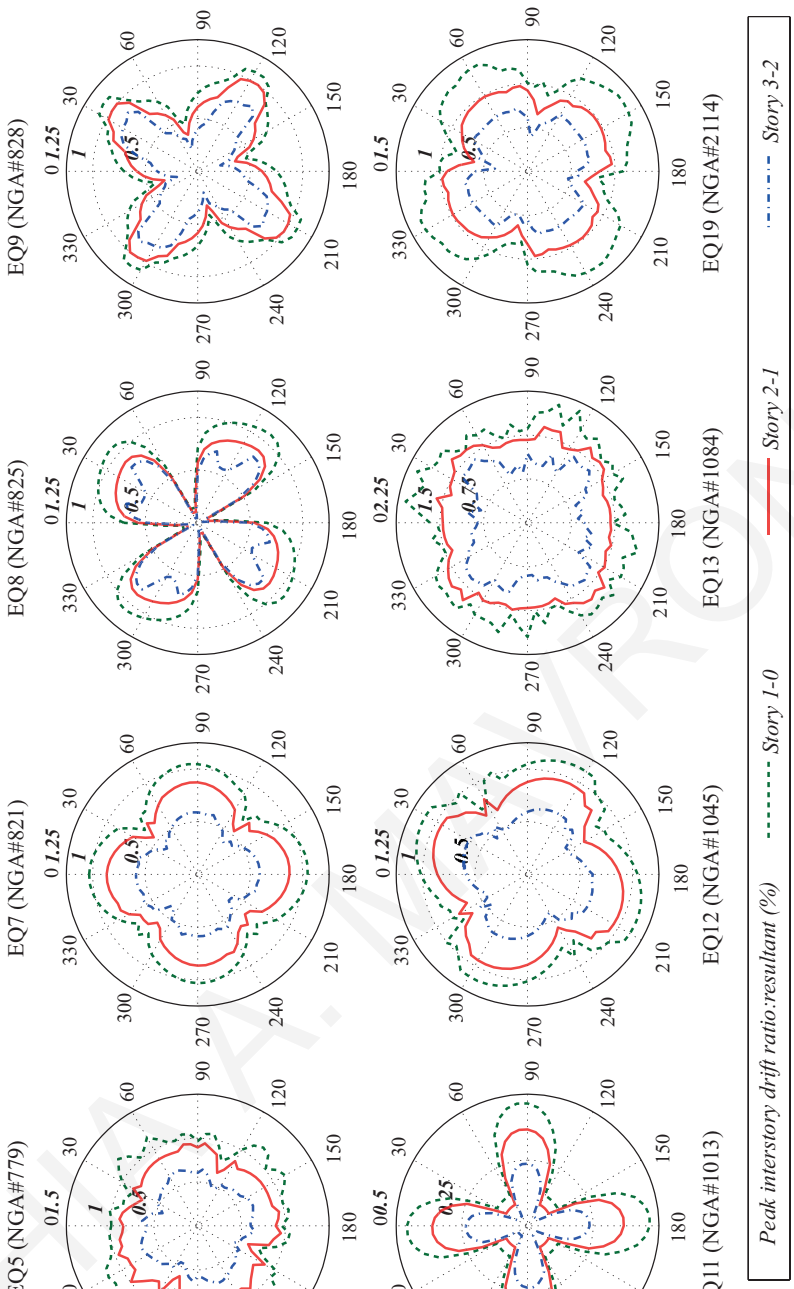

Figure 6.7 Polar plots of the peak resultant interstory drift ratios at each floor of the corner column A_1 for various seismic excitation angles: Case Study XY-5.

6.3 Variation of the Impact Parameters

The generated impact force depends on the constitutive model that is used. The deformability of the structures is taken into consideration through the impact stiffness coefficient, k_{imp}, which constitutes a composite elastic model generated through the impact, similar to Hertzian contact mechanics. The results presented in Section 0 assume a fixed value of the k_{imp} resulting from a fixed value of the elastic modulus of concrete equal to 30 GPa, which corresponds to typical values for medium/high grade concrete. In order to examine the influence of the k_{imp} on the overall structural response of a base-isolated building with retaining walls on two sides (Case Study X-5) the elastic modulus of concrete, E_{st}, is varied between 10 and 35 GPa.

Figure 6.8 shows the effect of the impact stiffness on the peak interstory drift ratio normalized by the corresponding response presented in the previous section for $E_{st} = 30\,\text{GPa}$ and $e = 0.65$ for the 10 selected seismic excitations. Each plot contains the results from 42 simulations obtained at a 7×6 grid. It is evident that while the stiffness of the material affects, as expected, the overall seismic structural response its contribution is limited within -15% to +10%, effects which can be considered relatively insignificant compared to the amplification effects, observed due to the angle of incidence. A similar conclusion can be drawn for the effect of the coefficient of restitution, as shown in Figure 6.9 for a single seismic excitation.

Furthermore, Figure 6.10 shows the variation of peak interstory drift ratios as a function of the angle of incidence for 5 seismic excitations: the influence of k_{imp} is highlighted in the results of the first row, whereas the influence of e is quantified in the second row. These results justify the statement made earlier regarding the relative insignificance of the contribution of k_{imp} and e on the overall peak dynamic structural response compared to the effect of the incidence angle of the seismic excitation. In general, the results show that, the choice of the constitutive impact model and its involved parameters affect the overall response; nevertheless, this is relatively of secondary nature compared to the effect of the directionality of the seismic excitation on the computed peak response.

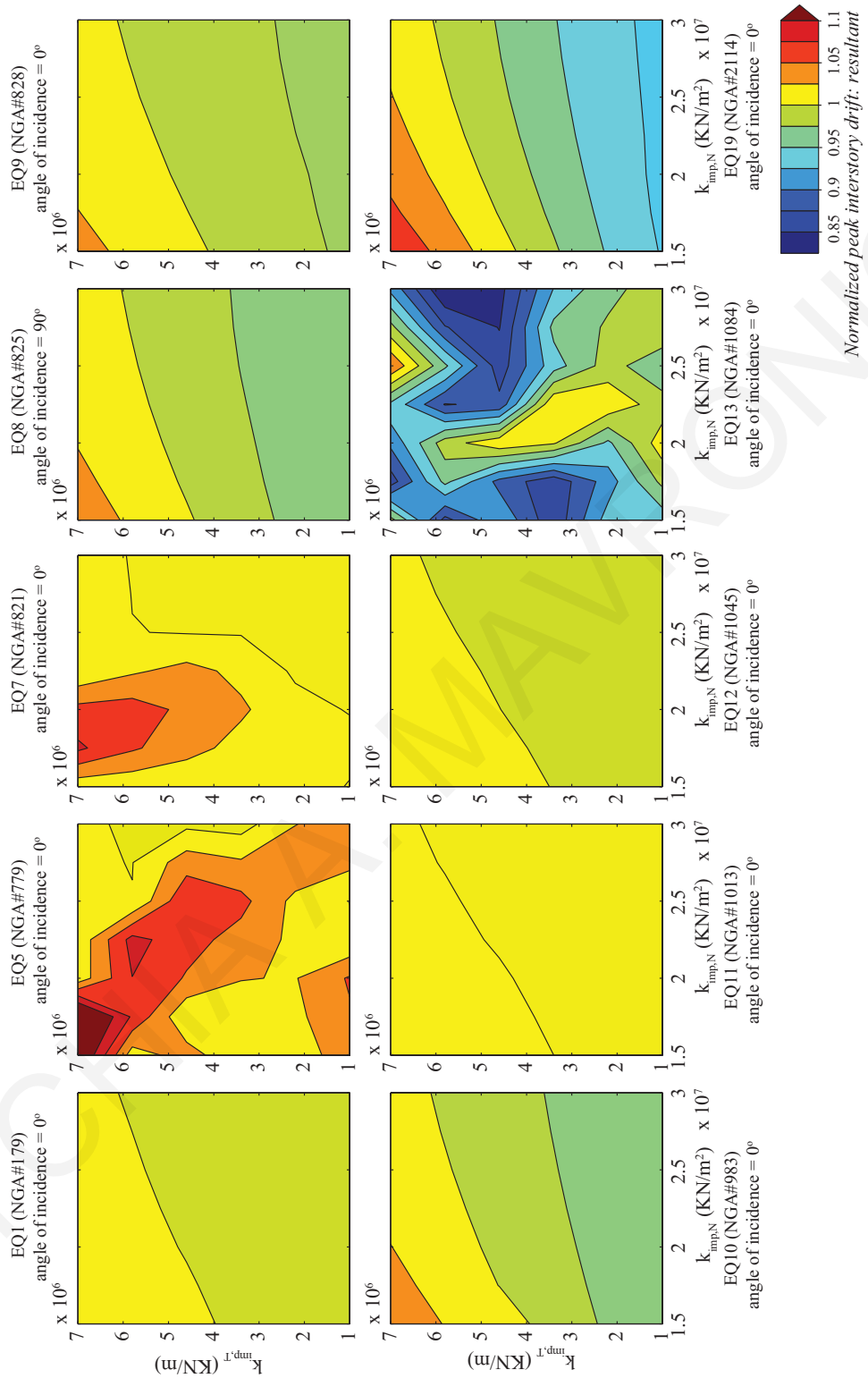

Figure 6.8 Peak interstory drifts among all corner columns, considering various combinations of impact stiffnesses in normal and tangential directions, e = 0.65 and gap size=20 cm, normalized with respect to the corresponding peak response while considering constant $k_{imp,N}$=2.58×10^7 kN/m^2, $k_{imp,T}$=5.74×10^6 *kN/m* and *e*=0.65 values.

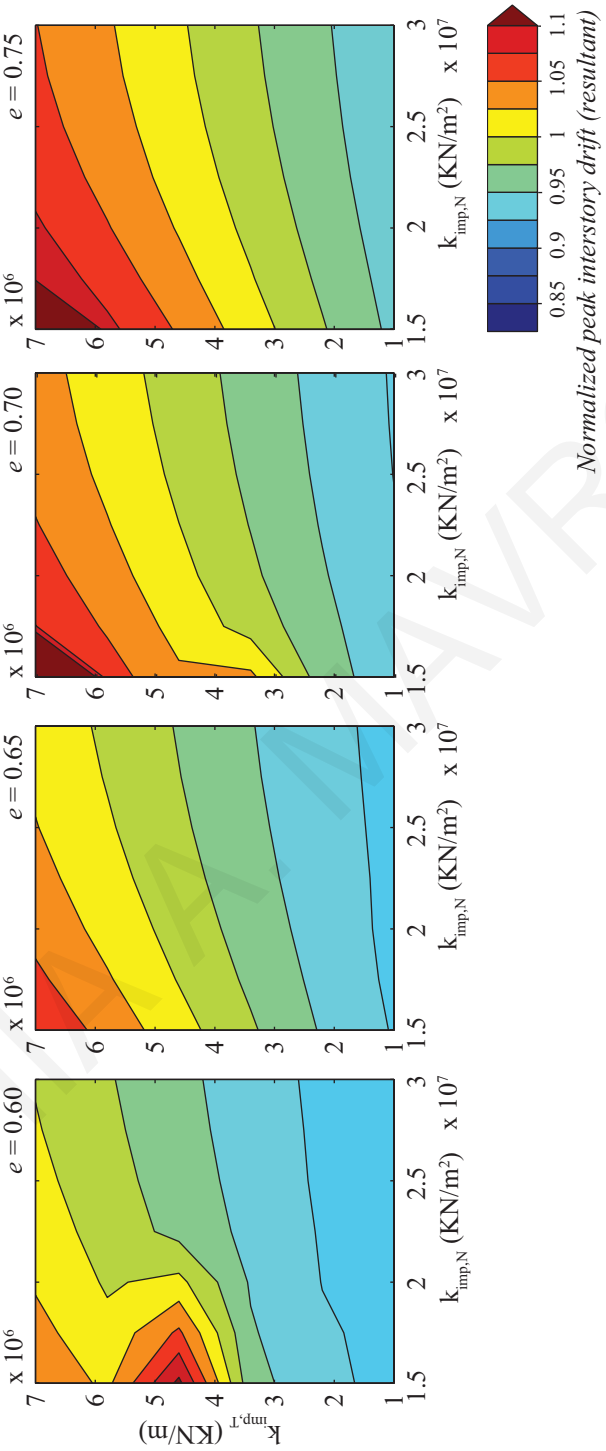

Figure 6.9 Peak interstory drifts among all corner columns under the Denali earthquake (EQ19) considering various combinations of impact parameters (k_{imp}, e) and a fixed gap size of 20cm, normalized with respect to the corresponding response while considering constant k_{imp} and e values.peak

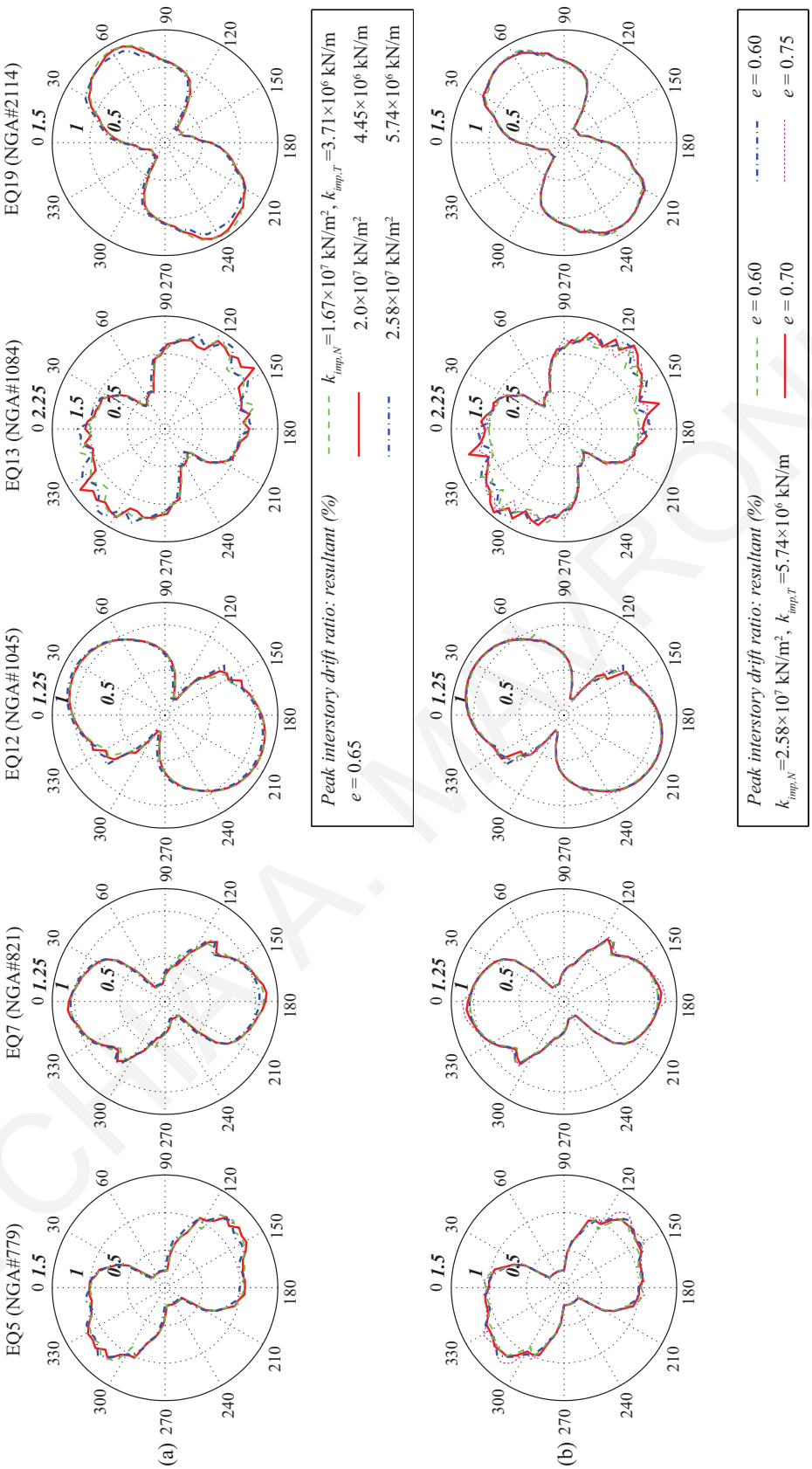

Figure 6.10 Polar plot envelopes of peak interstory drift ratios among all corner columns for various excitation angles and different impact parameters (k_{imp}, e) considering a gap size of 20 cm, Case Study X-5.

6.3.1 Effect of Contact Friction during Impact

The effect of the magnitude of the tangential impact forces and the friction between the colliding bodies on the peak structural response, can be examined only through spatial dynamic analysis. Wriggers (Wriggers, 2006) reported that the coefficient of friction for concrete-to-concrete contact varies from 0.5 to 1.0, depending on the material pairing of the solids in contact. Table 6.2 reports the friction coefficients for various material pairs. Jankowski used a value of 0.5 for impact between concrete structures (Jankowski, 2012). In another recent study, the value of the coefficient of static friction $\mu_s = 0.5$ and the value of the kinetic friction $\mu_k = 0.4$ were used (Pant and Wijeyewickrema, 2014), considering that the coefficient of kinetic friction μ_k is about 25% less than μ_s.

Table 6.2 Friction coefficient for different material pairings (Wriggers, 2006).

Material pairing	Friction coefficient, μ
concrete – concrete	0.5 – 1.0
concrete – sand	0.35 – 0.6
concrete – steel	0.2 – 0.4
metal – wood	0.3 – 0.65
rubber – steel	0.15 – 0.65
steel – steel	0.2 – 0.8
steel – teflon	0.04 – 0.06
steel – concrete	0.2 – 0.4
wood – steel	0.5 – 1.2
wood – wood	0.4 – 1.0

The effect of using different values for the coefficient of static friction, μ_s, and the coefficient of kinetic friction, μ_k, is examined next. In doing so, several pounding analyses by neglecting friction, are also carried out to understand the contribution of frictional forces. The peak interstory drift ratios for various combinations of friction coefficients and two different seismic gaps, 15 and 20 cm are plotted in Figure 6.11(a) and (b), respectively. The arrangement introduced in Case Study XY-5 is considered.

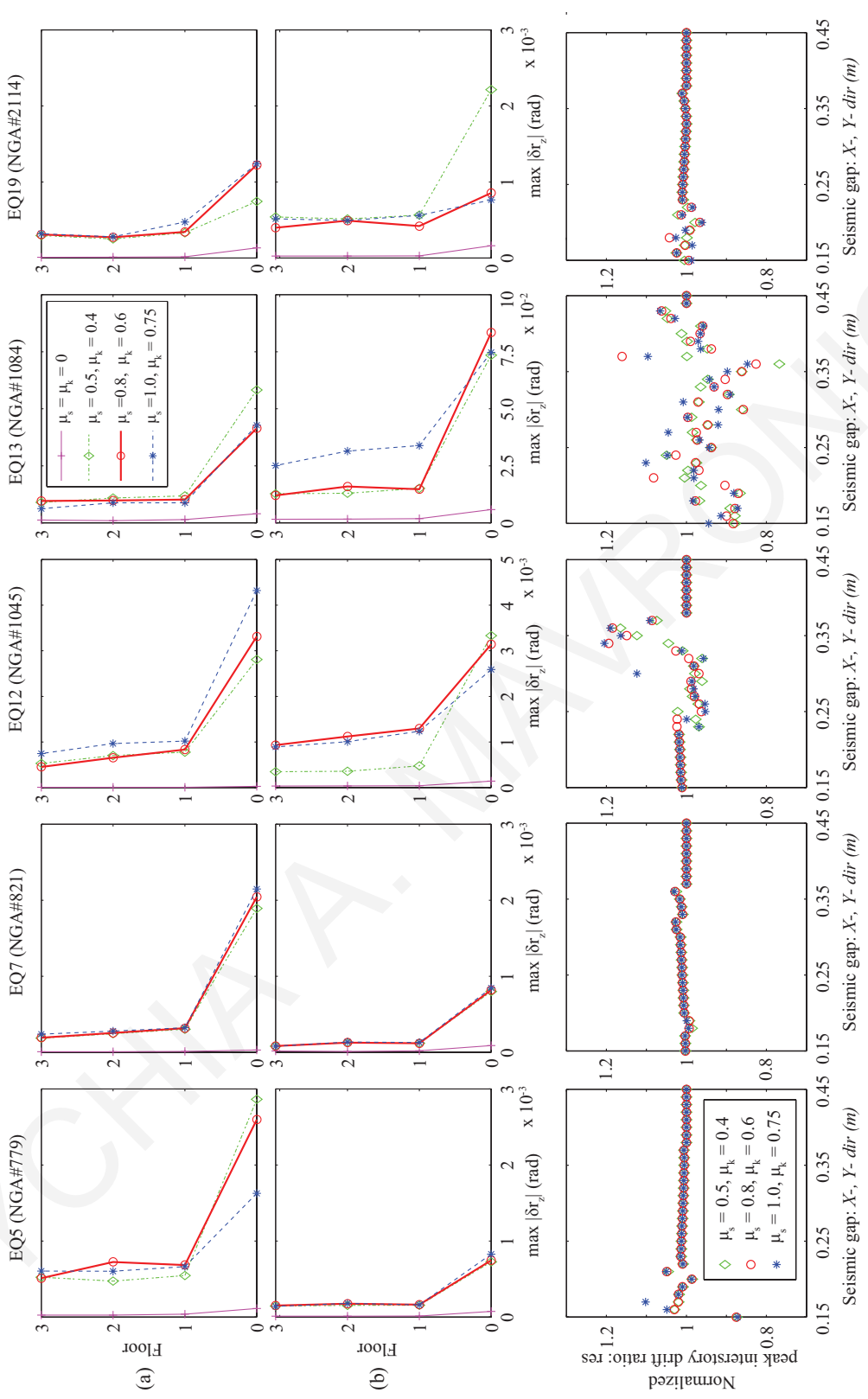

Figure 6.11 Peak absolute values of the interstory deflections (rotational) for various values of friction during impacts, considering seismic gaps equal to (a) 15 cm, and (b) 20 cm, and (c) peak interstory deflections ratio among corner columns considering different friction coefficients normalized to the corresponding response of frictionless models for various seismic gaps.

It becomes apparent that torsional responses are increased when the frictional impact forces are considered. The peak interstory drift ratios considering different friction values normalized with respect to the corresponding response while frictional impact forces are not taken into account are shown in Figure 6.11(c), for a range of seismic gap. In general, the coefficient of friction appears to play a secondary role in the response of base-isolated buildings when pounding occurs.

6.4 Variation of the Superstructure's Stiffness

The effects of the superstructure's flexibility on the overall dynamic response are considered in this section. The peak interstory drifts are obtained for different fundamental eigenperiods of the superstructure for the examined 3-story base-isolated building with impact conditions under 5 seismic excitations, as shown in Figure 6.12. Different stiffnesses of the superstructure are obtained by considering different cross-sections of the columns. The considered isolation system consists of lead-rubber bearings with normalized characteristic strength of 0.05 in both directions, with seismic gaps of 20 cm around all four sides of the structure, Case Study XY-5.

These plots demonstrate that the deflections of the superstructure, as expected, increase as the fundamental eigenperiod of the corresponding superstructure increases. This implies that the behavior of the base-isolated building during impact becomes inferior for superstructures with lower flexibility. Furthermore, the stiffness of the superstructure does not seem to influence the excitation angle that dominates the peak response. Structures with equal horizontal stiffnesses along the two axes of symmetry (*X* and *Y*), where $T_{x,fixed} = T_{y,fixed}$, exhibit two separate peaks for the Loma Prieta excitation (EQ5), at $\theta = 65°$ and $\theta = 145°$, leading to a petal-like shape with double symmetry. Structures with unequal eigenperiods in the two directions, exhibit a single peak and the polar plots display a shape with unequal "petal" size. Subsequently, the similar response of interstory deflections in the *X*-direction in Figure 6.12(a) and (d), relate to the almost identical superstructure stiffnesses in the *X*-direction.

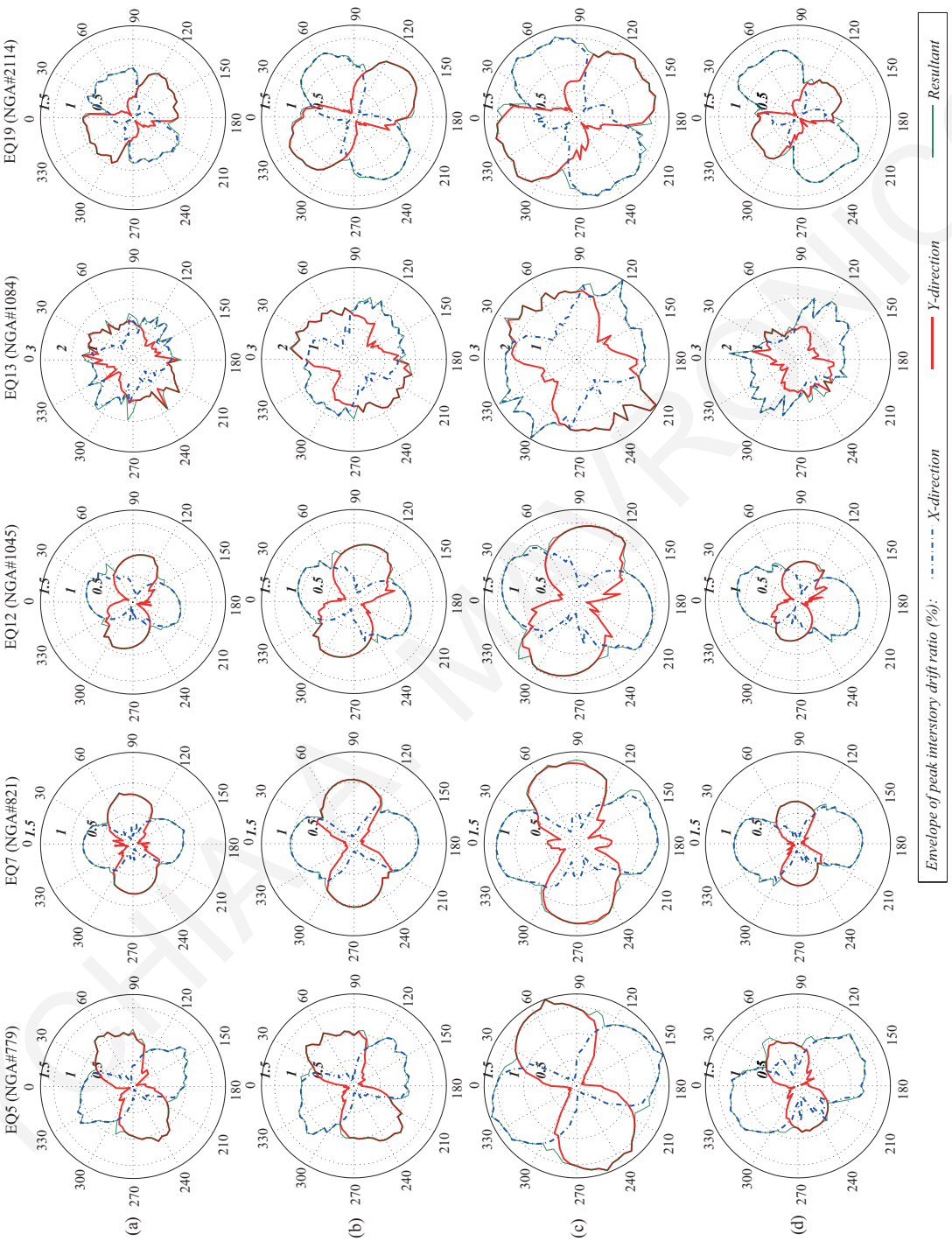

Figure 6.12 Polar plots of envelope responses of peak interstory deflections for the buildings ' corner column A_1 considering superstructure stiffness values ($T_{x,fixed}$=$T_{y,fixed}$) equal to: (a) 0.25 s, (b) 0.311 s, (c) 0.394 s, and (d) $T_{x,fixed}$=0.322 s, $T_{y,fixed}$ = 0.215 s.

6.5 Effect of Separation Distance on Superstructure Response

In base-isolated structures, the separation seismic gap is provided to accommodate the displacements at the isolation level. However, due to sometimes practically limited width of the seismic gap, the possibilities of impact under very strong seismic excitations are increased and, therefore, it is important to study the effect of the separation gap size on the impact response of base-isolated structures. For this reason, almost 5,000 analyses are carried out for the 5 near-fault excitations that induce the largest resultant base displacements. The width of the seismic gap is systematically varied from 15 up to 65 cm, with an increment step of 2.5 cm. The effects of the variation in the separation gap distance on the peak interstory drift ratios among all corner columns (A_1, D_1, A_4 and D_4), which are studied during different earthquakes for the torsionally coupled three-story isolated structures with LRBs, are shown in Figure 6.13. The results are provided for various angles of incidence and considering that the surrounding moat walls in any direction (*X* or *X/Y)* stand at equal distances on each side.

The contour polar plots illustrate that the envelope of the peak superstructure response due to pounding depends on the ground motion characteristics and the available clearance, in relation to the maximum unobstructed displacement under each angle of incidence of the near-fault ground motions. It becomes evident, that the direction of the seismic excitation affects substantially the maximum response of the superstructure, especially during pounding with the surrounding moat walls in only one direction. In general, it is observed that for a range of values of the width of the seismic gap near the maximum unobstructed relative displacement at the isolation level, i.e. the "critical gap size", the envelope of the superstructure's drifts resultant ratio is rapidly increasing and, then, slightly decreases with further reduction in the separation. An evaluation of the results, demonstrate that the maximum interstory drift ratios, over all examined orientations and available gap sizes, seem to be polarized in the direction in which the peak response is obtained when sufficient clearance is provided around the structure ('no pounding case'). The polar plots exhibit perfect symmetry, for this symmetric-plan building, owing to the fact that the structural response among all corner columns has been investigated and the peak response noted.

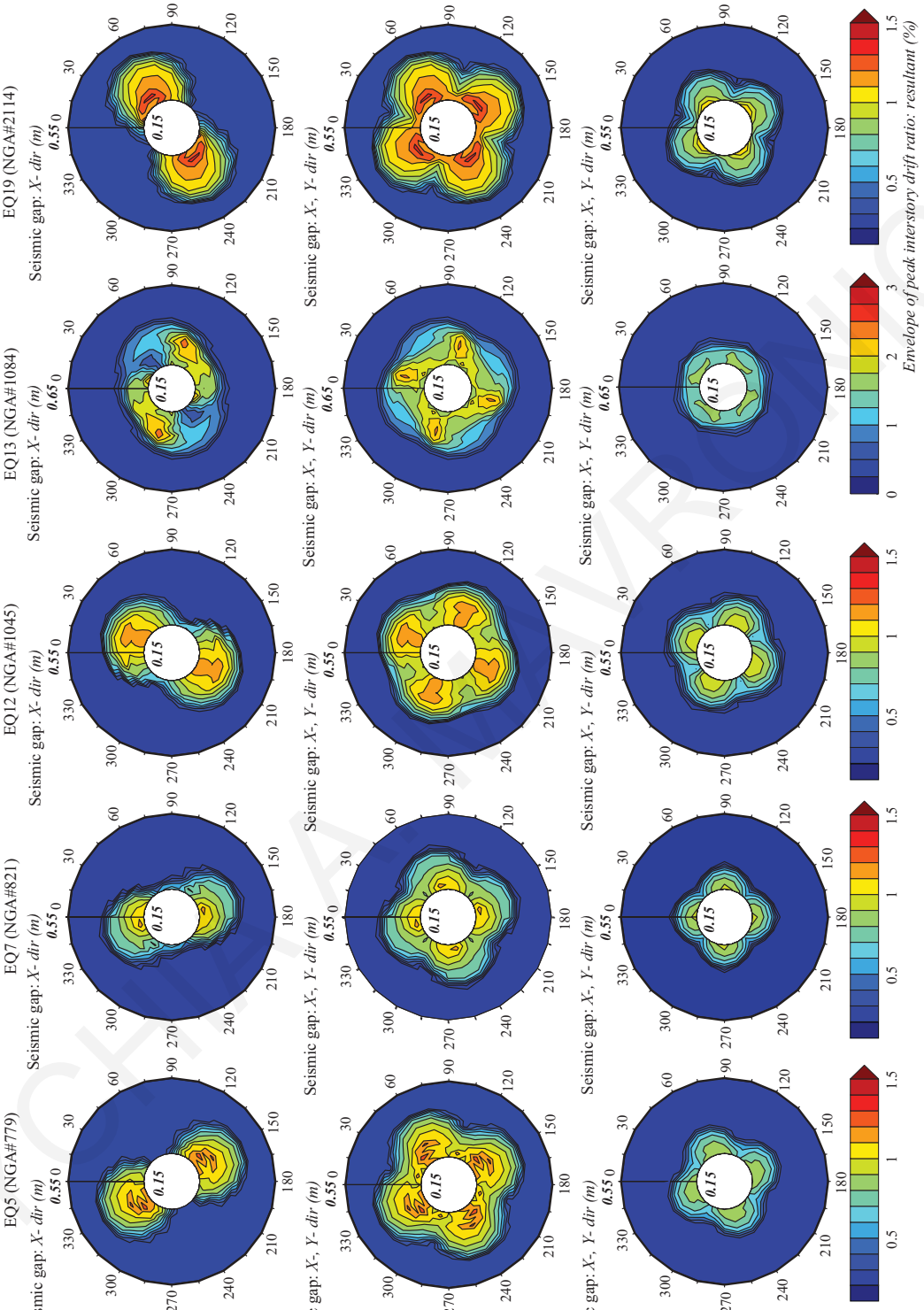

Figure 6.13 Contour plots of the envelope interstory deflection resultant ratio among corner columns, for various angles of incidence and available gap sizes (a) Case Study X-5, (b) Case Study XY-5, and (c) Case Study XY-10.

The value of the maximum interstory drift ratio, due to the Northridge earthquake, for Case Studies X-5 and XY-5, indicate significant amplification of the peak interstory drift ratios at the first story for a limited seismic gap. Structural response due to other earthquakes are significantly lower for all the cases examined. On the other hand, the increase in drift demands due to pounding in Case Study XY-10 is smaller compared to Case Study XY-5 for all examined ground motions, as shown in Figure 6.13(b) and (c), respectively. This is mainly attributed to the fact that the available gap size is more restricted in the first case compared to the corresponding maximum unobstructed displacement of the base-isolated building. An investigation of the peak response suggests that up to a gap size of 80% of the critical gap, the story drift ratios follow a monotonically increasing dependency for the selected excitations, which varies for different excitation angles.

Therefore, the earthquake characteristics in combination with the characteristics of the seismic isolation system and the relation between the available seismic gap and the maximum relative displacements of the building for each earthquake record seem to play a significant role in the severity of the structural impact and its consequences. Also, results demonstrate that rotating ground motions to Fault-Normal (FN) / Fault-Parallel (FP) directions does not always lead to the maximum responses over all angles. Therefore, if the performance assessment and design verification are conducted against worst-case scenarios, then bidirectional ground motions should be applied at various angles with respect to the structure's principal directions to take into account all possible peak responses. Although this might not be a practical solution, it could still be worth conducting for certain projects, even in cases where the specific structures are plan-regular buildings.

6.6 Effect of Number of Stories

Peak resultant interstory drifts for a range of separation distances between the building and the retaining walls are plotted in Figure 6.14, while the number of stories varies between 1 and 6. Various geometrical arrangements for the surrounded walls and isolators' characteristics are considered. Without pounding incidences, the interstory drift ratio variations for the various numbers of stories are similar for all examined excitations. It is noteworthy that the variation trend in peak structural response is similar irrespective of the type of ground motion and the number of stories on the superstructure. More specifically, the resultant of the drifts ratio increases when the separation distance between structures decreases or the number of stories increases.

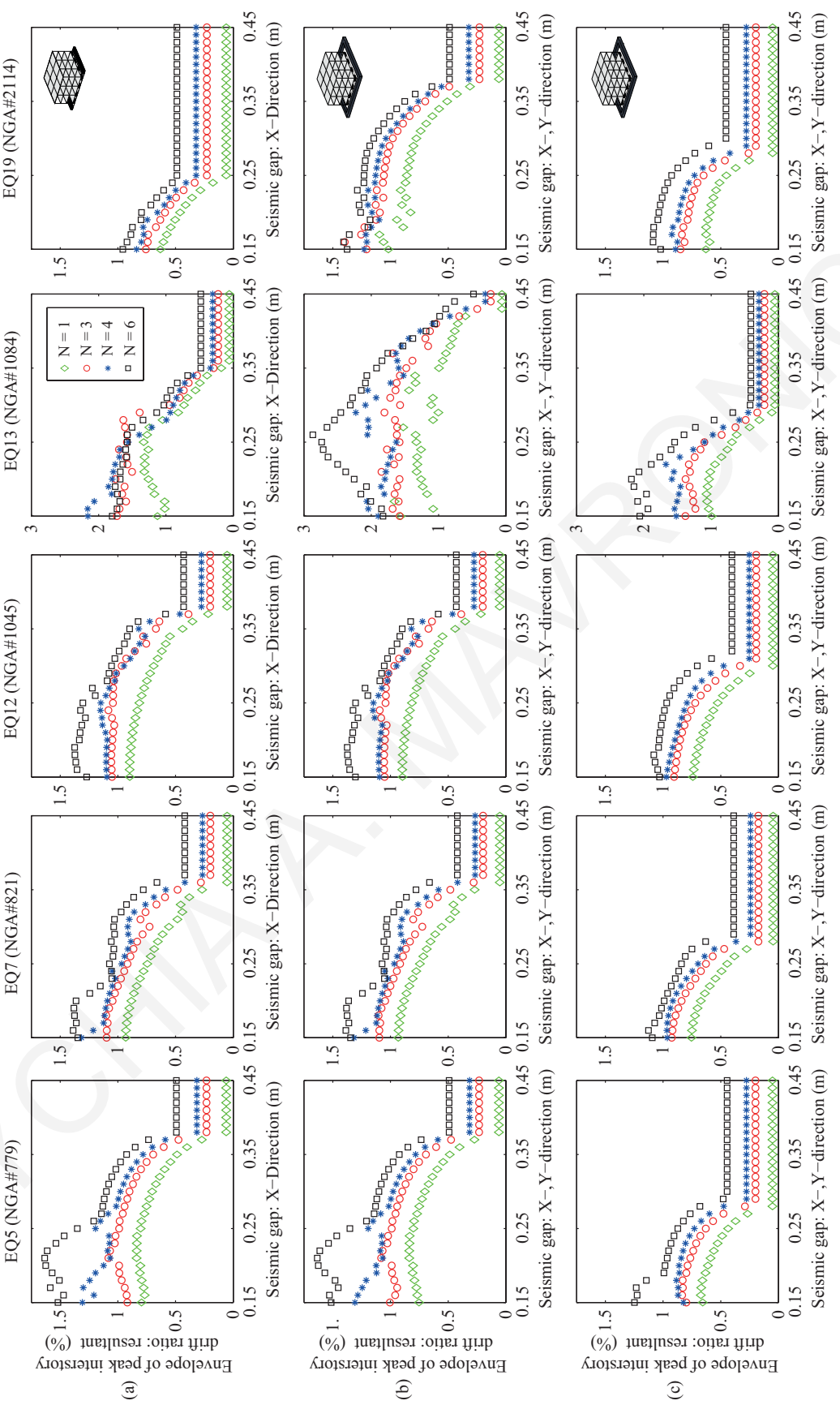

Figure 6.14 Envelope of resultant interstory deflection ratios among corner columns while varying the available gap size, considering different number of stories (N) and configurations.

6.7 Influence of Mass Eccentricities

Torsional effects can potentially occur even in fully symmetric structures due to non-uniform distributions of floor loads, non-symmetric brick partition wall locations and non-symmetric balconies, which are common causes of mass eccentricities in buildings. Torsional effects in buildings were considered by Anagnostopoulos *et al.* (Anagnostopoulos *et al.*, 2015b) in a recent review paper, where the modeling approaches in the field of earthquake induced torsion in buildings were summarized. That research work noted that simplified assumptions and idealizations made towards developing code provisions may lead to inaccurate conclusions, suggesting that the topic requires further in-depth investigation.

Modern codes for earthquake resistant building design require consideration of the so-called accidental design eccentricity, to account for torsional response. Eurocode 8 and the International Building Code (IBC) specify this eccentricity at 5% of the maximum dimension of the floor layout in the considered direction, while the New Zealand and Canadian codes suggest a value of 10%. The above codes require that the mass center in each of the building's floor is transferred along the *X* and *Y* axes, in both positive and negative directions (Anagnostopoulos *et al.*, 2015a). Tena-Colunga and Escamilla-Cruz (Tena-Colunga and Escamilla-Cruz, 2007) studied the torsional response of base-isolated structures when eccentricities occur in the superstructure. They concluded that the eccentricity related to the position of the center of mass in the superstructure leads to higher torsional amplifications for the displacements of the isolation system than eccentricity related to differences in the lateral stiffness of the resisting elements. Furthermore, they noted that peak amplification/reduction factors do not necessarily occur for the highest static eccentricity.

In this section, nonlinear dynamic analyses of a typical three-story building are used to study peak responses for different mass eccentricities, incorporated at all levels of the superstructure with and without considering seismic pounding. The eccentricities are introduced by shifting the center of mass of each floor from their respective center of stiffness, which are located in the geometric center of the plan, as depicted in Figure 6.15. All simulations are for nonlinear isolator systems with yield forces of 5% of the weight of the entire structure. Note that in all examined case studies, the structural plan aspect ratio is $L/B=1$. Among the 16 isolators, 4 are selected to monitor the nonlinear response: these are the corner isolators A_1, A_4, D_1 and D_4, which have the most extreme demands. For the completely symmetric systems, in which the location of the center of mass is not altered in

any way ($e_{s,x} = e_{s,y} = 0$), all isolators experience the same peak responses, since the imposed ground motions induce no torsional response.

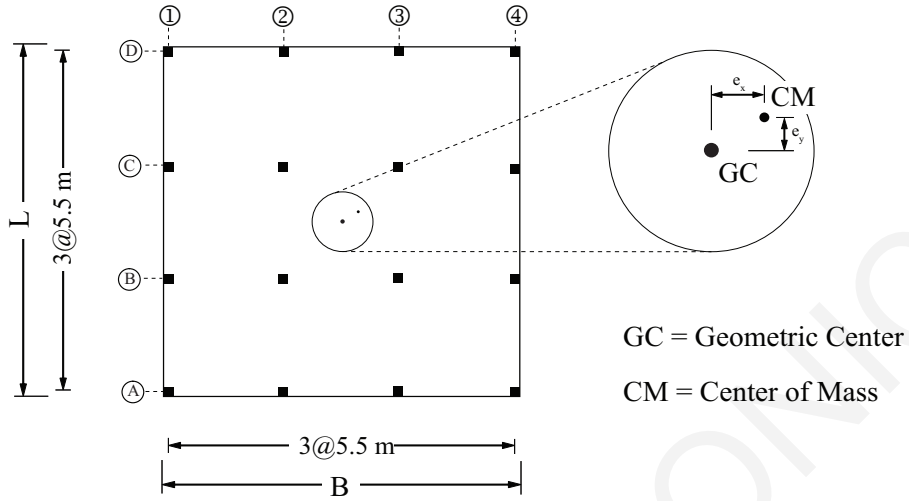

Figure 6.15 Definition of accidental floor mass eccentricity for the base-isolated building.

The envelopes of the peak base displacements and the interstory drift ratios among all corner elements, are contrasted in Figure 6.16 for the case of unidirectional or bidirectional eccentricity versus the peak response of the corresponding symmetric structure without eccentricities. The plots indicate that symmetric systems with mass eccentricities at the superstructure experience very significant response amplifications. The asymmetry introduced by the presence of eccentricity induces rotations at the diaphragms of the structure, leading to enhanced base resultant drifts among all examined ground motions. Such an increase leads to a significant amplification of the peak response of the superstructure, compared to the corresponding results of the symmetric building. The values of $u_{b,\,res}^{eccentr}$ for bidirectional eccentricities of 10% and 5% of the floor plan dimension at all floors, considered for all 20 ground motions, indicate that, on average, the peak base displacement is up to 22% and 17% larger, respectively, than that of the corresponding symmetric structure $u_{b,\,res}^{no\text{-}eccentr}$. The average $\Delta U_{superstr,\,res}^{eccentr} / \Delta U_{superstr,\,res}^{no\text{-}eccentr}$ ratios reach values of approximately 1.25 and 1.2 when considering bidirectional mass eccentricities of 10% and 5%, respectively. In contrast, it is observed that the average structural response ratios due to unidirectional mass eccentricities are kept within lower deviation bounds.

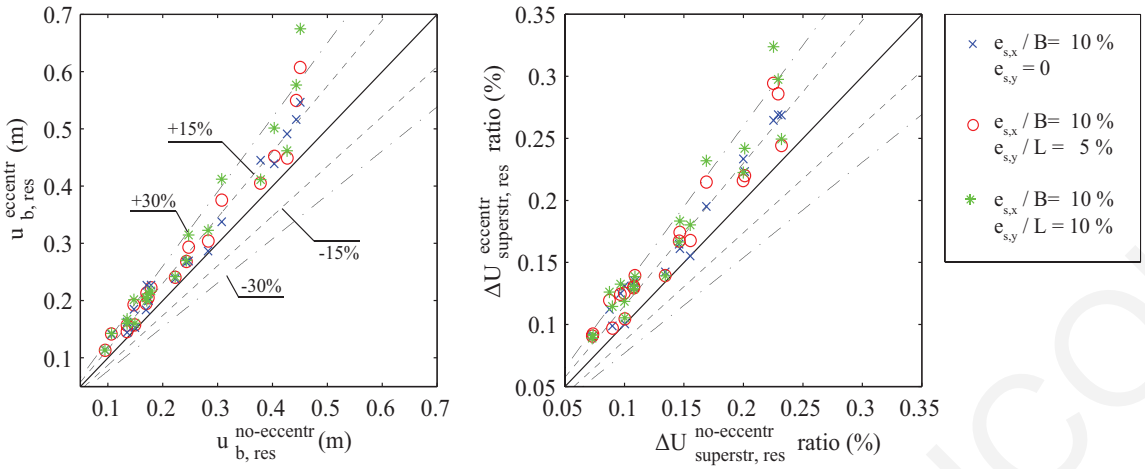

Figure 6.16 Comparison of the peak response considering a symmetric system of reference, no-eccentricity, and building with bidirectional mass eccentricities at all floors (no pounding case).

Similarly, it is important to assess the relative difference on peak structural demands due to mass eccentricity on the superstructure when base isolated buildings are subjected to bidirectional input of the ground motions in the presence of surrounding moat walls. The effect of the mass eccentricity value is parametrically studied, considering isolators with normalized characteristic strength equal to 5% and retaining walls in all four sides (Case Study XY-5). A total of 44 different cases are considered, where, instead of having the floor masses of the base-isolated building lumped at the center of gravity of each floor, a mass eccentricity is assumed in the *X* and/or *Y* directions. The angle of incidence for all ground motions is taken equal as 0° in this investigation.

The percentage deviation of superstructure drifts due to mass eccentricities compared to the corresponding response without any eccentricities are presented in Figure 6.17. The percentage deviation used for generating Figure 6.17 have been calculated using the mean deviation values between among the 10 earthquakes used herein. The amplification factors for the maximum interstory drift ratios of the asymmetric system with respect to the symmetric system, when pounding occurs due to the presence of walls at 20 cm from the base, increase as the mass eccentricity at the superstructure increases, reaching values up to 30-35%. In general, it is observed that the envelope of the interstory drift ratios of all four columns located at the corners of the structure is significantly amplified due to mass eccentricities at the superstructure when pounding occurs. These are the average results among all 10 earthquakes considered herein and, as expected, different values of the peak responses under individual earthquakes are recorded. As already mentioned, mass eccentricity of superstructures significantly amplifies the peak relative displacements at the isolation level compared to the response of the corresponding symmetric structure.

Therefore, specific attention should be placed on this aspect when pounding can potentially occur.

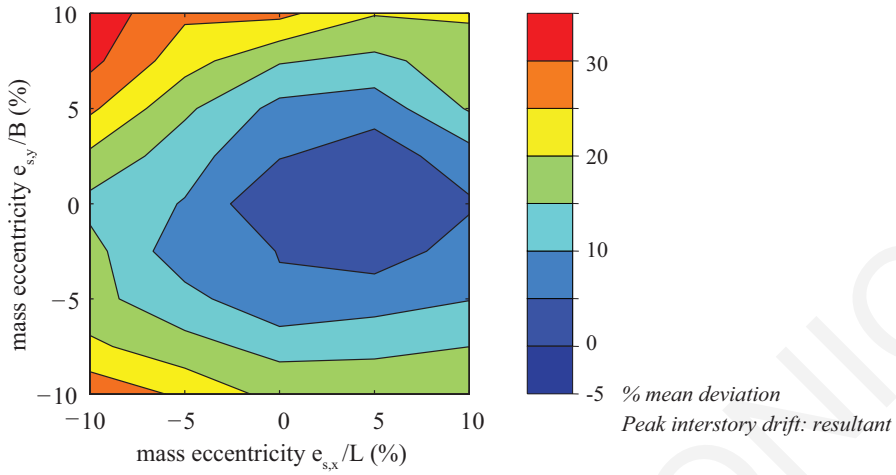

Figure 6.17 Percentage deviation of the peak interstory drifts among all corner columns due to collisions for various accidental mass eccentricities. Average value for the 10 ground motions that pounding occurs for gap size set at 20 cm – no eccentricity case.

It should be stressed that the symmetrical response is retained only in the absence of collisions. In case of collisions with the moat wall, the response depends highly on the location of the impact, which in turn depends on the torsional response of the building. Since the deformed position of the building differs, as shown in Figure 6.18 for the two cases of mass eccentricities (i.e. $e_{s,x}/L=-10\%$, $e_{s,y}/B=-10\%$ and $e_{s,x}/L=10\%$, $e_{s,y}/B=10\%$) the impact locations are also different for the two cases. Therefore, the overall response during pounding is different and there is no symmetry of the response.

Next, the effect of mass eccentricity on the peak seismic response is quantified. Figure 6.19 presents the effects of the incidence angle on the interstory drift amplification, considering a value of unidirectional and bidirectional mass eccentricity of 10% of the floor plan dimension, while the gap size around the building is set at 20 cm. For design purposes, the envelope of the peak interstory drifts ratios among the 4 corner columns is presented. Given the mass eccentricity that exists in the examined structure, the response of each corner column can vary significantly and the consideration of an envelope is deemed necessary. In general, the response amplification tends to increase for buildings with such irregularities, although the incidence angle continues to be the dominant factor influencing the overall response.

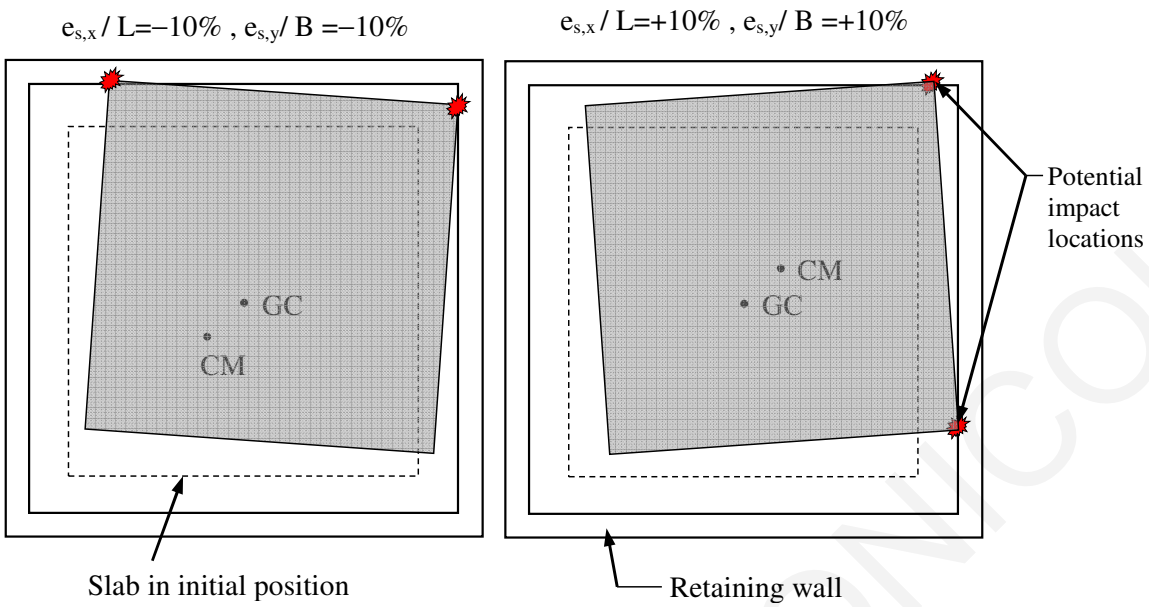

Figure 6.18 Deformed structural positions for two cases of mass eccentricities.

The effects of the incidence angle and the gap size on the peak seismic response of structures with mass eccentricities are also parametrically simulated and studied. Specifically, Figure 6.20 presents the effects of the angle of incidence and the gap width on the interstory drift amplification, considering two cases of unidirectional and bidirectional mass eccentricities. It can be observed that pounding is practically eliminated only when the gap is sufficient. However, the critical gap size required to avoid pounding is now significantly larger due to mass eccentricities among all orientations of the ground motions. The obtained response, as exemplified from the results, is strongly affected by the orientation, frequency content and intensity of the excitation.

As expected, the effect of the angle of incidence on the structural response is significantly different in symmetrical and unsymmetrical conditions. These investigations indicate that, in general, elements in asymmetric-plan systems due to bidirectional mass eccentricities are likely to experience higher interstory drifts, whereas elements on symmetric structures are expected to experience lower interstory drifts compared to those in the reference system (no eccentricity) given in Figure 6.13(b). The extent at which the orientation of the seismic records influences the peak interstory drift ratio depends on the structural system and the available seismic gap provided around the building. As a consequence, the common practice of applying the earthquake records along the structural axes can lead to significant underestimation of the peak structural response. Also, it is shown that the structural eccentricity, as well as the impact of the earthquake orientation, can lead to significantly different seismic response.

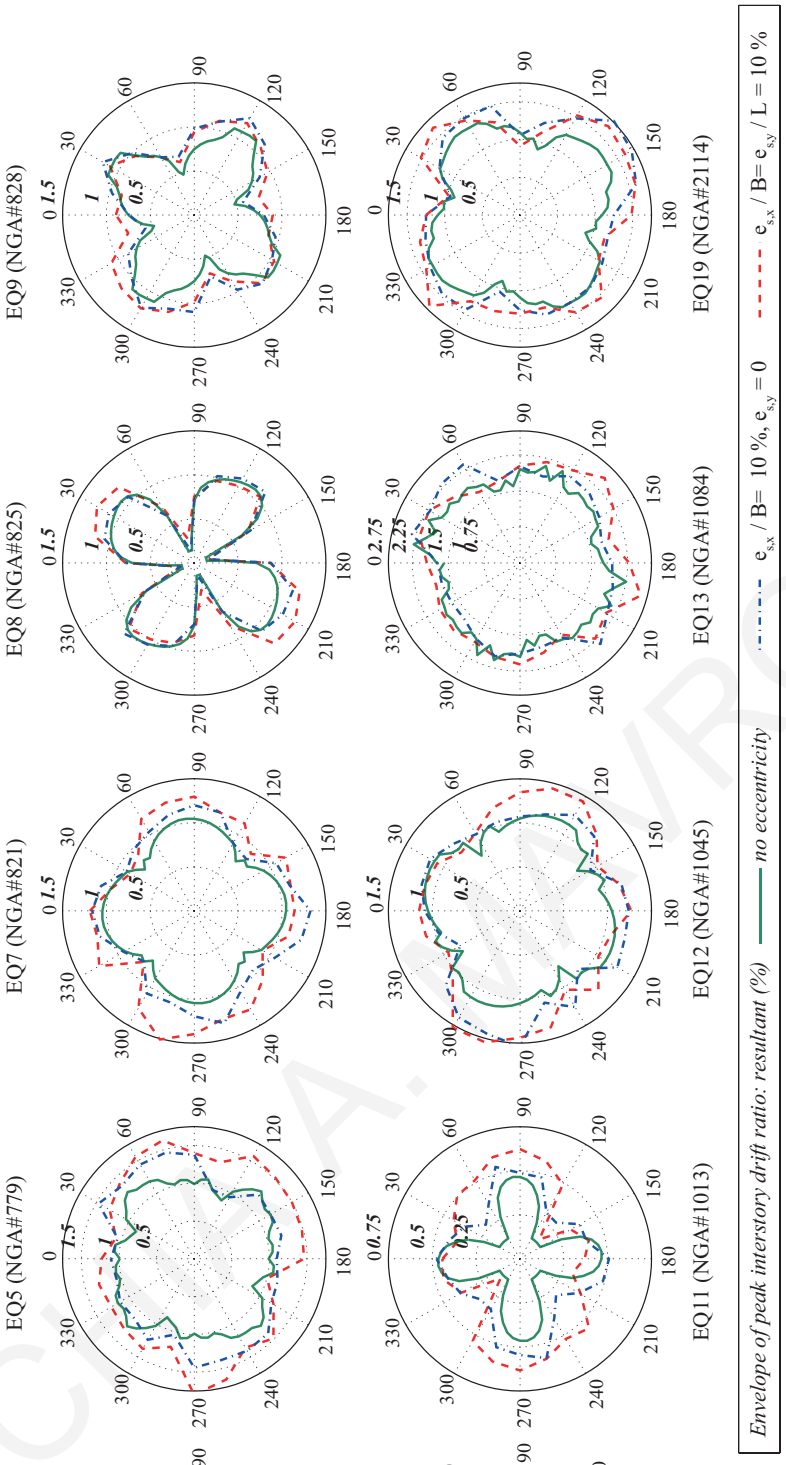

Figure 6.19 Plot of the envelope of the peak interstory deflection resultant ratio among corner columns with/without accidental mass eccentricity at the superstructure, assuming an available seismic gap between the simulated structure and the retaining walls of 20 cm.

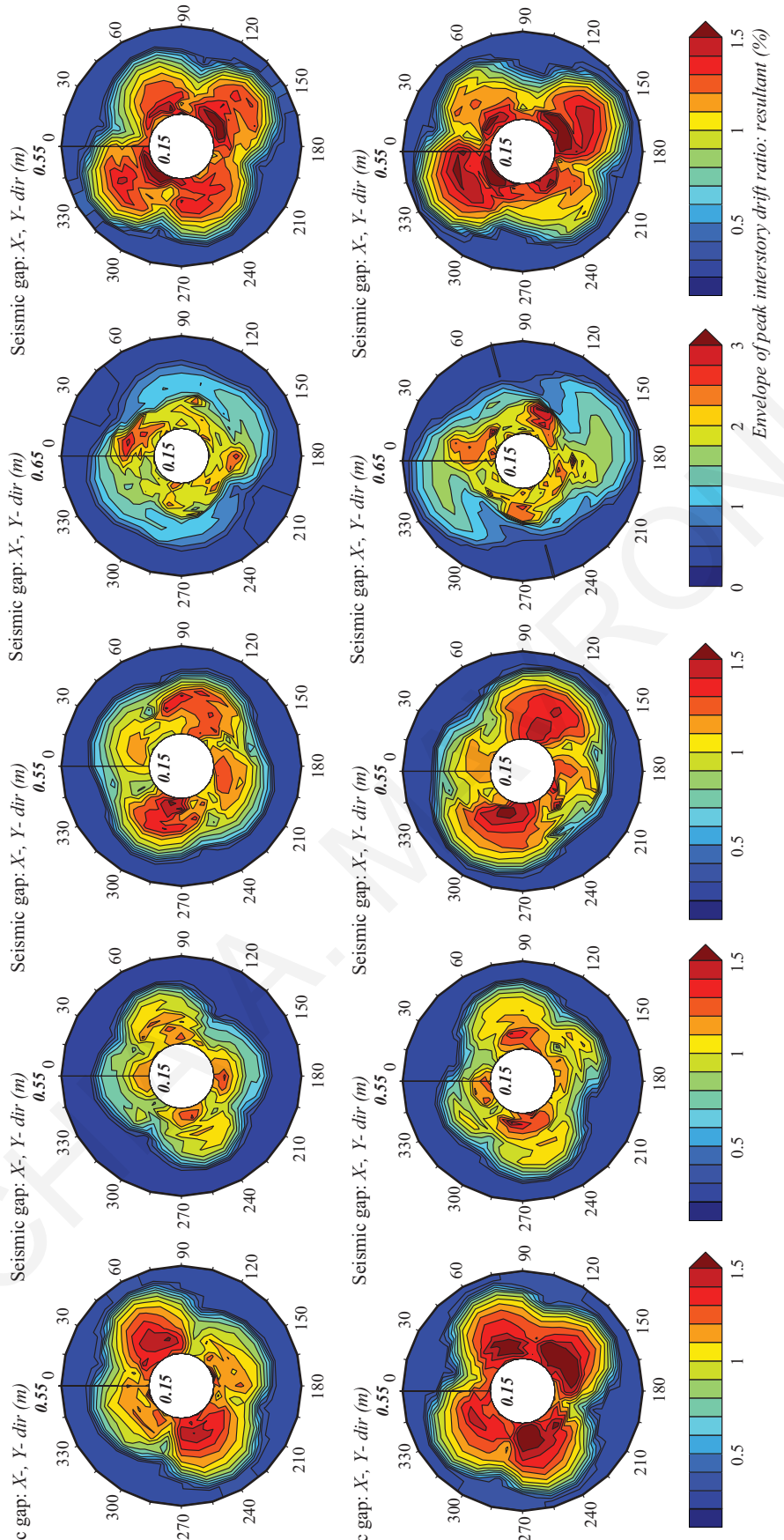

Figure 6.20 Contour plots of the envelope interstory deflection resultant ratio among corner columns considering accidental mass eccentricities of the superstructure: (a) unidirectional: $e_{s,x}/L=10\%$, $e_{s,y}=0$, and (b) bidirectional: $e_{s,x}/L=10\%$, $e_{s,y}/B=10\%$.

It is concluded that the process of determining the critical incidence angle is more complex when considering accidental mass eccentricities. Since it is not possible to know *a priori* the incidence direction that may generate the highest seismic response, it is necessary to perform numerous analyses for different incidence angles. Different models should also be used to explicitly evaluate various locations of accidental mass eccentricities, as well as different angles of incidence. The findings of this investigation, suggest that in order to take into account properly such effects, additional response time-history analyses should be performed to identify "the worst-case scenario". Alternatively, if an approach that does not explicitly account for accidental mass eccentricity is employed, appropriate safety factors should be used.

6.8 Concluding Remarks

The present study demonstrates the importance of implementing an efficient methodology with simple structural and impact modeling capabilities in three-dimensions, in order to be able to investigate the influence of the ground motion orientation on the pounding response of MDOF systems. Furthermore, the specifically designed, developed and extended software utilized herein provides the unique capability to efficiently and effectively perform spatial numerical simulations and parametric analyses of seismically isolated buildings with automatic impact detection and resolution capabilities.

Initially, analysis results have revealed the significant effects of the bidirectional coupled modeling of seismic isolation bearings in comparison with independent unidirectional modeling. Simultaneous seismic excitation loadings along each horizontal axis of a structure can substantially increase the maximum isolator displacement and decrease the superstructure response. Therefore, parametric studies for simulating earthquake induced pounding of seismically isolated buildings have been conducted in three-dimensions, with the earthquake excitations applied in two orthogonal directions simultaneously.

Parametric studies have revealed the factors that affect the spatial dynamic responses of seismically isolated buildings. Specifically, the seismic responses of typical three-story base-isolated buildings during impact with adjacent moat walls have been investigated. The comparative performances of isolation systems, while varying some characteristic parameters during various impact conditions, have been studied under various angles of incidence of selected near-fault ground motions. Furthermore, the amplification of the pounding response of base-isolated structures due to accidental mass eccentricities has

been quantified, while the influence of the angle of incidence due to such asymmetric conditions has also been discussed.

From the simulation results, the following conclusions can be drawn:

(1) The excitation angle can significantly affect the overall structural response, even when pounding does not occur. Therefore, this should be taken into consideration for defining the width of the seismic gap that is required to avoid collisions with the surrounding moat walls during the design phase of new buildings or reassessment of existing ones.

(2) The peak interstory drift ratio among all floors of a base-isolated building increases significantly when impact with a moat wall takes place during an earthquake.

(3) The detrimental effects of pounding may become more severe for certain values of the excitation angle. The incidence angle along which the amplification of the superstructure's peak response due to pounding obtains its maximum value, generally coincides with the angle along which the peak unobstructed base relative displacement occurs.

The amplification of the peak seismic response due to pounding is significantly influenced by the characteristics of the excitation, namely the orientation, frequency content and intensity. The extent at which the orientation of the seismic records influences the peak response depends on the structural system, the available clearance that is provided around the building and the surrounding wall arrangement.

(4) As the width of the provided seismic gap between the base-isolated building and the adjacent wall decreases, there is an increase in the deflections of the superstructure up to a certain value of the gap distance and, then, onwards the deflections of superstructure decrease.

(5) Potential mass eccentricities at the superstructure may influence significantly the interstory drifts during impact with adjacent structures. Structural elements in such asymmetric-plan systems are likely to experience higher interstory drift ratios. In such cases, the peak structural response that is obtained by applying the ground motion records along the principal axes may substantially underestimate the peak structural response prediction. The determination of the critical angle of incidence is expected to be more complicated in such a case. Therefore, rational amplification factors should be established to take into account the effects of accidental mass eccentricities and the angle of incidence of the seismic excitation.

CHAPTER 7 THREE-DIMENSIONAL STRUCTURAL POUNDING WITH ADJACENT BUILDINGS

7.1 Introduction

7.1.1 Introductory Remarks

This chapter is devoted to the investigation of seismically isolated buildings pounding with adjacent fixed-supported structures, with the computed results contrasted to the corresponding earlier investigations presented in Chapter 6, which considered pounding incidences solely against the moat wall. In practice, the possibility of pounding between structures is more likely to occur in cases where an existing building, in relatively close distance to other fixed-supported buildings, is seismically isolated, e.g. through a retrofit and structural upgrade process. Under such circumstances, the base-isolated building experiences large relative displacements, which might eventually lead to structural collisions either at the base or at the floors of adjacent buildings due to the deformations of the superstructures of the closely adjacent buildings.

7.1.2 Simulation Details

In the simulations performed within this chapter, the 3-story seismically isolated building that has been used in the Chapter 6 (Configuration A – Section 6.1) is considered to be adjacent to 2, 3, or 4-story fixed-supported buildings, which are located either on one or both sides of the base-isolated building (Figure 7.1). The adjacent buildings are simulated as linear MDOF systems, possess the same superstructures' characteristics as the base-isolated building (except otherwise stated in the text) and are located in the same distance as the adjacent moat wall, which has the same characteristics as those considered in Section 6.1. For simplicity, it is assumed that the floors of the neighboring buildings are located at the same levels, leading to potential slab-to-slab collisions without any slab-column interactions. In cases when adjacent structures are located on both sides of the base-isolated building, the separation gap is considered to be the same.

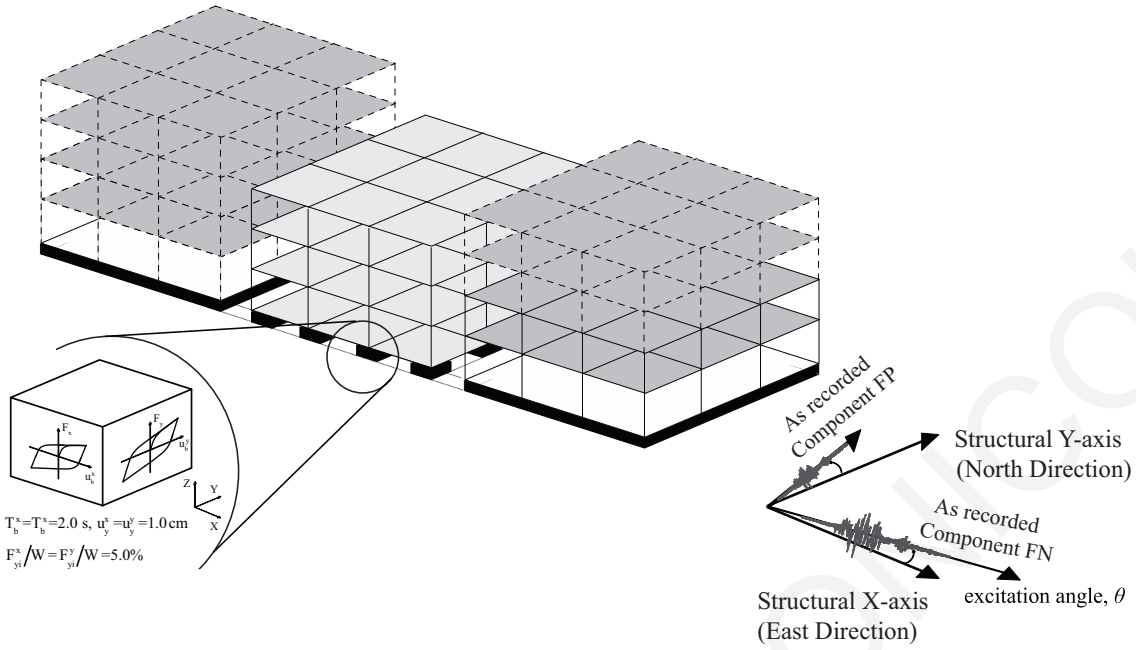

Figure 7.1 Schematic configuration of simulating a base-isolated building subjected to a bidirectional excitation with adjacent fixed-supported buildings.

7.1.3 Effect of Seismic Orientation on the Peak Seismic Response

Before proceeding with the investigation of structural collisions, a series of simulations of the individual dynamic responses of the base-isolated and the fixed-supported buildings considered herein is conducted. The peak unobstructed relative displacements of the buildings in the *X*-direction are illustrated in Figure 7.2. The structures are analyzed for the 5 bidirectional ground-motions records presented in Table 6.1 (EQ6, EQ7, EQ12, EQ13, EQ19), each one rotated with a constant step of 5° in the range of 0° to 360°. The main results arising from these simulations with regards to the ground motion orientation effect, are in line with previous observations: (i) the incidence angle of the seismic excitation significantly affects the maximum response of the structures in the *X*-direction, (ii) the critical angle corresponding to the peak response over all possible excitation orientations varies with the selected ground motion and the dynamic characteristics of the structures, and (iii) the *FN/FP* drifts (θ=0°) are not always conservative.

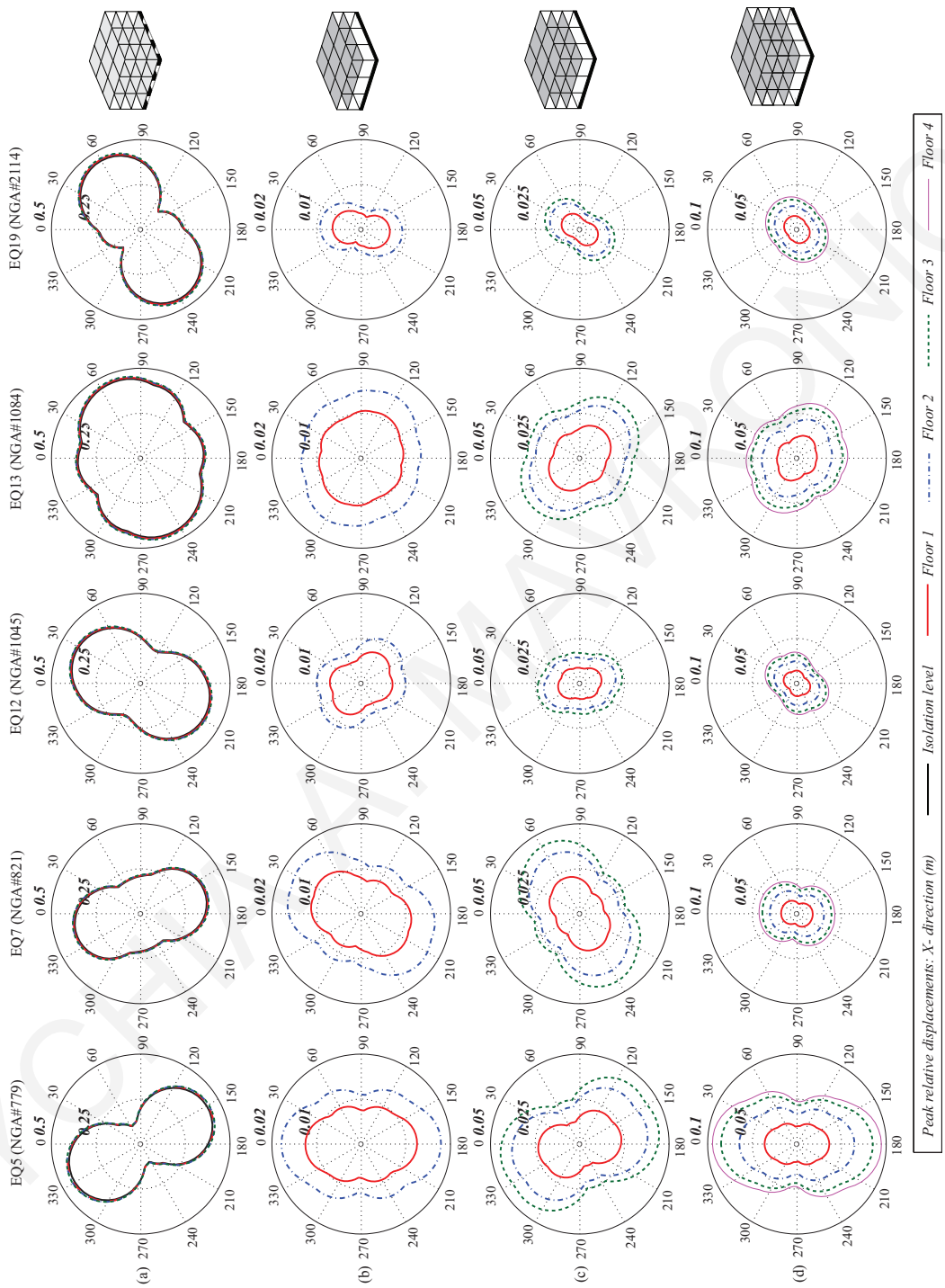

Figure 7.2 Peak unobstructed relative displacements [m] of (a) the 3–story base-isolated building, and (b) the 2–story, (c) 3–story, and the (d) 4–story; fixed–supported adjacent building, in the *X*-direction, in terms of the incidence angle.

7.2 Effect of Structural Arrangements of Adjacent Buildings

Given that the seismic response of base-isolated structures subjected to strong excitations depends on the excitation characteristics, specifically the frequency content and horizontal ground-motion directionality, the sensitivity of the calculated nonlinear dynamic response of a 3-story seismically isolated building during pounding against other fixed-supported buildings and/or the surrounding moat wall is parametrically examined. Numerous nonlinear time-history analyses are performed using selected pairs of orthogonal components of recorded horizontal ground-motions.

The peak responses of the examined seismically isolated building are discussed next, assuming an available seismic gap between the simulated building and the adjacent structures of 20 cm. Figure 7.3 and Figure 7.4 present the peak interstory drift ratios (resultant) at each floor of the base-isolated building among all corner columns during collisions with the adjacent structures located on both sides or on a single side (east), for different orientations of the ground motions. Records are rotated to 73 different horizontal angles of incidence with respect to the building's structural axes. It can be observed from Figure 7.3(a) that the peak interstory deflection ratios for the case of the base-isolated building pounding against the surrounding moat wall occur at the isolation level, the 1-0 interface, and are in general higher than for the case of buildings in series, as given in Figure 7.3(b)-(d). Furthermore, the peak response of the base-isolated building decreases when moving from the ground floor upwards. This is in contrast to the response of buildings in series, which suggests that higher modes of deformation are activated in those cases, an observation that is persistent for all earthquake excitations considered herein.

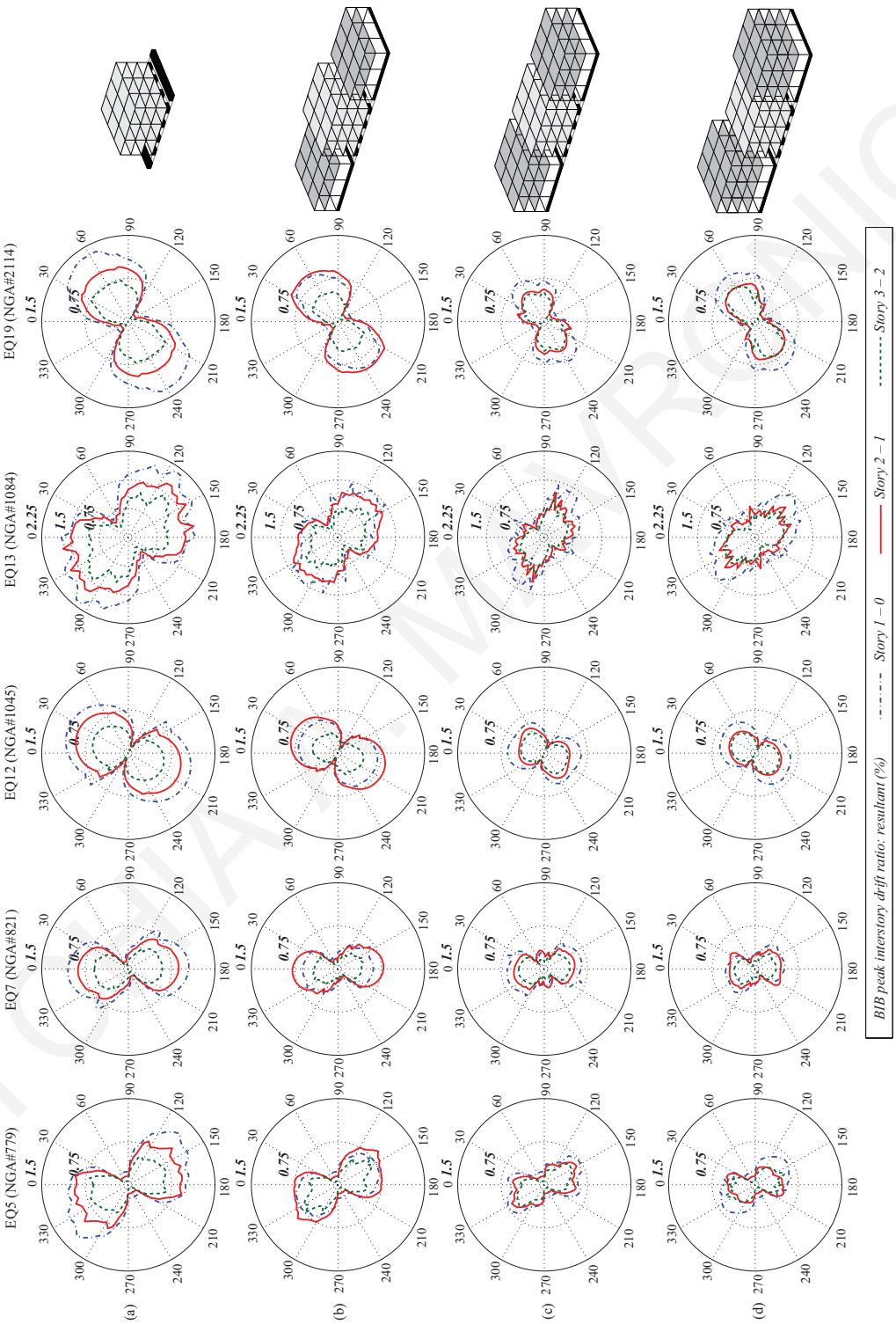

Figure 7.3 Peak responses of the 3-story base-isolated building (BIB) among all corner columns in terms of the angle of incidence, during collisions with the (a) moat wall, and (b) 2-story, (c) 3-story (d) 4-story fixed-supported structures, located on both sides (west and east) of the base-isolated structure.

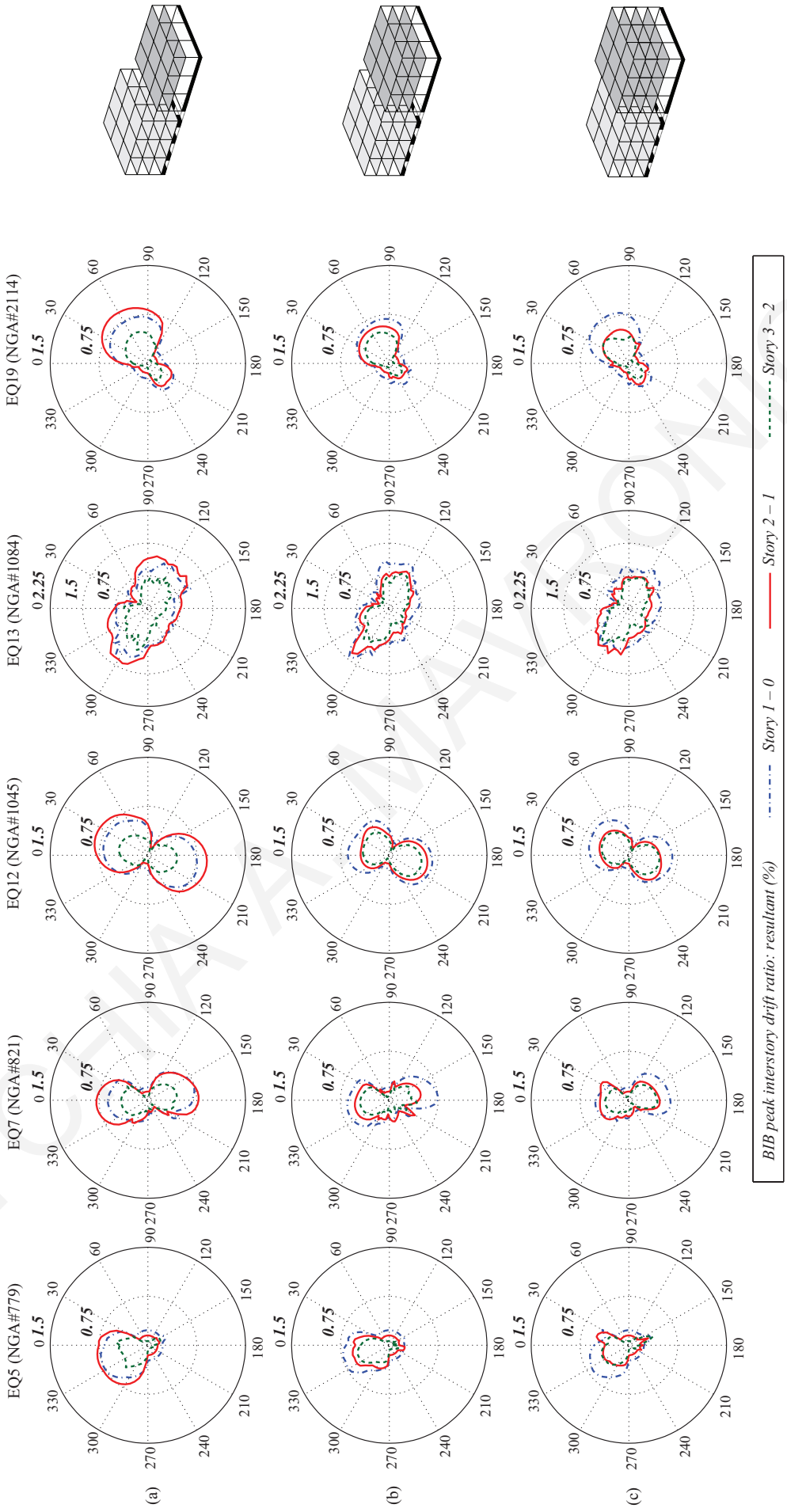

Figure 7.4 Peak responses of the 3-story base-isolated building (BIB) among all corner columns in terms of the angle of incidence, during collisions with the (a) 2-story, (b) 3-story (c) 4-story fixed-supported structures, located on the east side of the seismically isolated building.

In fact, a closer investigation on the peak deformation floor characteristics suggests that the presence of buildings adjacent to the base-isolated one induce structural collisions at higher floors, which eventually lead to the activation of higher modes of deformation, as evident in Figure 7.5 and, subsequently, less intense interstory drift ratios. In essence, the adjacent buildings act as containers/restrainers, preventing the large horizontal displacements that might take place when the base-isolated building hits only against the surrounding wall at the isolation level.

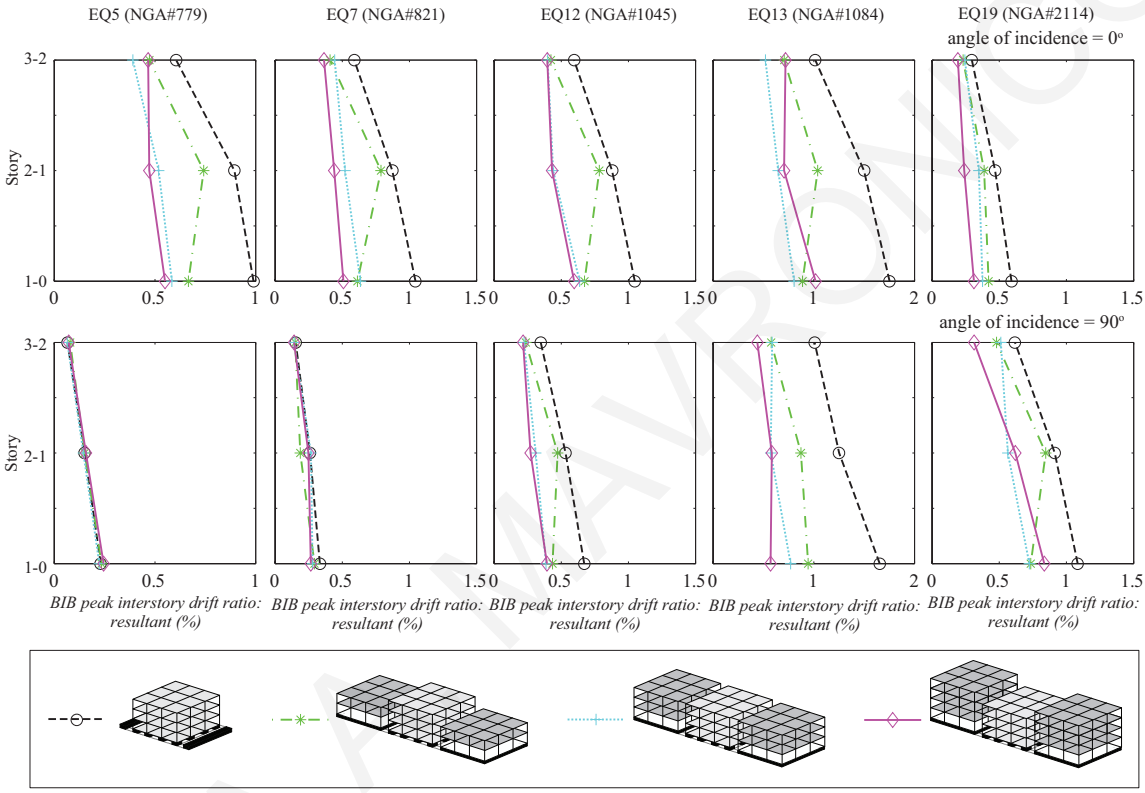

Figure 7.5 Peak resultant interstory drift ratios of the base-isolated building (BIB), when the available seismic gap with adjacent structures is set at 20 cm, for two different orientations of the bidirectional ground-motions.

In the specific parametric analyses, the peak response ratios are located (i) at the isolation level, for the cases when only moat walls surround the building, and when the seismically isolated building is of equal height or shorter than the neighboring fixed-supported buildings, or (ii) at the same floor level as the roof of the adjacent fixed-base structures, which occurs when the adjacent structures are shorter than the base-isolated one, among all incidence angles of the excitations. In general, the polar plots suggest that the critical envelope for all excitation angles may not be dominated by the response of a specific floor but rather of the combination of the peak responses of several floors when the base-isolated building hits against the adjacent MDOF structures. In general, the effect of the ground motion directionality, in combination with the number of stories and, consequently, the fundamental eigenperiod of the adjacent structures, seems to play a

significant role to the severity of the structural response. It should be noted, however, that in the cases of buildings in series, the floor that dominates the critical envelope might change as the provided gap size is modified, which is further investigated below.

In order to assess the effect of specific structural arrangement (fixed-supported building on one side *vs.* both sides) on the overall dynamic response, a re-presentation of the results shown in Figure 7.3 and Figure 7.4 is provided in Figure 7.6. More specifically, Figure 7.6 provides polar plots of the envelopes of peak interstory drift ratios during the five selected ground motions that are compared for six different configurations regarding: (i) the location of the adjacent fixed-supported buildings and (ii) the number of floors of the adjacent building (2, 3 or 4). In general, the variation of the response ratios, seems to be influenced by the earthquake excitation's characteristics (frequency content and directionality); as these plots show that peak interstory deflection ratios can vary by a factor of 2.5 over all possible angles, at least for the gap size of 20 cm considered herein. It is interesting to note that, in general, the incidence angle at which the maximum amplification of the superstructure response due to pounding occurs coincides with the critical angle that corresponds to the peak unobstructed relative displacement at the isolation level, as shown Figure 7.2(a). We can also observe that when adjacent buildings are located on both sides of the base-isolated building, Figure 7.6(a), the polar plots of its peak responses for each floor exhibit 8-shape figures (a consequence of double symmetry), a characteristic that breaks down when a building is located only on one side, which leads to asymmetric response shapes as shown in Figure 7.6(b).

Furthermore, the presence of adjacent fixed-supported buildings on both sides of the seismically isolated building has minor influences on the peak seismic response during pounding for the ground motion critical orientation. For example, in the case of the Loma Prieta 1989 ground motion (NGA#779), the range of critical angles between 300° to 360°, and the envelope of the peak responses among all floors are relatively close irrespective of whether adjacent buildings are located on both sides or only one side (in this case, the east side).

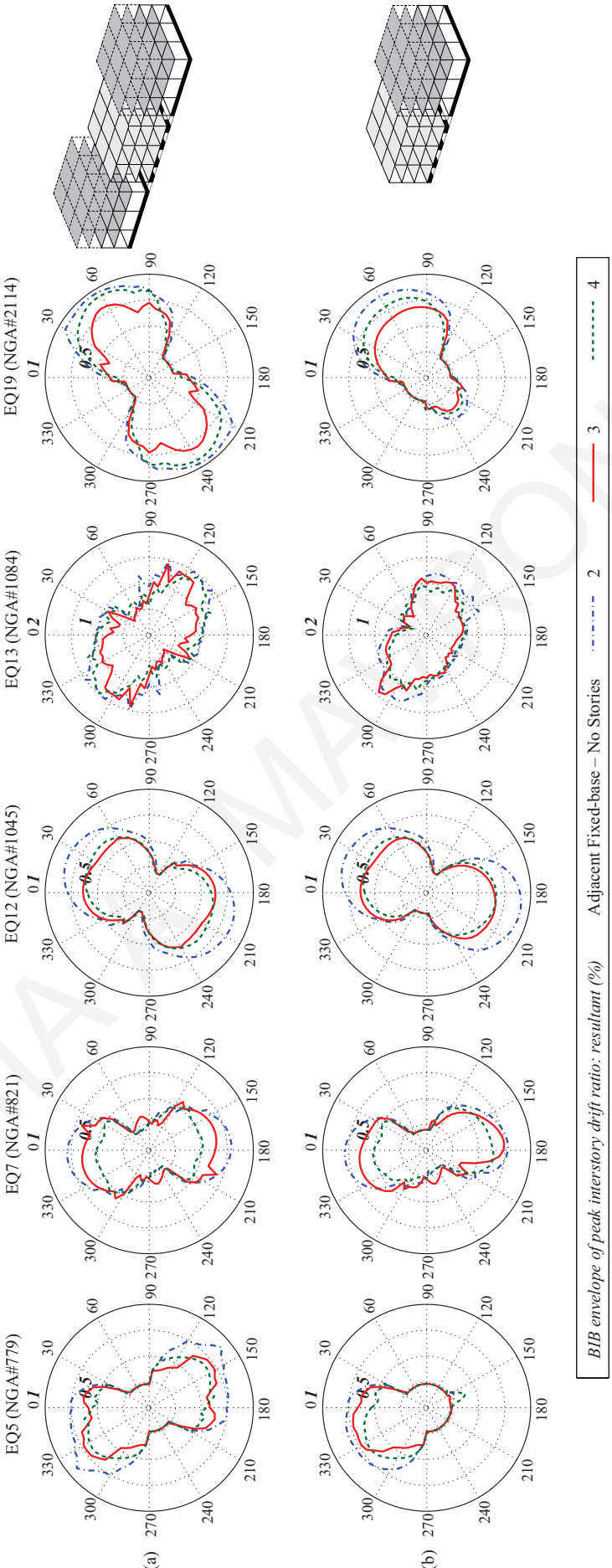

Figure 7.6 Envelope of peak resultant interstory drifts ratio of the base-isolated building (BIB) during collisions, in terms of the angle of incidence considering a gap size of 20 cm and various configurations of the adjacent fixed-supported structures, located (a) on both sides, (b) on the east side of the 3-story base-isolated structure.

As anticipated, the location of the adjacent buildings, in combination with the excitations' characteristics affect the envelope of the peak response of the seismically isolated building during impact. Furthermore, Figure 7.6 suggests that the number of floors of the adjacent buildings can significantly affect the overall dynamic response of the base-isolated structure. Nevertheless, one cannot generalize the severity of the influence based on the number of floors. Results that are presented in the following sections, suggest that the number of floors by its own is not the only structural characteristic that defines the dynamic response of the base-isolated building. Other parameters such as stiffness, fundamental eigenperiod, etc. might shift the relative importance of having short *vs.* high adjacent buildings. What one can generalize is that the critical response is polarized at a specific direction irrespective of the number of stories of surrounding buildings. Considering that the critical angle varies significantly with the arrangement type, its estimation, without a detailed investigation, is difficult.

The incidence angle of the imposed seismic excitation seems to be an important factor while computing the peak seismic response of buildings. For design purposes, the evaluation of the critical conditions for each specific case, which could ensure the more reliable prediction of the peak structural response, is crucial. Therefore, it might be a mandate to perform 3D nonlinear analysis and use an advanced modeling approach to computationally assess the critical response for each case, considering multiple angles of incidence.

7.3 Effect of the Separation Distance

In order to investigate the influence of the gap size between adjacent structures, the base-isolated building is assumed to be separated by various distances from the adjacent structures. In Figure 7.7, the peak seismic responses of the 3-story seismically isolated building are computed under four different configurations regarding the number of floors (2-, 3- and 4-floors) of the adjacent fixed-based structures located at both sides (in the east and west directions). The computed results for a single incidence angle (θ=0°) for five ground motions are presented. As anticipated, the location and the characteristics of the adjacent structures, in combination with the excitation characteristics, affect the peak response of the seismically isolated structure during impact.

Figure 7.7 suggests that the peak interstory drift ratios of the base-isolated structure pounding with the moat wall given in Figure 7.7(a) are, in general, higher than those for the case of buildings in series. The fact that the base-isolated building pounds with the fixed-base building before it can impact the rigid retaining wall at the base, reduces the

severity of impact at the base of the building for the range of separation distances that are examined. Furthermore, the ground floor of the base-isolated building dominates the peak response when only pounding with the surrounding wall at the base is considered. On the other hand, upper stories may experience higher drifts compared to lower level stories when pounding with adjacent fixed-base buildings is considered. More specifically, in the latter case the floor that dominates the critical envelope may change as the available gap size is modified. Also, it can be observed from Figure 7.7, that the critical gap size to avoid pounding, slightly increases in case of buildings in series. This is reasonable, considering that the seismically isolated building may pound against the neighboring buildings at the upper floors due to the deformations of the superstructures of the buildings in series before impacting the surrounding moat wall.

The plots of Figure 7.8 present the envelopes of the peak interstory deflection ratios, for all six configurations of the base-isolated building (regarding the number of floors and the location of the adjacent fixed-supported buildings) and for the selected bidirectional near-fault ground-motions. The first row of Figure 7.8 presents the envelopes of the maximum responses considering potential collisions on both sides of the seismically isolated building, while the second row plots the corresponding maximum responses considering only one-sided impacts with the adjacent structure on the east side of the seismically isolated buildings. It is observed that as the separation distance increases the amplifying effects resulting from collisions decrease. Also, the number of stories of the adjacent fixed-supported buildings, and the characteristics of the adjacent structures seem to influence the severity of the impact. Nevertheless, a clear trend cannot be identified. The response of the base-isolated building with adjacent buildings on both sides deviates significantly from the corresponding response in the case of one-sided building for the case of the Northridge earthquake (EQ13), while, for all other excitations considered herein, the response is similar. This particular deviation can be attributed to the combined differences in structural arrangement (one side *vs.* both side) and the excitation characteristics. It should be noted that a similar response could be observed for the other seismic excitations presented in Figure 7.8 if a different incidence angle is considered.

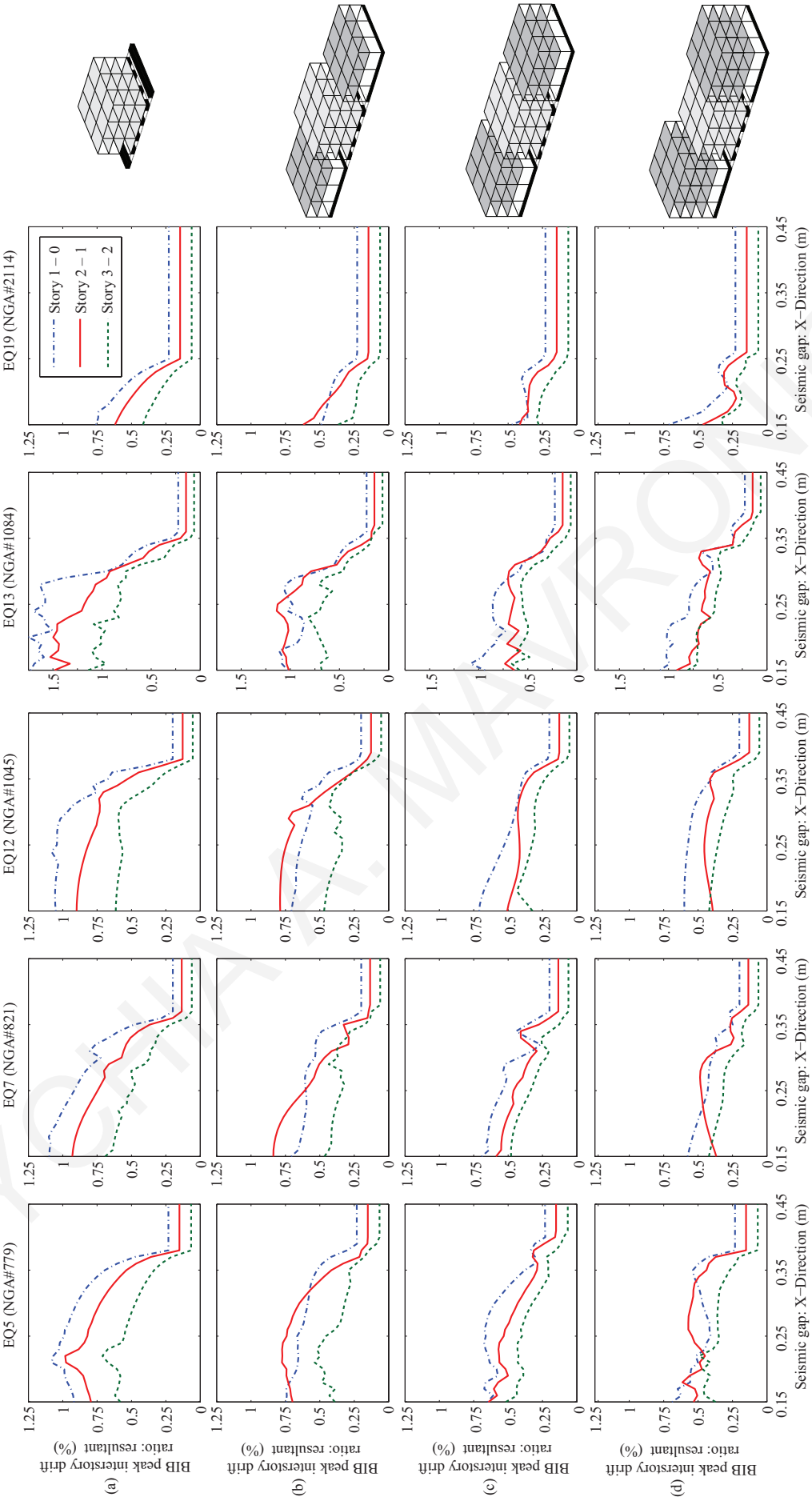

Figure 7.7 Peak responses at each floor of the 3-story base-isolated building (BIB) among corner columns in terms of the available gap size for four configurations of the adjacent structures and a fixed angle of incidence set at 0°.

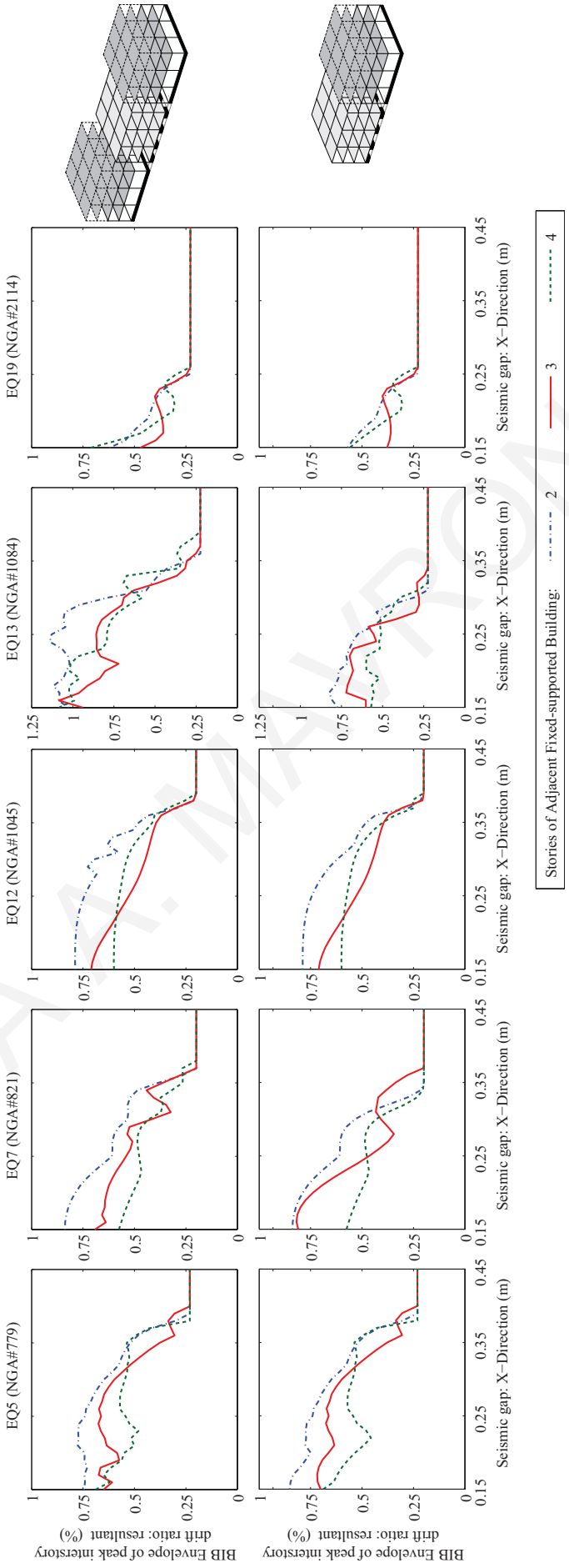

Figure 7.8 Envelope of peak responses of the base-isolated building (BIB) among corner columns in terms of the available gap size for different arrangement of the adjacent structures (angle of incidence = 0°).

In order to identify some of the trends that may be observed due to pounding interactions, the response of multiple pairs of buildings (a 3-story base-isolated building and a multi-story fixed-base structure), when subjected to the 5 selected bidirectional excitations of different orientations, are studied. Similar sets of analyses, as those described in the previous subsection, are performed. The structural characteristics of the base-isolated buildings, as well as the isolation characteristics are kept the same. The width of the seismic gap varies with a step of 2.5 cm in the range of 15 cm to 60 cm, while the incidence angle θ varies from 0° to 360° with a step of 15°. The results of those simulations are presented in Figure 7.9 in terms of polar plots where the envelope of the peak resultant interstory drift ratios is color-coded, with the radius of the polar plot representing the magnitude of the seismic gap. The results from more than 6,500 simulations are contained within this figure.

Consistent with previous observations, these contour plots indicate that the direction of the seismic excitation significantly affects the peak interstory drift ratio. It is also observed that pounding is practically eliminated only when the gap is sufficient, with the critical gap size being a function of the earthquake excitation and the structural characteristics. Also, plots in Figure 7.9 indicate that the characteristics of the adjacent fixed-supported structure seem to play a significant role to the severity of the structural impact. Furthermore, the extent at which the incidence angle influences the peak response depends on the structural systems (e.g. number of stories) and the separation distance. In such circumstances, the term 'building interaction' more appropriately describes the overall behavior of the base-isolated building. As expected, the effect of the angle of incidence on the structural response is significantly different due to the location of a fixed-supported building on one side (east). Finally, one can conclude that the process of determining the critical incidence angle is more complex when considering adjacent multistory structures and since generalizations cannot be made, specific case parametric simulations should be performed for more reliable investigations.

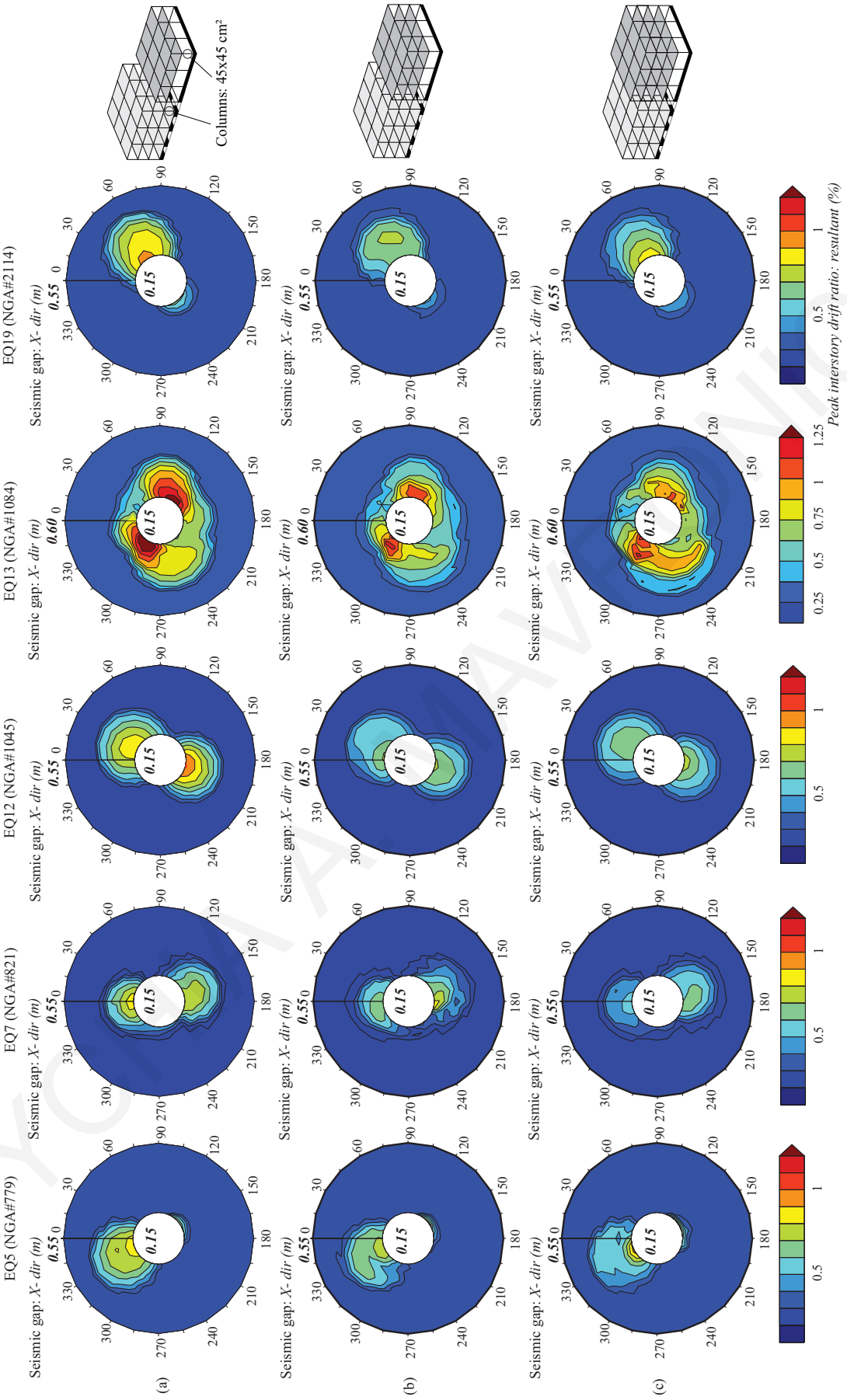

Figure 7.9 Contour plots of the envelope interstory drifts resultant ratio of the 3-story seismically isolated building among corner columns, for various orientations of the ground motions and separation distance, and 3 different configurations of the adjacent structures.

7.4 Effect of the Adjacent Structure Characteristics

In the above discussion, the superstructures' flexibilities of both buildings (base-isolated and fixed-based) are assumed to be the same. With the characteristics of the base-isolated structures unchanged, the flexibility of the adjacent buildings is parametrically examined next. Different stiffnesses of the superstructure are obtained in this section, by considering different cross-sections of the columns (35 x 35 cm^2). The peak resultant interstory drift ratios are obtained under 5 seismic excitations, considering a seismic gap of 20 cm. Figure 7.10 presents the peak response at each floor of the 3-story base-isolated building during collisions with the adjacent fixed-based structures, for all possible orientations of the ground motions. The results of the study show that the peak seismic response of the base-isolated structure could be much different from its peak response impacting to stiffer structures, as given in Figure 7.4.

The envelope of peak responses considering different flexibility of the adjacent multistory building are given in Figure 7.11, by red and green lines, and are compared to the corresponding results due to impact with the moat walls located on both sides of the seismically isolated building (Section 6, Case Study X-5), shown by blue lines. Figure 7.11 shows the angular dependence of the computed results for various arrangements. It becomes evident from the computed results, that the direction of the seismic excitation, in combination with the characteristics of the buildings in series, affects substantially the maximum response of the seismically isolated building. In general, the peak interstory drift ratios during collisions for the case of buildings in series are, in general, smaller than those when impacts occur only with the surrounding moat wall.

The effects of the incidence angle and the gap size on the seismic response of structures considering fixed-based structures with increased flexibility are also parametrically studied. Specifically, Figure 7.12 presents the effects of the angle of incidence and the gap width on the interstory drift amplification, under the Loma Prieta (1989) and Northridge (1994) earthquakes. It can be observed that the obtained response is strongly affected by the orientation of the imposed seismic excitation. The stiffness of the adjacent fixed-supported buildings significantly influences the peak response of the base-isolated structure during impact. Amplified results due to pounding to adjacent 3- and 4-story fixed-supported buildings deviate substantially from the corresponding results presented in Figure 7.9.

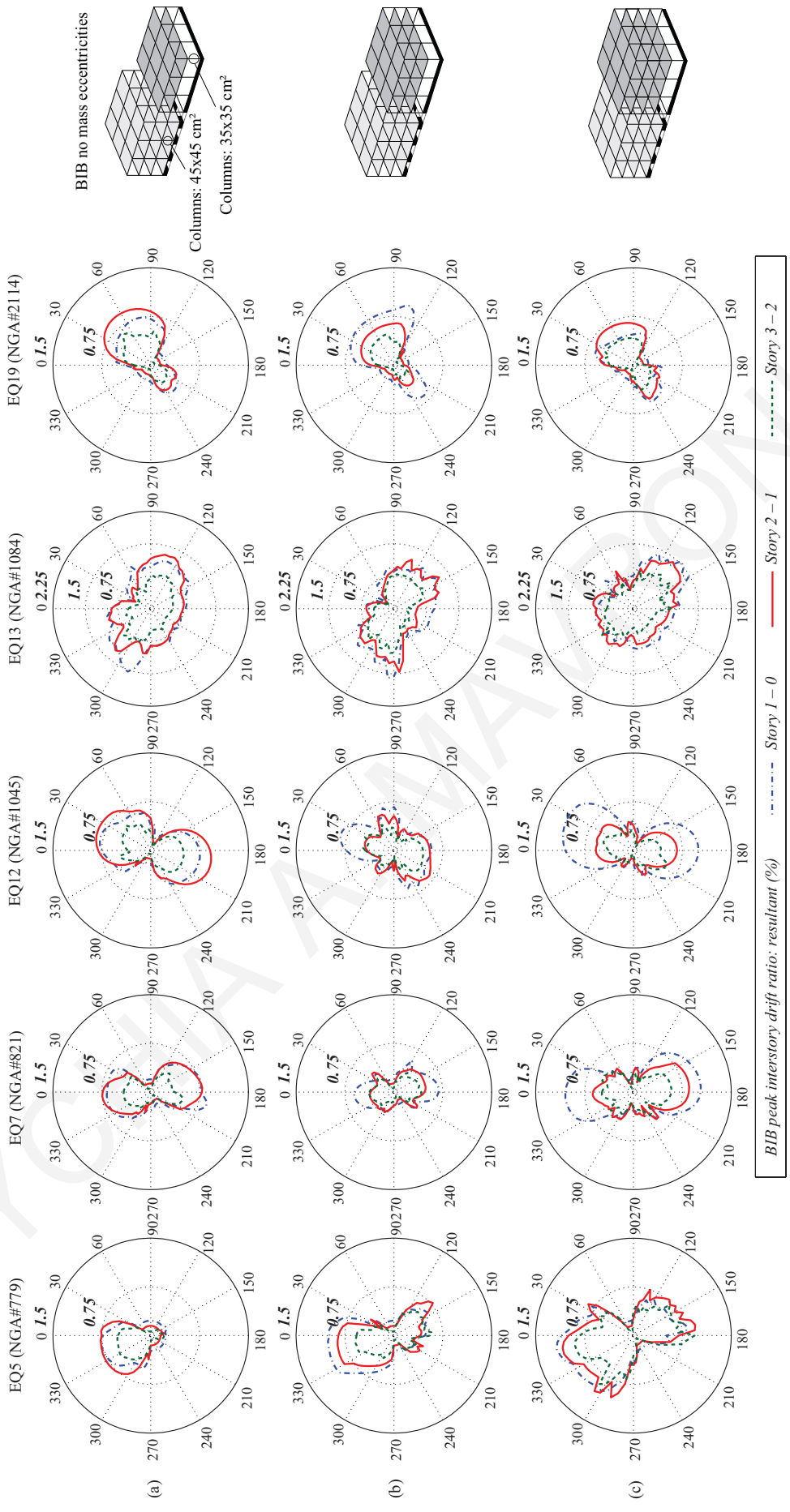

Figure 7.10 Peak responses of the 3-story base-isolated building (BIB), among all corner columns due to collisions to adjacent fixed supported buildings located at the east side of the seismically isolated building for 73 different orientations of each ground motions.

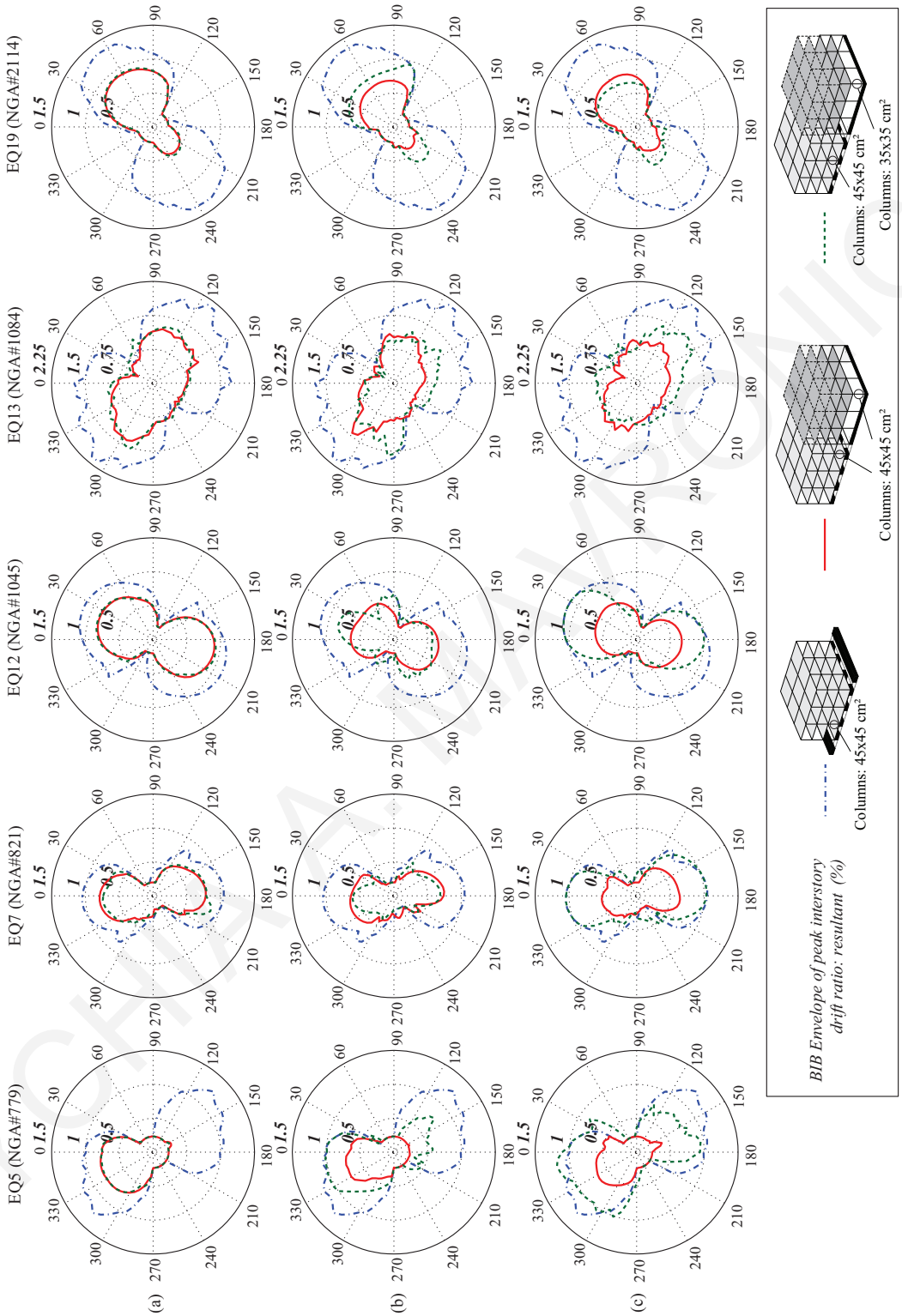

Figure 7.11 Polar plots of the base-isolated building (BIB) peak interstory deflections envelope among all corner columns due to collisions to adjacent moat walls; and fixed-base buildings of (a) 2-, (b) 3- and (c) 4-stories, with different flexibility of the superstructure.

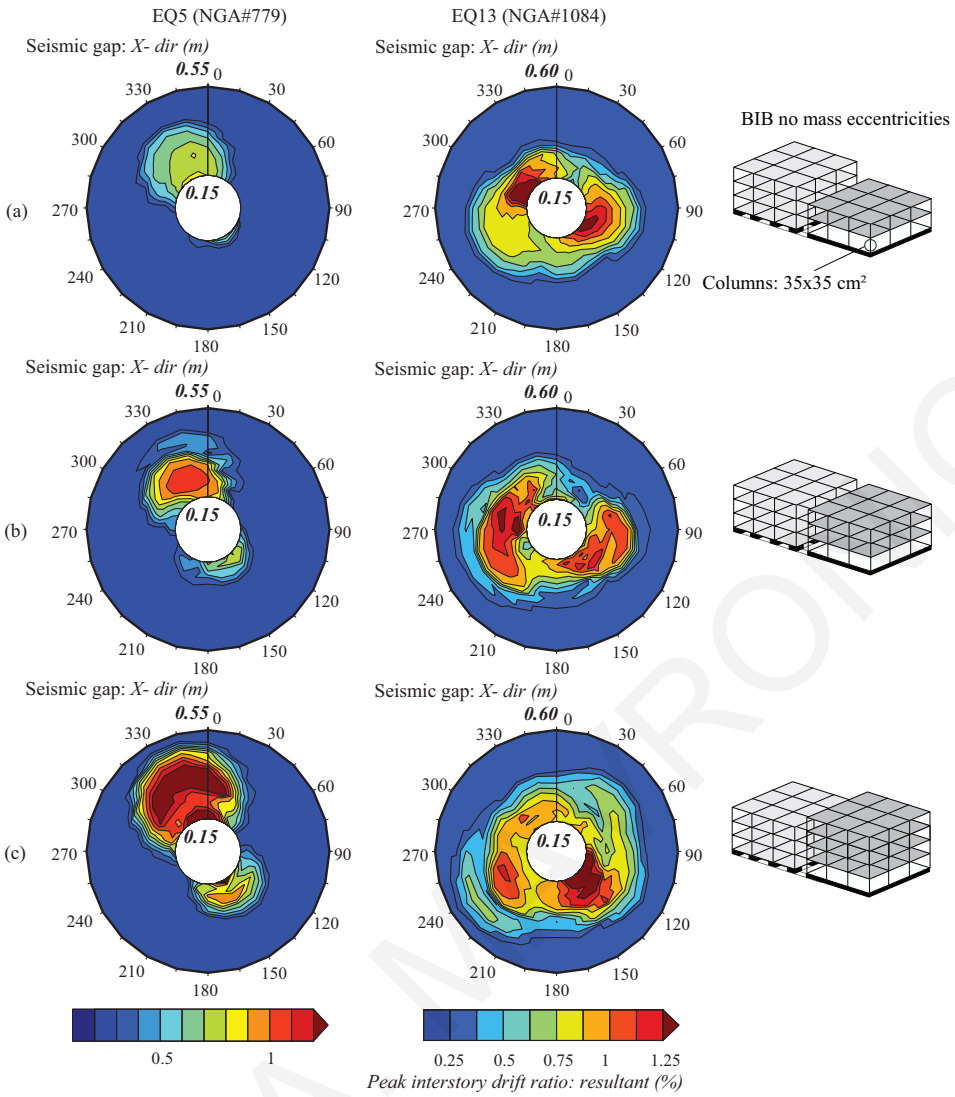

Figure 7.12 Contour plots of the envelope interstory drift resultant ratio of the 3-story seismically isolated building ratio among corner columns with different flexibility of the adjacent (a) 2-story (b) 3-story, and (c) 4-story; fixed-supported building for various orientations of the ground motions and available gap sizes.

The critical gap size required to avoid pounding is, in general, significantly larger in case of buildings in series, especially among critical orientations of the ground motions. Special attention should be given in the peak responses of the base-isolated building under the Loma Prieta excitation (EQ5) presented in Figure 7.12(c), as the results suggest that the peak resultant interstory drift ratio, for incidence angles in the critical range, can reach values higher than the ones corresponding to collisions in cases where collisions can occur only with the wall as there as there no adjacent buildings (relevant results are presented in Figure 6.13(a)). This highlights the fact that the interaction between the adjacent structures eventually defines the critical incidence angle, the critical gap size and the severity of potential structural pounding.

7.5 Effect of the Accidental Mass Eccentricities

As mentioned in Chapter 6, eccentricity in the superstructure can be due to two different reasons: stiffness and mass eccentricity. Herein, it is assumed that there is as mass eccentricity. Therefore, a 3-story seismically isolated building with eccentric mass at the superstructure is subjected to unscaled bidirectional ground motions. The selected level of mass eccentricity values is chosen as 10% of the plan dimensions of the floors in both horizontal directions. The variation of the peak values of interstory drift ratios among various incidence angles for the Loma Prieta (EQ5) and the Northridge (EQ13) excitations, based on the specific level of eccentricities are given in Figure 7.13.

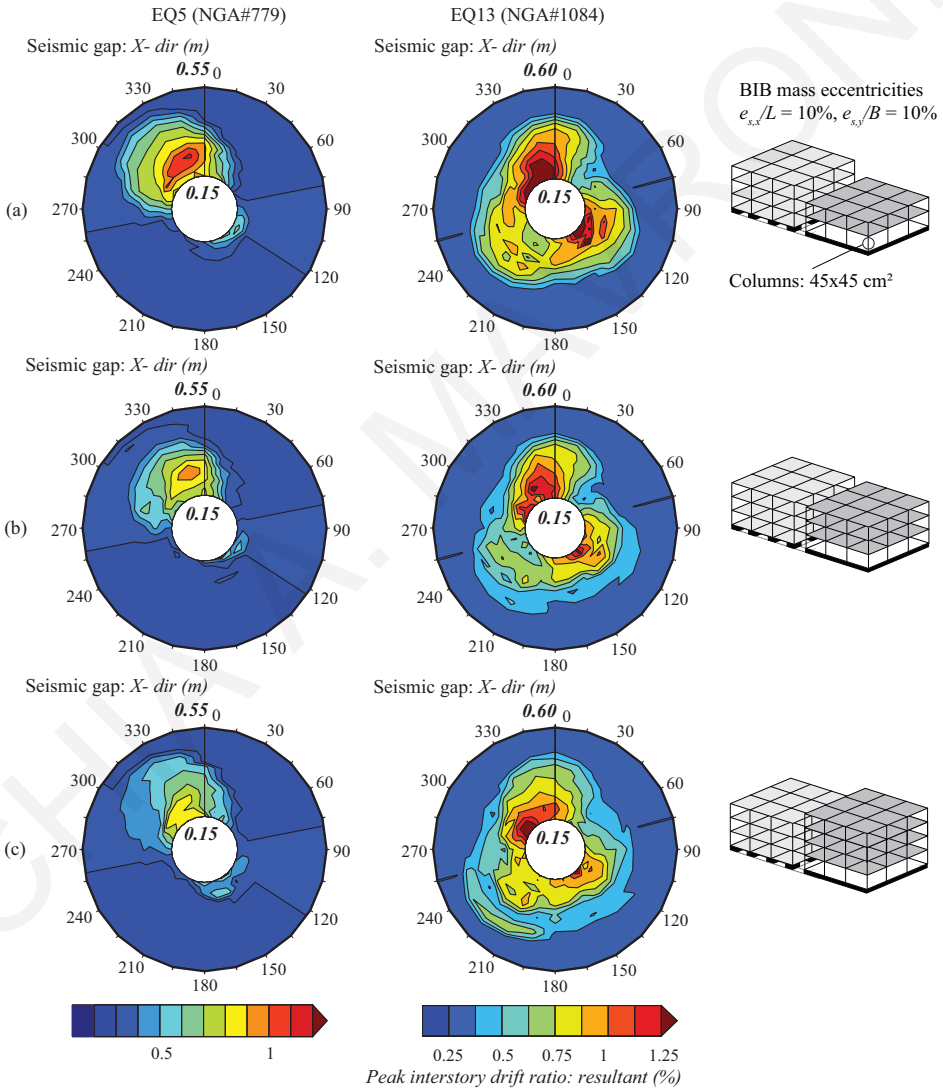

Figure 7.13 Contour plots of the envelope of the peak interstory drift resultant ratio of the 3-story seismically isolated building, among corner columns with accidental mass eccentricity of the superstructure, for various available gap sizes and angles of incidence of the Loma Prieta (EQ5) and the Northridge (EQ13) earthquake excitations.

These investigations indicate that, in general, irregular structures are likely to experience more significant response amplifications. Also, it is shown that the characteristics of the adjacent structures, as well as the impact of the earthquake orientation, can lead to significantly different response results. A comparison with the corresponding results presented in Figure 7.9 (results for the specific earthquake are given in the first and fourth columns) indicates that due to mass eccentricity, the peak response may occur under different gap size-incidence angle combination for the various configurations. Also, the critical gap size that would be required in order to avoid pounding could vary significantly due to mass eccentricities among all orientations of the ground motions. The angle of the seismic excitation is obviously one important parameter that should be examined in each case through parametric studies in order to identify the critical combination.

7.6 Concluding Remarks

Parametric studies for simulating earthquake-induced pounding of seismically isolated buildings with both the surrounding moat wall and adjacent conventionally fixed-supported buildings have been conducted in three-dimensions in order to investigate the influence of the incidence angle, the width of the seismic gap, the flexibility of the superstructure and the accidental mass eccentricity on the peak response of a base-isolated building.

Simulation results show that the impacts are particularly unfavourable for the base-isolated structure, since they significantly amplify interstory deflections of the building. Furthermore, they reveal that the detrimental effects of pounding may become more severe for certain values of the excitation angle, which, in general, is different from 0 degrees, the most commonly employed direction in practice when performing time-history analysis for design and analysis purposes. The critical incidence angle, in which the amplification of the superstructure response for the case of pounding only to the surrounding moat wall, generally coincides with the angle in which the peak unobstructed base displacement occurs.

Furthermore, it is evident that the torsional vibration that the seismically isolated building experiences due to the potential mass eccentricities increases the detrimental effects of pounding on the seismic performance of the structure. It is expected that similar effects on the response of the seismically isolated building will have the stiffness eccentricity due to asymmetric stiffness distribution to the floor due to the location and size of the columns. Therefore, this important parameter should not be omitted by simplifying

the structure to a planar frame model and performing 2D analysis, since its effect on the response during pounding seems to be significant.

In general, one can conclude that the process of determining the critical incidence angle is more complex while considering collisions to adjacent multistory buildings. Since generalizations cannot be adopted, specific simulations should be performed for each particular case in order to obtain a more reliable assessment of the expected peak seismic response. Therefore, it should be noted that the results presented herein cannot be generalized. In cases of adjacent multistory buildings, a unique critical angle of incidence cannot be identified *a priori* from the individual responses and multi-structural simulations and parametric analyses are required, in order to identify the most critical seismic response.

CHAPTER 8 CONCLUDING REMARKS

8.1 Research Summary

This research work has focused in the numerical investigation of the effects of earthquake-induced collisions of base-isolated buildings with adjacent structures. A typical seismically isolated building design requires a clearance at the isolation level in which the building is free to move sideways without impacting the surrounding moat wall. Pounding of base-isolated buildings to the surrounding moat wall has already been reported in the scientific literature and can be expected to take place in future severe earthquakes. Consequently, it is important to thoroughly investigate the possibility of collisions of base-isolated buildings in order to understand their peak consequences on their seismic response and seismic performance during very strong earthquakes.

This investigation has been accomplished in two stages. The first stage has involved the investigation of collisions in the 2D domain, where the majority of the relevant scientific literature that is available has been focusing. The second stage extends the investigation into the 3D domain, where additional phenomena, such as the torsional response of buildings and the excitation angle with respect to the structural arrangement, can be studied, since they can greatly influence the overall peak response. The impact of base-isolated buildings to the moat wall and/or adjacent fixed-supported buildings have been considered in the performed simulations and parametric studies.

In particular, an important aspect in the simulation of the seismic behavior of base-isolated structures is the incorporation of the appropriate model for the isolators. In the corresponding scientific literature, a sharp bilinear model has often been used for capturing the hysteretic behavior of the LRBs in the analysis of seismically-isolated structures, although the actual behavior of the LRBs can be more accurately represented utilizing smoothed plasticity, as expressed by the Bouc-Wen model. Therefore, at the initial stage of this thesis, a series of parametric studies in 2D have been performed to assess the effect of certain parameters on the accuracy of the computed peak structural responses without structural pounding. Inaccuracies in the computed peak seismic response when the sharp bilinear model is employed for modeling the LRBs, instead of the more accurate and

smoother Bouc-Wen model, have been quantified and certain decisions regarding the modeling of the seismic isolators, afterwards, have been taken.

In order to better understand the consequences of impact on the superstructure, the dynamic response of buildings during collisions has been investigated thoroughly though planar (2D) simulations. For the modeling of structural collisions, the major structural impact models have been considered and assessed. An important issue that has been raised, is the way of considering impacts, which are typically simulated using different types of force-based impact models. Thus, the influence of the characteristics of impact modeling on the computed overall peak structural response of a base-isolated building, which is subjected to earthquake induced structural pounding, have been examined. Specifically, four recently proposed variations of the classical linear viscoelastic impact model, have been compared considering as a benchmark model the classical Kelvin-Voigt model using the formula provided by Anagnostopoulos (Anagnostopoulos, 1988, 2004) for the estimation of the impact damping coefficient.

In effectively and efficiently conducting this investigation, a specialized software application has been utilized, which has been specifically developed to simulate buildings subjected to pounding. The influence of impact parameters, under different cases of gap sizes and isolator's characteristics, on the peak seismic response of a base-isolated building under strong seismic excitations has been examined to assess the relative accuracy of the computed overall peak seismic response during pounding using different impact models for the estimation of the corresponding impact forces.

At the second stage of this thesis, the dynamic response of buildings during collisions has been studied through spatial (3D) numerical simulations and parametric analyses of buildings, which are modeled as MDOF systems with automatic impact capabilities. Performing simulations in three dimensions has enabled the consideration of torsional effects and their effect on structural collisions. Large numbers of numerical simulations and parametric analyses of base-isolated buildings have been performed, in order to investigate the effect of certain factors on the peak seismic performance of these structures under earthquake-induced collisions. The effect of critical factors, such as the consideration of both orthogonal seismic components, the angle of seismic incidence, friction phenomena that occur during pounding, non-eccentric impacts, irregularities or asymmetries in the plan view of the colliding structures, which may excite the torsional vibration of a building and further increase the possibility of impacts during earthquakes, have been also taken into account.

In order to efficiently and effectively estimate the impact forces that should be applied at detected impact points on each structure in contact, an appropriate 3D impact model has been employed. More precisely, a "penalty" method has been implemented, in which a small interpenetration among two colliding bodies is allowed and used in combination with an impact stiffness coefficient to calculate the elastic impact forces that should be applied on the colliding bodies. Contrary to the corresponding 2D impact models, the 3D impact model is able to calculate not only the normal impact forces, but also the frictional forces that may arise between the colliding structures.

Based on this approach, a software has been properly extended, using modern Object-Oriented Design and Programming (OOD/OOP) and the Java programming language to efficiently perform the necessary numerical analyses and parametric studies. The specially developed software provides the desired flexibility, maintainability and extensibility in order to fulfill not only the needs of the current research work, but also facilitate potential future extensions of this research work. Using the aforementioned software, parametric analyses have been executed by automatically varying certain parameters, though a user-specified range of values, so as to assess their influence on the peak seismic response of the simulated base-isolated buildings, while taking into consideration pounding incidences. The results of the conducted simulations and parametric studies provide useful information regarding potential consequences of collisions on the peak response of seismically isolated buildings.

8.2 Major Research Findings

8.2.1 Modeling Considerations of LRBs

The results of the parametric studies have highlighted the discrepancies of the computed peak responses of interest of MDOF base-isolated buildings while using the commonly employed bilinear inelastic and the equivalent linear elastic analysis procedures, instead of a more accurate nonlinear model, such as the Bouc-Wen model. The characteristics of the isolation systems do not considerably influence the peak relative displacements at the isolation level, which seems to be influenced mostly by the characteristics of the earthquake excitations. Considering the dispersion of the errors of the base drifts, the response can be either underestimated or overestimated when the bilinear inelastic model is used for the isolation system. Therefore, the maximum relative displacement can be predicted with high confidence from a safety point of view using the bilinear inelastic model for the LRBs when appropriate safety factors are introduced.

The results have also revealed that the peak responses of the superstructure (i.e. peak floor accelerations and interstory deflections) are overestimated when the bilinear model for the LRBs is used, compared to the more accurate and smoother force-displacement curves of the Bouc-Wen model, due to the more significant contribution of the higher eigenmodes resulting from the sudden stiffness changes of the isolation system. Considering the deviation of the peak responses examined herein, the Bouc Wen model should be used to more accurately assess the peak responses of base-isolated structures.

8.2.2 2D Pounding with the Surrounding Moat Wall

The results of the parametric 2D analysis showed the effect of using five different impact models for the calculation of the impact forces on the overall peak seismic response during pounding. Although, the classical Kelvin-Voigt model and the modified linear viscoelastic model by Ye *et al.* were introduced to provide a reasonable physical explanation of the pounding mechanism, they do not always avoid the appearance of tensile forces just before the end of the retraction phases. Furthermore, both the linear viscoelastic impact model and the Mahmoud and Jankowski model exhibit initial jumps at the impact force values due to the viscous damping term.

The relative performance of the structure is evaluated based on the peak absolute floor accelerations and interstory drifts for various gap sizes and different impact parameters. The presented results from the relevant simulations have shown that the modification proposed by Komodromos *et al.* for the linear viscoelastic model does not influence considerably the peak response values. On the other hand, the maximum impact forces obtained using the linear impact models proposed by Ye *et al.* and Pant and Wijeyewickrema are much higher, than those obtained using the linear viscoelastic impact model with the usage of the formula provided by Anagnostopoulos, leading to significant overestimation of the peak absolute accelerations. Furthermore, the impact parameters seem to influence in a systematic manner the peak response among the examined impact models. On the other hand, the computed peak interstory deflections are relatively insensitive to the impact model that is used, while the minor differences that are observed relate to the different dissipation capacities predicted by each model.

8.2.3 3D Pounding with Adjacent Structures

When a seismically isolated building is subjected to a bidirectional near-fault ground-motion, it may undergo large relative horizontal displacements in both directions. If the separation distance for the adjacent structures is smaller than the peak unobstructed relative

displacements of the structures, collisions occur in either one or both directions. The performed numerical simulations have revealed that the impacts are particularly unfavourable for the seismically isolated structure since they amplify significantly the interstory deflections of the building.

The computed peak seismic responses obtained by considering the bidirectional coupled interaction of bearing restoring force have been compared with the corresponding peak seismic response while ignoring the bidirectional coupled interaction. It has been shown that the bi-directional coupled interaction of the restoring forces of LRB has considerable effects on the seismic responses of the isolated building. If the coupled interaction effects are ignored, the peak bearing displacements are underestimated, which can be crucial for the proper design of base-isolated structures.

The normalized characteristic strength ratio of the seismic isolators significantly influences the peak response of a base-isolated structure during impact. This can be explained by considering that with an increase of the aforementioned ratio, the relative displacements at the isolation level decrease substantially, in combination to the influence of the width of the available seismic gap compared to the corresponding maximum unobstructed relative displacements during those seismic excitations.

Furthermore, the performed simulations have revealed that the peak resultant interstory drift ratio response on a doubly-symmetric base-isolated structure does not vary as a function of the incidence angle. Conversely, the peak response along the *X* or *Y* directions vary considerably depending on the incidence angle. Therefore, a special attention has been devoted on the influence of the seismic incidence angle in 3D analyses.

The results of the parametric studies have also revealed that the detrimental effects of pounding may become more severe for certain values of the excitation angle. Specifically, according to the computed results, the detrimental effects of pounding may become more severe for certain values of the excitation angle, different from 0 degrees, which is the most commonly applied incidence angle in practice while performing dynamic time-history analysis. The incidence angle, along which the amplification of the superstructure response due to pounding with the adjacent building obtains its maximum value, generally coincides with the angle along which the peak unobstructed base displacement occurs, for the case of pounding to the surrounding wall. However, the degree by which the incidence angle affects the interstory deflections seems to be significantly affected by the characteristics and the arrangement of the adjacent structures, in case of buildings in series.

As the separation distance between the base-isolated building and the adjacent structures decreases, there is an increase in the deflections of the superstructure up to a certain value of the seismic gap width and, then, onwards the deflections of the superstructure decrease. Taking into account the examined arrangements, the peak interstory deflection ratios for the case of buildings in series are, in general, smaller than those when impacts occur only with the surrounding moat wall.

The effect of the values of the impact parameters, such as the impact stiffnesses, the coefficient of restitution and the friction coefficient, which are used for the evaluation of the overall response of the seismically isolated structures, has been found to be much less significant that the effect of the directionality of the seismic excitation. The most sensitive responses to the variation of the excitation angle, as well as to the mass eccentricity effects, are the interstory deflections in the direction of pounding and especially those of relatively more flexible building.

Using results from extensive parametric analysis, the influence of certain parameters can be investigated and some general trends in the expected response of the structures can be identified. However, their use and range of applicability becomes limited to the chosen combination of values or range of values of the considered parameters. Although response variation contour plots may be generated, these plots are specific for the imposed earthquake excitations and the characteristics of the adjacent structures that are simulated, rendering the observed trends not suitable to be extrapolated for different combinations.

8.3 Potential Research Extensions

Many other aspects of earthquake-induced collisions of seismically isolated buildings can be considered as potential research issues to be addressed in future extensions of this research work.

Despite the extensive parametric investigations presented within this thesis regarding the dynamic response of base-isolated structures, there are still important aspects regarding that remain to be studied. More specifically, the base isolation system used in all simulations related to the lead-rubber bearing configuration. While LRBs are the most commonly used isolation units, other systems such as friction-pendulum devices are also employed in practice and need to be properly modelled and accordingly investigated.

In the simulations performed within this thesis, the response of regular and symmetric base-isolated buildings has been examined in order to more easily identify the effects of the various parameters on the peak response during pounding. However, it would also be

useful to examine the case of asymmetric structural systems with both vertical stiffness irregularities and vertical geometric irregularities. Another configuration of seismically isolated building that can be examined, considering pounding with the adjacent structures, may refer to the case that seismic isolation is implemented at various elevations.

Firstly, the utilization of seismic isolation results to significantly lower seismic loads acting on the superstructure. Therefore, both floor accelerations and interstory deflections can be significantly reduced, and the superstructure of a seismically isolated building exhibit linear elastic behavior. However, computed peak responses, assuming linear elastic behavior of the superstructure indicate that the significant contact forces generated due to pounding could induce yielding in the superstructure. Therefore, a major future research extension of this study is to examine the effect of nonlinearities of the superstructure on the overall response due to collisions. An extension of the current software is required for the accomplishment of such an investigation as the superstructure should be able to yield and behave nonlinearly and inelastically.

In the current study, the slabs of neighboring buildings are assumed to be at the same level, leading to slab-slab collisions. However, the worst-case scenario corresponds to unaligned slabs, which would lead to floor-to-column collisions, since the impact of massive and rigid slabs against the mid-height of columns can lead to overall structural collapses. Therefore, it would be intriguing to investigate such cases, simulating base-isolated and fixed-base building under such circumstances.

The peak absolute accelerations and deformations of base-isolated structures, are expected to be relatively very limited. Therefore, the detrimental effects of potential collisions during very strong earthquakes are absolutely unacceptable and should be mitigated. Even in cases of extremely strong earthquakes, the isolators should never lose their capability of supporting the vertical loads. Thus, the adoption of a horizontal fail-safe system to limit the isolator deformation could be parametrically assessed. Therefore, an evaluation of the response of base-isolated structures associated with the impacts of the structure against the retaining surrounding wall that can be used as fail-safe system could be studied, and various options of placing bumpers on the active side of the wall could be evaluated. The effectiveness of attaching layers of rubber at potential impact locations, to act as collision bumpers, in order to mitigate the detrimental effects of collisions on the overall response of a seismically isolated building, should be also examined and assessed.

Last but not least, the conclusions drawn from this thesis and any past/future relevant investigations need to be incorporated into standards and codes of practice such as the

effect of incidence angle of seismic excitation, mass eccentricities, etc. are incorporated into the design guidelines for seismically isolated structures.

REFERENCES

Abe, M., Yoshida, J., and Fujino, Y. (2004). Multiaxial Behaviors of Laminated Rubber Bearings and Their Modeling. II: Modeling. *J. Struct. Eng.* 130, 1133–1144. doi:10.1061/(ASCE)0733-9445(2004)130:8(1133).

Agarwal, V. K., Niedzwecki, J. M., and van de Lindt, J. W. (2007). Earthquake induced pounding in friction varying base isolated buildings. *Eng. Struct.* 29, 2825–2832. doi:10.1016/j.engstruct.2007.01.026.

Anagnostopoulos, S. A. (1988). Pounding of buildings in series during earthquakes. *Earthq. Eng. Struct. Dyn.* 16, 443–456. doi:10.1002/eqe.4290160311.

Anagnostopoulos, S. A. (1996). Building pounding re-examined: How serious a problem is it? in *the 11th World Conference on Earthquake Engineering Proceedings* (Acapulco: Elsevier).

Anagnostopoulos, S. A. (2004). Equivalent viscous damping for modeling inelastic impacts in earthquake pounding problems. *Earthq. Eng. Struct. Dyn.* 33, 897–902. doi:10.1002/eqe.377.

Anagnostopoulos, S. A., and Karamaneas, C. E. (2008). Use of collision shear walls to minimize seismic separation and to protect adjacent buildings from collapse due to earthquake-induced pounding. *Earthq. Eng. Struct. Dyn.* 37, 1371–1388. doi:10.1002/eqe.817.

Anagnostopoulos, S. A., Kyrkos, M. T., Papalymperi, A., and Plevri, E. (2015a). Should accidental eccentricity be eliminated from Eurocode 8? *Earthquakes Struct.* 8, 463–484. doi:10.12989/eas.2015.8.2.463.

Anagnostopoulos, S. A., Kyrkos, M. T., and Stathopoulos, K. G. (2015b). Earthquake induced torsion in buildings: critical review and state of the art. *Earthquakes Struct.* 8, 305–377. doi:10.12989/eas.2015.8.2.305.

Anagnostopoulos, S. A., and Spiliopoulos, K. V. (1992). An investigation of earthquake induced pounding between adjacent buildings. *Earthq. Eng. Struct. Dyn.* 21, 289–302. doi:10.1002/eqe.4290210402.

Athanassiadou, C. J., Penelis, G. G., and Kappos, A. J. (1994). Seismic response of adjacent buildings with similar or different dynamic characteristics. *Earthq. Spectra* 10, 293–317. doi:10.1193/1.1585775.

Athanatopoulou, A. M. (2005). Critical orientation of three correlated seismic components. *Eng. Struct.* 27, 301–312. doi:10.1016/j.engstruct.2004.10.011.

Baker, J. W. (2007). Quantitative classification of near-fault ground motions using wavelet analysis. *Bull. Seismol. Soc. Am.* 97, 1486–1501. doi:10.1785/0120060255.

Barros, R. C., Naderpour, H., Khatami, S. M. M., and Mortezaei, A. (2013). Influence of Seismic Pounding on RC Buildings with and without Base Isolation System Subject to Near-Fault Ground Motions. *J. Rehabil. Civ. Eng.* 1, 39–52.

Basu, B., Bursi, O. S., Casciati, F., Casciati, S., Del Grosso, A. E., Domaneschi, M., et al. (2014). A European Association for the Control of Structures joint perspective. Recent studies in civil structural control across Europe. *Struct. Control Heal. Monit.* 21, 1414–1436. doi:10.1002/stc.1652.

Bessason, B. (1992). Assessment of Earthquake Loading and Response of Seismically Isolated Bridges.

Bouc, R. (1967). Forced vibration of mechanical systems with hysteresis. in *the 4th Conference on Nonlinear Oscillation Proceedings* (Prague, Czechoslovakia).

Constantinou, M., Mokha, A., and Reinhorn, A. M. (1990). Teflon Bearings in Base Isolation II: Modeling. *J. Struct. Eng.* 116, 455–474. doi:10.1061/(ASCE)0733-9445(1990)116:2(455).

DesRoches, R., and Muthukumar, S. (2002). Effect of Pounding and Restrainers on Seismic Response of Multiple-Frame Bridges. *J. Struct. Eng.* 128, 860–869. doi:10.1061/(ASCE)0733-9445(2002)128:7(860).

Dimitrakopoulos, E., Makris, N., and Kappos, A. J. (2009). Dimensional analysis of the earthquake-induced pounding between adjacent structures. *Earthq. Eng. Struct. Dyn.* 38, 867–886. doi:10.1002/eqe.872.

Fenves, G. L., Huang, W. H., Whittaker, A. S., Clark, P. W., and Mahin, S. A. (1998). Modeling And Characterization Of Seismic Isolation Bearing. in *the U.S. Italy Workshop on Seismic Protective Systems for Bridges Proceedings* (New York), 1–15.

Filiatrault, A., Wagner, P., and Cherry, S. (1995). Analytical prediction of experimental building pounding. *Earthq. Eng. Struct. Dyn.* 24, 1131–1154.

doi:10.1002/eqe.4290240807.

Gavin, H. P., and Nigbor, R. L. (2012). Performance of the Base-Isolated Christchurch Women's Hospital in the September 4, 2010, Darfield Earthquake and the February 22, 2011, Christchurch Earthquake. in *the 20th Analysis and Computation Specialty Conference Proceedings* (Chicago, Illinois, United States: American Society of Civil Engineers), 554–563. doi:10.1061/9780784412374.049.

Gavin, H. P., and Wilkinson, G. (2010). Preliminary observations of the effects of the 2010 Darfield earthquake on the base-isolated christchurch women's hospital. *Bull. New Zeal. Soc. Earthq. Eng.* 43, 360–367.

Goldsmith, W. (1960). *Impact: the Theory and Physical Behaviour of Colliding Solids*. , ed. E. Arnold London.

Guo, A., Cui, L., and Li, H. (2012). Impact Stiffness of the Contact-Element Models for the Pounding Analysis of Highway Bridges: Experimental Evaluation. *J. Earthq. Eng.* 16, 1132–1160. doi:10.1080/13632469.2012.693243.

Guo, A., Li, Z., Li, H., and Ou, J. (2009). Experimental and analytical study on pounding reduction of base-isolated highway bridges using MR dampers. *Earthq. Eng. Struct. Dyn.* 38, 1307–1333. doi:10.1002/eqe.903.

Hameed, A., Koo, M.-S., Do, T. D., and Jeong, J.-H. (2008). Effect of lead rubber bearing characteristics on the response of seismic-isolated bridges. *KSCE J. Civ. Eng.* 12, 187–196. doi:10.1007/s12205-008-0187-9.

Higashino, M., and Okamoto, S. (2006). *Response Control and Seismic Isolation of Buildings*. , ed. Taylor & Francis Oxon, UK doi:10.4324/9780203018866.

Huang, W., Fenves, G. L., Whittaker, A. S., and Mahin, S. A. (2000). Characterization of Seismic Isolation Bearings for Bridges From Bi-Directional Testing. in *the 12th World Conference on Earthquake Engineering Proceedings* (Auckland, New Zealand).

Jangid, R. S. (2007). Optimum lead-rubber isolation bearings for near-fault motions. *Eng. Struct.* 29, 2503–2513. doi:10.1016/j.engstruct.2006.12.010.

Jankowski, R. (2005). Non-linear viscoelastic modelling of earthquake-induced structural pounding. *Earthq. Eng. Struct. Dyn.* 34, 595–611. doi:10.1002/eqe.434.

Jankowski, R. (2008). Earthquake-induced pounding between equal height buildings with substantially different dynamic properties. *Eng. Struct.* 30, 2818–2829.

doi:10.1016/j.engstruct.2008.03.006.

Jankowski, R. (2009). Non-linear FEM analysis of earthquake-induced pounding between the main building and the stairway tower of the Olive View Hospital. *Eng. Struct.* 31, 1851–1864. doi:10.1016/j.engstruct.2009.03.024.

Jankowski, R. (2010). Experimental study on earthquake-induced pounding between structural elements made of different building materials. *Earthq. Eng. Struct. Dyn.* 39, 343–354. doi:10.1002/eqe.941.

Jankowski, R. (2012). Non-linear FEM analysis of pounding-involved response of buildings under non-uniform earthquake excitation. *Eng. Struct.* 37, 99–105. doi:10.1016/j.engstruct.2011.12.035.

Jankowski, R., and Mahmoud, S. (2015). *Earthquake-Induced Structural Pounding*. Cham: Springer International Publishing doi:10.1007/978-3-319-16324-6.

Jankowski, R., Wilde, K., and Fujino, Y. (1998). Pounding of superstructure segments in isolated elevated bridge during earthquakes. *Earthq. Eng. Struct. Dyn.* 27, 487–502. doi:10.1002/(SICI)1096-9845(199805)27:5<487::AID-EQE738>3.0.CO;2-M.

Jin, J. J., Huang, X. Y., and Zhuang, X. Z. (2008). Study on Preyield Shear Stiffness of Differential Restoring Force Model for Lead Rubber Bearing. in *the 14th World Conference on Earthquake Engineering Proceedings* (Beijing, China), 1–8.

Kalkan, E., and Kwong, N. S. (2014). Pros and Cons of Rotating Ground Motion Records to Fault-Normal/Parallel Directions for Response History Analysis of Buildings. *J. Struct. Eng.* 140, 4013062. doi:10.1061/(ASCE)ST.1943-541X.0000845.

Kalpakidis, I. V., Constantinou, M. C., and Whittaker, A. S. (2010). Modeling strength degradation in lead-rubber bearings under earthquake shaking. *Earthq. Eng. Struct. Dyn.* 39, 1533–1549. doi:10.1002/eqe.1039.

Kampas, G., and Makris, N. (2012). Time and frequency domain identification of seismically isolated structures: advantages and limitations. *Earthquakes Struct.* 3, 249–270. doi:10.12989/eas.2012.3_3.249.

Kikuchi, M., and Aiken, I. A. N. D. (1997). An analytical hysteresis model for elastomeric seismic isolation bearings. *Earthq. Eng. Struct. Dyn.* 26, 215–231. doi:10.1002/(SICI)1096-9845(199702)26:2<215::AID-EQE640>3.0.CO;2-9.

Kim, S.-H., and Shinozuka, M. (2003). Effects of Seismically Induced Pounding at Expansion Joints of Concrete Bridges. *J. Eng. Mech.* 129, 1225–1234.

doi:10.1061/(ASCE)0733-9399(2003)129:11(1225).

Komodromos, P. (2000). *Seismic Isolation for Earthquake Resistant Structures*. Southampton: WIT Press.

Komodromos, P. (2008). Simulation of the earthquake-induced pounding of seismically isolated buildings. *Earthq. Eng. Struct. Dyn.* 86, 618–626. doi:10.1016/j.compstruc.2007.08.001.

Komodromos, P., Polycarpou, P. C., Papaloizou, L., and Phocas, M. C. (2007). Response of seismically isolated buildings considering poundings. *Earthq. Eng. Struct. Dyn.* 36, 1605–1622. doi:10.1002/eqe.692.

Kostinakis, K., Athanatopoulou, A., and Morfidis, K. (2015). Correlation between ground motion intensity measures and seismic damage of 3D R/C buildings. *Eng. Struct.* 82, 151–167. doi:10.1016/j.engstruct.2014.10.035.

Kostinakis, K. G., Athanatopoulou, A. M., and Avramidis, I. E. (2012). Orientation effects of horizontal seismic components on longitudinal reinforcement in R/C frame elements. *Nat. Hazards Earth Syst. Sci.* 12, 1–10. doi:10.5194/nhess-12-1-2012.

Kulkarni, J. A., and Jangid, R. S. (2002). Rigid body response of base-isolated structures. *J. Struct. Control* 9, 171–188. doi:10.1002/stc.11.

Layton, H. (1999). Principles and techniques for desiging precision machines.

Leibovich, E., Rutenberg, A., and Yankelevsky, D. (2012). Pounding Response of Adjacent Concrete Rods: An Experimental Study. *Int. J. Prot. Struct.* 3, 355–374. doi:10.1260/2041-4196.3.3.355.

Liang, Z., and Lee, G. C. (2003). Principal axes of M-DOF structures Part II: Dynamic loading. *Earthq. Eng. Eng. Vib.* 2, 39–50. doi:10.1007/BF02857537.

Liolios, A. A. (2000). A Linear Complementarity Approach for the Non-convex Seismic Frictional Interaction between Adjacent Structures under Instabilizing Effects*. *J. Glob. Optim.* 17, 259–266. doi:10.1023/A:1026789817828.

Lopez, O. A., Chopra, A. K., and Hernandez, J. J. (2000). Critical response of structures to multicomponent earthquake excitation. *Earthq. Eng. Struct. Dyn.* 29, 1759–1778. doi:10.1002/1096-9845(200012)29:12<1759::AID-EQE984>3.0.CO;2-K.

López, O. A., and Torres, R. (1997). The critical angle of seismic incidence and the maximum structural response. *Earthq. Eng. Struct. Dyn.* 26, 881–894. doi:10.1002/(SICI)1096-9845(199709)26:9<881::AID-EQE674>3.0.CO;2-R.

Magliulo, G., Maddaloni, G., and Petrone, C. (2014). Influence of earthquake direction on the seismic response of irregular plan RC frame buildings. *Earthq. Eng. Eng. Vib.* 13, 243–256. doi:10.1007/s11803-014-0227-z.

Mahmoud, S., Abd-Elhamed, A., and Jankowski, R. (2013). Earthquake-induced pounding between equal height multi-storey buildings considering soil-structure interaction. *Bull. Earthq. Eng.* 11, 1021–1048. doi:10.1007/s10518-012-9411-6.

Mahmoud, S., and Jankowski, R. (2010). Pounding-involved response of isolated and non-isolated buildings under earthquake excitation. *Earthquakes Struct.* 1, 231–252. doi:10.12989/eas.2010.1.3.231.

Mahmoud, S., and Jankowski, R. (2011). Modified linear viscoelastic model of earthquake-induced structural pounding. *Iran. J. Sci. Technol. Trans. B Eng.* 35, 51–62.

Maison, B. F., and Kasai, K. (1990). Analysis for a Type of Structural Pounding. *J. Struct. Eng.* 116, 957–977. doi:10.1061/(ASCE)0733-9445(1990)116:4(957).

Maison, B. F., and Venture, C. E. (1992). Seismic Analysis of Base-Isolated San Bernardino County Building. *Earthq. Spectra* 8, 605–633. doi:10.1193/1.1585698.

Makris, N., and Black, C. (2003). *Dimensional analysis of inelastic structures subjected to near fault ground motions*. California, Berkeley: Earthquake Engineering Research Center.

Makris, N., and Black, C. J. (2004). Dimensional Analysis of Bilinear Oscillators under Pulse-Type Excitations. *J. Eng. Mech.* 130, 1019–1031. doi:10.1061/(ASCE)0733-9399(2004)130:9(1019).

Makris, N., and Vassiliou, M. F. (2011). The existence of "complete similarities" in the response of seismic isolated structures subjected to pulse-like ground motions and their implications in analysis. *Earthq. Eng. Struct. Dyn.* 40, 1103–1121. doi:10.1002/eqe.1072.

Malhotra, P. K. (1997). Dynamics of seismic impacts in base-isolated buildings. *Earthq. Eng. Struct. Dyn.* 26, 797–813. doi:10.1002/(SICI)1096-9845(199708)26:8<797::AID-EQE677>3.0.CO;2-6.

Martelli, A., Forni, M., and Clemente, P. (2012). Recent Worldwide Application of Seismic Isolation and Energy Dissipation and Conditions for Their Correct Use. in *the 15th World Conference on Earthquake Engineering Proceedings* (Lisbon, Portugal).

Masroor, A., and Mosqueda, G. (2012). Experimental simulation of base-isolated buildings pounding against moat wall and effects on superstructure response. *Earthq. Eng. Struct. Dyn.* 41, 2093–2109. doi:10.1002/eqe.2177.

Masroor, A., and Mosqueda, G. (2013a). Impact model for simulation of base isolated buildings impacting flexible moat walls. *Earthq. Eng. Struct. Dyn.* 42, 357–376. doi:10.1002/eqe.2210.

Masroor, A., and Mosqueda, G. (2013b). Seismic response of base isolated buildings considering pounding to moat walls: MCEER-13-0003.

Matsagar, V. A., and Jangid, R. S. (2003). Seismic response of base-isolated structures during impact with adjacent structures. *Eng. Struct.* 25, 1311–1323. doi:10.1016/S0141-0296(03)00081-6.

Matsagar, V. A., and Jangid, R. S. (2004). Influence of isolator characteristics on the response of base-isolated structures. *Eng. Struct.* 26, 1735–1749.

Matsagar, V. A., and Jangid, R. S. S. (2010). Impact Response of Torsionally Coupled Base-isolated Structures. *J. Vib. Control* 16, 1623–1649. doi:10.1177/1077546309103271.

Mavroeidis, G., Dong, G., and Papageorgiou, A. S. (2004). Near-fault ground motions, and the response of elastic and inelastic single-degree-of-freedom (SDOF) systems. *Earthq. Eng. Struct. Dyn.* 33, 1023–1049. doi:10.1002/eqe.391.

Mavronicola, E. A., Polycarpou, P. C., and Komodromos, P. (2016). Effect of Planar Impact Modeling on the Pounding Response of Base-Isolated Buildings. *Front. Built Environ.* 2, 11. doi:10.3389/fbuil.2016.00011.

Mavronicola, E., and Komodromos, P. (2011). Assessing the suitability of equivalent linear elastic analysis of seismically isolated multi-storey buildings. *Comput. Struct.* 89, 1920–1931. doi:10.1016/j.compstruc.2011.05.010.

Mavronicola, E., and Komodromos, P. (2012). The effect of non-linear parameters on the modeling of multi-storey seismically isolated buildings. in *the 15th World Conference on Earthquake Engineering Proceedings* (Lisbon, Portugal).

Mavronicola, E., Polycarpou, P. C., and Komodromos, P. (2015a). The effect of modified linear viscoelastic impact models in the pounding response of a base-isolated building with adjacent structures. in *the 5th International Conference on Computational Methods in Structural Dynamics and Earthquake Engineering Proceedings* (Crete Island, Greece).

Mavronicola, E., Polycarpou, P., Papaloizou, L., and Komodromos, P. (2015b). Computer-aided investigation of special issues of the response of seismically isolated buildings. *Int. J. Comput. Methods Exp. Meas.* 3, 21–32. doi:10.2495/CMEM-V3-N1-21-32.

van Mier, J. G. M., Pruijssers, A. F., Reinhardt, H. W., and Monnier, T. (1991). Load-Time Response of Colliding Concrete Bodies. *J. Struct. Eng.* 117, 354–374. doi:10.1061/(ASCE)0733-9445(1991)117:2(354).

Mohammed, S., and Al-Amawee, A. H. (2006). The Ratio between Static and Dynamic Modulus of Elasticity in Normal and High Strength Concrete. *J. Eng. Dev.* 10, 163–174.

Moustafa, A., and Mahmoud, S. (2014). Damage assessment of adjacent buildings under earthquake loads. *Eng. Struct.* 61, 153–165. doi:10.1016/j.engstruct.2014.01.004.

Muthukumar, S., and DesRoches, R. (2006). A Hertz contact model with non-linear damping for pounding simulation. *Earthq. Eng. Struct. Dyn.* 35, 811–828. doi:10.1002/eqe.557.

Naeim, F., and Kelly, J. M. (1999). *Design of seismic isolated structures: From theory to practice*. Hoboken NJ, USA: John Wiley & Sons Inc.

Nagarajaiah, S., Reinhorn, A. M., and Constantinou, M. C. (1991). Nonlinear Dynamic Analysis of 3D Base Isolated Structures. *J. Struct. Eng.* 117, 2035–2054. doi:10.1061/(ASCE)0733-9445(1991)117:7(2035).

Nagarajaiah, S., and Sun, X. (2001). Base-Isolated FCC Building: Impact Response in Northridge Earthquake. *J. Struct. Eng.* 127, 1063–1075.

Nagarajaiah, S., and Xiaohong, S. (2000). Response of Base-Isolated USC Hospital Building in Northridge Earthquake. *J. Struct. Eng.* 126, 1177–1186. doi:10.1061/(ASCE)0733-9445(2000)126:10(1177).

Ozdemir, G. (2014). Lead core heating in lead rubber bearings subjected to bidirectional ground motion excitations in various soil types. *Earthq. Eng. Struct. Dyn.* 43, 267–285. doi:10.1002/eqe.2343.

Pant, D. R., and Wijeyewickrema, A. C. (2012). Structural performance of a base-isolated reinforced concrete building subjected to seismic pounding. *Earthq. Eng. Struct. Dyn.* 41, 1709–1716. doi:10.1002/eqe.2158.

Pant, D. R., and Wijeyewickrema, A. C. (2014). Performance of base-isolated reinforced concrete buildings under bidirectional seismic excitation considering pounding with

retaining walls including friction effects. *Earthq. Eng. Struct. Dyn.* 43, 1521–1541. doi:10.1002/eqe.2409.

Pant, D. R., Wijeyewickrema, A. C., and Ohmachi, T. (2010). Seismic pounding between reinforced concrete buildings : A study using two recently proposed contact element models. in *the 14th European Conference on Earthquake Engineering Proceesings* (Ohrid).

Papadrakakis, M., Mouzakis, H., Plevris, N., and Bitzarakis, S. (1991). A lagrange multiplier solution method for pounding of buildings during earthquakes. *Earthq. Eng. Struct. Dyn.* 20, 981–998. doi:10.1002/eqe.4290201102.

Park, J.-G., and Otsuka, H. (1999). Optimal yield level of bilinear seismic isolation devices. *Earthq. Eng. Struct. Dyn.* 28, 941–955. doi:10.1002/(SICI)1096-9845(199909)28:9<941::AID-EQE848>3.0.CO;2-5.

Park, Y. J., Wen, Y.-K., and Ang, A. (1986). Random vibration of hysteretic systems under bi-directional ground motions. *Earthq. Eng. Struct. Dyn.* 14, 543–557. doi:10.1002/eqe.4290140405.

PEER Pacific Earthquake Engineering Research Center (2011). Ground motion database. Available at: http://peer.berkeley.edu/peer_ground_motion_database [Accessed November 23, 2011].

Penzien, J., and Watabe, M. (1974). Characteristics of 3-dimensional earthquake ground motions. *Earthq. Eng. Struct. Dyn.* 3, 365–373. doi:10.1002/eqe.4290030407.

Polycarpou, P. C., and Komodromos, P. (2010a). Earthquake-induced poundings of a seismically isolated building with adjacent structures. *Eng. Struct.* 32, 1937–1951. doi:10.1016/j.engstruct.2010.03.011.

Polycarpou, P. C., and Komodromos, P. (2010b). On poundings of a seismically isolated building with adjacent structures during strong earthquakes. *Earthq. Eng. Struct. Dyn.* 39, 1397–1951. doi:10.1002/eqe.975.

Polycarpou, P. C., and Komodromos, P. (2011). Numerical investigation of potential mitigation measures for poundings of seismically isolated buildings. *Earthquakes Struct.* 2, 1–24. doi:10.12989/eas.2011.2.1.001.

Polycarpou, P. C., Mavronicola, E. A., and Komodromos, P. (2015a). Planar and spatial numerical investigation of the effects of earthquake-induced pounding of base isolated buildings. in *the 14th World Conference on Seismic Isolation, Energy Dissipation and Active Vibration Control of Structures Proceedings* (San Diego, USA).

Polycarpou, P. C., Papaloizou, L., and Komodromos, P. (2014). An efficient methodology for simulating earthquake-induced 3D pounding of buildings. *Earthq. Eng. Struct. Dyn.* 43, 985–1003. doi:10.1002/eqe.2383.

Polycarpou, P. C., Papaloizou, L., Komodromos, P., and Charmpis, D. C. (2015b). Effect of the seismic excitation angle on the dynamic response of adjacent buildings during pounding. *Earthquakes Struct.* 8, 1127–1146. doi:DOI: http://dx.doi.org/10.12989/eas.2015.8.5.1127.

Popov, V., and Heß, M. (2015). *Method of Dimensionality Reduction in Contact Mechanics and Friction*. Springer-Verlag Berlin Heidelberg doi:10.1007/978-3-642-53876-6.

Pranesh, M., and Sinha, R. (2000). VFPI: an isolation device for aseismic design. *Earthq. Eng. Struct. Dyn.* 29, 603–627. doi:10.1002/(SICI)1096-9845(200005)29:5<603::AID-EQE927>3.0.CO;2-W.

Providakis, C. (2008). Effect of LRB isolators and supplemental viscous dampers on seismic isolated buildings under near-fault excitations. *Eng. Struct.* 30, 1187–1198. doi:10.1016/j.engstruct.2007.07.020.

Ramallo, J. C., Johnson, E. A., and Spencer, J. B. F. (2002). "Smart"' Base Isolation Systems. *J. Eng. Mech.* 128, 1088–1099. doi:10.1061/(ASCE)0733-9399(2002)128:10(1088).

Robinson, W. (2011). Lead-rubber hysteretic bearings suitable for protecting structures during earthquakes. *Seism. Isol. Prot. Syst.* 2, 5–19. doi:10.2140/siaps.2011.2.5.

Sain, P. M., Sain, M. K., and Spencer, B. F. (1997). Models for hysteresis and application to structural control. in *the 1997 American Control Conference Proceedings* (Albuquerque, New Mexico). doi:10.1109/ACC.1997.611746.

Sato, E., Furukawa, S., Kakehi, A., and Nakashima, M. (2011). Full-scale shaking table test for examination of safety and functionality of base-isolated medical facilities. *Earthq. Eng. Struct. Dyn.* 40, 1435–1453. doi:10.1002/eqe.1097.

Shrimali, M. K., and Jangid, R. S. (2002). Non-linear seismic response of base-isolated liquid storage tanks to bi-directional excitation. *Nucl. Eng. Des.* 217, 1–20. doi:10.1016/S0029-5493(02)00134-6.

Skinner, R. I., Robinson, W. H., and McVerry, G. H. (1993). *An introduction to seismic isolation*. West Sussex, UK: John Wiley & Sons Ltd.

Slafak, E., and Bendimerad, M. F. (1988). Peak response of 2-DOF uncoupled oscillator under two-directional base motion. *Earthq. Eng. Struct. Dyn.* 16, 1061–1072. doi:10.1002/eqe.4290160708.

Spiliopoulos, K. V., and Anagnostopoulos, S. A. (1996). Measures against earthquake pounding between adjacent buildings. in *the 11th World Conference on Earthquake Engineering Proceedings* (Acapulco: Elsevier).

Taskari, O., and Sextos, A. (2015). Multi-angle, multi-damage fragility curves for seismic assessment of bridges. *Earthq. Eng. Struct. Dyn.* 44, 2281–2301. doi:10.1002/eqe.2584.

Tena-Colunga, A., and Escamilla-Cruz, J. L. (2007). Torsional amplifications in asymmetric base-isolated structures. *Eng. Struct.* 29, 237–247. doi:10.1016/j.engstruct.2006.03.036.

Torbol, M., and Shinozuka, M. (2012). Effect of the angle of seismic incidence on the fragility curves of bridges. *Earthq. Eng. Struct. Dyn.* 41, 2111–2124. doi:10.1002/eqe.2197.

Tsai, H. C. (1997). Dynamic analysis of base-isolated shear beams bumping against stops. *Earthq. Eng. Struct. Dyn.* 26, 515–528. doi:10.1002/(SICI)1096-9845(199705)26:5<515::AID-EQE654>3.0.CO;2-C.

Uz, M., and Hadi, M. (2011). "Investigating the effects of pounding for inelastic base isolated adjacent buildings under earthquake excitations," in *Incorporating Sustainable Practice in Mechanics of Structures and Materials*, eds. S. Fragomeni, S. Venkatesan, N. Setunge, and L. S. (Netherlands: CRC Press), 329–334. Available at: http://ro.uow.edu.au/engpapers/2683 [Accessed March 28, 2017].

Varnava, V., and Komodromos, P. (2013). Assessing the effect of inherent nonlinearities in the analysis and design of a low-rise base isolated steel building. *Earthquakes Struct.* 5, 499–526.

Vassiliou, M. F., Tsiavos, A., and Stojadinović, B. (2013). Dynamics of inelastic base-isolated structures subjected to analytical pulse ground motions. *Earthq. Eng. Struct. Dyn.* 42, 2043–2060. doi:10.1002/eqe.2311.

Watanabe, G., and Kawashima, K. (2004). Numerical Simulation of Pounding of Bridge Decks. in *the 13th World Conference on Earthquake Engineering Proceedings* (Vancouver, B.C.).

Wen, Y.-K. (1976). Method for random vibration of hysteretic systems. *J. Eng. Mech. Div.*

102, 249–263.

Whittaker, A. S., Kumar, M., and Kumar, M. (2014). Seismic Isolation of Nuclear Power Plants. *Nucl. Eng. Technol.* 46. doi:10.5516/NET.09.2014.715.

Wilson, E. L., and Button, M. R. (1982). Three-dimensional dynamic analysis for multi-component earthquake spectra. *Earthq. Eng. Struct. Dyn.* 10, 471–476. doi:10.1002/eqe.4290100309.

Wriggers, P. (2006). "Constitutive Equations for Contact Interfaces," in *Computational Contact Mechanics* (Berlin, Heidelberg: Springer Berlin Heidelberg), 69–108. doi:10.1007/978-3-540-32609-0_5.

Ye, K., Li, L., and Zhu, H. (2009a). A modified Kelvin impact model for pounding simulation of base-isolated building with adjacent structures. *Earthq. Eng. Eng. Vib.* 8, 433–446. doi:10.1007/s11803-009-8045-4.

Ye, K., Li, L., and Zhu, H. (2009b). A note on the Hertz contact model with nonlinear damping for pounding simulation. *Earthq. Eng. Struct. Dyn.* 38, 1135–1142. doi:10.1002/eqe.883.

Zhu, P., Abe, M., and Fujino, Y. (2002). Modelling three-dimensional non-linear seismic performance of elevated bridges with emphasis on pounding of girders. *Earthq. Eng. Struct. Dyn.* 31, 1891–1913. doi:10.1002/eqe.194.